UNIVERSIDADE ESTADUAL DE CAMPINAS
INSTITUTO DE GEOCIÊNCIAS

PAULO MIGUEL HADDAD MARTIM

FRACTAIS E IMPLICAÇÕES PARA MAPAS DE FAVORABILIDADE MINERAL: O EXEMPLO DOS DEPÓSITOS *IRON OXIDE-COPPER-GOLD* DE CARAJÁS (PA)

CAMPINAS
2017

PAULO MIGUEL HADDAD MARTIM

FRACTAIS E IMPLICAÇÕES PARA MAPAS DE FAVORABILIDADE MINERAL: O EXEMPLO DOS DEPÓSITOS *IRON OXIDE-COPPER-GOLD* DE CARAJÁS (PA)

DISSERTAÇÃO APRESENTADA AO INSTITUTO DE GEOCIÊNCIAS DA UNIVERSIDADE ESTADUAL DE CAMPINAS PARA OBTENÇÃO DO TÍTULO DE MESTRE EM GEOCIÊNCIAS NA ÁREA DE GEOLOGIA E RECURSOS NATURAIS

ORIENTADOR: PROF. DR. CARLOS ROBERTO DE SOUZA FILHO

COORIENTADOR: PROF. DR. EMMANUEL JOHN M. CARRANZA

ESTE EXEMPLAR CORRESPONDE À VERSÃO FINAL DA DISSERTAÇÃO DEFENDIDA PELO ALUNO PAULO MIGUEL HADDAD MARTIM E ORIENTADA PELO PROF. DR. CARLOS ROBERTO DE SOUZA FILHO

CAMPINAS

2017

Agência(s) de fomento e nº(s) de processo(s): FAPESP, 2015/11186-3; CNPq, 401316/2014-9

Ficha catalográfica
Universidade Estadual de Campinas
Biblioteca do Instituto de Geociências
Marta dos Santos - CRB 8/5892

H117f

Haddad Martim, Paulo Miguel, 1985-
Fractais e implicações para mapas de favorabilidade mineral: o exemplo dos depósitos *iron oxide-copper-gold* de Carajás (PA) / Paulo Miguel Haddad Martim. – Campinas, SP : [s.n.], 2017.

Orientador: Carlos Roberto de Souza Filho.
Coorientador: Emmanuel John Muico Carranza.
Dissertação (mestrado) – Universidade Estadual de Campinas, Instituto de Geociências.

1. Metalogenia. 2. Alteração hidrotermal. 3. Depositos de oxido de Fe-Cu-Au - Carajas, Serra dos (PA). 4. Fractais. 5. Prospecção mineral. I. Souza Filho, Carlos Roberto de, 1965-. II. Carranza, Emmanuel John Muico. III. Universidade Estadual de Campinas. Instituto de Geociências. IV. Título.

Informações para Biblioteca Digital

Título em outro idioma: Fractals and implications for mineral favorability maps: the example of iron oxide-copper-gold deposits from Carajás (PA)
Palavras-chave em inglês:
Metallogenesis
Hydrothermal alteration
Iron oxide-copper-gold deposits - Carajas, Serra dos (PA)
Fractals
Prospecting
Área de concentração: Geologia e Recursos Naturais
Titulação: Mestre em Geociências
Banca examinadora:
Carlos Roberto de Souza Filho [Orientador]
Roberto Perez Xavier
Adelir José Strieder
Data de defesa: 27-09-2017
Programa de Pós-Graduação: Geociências

UNIVERSIDADE ESTADUAL DE CAMPINAS
INSTITUTO DE GEOCIÊNCIAS

AUTOR: Paulo Miguel Haddad Martim

FRACTAIS E IMPLICAÇÕES PARA MAPAS DE FAVORABILIDADE MINERAL: O EXEMPLO DOS DEPÓSITOS *IRON OXIDE-COPPER-GOLD* DE CARAJÁS (PA)

ORIENTADOR: Prof. Dr. Carlos Roberto de Sousa Filho
COORIENTADOR: Prof. Dr. Emmanuel John Muico Carranza

Aprovado em: 27 / 09 / 2017

EXAMINADORES:

Prof. Dr. Carlos Roberto de Sousa Filho - Presidente

Prof. Dr. Roberto Perez Xavier

Prof. Dr. Adelir José Strieder

A Ata de Defesa assinada pelos membros da Comissão Examinadora, consta no processo de vida acadêmica do aluno.

Campinas, 27 de setembro de 2017.

SÚMULA CURRICULAR

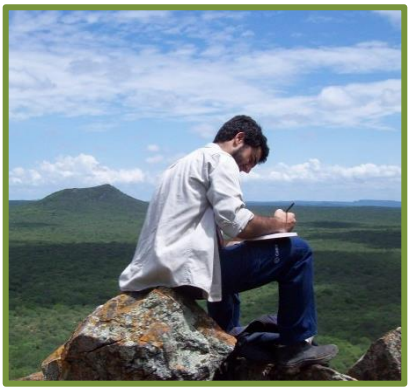

Paulo Miguel Haddad Martim concluiu sua graduação em geologia pelo Instituto de Geociências da Universidade de São Paulo em 2007.

Entre 2008 e 2015 trabalhou com exploração mineral em diferentes regiões do Brasil. Os projetos de prospecção em que esteve envolvido incluíram diversos bens minerais: bauxita (ES, RJ, MG), ferro (BA), ferro, níquel e calcário (PI, PE), ouro (norte de MT), cobre, chumbo e zinco (sudoeste de MT). Durante este período suas principais atribuições estavam relacionadas a atividades de mapeamento geológico em diversas escalas, coleta de amostras para geoquímica de superfície e descrição de sondagens para investigação de subsuperfície.

A experiência profissional na área de prospecção mineral permitiu a aquisição de experiência com Sistemas de Informações Geográficas (SIG) e dados espaciais de geologia, geoquímica, geofísica, imagem de satélite e topografia, além de georreferenciamento, vetorização e manipulação de dados espaciais para criação de mapas multitemáticos.

O autor ingressou no programa de pós-graduação da Universidade Estadual de Campinas em agosto de 2015. Atualmente, seus interesses estão concentrados nas diversas aplicações das geotecnologias na investigação de problemas geológicos.

AGRADECIMENTOS

Gostaria de expressar meus agradecimentos à Fundação de Amparo à Pesquisa do Estado de São Paulo (FAPESP), em convênio com a Coordenação de Aperfeiçoamento de Pessoal de Nível Superior (CAPES) pela bolsa de estudos para o desenvolvimento desta pesquisa (processo nº 2015/11186-3). Agradeço também ao Conselho Nacional de Desenvolvimento Tecnológico e Científico (CNPq) pelo apoio financeiro do qual este mestrado também se utilizou (processo nº 2014-9/401316).

Aos orientadores do projeto, Professores Carlos Roberto de Souza Filho e Emmanuel John M. Carranza pelo apoio e incentivo durante todo o desenvolvimento das pesquisas.

Ao Serviço Geológico do Brasil (CPRM) pela disponibilização dos dados aerogeofísicos da região de Carajás.

À Vale pelo apoio em longo prazo à UNICAMP para pesquisa na região de Carajás, e pela autorização de acesso à Mina de Sossego. Agradecemos também pela organização e acompanhamento das atividades de campo, estendendo agradecimentos especiais aos colegas: Roberto Albuquerque, Petterson Barbosa, Fabricio Franco, Rafael Sposito, Fernando Matos, Sergio B. Huhn, Valmir e Ivan. Agradecimentos também à equipe do planejamento de curto prazo da Mina de Sossego pela ajuda com a amostragem nas cavas da mina: Vitor, Maureny, Antônio, Ricardo e Luiz.

Agradeço especialmente à Professora Lena Monteiro, da Universidade de São Paulo, pelo auxílio com a preparação e confecção dos primeiros lotes de lâminas. Também ajudaram na preparação e serragem das amostras os colegas Rodrigo e Bruna. A preparação das amostras dependeu ainda da indispensável ajuda de Marco, da Universidade Federal de Ouro Preto.

À Professora Maryelle Ferreira pelo compartilhamento da íntegra de sua dissertação de mestrado, e ao Professor Emilson Leite pelo auxílio aos trâmites da pós-graduação.

Aos Professores Roberto Xavier e Carolina Moreto pelas críticas construtivas durante o exame de qualificação.

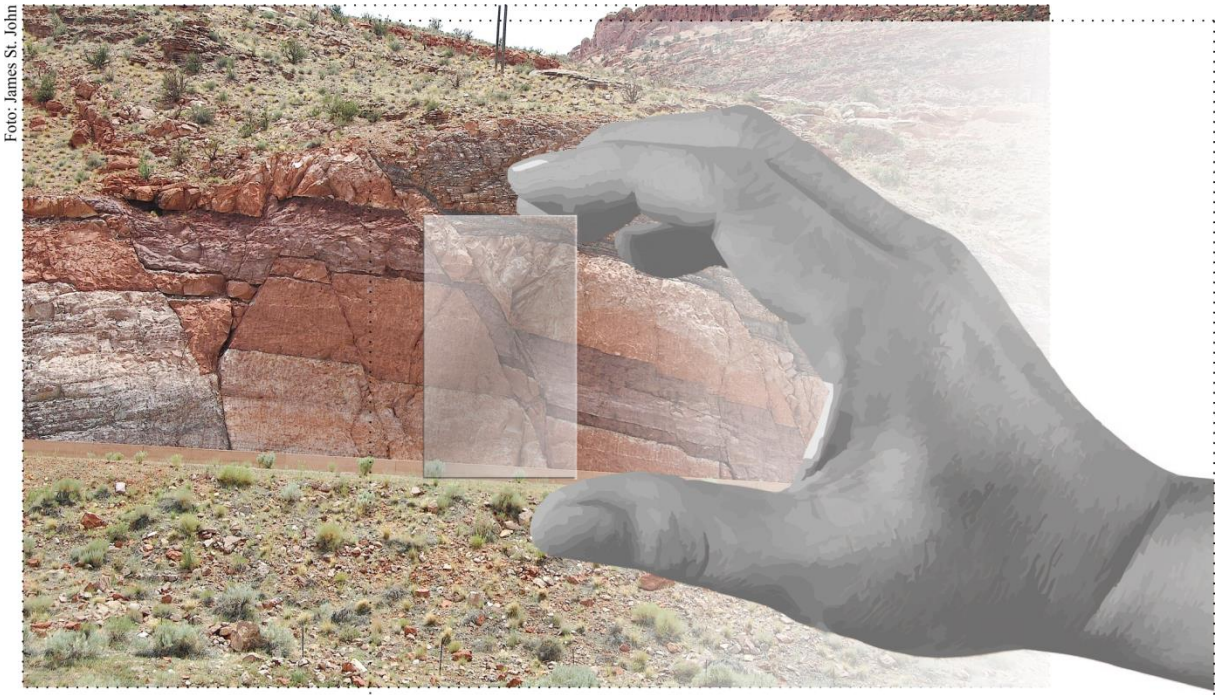

During their earliest field training, geologists are taught to place an object of known size, such as a rock hammer or a lens cap, in photographs of outcrops in order to convey a sense of scale. Why?

Christopher C. Barton e Paul R. La Pointe,

Fractals in the Earth Sciences

RESUMO

Desde a definição do conceito da geometria fractal na segunda metade do século XX, a importância dos fractais para a descrição e entendimento de feições geológicas gradualmente ganhou importância. Mais recentemente, diversos trabalhos têm sugerido que a distribuição espacial de depósitos minerais apresenta geometria fractal, a qual representaria a complexa interação de processos geológicos necessários para a gênese de uma mineralização. A manifestação da geometria fractal se dá através da invariância escalar, ou seja, a propriedade de uma feição conservar suas características geométricas independente da escala espacial. Esta característica é promissora para o estudo de depósitos minerais, pois sugere a possibilidade de que informações sobre a geometria da mineralização em uma escala possa ser usada para inferir aspectos da geometria em outras escalas. Uma vez que a geometria das mineralizações é consequência dos controles que atuaram durante e após sua formação, a possibilidade de estudos com uma abordagem fractal tem aplicações teóricas e práticas. Considerando o exposto, a presente pesquisa dedicou-se a investigar se de fato a geometria de depósitos minerais apresenta invariância escalar, e em caso positivo, que informações ela permite inferir sobre os controles de mineralização. Para esta investigação foi escolhida como área de estudo a região do depósito *Iron Oxide-Copper-Gold* (IOCG) de Sossego, na Província Mineral de Carajás (PA). Depósitos IOCG apresentam forte controle estrutural, que somados a farta disponibilidade de dados nas escalas regional, local e microscópica tornam a área da mina de Sossego ideal para a pesquisa proposta. Assim, os dados já disponíveis na literatura foram integrados com novas medidas estruturais e novas lâminas orientadas de amostras coletadas nas cavas da mina. A geometria da mineralização foi avaliada em três diferentes escalas: na escala regional examinou-se a distribuição espacial dos depósitos IOCG conhecidos; na escala local examinou-se a geometria das estruturas e corpos mineralizados no depósito de Sossego; na escala microscópica foi avaliada a geometria da distribuição espacial e da forma dos grãos de minerais de minério. O conjunto de resultados indica que os depósitos IOCG da região de Carajás, e em particular o depósito de Sossego, apresentam geometria fractal, conservando a orientação e anisotropia nas diferentes escalas. A orientação e anisotropia das mineralizações são aspectos geométricos que resultam diretamente do controle exercido pela trama estrutural subjacente. Desta forma, os resultados indicam que o controle estrutural gera a invariância escalar devido à influência que exerce sobre a permeabilidade das rochas, um fator essencial para a geração de depósitos hidrotermais. A permeabilidade é definida em escala microscópica através de planos de foliação, microfraturas e vênulas, as quais se relacionam diretamente com estruturas de escalas maiores, tais como zonas de cisalhamento, falhas e veios, criando uma rede permeável consistente através das escalas. No caso de Carajás, a geometria destas áreas permeáveis reflete a interação entre uma trama dúctil anterior, de permeabilidade difusa, e uma trama rúptil posterior, com permeabilidade focada. Os resultados deste trabalho sugerem que a abordagem fractal para o estudo da gênese de depósitos minerais tem potencial concreto para gerar resultados relevantes, inclusive para a avaliação da favorabilidade mineral de áreas em exploração.

Palavras-chave: Metalogenia, Alteração hidrotermal, Depositos de oxido de Fe-Cu-Au - Carajas, Serra dos (PA), Fractais, Prospecção mineral.

ABSTRACT

Since the concept of fractal geometry was defined in the second half of the twentieth century, the importance of fractals for the description and understanding of geological features has gradually gained importance. More recent work has suggested that the spatial distribution of mineral deposits presents fractal geometry, which represents the complex interaction of geological processes necessary for the genesis of a mineralization. The manifestation of fractal geometry occurs through scale invariance, i.e. the property of a feature that conserves its geometrical characteristics independent of the spatial scale. This property is promising for the study of mineral deposits because it suggests the possibility that information about the geometry of a mineralization at one scale can be used to infer aspects of its geometry at other scales. Since mineralization geometry is a consequence of controls that acted during and after its formation, studies with a fractal approach have theoretical and practical applications. Considering the above, the present research investigated if the geometry of mineral deposits presents scale invariance, and if so, what information it permits to infer about the mineralization controls. For this investigation the study area chosen was the iron oxide-copper-gold (IOCG) Sossego deposit, in the Carajás Mineral Province (PA). IOCG deposits present strong structural control, which taken in conjunction with data availability at the regional, local and microscopic scales make the Sossego deposit area ideal for the proposed research. Thus, data already available in the literature were integrated with new structural measurements and new oriented thin sections of samples collected in the mine pits. Mineralization geometry was evaluated at three different scales: in the regional scale the spatial distribution of the known IOCG deposits was examined; in the local scale the geometry of the mineralized structures and orebodies at the Sossego deposit was examined; in the microscale the geometry of the spatial distribution and the shape of ore mineral grains were evaluated. The bulk of results indicate that the IOCG deposits of Carajás province, and in particular the Sossego deposit, present fractal geometry, conserving the orientation and anisotropy at the different scales. The orientation and anisotropy of the mineralization are geometric aspects that result directly from the control exerted by the underlying structural framework. As a consequence, the results indicate that the structural control generates the scale invariance due to its influence on rock permeability, an essential factor for the genesis of hydrothermal deposits. Permeability is defined at the microscale through foliation planes, microfractures and veinlets, which are directly related to structures of larger scales, such as shear zones, faults and veins, creating a consistent permeable network throughout the scales. In the case of Carajás, the geometry of these permeable areas reflects the interaction between an older ductile framework with diffuse permeability, and a posterior brittle network with focused permeability. The results of this work suggest that the fractal approach to the study of the genesis of mineral deposits has concrete potential to generate relevant results, including for the evaluation of the mineral favorability on exploration areas.

Keywords: Metallogenesis, Hydrothermal alteration, Iron oxide-copper-gold deposits - Carajas, Serra dos (PA), Fractals, Prospecting.

LISTA DE ILUSTRAÇÕES

CAPÍTULO 1 - REFERENCIAL TEÓRICO E METODOLÓGICO

CAPÍTULO 2 - ANÁLISE ESPACIAL DA DISTRIBUIÇÃO DE DEPÓSITOS MINERAIS: REVISÃO DE MÉTODOS E IMPLICAÇÕES PARA OS CONTROLES ESTRUTURAIS DAS MINERALIZAÇÕES *IRON OXIDE-COPPER-GOLD* EM CARAJÁS, BRASIL

CAPÍTULO 3 - CONTROLES ESTRUTURAIS EM MINERALIZAÇÕES EPISÓDICAS IOCG DA PROVÍNCIA MINERAL DE CARAJÁS: EVIDÊNCIAS DA ANÁLISE GEOMÉTRICA E DE PALEOTENSÃO DO DEPÓSITO DE SOSSEGO

LISTA DE TABELAS

CAPÍTULO 3 - CONTROLES ESTRUTURAIS EM MINERALIZAÇÕES EPISÓDICAS IOCG DA PROVÍNCIA MINERAL DE CARAJÁS: EVIDÊNCIAS DA ANÁLISE GEOMÉTRICA E DE PALEOTENSÃO DO DEPÓSITO DE SOSSEGO

SUMÁRIO

CAPÍTULO 1 REFERENCIAL TEÓRICO E METODOLÓGICO

1. Introdução e justificativa

Nas últimas décadas diversos autores propuseram a ideia de que a distribuição espacial de depósitos minerais é fractal (Mandelbrot 1983; Carlson 1991; Blenkinsop & Sanderson 1999; Carranza 2009). Em geral esta característica é interpretada como consequência de que vários dos processos metalogenéticos são fractais, incluindo a geometria da trama estrutural subjacente (Blenkinsop & Sanderson 1999; Hodkiewicz *et al.* 2005; Ord *et al.* 2016). Esta interpretação é suportada por diversos estudos que demonstram que diferentes tipos de estruturas geológicas apresentam geometria fractal (Kruhl 2013). Entre elas pode-se destacar: falhas (Jensen *et al.* 2011), fraturas, pares S-C (Hippertt 1999), veios (Johnston & McCaffrey 1996; Hippertt & Massucatto 1998) e fragmentos de brecha (Jébrak 1997), apenas para citar alguns exemplos.

A propriedade fractal de depósitos minerais implica na existência de padrões sistemáticos em sua geometria que se conservam independente da escala espacial, uma vez que a *invariância escalar* é uma propriedade fundamental de fractais (Turcotte & Huang 1995). Isto significa que apesar da complexidade inerente aos processos metalogenéticos, padrões geométricos consistentes devem ser encontrados nas diferentes escalas espaciais. Esta característica pode se tornar útil porque processos metalogenéticos atuam em diferentes escalas, e uma abordagem de estudo multiescalar pode fornecer um melhor entendimento de como depósitos minerais são formados (Turcotte 1989). Além disso, esta propriedade pode ser utilizada para melhorar a previsão da localização de depósitos, principalmente em *greenfields*. Se depósitos minerais são fractais e propriedades de seus controles podem ser descritas em lâminas e na escala local, então os controles de mineralização podem ser entendidos nestas escalas, e depois extrapolados para a escala regional.

Apesar da expressiva pesquisa na área, a relação entre a geometria dos depósitos nas escalas microscópica, local e regional nunca foi devidamente demonstrada. Pesquisas anteriores demonstraram relações geométricas entre mineralizações na escala regional e local, mas não simultaneamente na escala microscópica. Assim, para validar a noção de que a distribuição de determinados tipos de depósitos minerais é fractal, a presente pesquisa de mestrado investigou se as propriedades geométricas de depósitos minerais são consistentes

desde a escala microscópica até a regional. Para isso a pesquisa foi conduzida com um fluxo de trabalho marcado pela mudança de escala na coleta de informações e na interpretação dos resultados (Fig. 1).

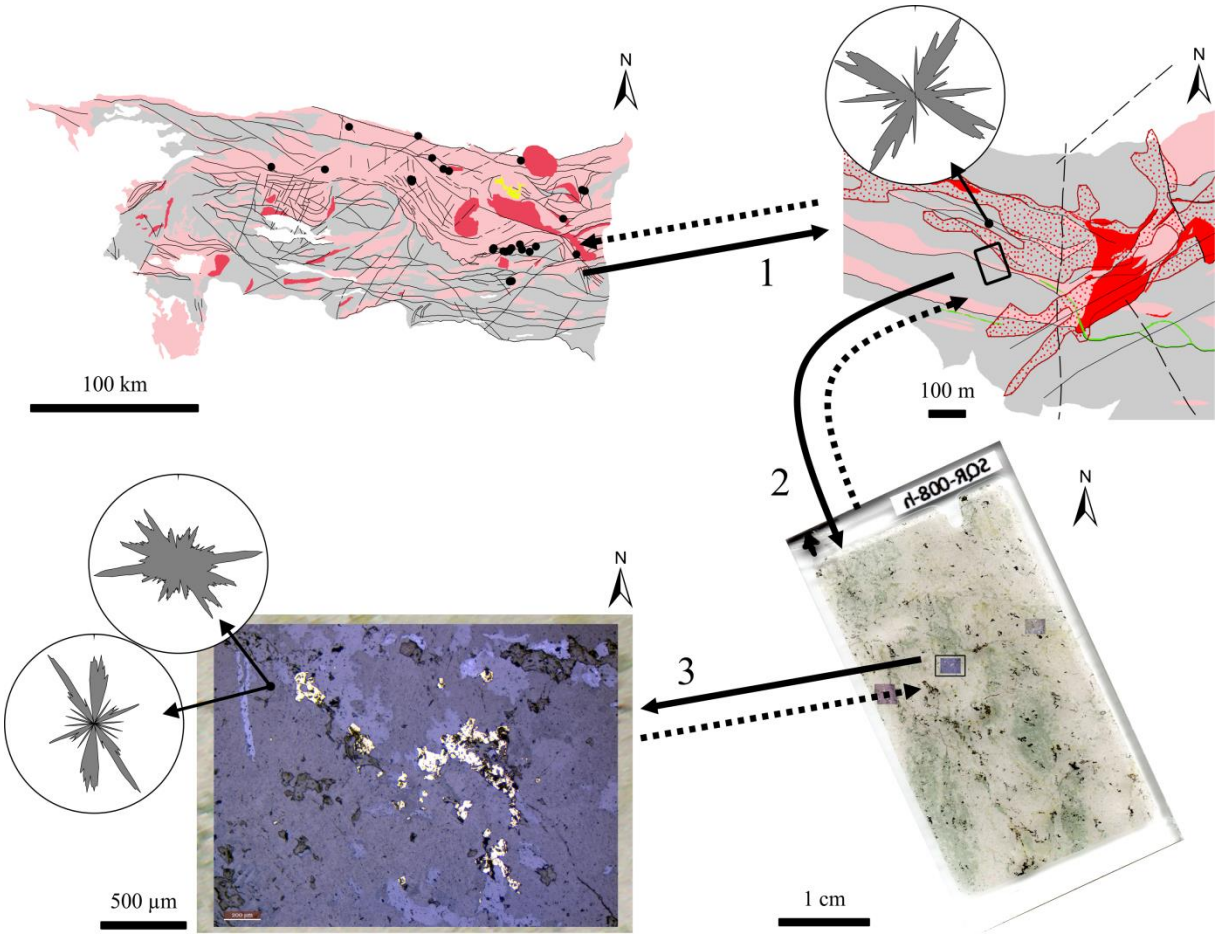

Fig. 1: Esquema do fluxo de trabalho adotado na pesquisa. Em sentido horário, a partir do canto superior esquerdo: geologia em escala regional; mapa de um afloramento da área mineralizada; lâmina orientada; detalhe de parte da lâmina ao microscópio. A pesquisa investigou se a geometria das estruturas que controlam a mineralização é consistente entre a escala regional (distribuição espacial de depósitos), escala local (mapas e dados estruturais) e escala microscópica (distribuição e forma dos minerais de minério). As setas indicadas por números representam a integração de dados e interpretações nas escalas regional, local e microscópica.

O fenômeno descrito acima deve ser particularmente observado em depósitos hidrotermais, tais como aqueles da tipologia *Iron Oxide-Copper-Gold* (IOCG). Isto porque uma das características mais marcantes de depósitos IOCG é que apesar das rochas encaixantes, fluidos mineralizantes e condições físico-químicas serem bastante variáveis, alguma forma de controle estrutural está sempre presente (Hitzman 2000; Williams *et al.* 2005). Assim como em outros tipos de depósitos minerais hidrotermais, a importância das estruturas para a formação de depósitos IOCG reside no fato de que estruturas são feições que aumentam expressivamente a permeabilidade do meio rochoso, viabilizando assim a passagem de quantidades suficientes de fluidos para a formação de acumulações econômicas de minerais (Sibson 1994; Oliver 1996; Sibson 1996; Cox *et al.* 2001). Uma vez que depósitos IOCG são controlados estruturalmente, é de se esperar que sua geometria também seja, ao menos em parte, fractal. Neste contexto, a Província Mineral de Carajás (Pará) mostra-se um laboratório ideal para investigar a geometria deste tipo de depósito, uma vez que possui a maior concentração de depósitos IOCG de alta tonelagem (> 100 Mt) do mundo (Xavier *et al.* 2012).

Dentro da Província Mineral de Carajás o depósito de Sossego apresenta destacada relevância, seja por sua importância econômica e abundância de ocorrências próximas, seja pela quantidade de estudos desenvolvidos na área já há mais de 10 anos (Morais & Alkmim 2005; Monteiro *et al.* 2008a; Monteiro *et al.* 2008b; Carvalho 2009; Domingos 2009; Moreto *et al.* 2015a; Moreto *et al.* 2015b). A origem destes depósitos no contexto da província é interpretada como resultado de uma evolução tectônica marcada por sucessivos eventos transcorrentes (Holdsworth & Pinheiro 2000; Pinheiro & Holdsworth 2000), eventualmente associados à magmatismo granítico e/ou máfico-ultramáfico (Vasquez *et al.* 2008). Esta evolução tectono-termal é que estaria potencialmente relacionada à origem e circulação dos fluidos responsáveis pelas mineralizações observadas (Moreto *et al.* 2015a).

Considerando o exposto acima, para testar a viabilidade da abordagem proposta foi escolhida a tipologia de depósito IOCG e a região da mina de Sossego. A investigação foi conduzida através da integração de novos dados estruturais de escala local, obtidos nas cavas da mina, e em novos dados mineralógicos de escala microscópica, obtidos em lâminas polidas orientadas. Através da análise de padrões de mineralização nas escalas microscópica, local e regional, buscou-se confirmar a natureza fractal do sistema mineral em estudo, e identificar características relevantes para o controle estrutural nas diferentes escalas. As informações obtidas através da abordagem proposta nesta pesquisa podem ser então usadas na elaboração

de modelos conceituais para os metalotectos regionais, o que é vital para reduzir a incerteza na previsão da favorabilidade mineral

2. Objetivos

Considerando o exposto em epígrafe, este mestrado investiga a hipótese de que controles estruturais regionais de mineralização podem ser inferidos a partir de padrões de escala microscópica de minerais de minério e a partir de estruturas de escala local, próximas de depósitos minerais. Adicionalmente, a pesquisa avalia se as inferências sobre os controles nas diferentes escalas podem ser úteis para a previsão da favorabilidade mineral regional.

3. Síntese dos materiais e métodos

A pesquisa de mestrado lidou com dados compilados de trabalhos anteriores, assim como novos dados coletados, em especial na escala microscópica. Para cada escala de trabalho foram adotados diferentes conjuntos de dados e de métodos para a investigação do controle estrutural da mineralização. A seguir, apresenta-se uma breve descrição dos materiais usados e dos métodos empregados para analisa-los.

3.1. Escala regional

Na escala regional, a mineralização é representada pela distribuição espacial dos depósitos IOCG da Província Mineral de Carajás. Assim, um dos primeiros passos da pesquisa foi a compilação dos dados regionais. Estes dados incluem mapas geológicos, mapas estruturais, localização das principais ocorrências e depósitos IOCG, hidrografia, infraestrutura e imagens de sensoriamento remoto. Em seguida, todos os dados regionais compilados foram organizados em um Sistema de Informação Geográfica (SIG).

A distribuição espacial dos depósitos IOCG na escala regional foi estudada através dos seguintes métodos: (i) análise fractal da distribuição de pontos (Carlson 1991; Blenkinsop & Sanderson 1999; Carranza 2009); (ii) análise Fry (Fry 1979; Vearncombe & Vearncombe 1999); (iii) análise fractal do padrão de estruturas regionais (Weinberg *et al.* 2004; Ford & Blenkinsop 2008); (iv) análise de associação espacial entre depósitos IOCG e conjuntos selecionados de estruturas (Berman 1977; Carranza 2009).

3.2. Escala local

Na escala local, a mineralização é representada pelos conjuntos de corpos mineralizados do depósito de Sossego (Monteiro *et al.* 2008a), a saber: Pista-Sequeirinho-Baiano e Sossego-Curral. A equipe da empresa Vale forneceu diversos dados da área da mina, os quais foram complementados por dados compilados da bibliografia. O conjunto de dados resultantes inclui: mapas geológico e estrutural, medidas estruturais de trabalhos anteriores, modelos de falhas baseados em dados de sondagem, mapa de alteração hidrotermal e imagens de satélite obtidas no *Google Earth*. Adicionalmente, através de pesquisa bibliográfica, foi possível compilar dados referentes à geocronologia (Moreto *et al.* 2015a; Moreto *et al.* 2015b), características petrográficas e de alteração hidrotermal (Monteiro *et al.* 2008a; Monteiro *et al.* 2008b; Carvalho 2009) e da geologia estrutural do depósito (Domingos 2009).

Foram realizados dois trabalhos de campo à mina de Sossego, com o objetivo de coletar dados de escala local. A primeira etapa foi realizada entre 17/08 e 21/08/2015, compreendendo o reconhecimento da geologia regional e local, além da coleta de amostras na cava da mina. A segunda etapa de campo, ocorrida entre 09/11 e 20/11/2015, foi direcionada à coleta de dados propriamente dita. Nesta etapa, foram visitados pontos selecionados dentro das cavas dos corpos de minério de Sequeirinho, Sossego e Pista. Para cada ponto visitado foram coletados dados descritivos básicos, incluindo fotografias, medidas estruturais e amostras orientadas de minério e de suas rochas encaixantes. Durante as duas etapas de campo foram visitados 51 pontos, com a coleta de 193 medidas estruturais e 32 amostras orientadas de rocha (Fig. 2).

De maneira a adquirir um conhecimento mais profundo dos controles estruturais na escala local, os dados estruturais disponíveis foram analisados da seguinte forma: (i) definição dos domínios estruturais com base nos mapas geológico e estrutural, e com o auxílio de diagramas *strike vs*. distância transversal (Marshak & Mitra 1988); (ii) análise geométrica básica, com uso de estereogramas, diagramas de roseta, histogramas de *rake*, etc. (Marshak & Mitra 1988; Davis & Reynolds 1996); (iii) análise de paleotensão (Delvaux & Sperner 2003).

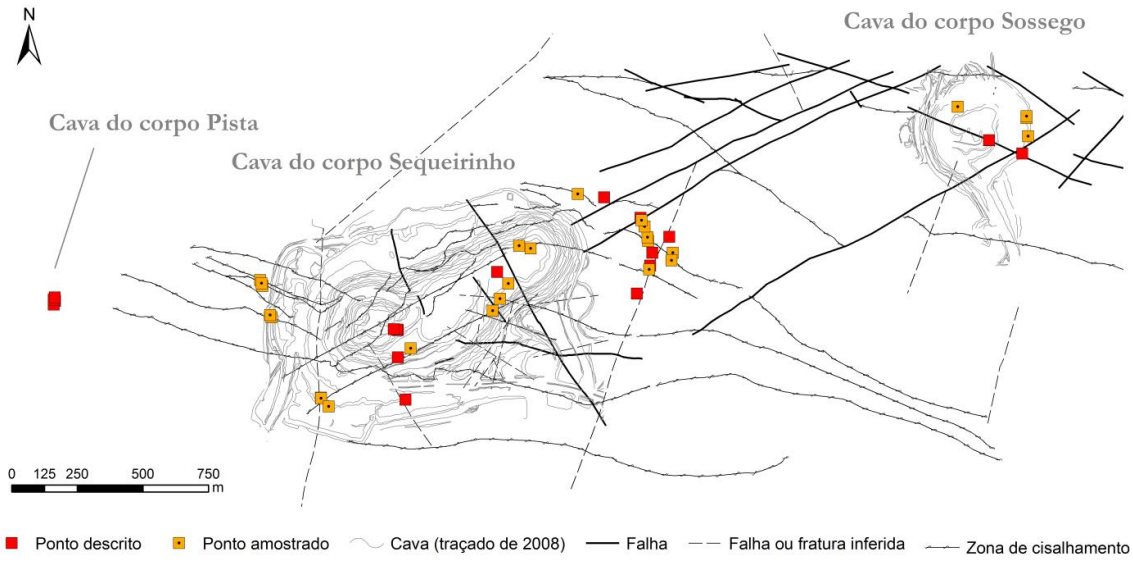

Fig. 2: Mapa simplificado ilustrando os pontos visitados durante os trabalhos de campo realizados na mina de Sossego. Mapa estrutural sobreposto para referência (compilado de mapa interno da companhia Vale; Domingos 2009; Moreto *et al.* 2015b).

3.3. Escala microscópica

Na escala microscópica a mineralização é representada pela ocorrência de minerais de minério (essencialmente calcopirita), dispersos pelas amostras de rocha coletadas nas paredes das cavas. Assim, as amostras foram preparadas para a extração de lâminas delgadas orientadas (Hansen 1990). Considerando que a ideia básica do projeto foi relacionar os dados microscópicos aos dados de escala local e regional, foi feita a opção de extrair as lâminas do plano horizontal das amostras, uma vez que os mapas de dados locais e regionais representam este plano. Desta forma, os dados adquiridos nas três escalas são diretamente comparáveis. Foram selecionadas 27 amostras extraídas das cavas da mina de Sossego e confeccionadas 27 lâminas delgadas polidas, das quais duas não apresentaram minerais de minério e, portanto, não foram submetidas a análises subsequentes.

A primeira etapa da coleta dos dados microscópicos foi o planejamento da rotina, com a definição do processo de aquisição de fotomicrografias, seu georreferenciamento em SIG, e a subsequente análise espacial da distribuição de minerais de minério. Simplificadamente, o processo de coleta de dados microscópicos consistiu em:

(i) Descrição macroscópica da amostra de mão;
(ii) Escaneamento da lâmina e georreferenciamento da imagem obtida em um SIG;
(iii) Inspeção da lâmina ao microscópio;
(iv) Seleção e coleta de fotomicrografias;
(v) Georreferenciamento das fotomicrografias obtidas (Fig. 3).

Para lâminas com estrutura homogênea, foram escolhidos três locais para obtenção das fotomicrografias, sempre que possível ao longo de perfil ortogonal à estruturação geral da lâmina (e.g. direção da foliação). Para amostras heterogêneas, foram escolhidas áreas consideradas representativas das diferentes formas de ocorrência de sulfetos na lâmina. Assim, ao final do processo, foram coletadas 72 fotomicrografias.

Para cada uma das 72 fotomicrografias obtidas durante a coleta de dados, distribuídas nas 25 lâminas analisadas, a geometria dos minerais de minério foi analisada segundo seis métodos (Fig. 3). Os métodos aplicados se utilizam da forma (área) ou da distribuição espacial dos grãos de sulfeto (centroides). A sequência de procedimentos adotados foi a seguinte:

(i) Conversão das fotomicrografias em imagens binárias e análise da forma de partículas no software Fiji (Heilbronner & Barrett 2014);
(ii) Georreferenciamento da imagem binária no software ArcMap™;
(iii) Análise dos centroides dos grãos: padrão de pontos (Kretz 1969; Jerram *et al.* 1996); análises fractais de *box-counting* e densidade radial (Raines 2008; Carranza 2009); análise Fry (Fry 1979; Vearncombe & Vearncombe 1999);
(iv) Análise da área dos grãos: *box-counting* (Wang *et al.* 2007) e análise de forma (*best-fit ellipses*, Heilbronner & Barrett 2014).

Ressalta-se que vários destes métodos são os mesmos usados para investigar a distribuição espacial dos depósitos IOCG em escala regional (Item 3.1). Esta consistência de métodos é importante para comparar os resultados das diferentes escalas.

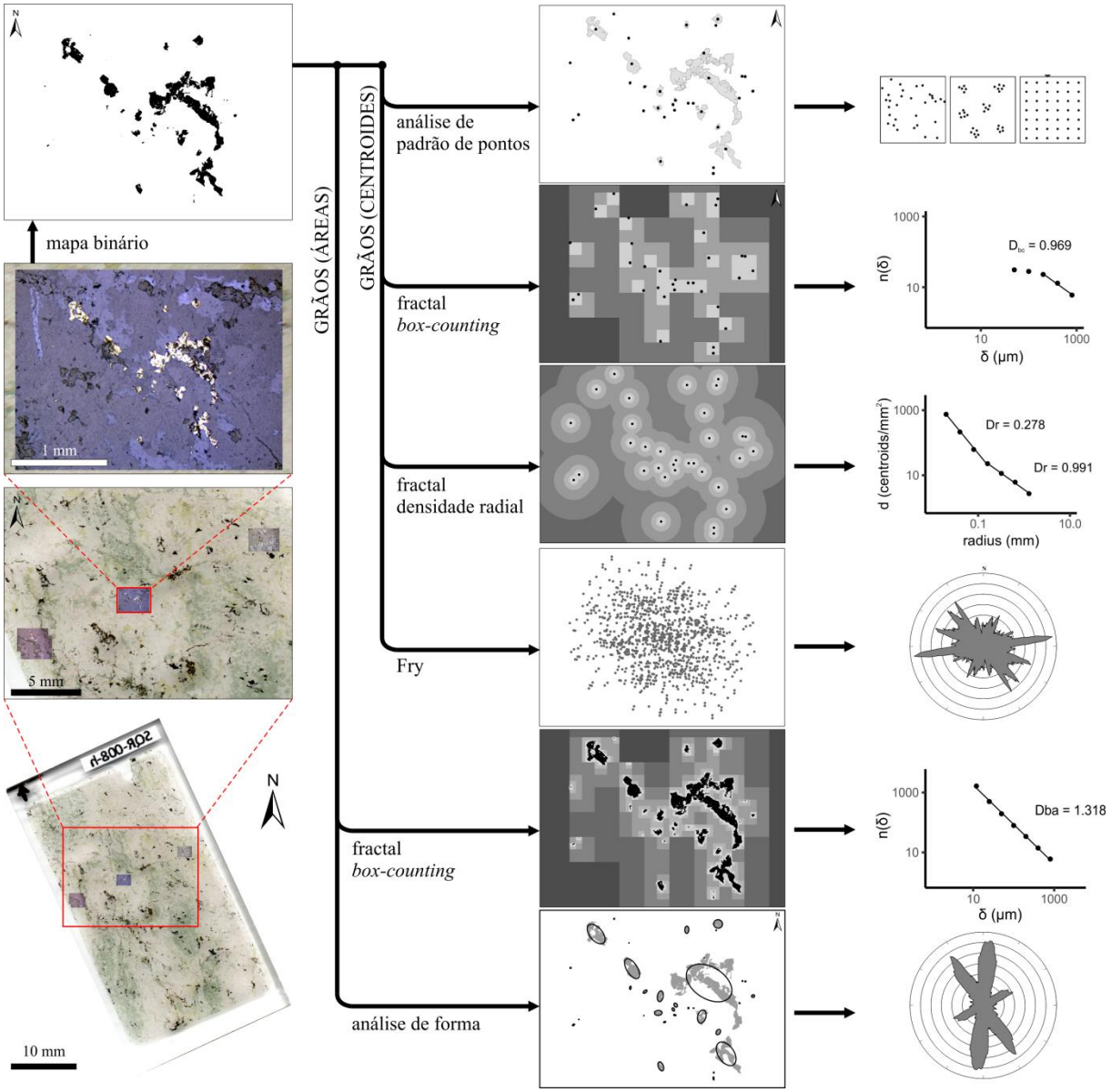

Fig. 3: Fluxo de trabalho para a coleta e análise de dados na escala microscópica. A imagem da lâmina foi georreferenciada em ambiente SIG, incluindo suas três fotomicrografias obtidas em luz refletida (canto inferior esquerdo). Durante esse processo, a escala e a orientação das imagens foram preservadas. A partir da fotomicrografia, obteve-se a imagem binária dos minerais de minério (canto superior esquerdo). A imagem binária foi então submetida a seis análises geométricas. O mesmo fluxo de trabalho foi seguido para cada uma das 72 fotomicrografias analisadas.

4. Contribuições e integração dos trabalhos

Conforme detalhado nas seções anteriores, esta pesquisa avaliou a geometria da mineralização IOCG nas escalas regional, local e microscópica, buscando entender seus controles estruturais, e principalmente verificando se a geometria da mineralização possui atributos coerentes nas diferentes escalas. Para conduzir esta avaliação, a pesquisa foi dividida em três partes principais, focadas nas escalas regional, local e microscópica. Considerando a variedade de dados e métodos descrita acima, cada uma das escalas estudadas foi separada em um capítulo próprio.

O CAPÍTULO 2 apresenta os resultados da escala regional, onde foi estudada a distribuição espacial dos depósitos IOCG na Província Mineral de Carajás. Neste trabalho é demonstrado que a distribuição espacial dos depósitos apresenta geometria fractal, que os padrões direcionais entre depósitos são consistentes com as estruturas regionais e que refletem algumas caraterísticas de seus controles estruturais, tais como direções preferenciais, densidade de estruturas, entre outras características.

O CAPÍTULO 3 apresenta os resultados da escala local. Nele foi investigado o controle estrutural do depósito de Sossego na tentativa de identificar quais estruturas foram determinantes para a mineralização, sendo gerado um modelo para descrever os eventos relacionados à sua formação. Enfoque especial foi dado para o fato de o depósito apresentar dois conjuntos de corpos mineralizados com características estruturais bem distintas entre si, e associados a intervalos temporais expressivamente separados (~780 Ma), apesar da grande proximidade espacial (< 1 km).

O CAPÍTULO 4 apresenta os resultados da escala microscópica. Nele foi demonstrado que a distribuição espacial dos minerais de minério na escala de lâmina não é aleatória, apresenta geometria fractal e possuiu padrões direcionais bem assinalados. É demonstrado ainda que a forma dos minerais de minério também é fractal, e possui direções de anisotropia bem marcadas. Estas características indicam que a mineralização nesta escala também mostra evidências de seu controle estrutural. Ainda neste capitulo é demonstrada a consistência da geometria da mineralização entre as escalas microscópica, local e regional, o principal objetivo de investigação da pesquisa.

Finalmente, no CAPÍTULO 5 são apresentadas as implicações dos resultados para a avaliação da favorabilidade mineral regional e as principais conclusões da pesquisa.

CAPÍTULO 2 ANÁLISE ESPACIAL DA DISTRIBUIÇÃO DE DEPÓSITOS MINERAIS: REVISÃO DE MÉTODOS E IMPLICAÇÕES PARA OS CONTROLES ESTRUTURAIS DAS MINERALIZAÇÕES *IRON OXIDE-COPPER-GOLD* EM CARAJÁS, BRASIL

Durante o desenvolvimento da pesquisa deste mestrado, o seguinte artigo foi preparado e publicado:

Paulo Miguel Haddad-Martim, Carlos Roberto de Souza Filho, Emmanuel John M. Carranza, *Spatial analysis of mineral deposit distribution: A review of methods and implications for structural controls on iron oxide-copper-gold mineralization in Carajás, Brazil*, ***Ore Geology Reviews***, Volume 81, Part 1, March 2017, Pages 230-244, ISSN 0169-1368, http://dx.doi.org/10.1016/j.oregeorev.2016.09.038.

Tipo: *Research paper*

Conceitos Qualis-CAPES do periódico: A2

Fator de impacto (2016): 3.095

Sítio para download direto:

http://www.sciencedirect.com/science/article/pii/S0169136816302049

O manuscrito como publicado é apresentado nas próximas páginas.

O material suplementar para este trabalho está disponível no APÊNDICE A.

Spatial analysis of mineral deposit distribution: A review of methods and implications for structural controls on iron oxide-copper-gold mineralization in Carajás, Brazil

Paulo Miguel Haddad-Martim [a], Carlos Roberto de Souza Filho [a], Emmanuel John M. Carranza [a,b]

[a] Institute of Geosciences, State University of Campinas (UNICAMP), Campinas, São Paulo, Brazil

[b] Economic Geology Research Centre (EGRU), James Cook University, Townsville, Queensland, Australia

Mineral deposits are formed by interaction of various geological processes and conditioned by controls that favor their formation and preservation. The understanding of mineralization controls is critical for mineral exploration because it allows focusing exploration on regions where these controls are concentrated. The analysis of the spatial distribution of mineral deposits, particularly on a regional scale, can provide information relevant to the understanding of regional-scale processes involved during their formation. Here we present a review of Fry and fractal methods for spatial analysis of mineral deposit distribution and an application using the iron oxide-copper-gold (IOCG) deposits of the Carajás Mineral Province (Brazil). Results show that different IOCG mineralization structural controls acted in scales of <10–15 km, 15 to 40 km, and >40 km. The IOCG deposits cluster at scales of <40 km, whereas different clusters of IOCG deposits form WNW-ESE alignments at scales larger than 40 km. Structures oriented to WNW-ESE, E-W and NW-SE, with secondary trends to ENE-WSW and NNE-SSW, host the main IOCG deposits in Carajás. Additionally, Carajás IOCG deposits are located in areas with intermediate to high fractal dimensions, reflecting tracts with intermediate to high complexity of structural patterns. Information yielded in this work provides relevant criteria for further exploration for IOCG deposits in the region, including an indication of a possible new WNW-ESE central trend, apart from the northern and southern copper belts in the Carajás Mineral Province.

Keywords: Fractal analysis; Fry analysis; Spatial analysis; IOCG deposit; Mineralization control; Mineral prospecting

1. Introduction

Predictive mineral potential modeling typically uses a combination of: (i) knowledge of geological processes leading to the formation of mineral deposits, (ii) empirical evidence of spatial association between mineral deposits and certain geological features representing those geological processes (Carranza and Hale, 2002a, 2002b; Carranza et al., 2008; Lisitsin, 2015). In an area with a relatively large number of known mineral deposits, which are invariably represented as *points* on broad-scale maps, their spatial distribution can provide critical information on mineralization processes that operated at a range of scales, especially in cases where these processes have only cryptic expressions in traditional geological datasets (Carranza, 2009; Zuo et al., 2009; Lisitsin, 2015).

Point pattern analysis (Diggle, 1983; Boots and Getis, 1988), Fry (Fry, 1979) and fractal (Mandelbrot, 1983) analyses are well developed and have been used in a variety of geological research, including the study of distribution of mineral deposits and their structural controls (Carlson, 1991; Ford and Blenkinsop, 2008a; Raines, 2008; Carranza, 2009; Agterberg, 2013). As each method only characterizes a particular aspect of a point pattern, reasonable inferences about the spatial distribution of deposits can be made only after the integration of results provided by different methods (Carranza, 2008, 2009; Lisitsin, 2015). This paper reviews the theoretical aspects of the Fry and fractal analyses and their applications to the study of the spatial distribution of mineral deposits. Furthermore, to illustrate their potential in comprehensive exploratory spatial analysis of deposits distribution, the methods are used here in combination to investigate the regional-scale spatial pattern of iron oxide-copper-gold (IOCG) deposits in the Carajás Mineral Province (CMP), southeast Amazon Craton, Brazil. The results are used in conjunction with existing knowledge of the structural geology of the CMP to infer the structural controls of IOCG mineralization, complementing resource assessment and exploration targeting in the region.

2. Fry analysis

Fry analysis is a graphical form of autocorrelation analysis developed by Fry (1979) to measure rock deformation using the relative positions of geological markers in thin sections. In this analysis, geological objects (such as porphyroblasts, ooids or mineral grains) are represented as points and their pre-deformation distribution is assumed to be largely non-random, because their existence is due to non-random geological events (Hanna and Fry, 1979). Section 1 of the Supplementary material contains a brief review of the main aspects of

randomness in point patterns, since these aspects are important to help understand the circumstances in which the use of Fry analysis is appropriate.

Fry analysis is performed through the construction of an autocorrelation diagram called Fry plot (Fig. 1). The diagram can be constructed manually or computationally, with the following procedure (Fry, 1979): (i) one of the points in the original distribution is placed at the center of the diagram, preserving the distances and orientation of all other points; (ii) the positions of every point of the original distribution are marked in the new diagram (i.e., "Fry points"); (iii) a second point in the original pattern is placed at the diagram center, and the positions of the remaining points are registered. This procedure is repeated until every point in the original distribution is used as the center of the diagram (Fig. 1).

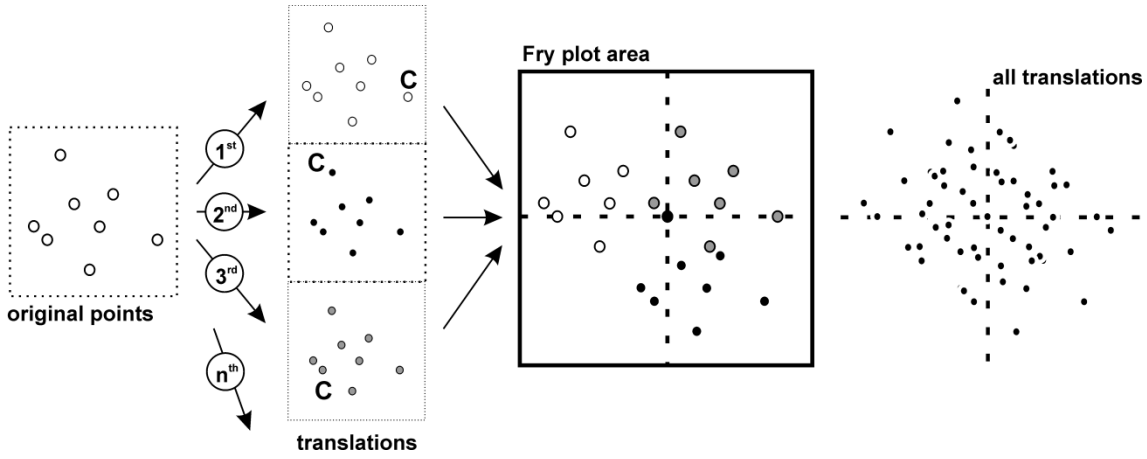

Fig. 1: Schematic procedure to construct a Fry plot. In the three translations shown, 'C' denotes the point used as center. When all original points are used as centers, all translations and the diagram are complete. For *n* original points there are n^2–*n* Fry points.

For Fry analysis to be efficient, the objects of interest must (Fry, 1979): (i) be well dispersed, so they can be represented as points in a homogeneously deformed matrix; (ii) allow for numerically relevant sampling (dozens to hundreds of objects); and (iii) have a relatively regular or clustered pre-strain distribution. The third condition is critical because the Fry diagram of a set of objects with random distribution does not present relevant results (Fig. 2a–d). Note that the diagrams in Fig. 2b and d are nearly indistinguishable.

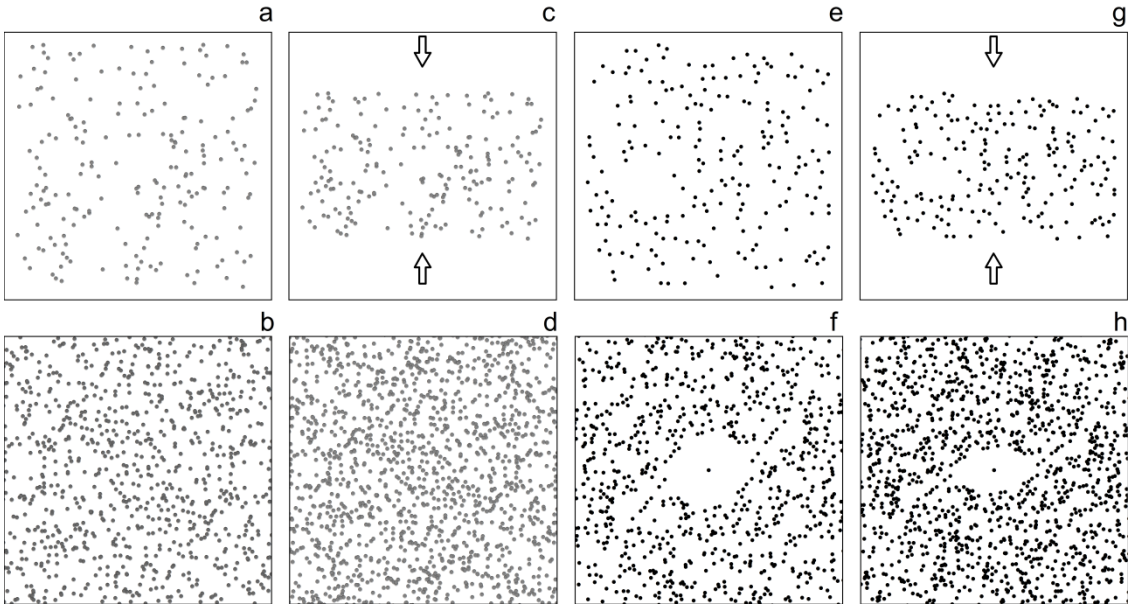

Fig. 2: Examples of Fry diagrams: (a) points with random distribution; (b) Fry diagram for points in (a); (c) distribution of points in (a) after compression indicated by arrows; (d) Fry diagram for points in (c); (e) points with an uniform distribution pattern; (f) Fry diagram for points in (e); (g) distribution of points in (e) after compression indicated by arrows; (h) Fry diagram for points in (g).

Fry analysis is able to highlight the existence of deformation that otherwise would not be evident by observing the patterns individually (Fig. 2e–h). Note in Fig. 2f the existence of a circular girdle at the center of the diagram, indicating the absence of deformation. In contrast, in Fig. 2h the ellipse at the center of the diagram indicates deformation. The ellipse shown by Fry analysis (Fig. 2h) represents how points – which were initially neighbors – shifted relative to each other, so that the girdle that appears in the center of the diagram can be used as an approximation to the measurement of the deformation ellipse (Fry, 1979).

Twenty years after the development of Fry analysis as a tool for the study of rock deformation, it has been successfully applied to study the spatial distribution of various types of mineral deposits, both at regional and local scales (Vearncombe and Vearncombe, 1999; Stubley, 2004; de Andrada and Carranza, 2005; Blenkinsop and Kadzviti, 2006; Kreuzer et al., 2007; Carranza, 2008, 2009). When applied to the investigation of mineral deposits, Fry analysis provides insight into directional controls on mineralization by using each and every spatial relationship between deposits (Vearncombe and Vearncombe, 1999). At regional scales, Fry analysis highlights patterns of direction and spacing associated with structures that control mineralization. At local scales, it can be applied to determine directions of orebodies

based on the distribution of positive drill holes intersections – thus representing an alternative to directional variography (Vearncombe and Vearncombe, 1999). In either case, the investigation can be detailed by analyzing point subsets defined by proximity or other relevant property, such as deposit reserves or the grade of a borehole segment. This alternative use for Fry analysis has been applied by several authors to study the spatial distributions of mineral deposits of Au, Cu, Pb and other elements (Stubley, 2004; Kreuzer et al., 2007; Austin and Blenkinsop, 2009; Carranza, 2009; Carranza and Sadeghi, 2014), even in three-dimensions (Blenkinsop and Kadzviti, 2006). The typical results of these studies are the: (i) identification of subtle preferential orientations in the distribution of mineral deposits, which are hardly perceived from their original map locations (Vearncombe and Vearncombe, 1999; Lisitsin, 2015); (ii) recognition of structural trends of mineral occurrences at different spatial scales (Austin and Blenkinsop, 2009; Carranza, 2008, 2009); or (iii) recognition of preferred corridors for mineralization (Vearncombe and Vearncombe, 2002; Carranza and Sadeghi, 2010). These results are then integrated and employed to interpret structural controls on mineralization.

3. Fractal analysis

Fractals comprise a unique geometrical approach that can be used to study the spatial distribution of mineral deposits (Carlson, 1991), and its concept has had a major impact in several areas of geology (Turcotte, 1989, 1997; Turcotte and Huang, 1995; Kruhl, 2013). A fractal "*is a feature whose Hausdorff-Besicovitch dimension is greater than its topological dimension*" (Mandelbrot, 1983). The Hausdorff-Besicovitch dimension – also known as fractal dimension – is the main parameter used to characterize natural fractals, as discussed below. For a brief review of some fundamental concepts that lead to the definition of the fractal dimension, the reader is referred to Section 2 of the Supplementary material.

3.1. Natural fractals and their properties

Fractals are entities that have a self-similar or self-affine geometry at different spatial scales, and various geological features present such properties (Turcotte, 1989; Xu et al., 1993; Goryainov et al., 1997). This means that geological features have similar geometry even when observed in ranges of scales separated by several orders of magnitude (Fig. 3) (Hodkiewicz et al., 2005).

The importance of fractal geometry is that it provides definitions and tools that allow to quantify complex geometries - a difficult or even impossible task with the use of Euclidean geometry (Kruhl, 2013). However, fractal geometry applied to the study of natural features has limitations that must be considered, including the fact that some geological features are simply not fractals (Walsh and Watterson, 1993). Additionally, unlike what is observed in theoretical fractal curves (Fig. 3, Supplementary material), natural fractal dimensions are not constant, although from a mathematical point of view fractals have to be self-similar in an infinite range of scales. For certain geological features, the self-similarity is generally restricted between one and four orders of magnitude, even though this range may be greater (Kruhl, 2013). Additionally, in natural fractals self-similarity or self-affinity is usually statistical, since the geometry of the pattern parts is not identical to that of the whole pattern, but similar. For this, natural fractals are also called statistical fractals (Xu et al., 1993).

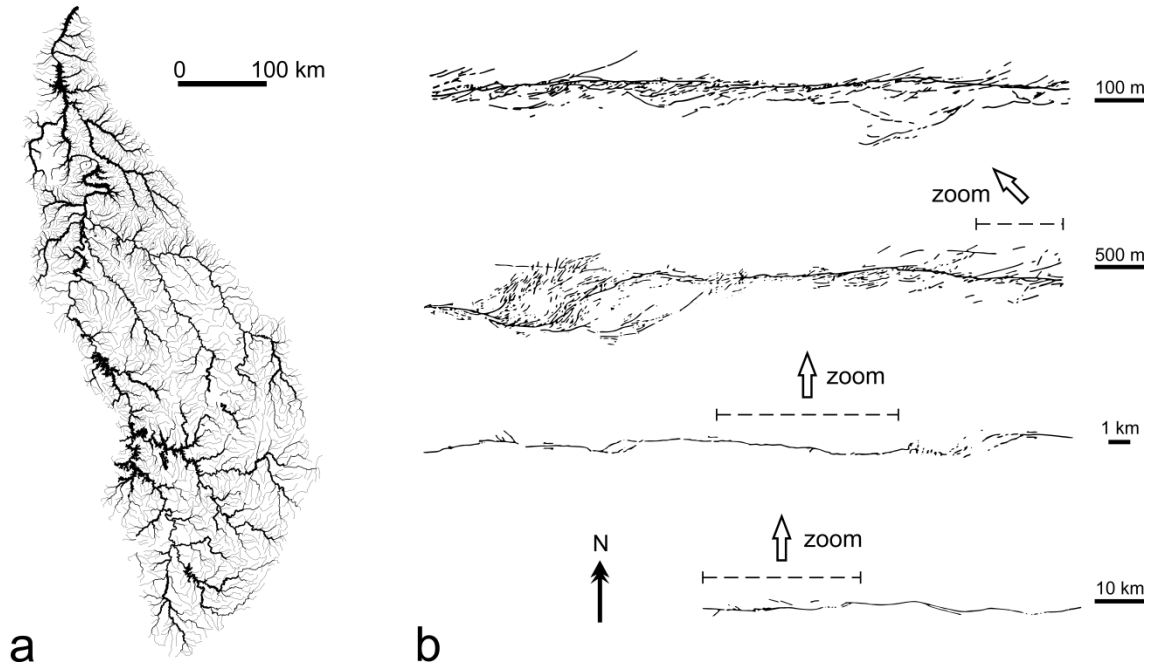

Fig. 3: Examples of geological features that have fractal geometries: (a) drainage pattern; (b) faults due to an earthquake in Iran, mapped in four different scales (adapted from Scholz, 1995). In both examples, the self-similarity is in the repeating geometric patterns at various scales.

It is also noteworthy that the objective of fractal geometry application to geological features is not to find an exact mathematical model to describe them. Instead, the main aim is to detect systematic patterns and their correlation to geologic processes. Rigorous mathematical precision is important, but not indispensable (Kruhl, 2013). In addition, variations in relation to fractal mathematical models should not be seen as defects, but as characteristics that provide information about the natural processes involved.

The main differences between natural and mathematical fractals are the fact that fractal dimensions of natural patterns vary over different (Kruhl, 2013): (i) scales (scaling); (ii) areas (heterogeneity); and (iii) directions (anisotropy). Self-similarity scaling leads to the recognition of multifractal patterns. Together with heterogeneity and anisotropy, self-similarity scaling reflects the fact that geological features usually result from the interaction among various materials and processes that are not constant across all orders of magnitude. The variation of fractal dimension in different scales, areas or directions does not preclude the establishment of a comprehensive fractal dimension to a feature, as commonly reported in the literature. In fact, each of these facets of fractal dimension represents a different aspect of the geometric complexity of the studied feature (Kruhl, 2013). However, it is important to note that the traditional methods for estimating the fractal dimension of natural patterns are designed to determine the overall dimension of the pattern. Changes need to be made in order to use them to quantify heterogeneity and anisotropy.

3.2. Study methods of fractal geometry

There are various methods for estimating the fractal dimension of a geological feature. Each of them evaluates an aspect of its geometric complexity, so that their results do not match exactly. For this reason, it is common that the fractal dimension takes the name of the method used to obtain it, such as (Kruhl, 2013): box-counting, radial-density, divider (also known as ruler - or Mandelbrot method), perimeter-area and number-area methods, just to name a few. To further increase the abundance of methods, many have been modified to assess the heterogeneity and anisotropy of the fractal dimension of a pattern (Fig. 4).

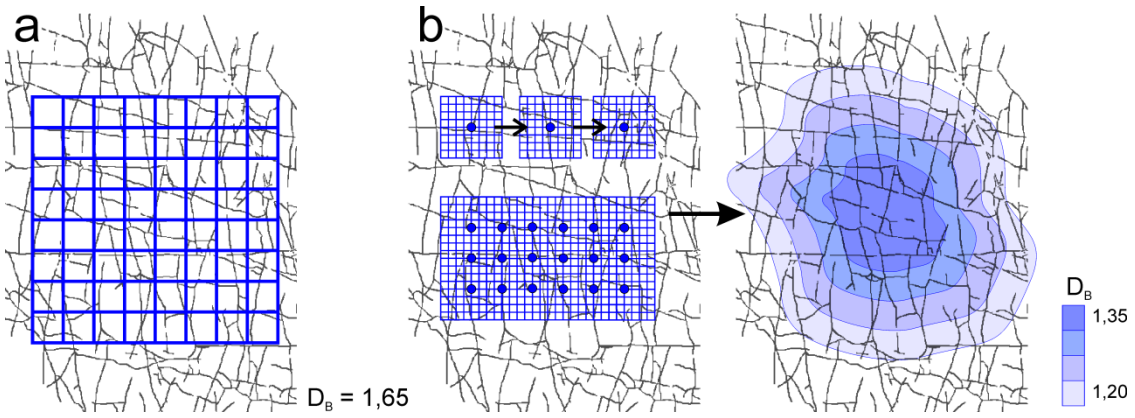

Fig. 4: Examples of methods for calculating the box-counting fractal dimension (D_B) of a fracture pattern: (a) cell count for the entire pattern, as described in Fig. 3 of the supplementary material; (b) moving box-counting method, adapted to measure heterogeneity of D_B. The single fractal dimension obtained in (a) represents the complexity of the pattern as a whole. In (b), values obtained for every box are interpolated to provide a map of D_B variation in space. Values for D_B are illustrative.

The three most commonly applied methods in the study of mineral deposits are presented below (Carlson, 1991; Weinberg et al., 2004; Ford and Blenkinsop, 2008a; Carranza, 2008, 2009): box-counting, moving box-counting and radial-density methods.

3.2.1. Box-counting fractal dimension (D_B)

The box-counting method is the most used in geological applications (Pruess, 1995), and can be applied in patterns of points, lines or areas (Fig. 3 in the Supplementary material and Fig. 4a). In this method, a grid with square cells with size δ is placed over the pattern under analysis, and the number of cells n that overlap the pattern is counted. The process is repeated for progressively smaller values of δ, and the results are plotted on a log-log graph of $n(\delta) \times \delta$. The fractal dimension is given by the slope of this graph (Fig. 3, Supplementary material).

It is important to note that to avoid spurious results, the size and layout of the chosen grid must take into account the maximum and minimum resolutions of the studied features (Pruess, 1995), as well as the shape and orientation of the study area borders (Walsh and Watterson, 1993). Additionally, it is recommended that the grids of different values of δ cover exactly the same area (Agterberg, 2013).

3.2.2. Moving box-counting fractal dimension (D_B)

This method has been applied to study the heterogeneity of the fractal dimension of a geological pattern (Hodkiewicz et al., 2005; Ford and Blenkinsop, 2008a; Zhao et al., 2011; Kruhl, 2013). The same procedure described above is applied in sectors of the pattern by a reduced grid, and the value of the fractal dimension obtained is assigned to the grid center. The grid is then moved, maintaining some level of overlap with the previous iterations, until the entire pattern area is covered. The dimension values found are then interpolated, providing a fractal dimension variation map (Fig. 4b). For this application, the degree of pattern detail (e.g., the base maps scales) must be uniform across the study area (Hodkiewicz et al., 2005).

3.2.3. Radial-density fractal dimension (D_R)

In the specific case of fractals composed of points, also called fractal dusts, Mandelbrot (1983) demonstrated the existence of a law of radial density according to Eq. (1):

$$d = C \times r^{D-2} \quad (1)$$

where d is the point density in a given location (the number of points per unit area), C is a constant of proportionality, r is the distance from a known point to the center of a cluster of points and D is the fractal dimension. If a given pattern behaves like a fractal dust, then the density of points around a reference point should decrease with distance, following this law (Carlson, 1991; Carranza, 2008, 2009).

In practice, circles of a given radius r are centered on all points of the pattern, and then the deposit density is calculated as the total number of deposits divided by the total area of circles, excluding overlaps. The procedure is repeated for increasingly larger radii. The relationship between $\log D \times \log r$ is defined by a best-fit line through the values and its slope equals $D_R - 2$ as in Eq. (1) (Agterberg, 2013).

3.3. Fractal geometry application to the study of mineral deposits

Considered on a regional scale, the spatial distribution of mineral deposits is an irregular cluster of points. Several mathematical models have been proposed to represent this type of point distribution, including a fractal dust model (Mandelbrot, 1983). A fractal dust is a point distribution where systematic clusters are found at different scales of existence, thus constituting an example of self-similarity.

The first work to deeply explore this possibility was conducted by Carlson (1991), who applied the box-counting and the radial-density methods to characterize the distribution of mineral deposits in the Basin and Range Province, and concluded that their distribution is fractal. A visual comparison of different types of point distributions reveals that the fractal dust is the most similar model to that of mineral deposits distribution (Fig. 5).

The pioneering work of Carlson (1991) motivated other researchers to investigate the spatial distribution of mineral deposits through fractal geometry, and, in general, later studies support his original conclusions (Blenkinsop and Sanderson, 1999; Raines, 2008; Carranza, 2009; Agterberg, 2013). In fact, fractal dimensions observed by different authors suggest that mineral deposits behave like fractals at scales varying from 1 to 1000 km. Moreover, D_B varies depending on scale, suggesting the occurrence of bifractal patterns (Raines, 2008) or even trifractal patterns (Carranza and Sadeghi, 2010, 2014), although some authors attribute this variation to sampling bias such as the roll-off effect (Blenkinsop and Sanderson, 1999; Ford and Blenkinsop, 2008a; Agterberg, 2013).

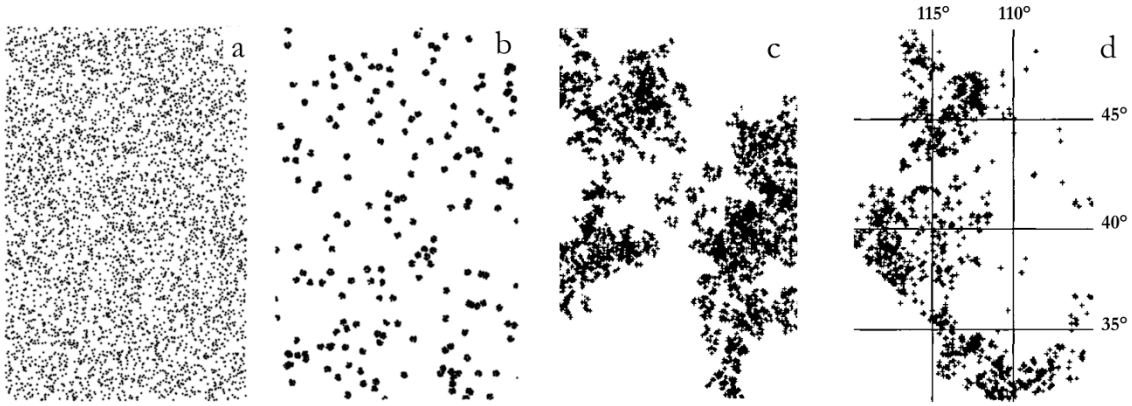

Fig. 5: Examples of spatial distribution of points used to model the distribution of mineral deposits (slightly modified from Carlson, 1991). The number of points in each image is similar. (a) random distribution. (b) Neyman-Scott distribution, in which the positions of the centers of clusters follow a standard random distribution. (c) fractal dust simulation using a seven-level recursive Poisson distribution. (d) distribution of 4775 metal deposits in the Basin and Range Province, USA.

What could be accounted for by a fractal distribution of mineral deposits? The existence of a cluster of deposits in a given scale implies the occurrence of non-random processes responsible for their concentration (Carlson, 1991). The fact that these clusters

occur in a wide range of spatial scales suggests that processes involved in mineralization are fractal, and in fact most of the processes considered important to the genesis or exposure of mineral deposits are fractals, such as hydrothermal systems, fracture systems and veins (Johnston and McCaffrey, 1996; Gumiel et al., 2010), plutonism (McCaffrey and Petford, 1997), the irregularity of rock exposures on the surface (Carlson, 1991; Xu et al., 1993), among others.

Considering the relationship between the fractal pattern in the distribution of mineral deposits to the fractal nature of their controls, several authors have used variations in the D_B and D_R dimensions to suggest variations in mineralization controls (Carranza, 2009). Others have suggested that D_B and D_R of mineral deposit distributions are useful parameters for estimating the degree of economic exploration of mineral provinces (Carlson, 1991; Blenkinsop and Sanderson, 1999), or even provide an estimate of the number of undiscovered deposits (Raines, 2008; Carranza et al., 2009; Carranza and Sadeghi, 2010; Carranza, 2011a). In addition, fractal dimension analysis can be used to quantify complex patterns of structures and lithologic contacts, which are conduits for fluid flow during hydrothermal formation of mineral deposits (Hodkiewicz et al., 2005). Considering this, the measurement of the heterogeneity of fractal dimension in mineralized regions may be related to variations in the density of faults and contacts (Weinberg et al., 2004; Hodkiewicz et al., 2005; Zhao et al., 2011), or their intersections and inflections (Ford and Blenkinsop, 2008a). The complexity of these geological features in a region, measured by fractal dimensions, may then be correlated to the density of mineral deposits, correlation which may be positive or not. If a positive correlation is confirmed such geological features may be assumed as good indicators for mineral prospectivity modeling (Ford and Blenkinsop, 2008a; Zhao et al., 2011; Herbert et al., 2014).

Other applications of fractal geometry related to mineral deposits include: separation of geochemical anomalies and background (Carranza, 2011b; Zuo et al., 2012; He et al., 2013; Luz et al., 2014), the estimation of mineral reserves based on the relationship between grade and ore volumes (Turcotte and Huang, 1995; Raines, 2008), and the analysis of frequency-size distributions (Agterberg, 2013). These analyses are not detailed here, since they are beyond the scope of this review.

4. Case study: IOCG deposits of Carajás, Brazil

The Carajás Tectonic Domain (Santos, 2003), formerly known as the Itacaiúnas Shear Belt, is located in the northern region of Brazil, more specifically in southeast Pará state. This domain is part of the Amazon craton, which was stabilized during the Archean. It is composed of two segments: (1) a Transition Subdomain, to the south, which possibly acts as basement to (2) the Cover Assemblage, to the north (Pinheiro, 1997; Pinheiro and Holdsworth, 1997a). The Transition Subdomain is composed mostly of Archean units such as gneisses from the Xingu Complex and granulites from the Pium Complex, whereas the Cover Assemblage is composed of two metamorphosed volcano-sedimentary units, the Rio Novo Group and the Itacaiúnas Supergroup, and a sedimentary unit, the Águas Claras Formation (Nogueira et al., 1995; Vasquez et al., 2008). The Transition Subdomain and the volcano-sedimentary units were intruded by layered mafic-ultramafic rocks (e.g., Luanga) and Neoarchean granites (*ca.* 2.7 Ga). All units were intruded by Paleoproterozoic anorogenic granites (*ca.* 1.88 Ga) (e.g., Central Granite) (Fig. 6).

Several tectonic models have been proposed for the Carajás region (Araújo and Maia, 1991; Pinheiro, 1997; Veneziani et al., 2004; Rosière et al., 2006; Tavares, 2015). Initially, the dominant structure was interpreted by Beisiegel et al. (1973) as a synclinorium with a WNW-ESE axis. This interpretation was later challenged by Araújo and Maia (1991), who reinterpreted this as a positive flower structure developed by transpression affecting moderately to steeply dipping, E-W and WNW-ESE-trending shear zones, represented by the Cinzento and Carajás strike-slip systems. Similarly, the tectonic model presented by Pinheiro (1997) is based on a history in which subsequent brittle-ductile and brittle tectonic reactivation events were geometrically controlled by pre-existing Archaean ductile fabrics developed initially in the basement. This model proposed an alternating series of transpressional and transtensional reactivations in four main stages (Domingos, 2009).

The Carajás Tectonic Domain comprises one of the most important mineral provinces in the world, encompassing several world-class mineral deposits including iron, manganese, nickel, copper, gold, platinum group elements and others (e.g., Monteiro et al., 2014). In order to demonstrate the relevance of Fry and fractal analyses to understand structural controls on mineralization based on the spatial distribution of mineral deposits, we applied these methods, on a regional scale, to the iron oxide-copper-gold (IOCG) deposits of Carajás, in order to highlight meaningful patterns that may provide further insights to their

structural controls. We chose the IOCG deposits in this domain because it is a class of deposits known for its ubiquitous structural control (Hitzman, 2000; Williams et al., 2005), and because Carajás contains the largest known concentration of large-tonnage (>100 Mt) IOCG deposits (Xavier et al., 2012). Considering their geographic positions, the Carajás IOCG deposits have been grouped in two clusters, the southern and northern copper belts (Moreto et al., 2015a). The southern copper belt encompasses IOCG deposits distributed mostly around the Sossego deposit, while the northern copper belt encompasses deposits with latitudes in the range between that of Bahia-Alemão and Salobo deposits (Fig. 6).

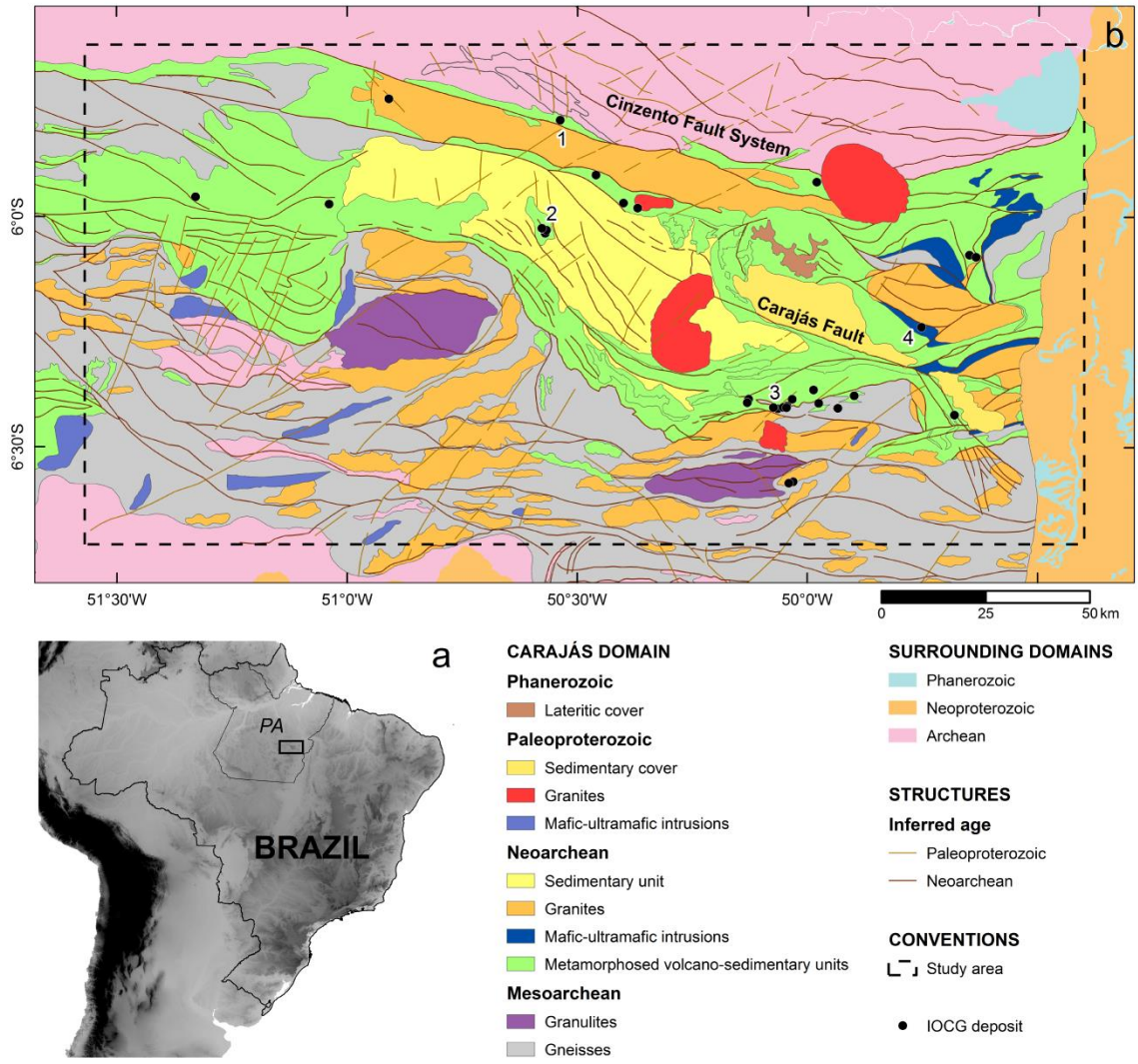

Fig. 6: (a) Location of the study area, in southeast Pará State (PA); (b) simplified geological-structural map of the study area (modified from Vasquez and Rosa-Costa, 2008). Structures and deposits mentioned in the text are indicated (1: Salobo; 2: Igarapé Bahia-Alemão; 3: Sossego; 4: Antas North).

The locations of the IOCG deposits were obtained from data made available by the Brazilian Geological Survey – CPRM (Vasquez and Rosa-Costa, 2008), which were revised to include new deposits under current development (e.g., Antas North). For deposits where different orebodies can be individualized, such orebodies were treated as separate objects to ensure that we have sufficient number of points for analysis. Therefore, deposit locations were adjusted, where appropriate, based on data available from the literature.

Geological and structural maps were compiled from geological databases and literature available for the region. The geological and structural maps were overlapped, compared and integrated in a GIS platform. The stratigraphic units and regional tectonic outline were extracted from the compilation provided in Vasquez and Rosa-Costa (2008), which is the only public map available that completely covers the study area. This map was overlapped by more detailed maps at the 1:250.000 scale (Araújo and Maia, 1991; Oliveira et al., 1994; Macambira and Vale, 1997), which were used to refine contact outlines and structures. Comparison between these two sets of maps indicated that they were satisfactorily compatible. More recently, the Brazilian Geological Survey produced new 1:100.000-scale maps in the Carajás region supported by the interpretation of high-resolution geophysical data (Tavares and Silva, 2013; Justo and Lopes, 2014; Tavares, 2014). The new available map sheets, however, only cover a small portion of the study area. Therefore, they were only used to adjust some of the contacts and structures within restricted areas. At each level of data integration, care was taken to include only those structures from more detailed maps that were compatible with structures depicted in coarse scale maps. In doing so, we avoided creating heterogeneities that could affect our analysis due to scale issues (Ford and McCuaig, 2010).

Fry analysis was performed using DotProc shareware. The box-counting and radial-density methods were implemented in ArcGIS® (Raines, 2008; Carranza, 2008, 2009). Rose diagrams were made using the Windows® version of MARD (Munro and Blenkinsop, 2012), and exploratory spatial association analysis was performed in the ILWIS software (http://www.ilwis.org/).

4.1. Fractal analysis applied to Carajás

Box-counting analysis was performed by covering the point pattern of 30 IOCG deposits/orebodies in Carajás (Fig. 6) by two adjacent boxes, each with 120 km side (δ). Then, the box size was halved seven times, resulting in a final box with 1.875 km side. Using the same grid area, a secondary sampling was performed using a grid with an initial box with

a side of 40 km and seven iterations, resulting in a final box side of 675 m. Radial-density analysis was performed by defining an initial circle with 25 m radius around each deposit/orebody, and then doubling the radius until the same study area used in the box-counting analysis was completely covered by the final circles, resulting in a maximum circle radius of 102.4 km (Fig. 7).

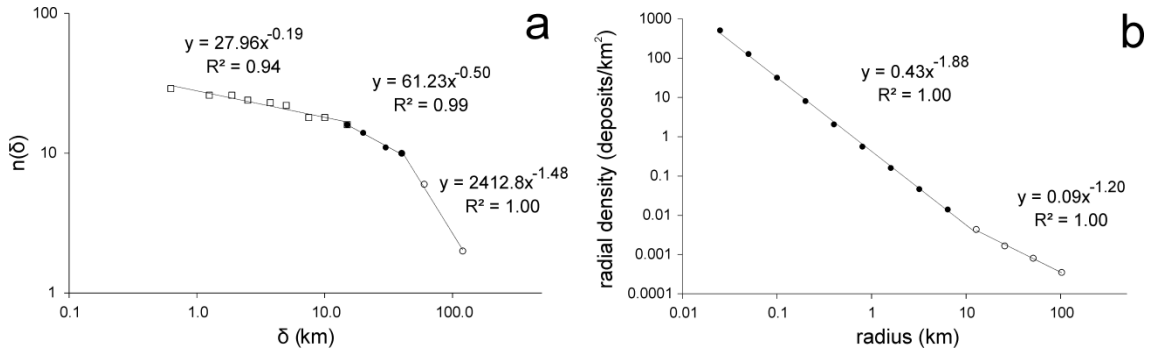

Fig. 7: Results for fractal analyses of IOCG deposits/orebodies in Carajás: (a) box-counting fractal dimensions; (b) radial-density fractal dimensions.

The Carajás IOCG deposits/orebodies exhibit a fractal spatial distribution, as indicated by the log x log plots (Fig. 7). However, the fractal dimensions obtained are not homogeneous throughout the range of scales analyzed, a feature that can be interpreted as scaling of the fractal dimension. The box-counting analysis reveals that the pattern of the Carajás IOCG deposits/orebodies has three fractal dimensions defined by breaks in the plots at around 15 and 40 km, and the fractal dimensions vary from 0.19 (≤15 km), 0.50 (between 15 and 40 km) to 1.48 (>40 km). In contrast, the radial-density analysis indicates that the pattern of the Carajás IOCG deposits/orebodies has two fractal dimensions defined by one break point at around 13 km, and the fractal dimensions are 0.12 (≤13 km) and 0.81 (>13 km).

The moving box-counting method was performed to analyze the structural map of the same study area. The pattern of structures was scanned with a smaller grid with an initial box size of 20 km. For each grid position, the box size was halved four times, resulting in a minimum box side of 1.25 km. After assigning the fractal dimension obtained to the center of a grid cell, it was moved 10 km, thus resulting in some overlap between iterations. The process was repeated until the whole area was covered, and fractal dimensions for each measured grid were interpolated using a two-dimensional minimum curvature spline

technique. This technique was chosen since it provides contours that honor original values, besides presenting the best results after visual comparison with other interpolation methods. Additionally, several authors have proposed that Carajás IOCG deposits formed in more than one mineralizing event, with clusters of ages around the Neoarchean (2.7 and 2.5 Ga) and the Paleoproterozoic (1.8 Ga, Monteiro et al., 2008; Xavier et al., 2012; Moreto et al., 2015a, 2015b). Therefore, in order to honor this information, the mapped structures in Carajás were classified according to their inferred ages based on interpretations of the original maps from where the structures were derived (Fig. 6). Ages of deposits were obtained from the compilation provided by Moreto et al. (2015b), complemented by data available elsewhere (Galarza and Macambira, 2002; Pimentel et al., 2003; Silva et al., 2005). Fig. 8 shows the results of the moving box-counting of structures considered to be of Neoarchean age or older (only including the 2.7 and 2.5 Ga systems), and structures considered to be Paleoproterozoic or older (and thus including all IOCG mineralizing systems).

The moving box-counting analysis of Neoarchean structures indicates fractal dimensions ranging from 0 to 1.78 (Fig. 8a), with the highest values over the Cover Assemblage at the western, central, southeastern and northeastern portions, as well as over the Estrela granite, while the lowest values are over parts of the sedimentary cover (Águas Claras Formation), the Chicrin-Cateté granulite and north of the Carajás Tectonic Domain. Fractal dimensions for Paleoproterozoic structures range from 0 to 1.89 (Fig. 8b), with the highest values covering the same areas as the Neoarchean pattern, but extending to the south of the Cover Assemblage, and the northern central portion. Fractal dimensions over the Paleoproterozoic granites and the sedimentary cover are usually low. In general, fractal dimensions of the Paleoproterozoic pattern are higher than those of the Neoarchean pattern, a logical result because the structures increased and thus became denser and more complex.

We applied our best efforts to perform the analysis to a homogenous structural map (Fig. 6). Nonetheless, because the mapped structures used to calculate the fractal dimensions were derived from different map sheets, prepared by different surveys at different times, some degree of heterogeneity is present. For example, the anomalously high fractal dimensions for Paleoproterozoic structures at the western portion (Fig. 8b) are due to dense mapped structures in one of the map sheets used.

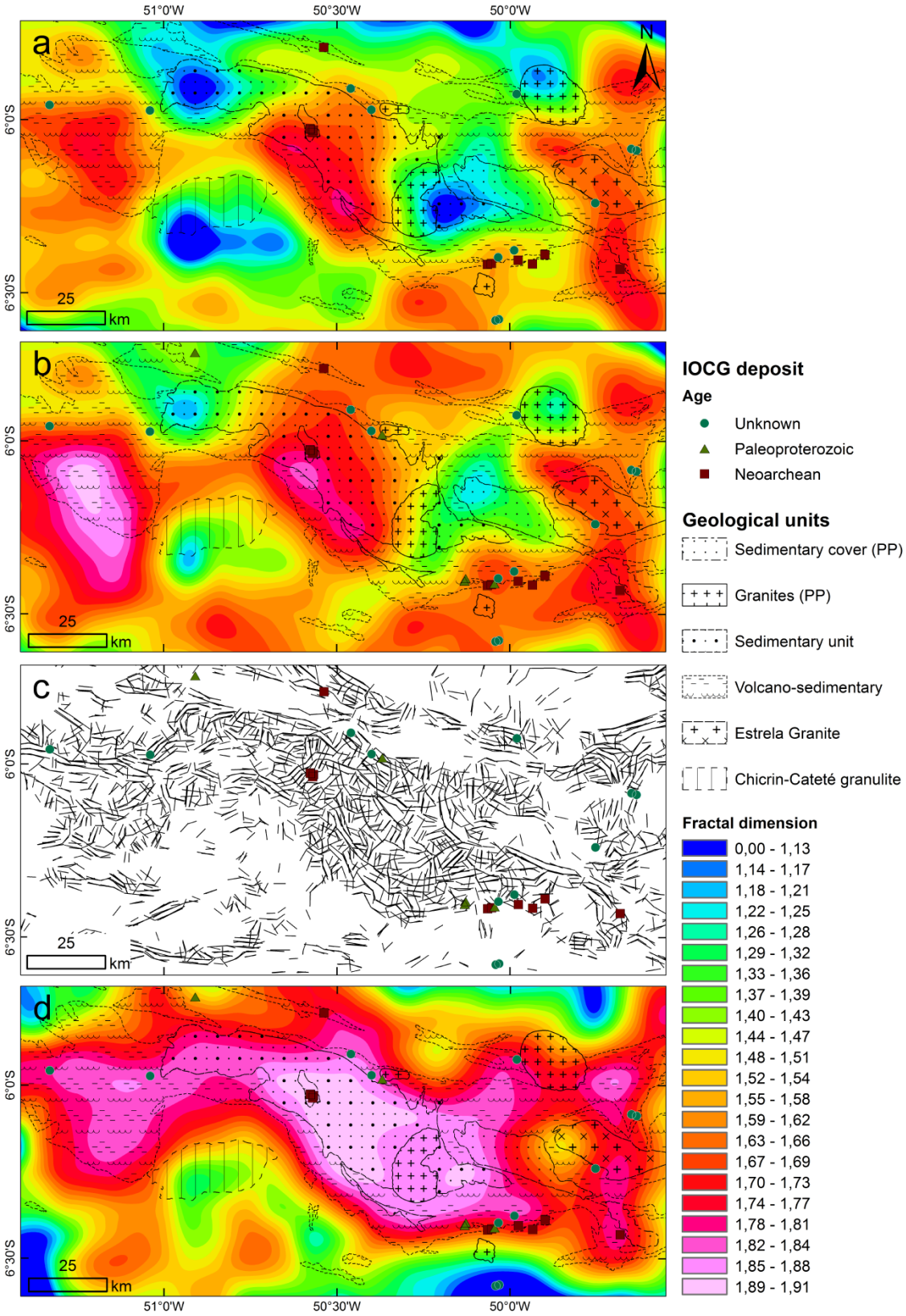

Fig. 8: Moving box-counting analysis of structures (Fig. 6) and lineaments in the Carajás Domain. (a) Neoarchean and older structures; (b) Paleoproterozoic and older structures; (c) lineament map of the Carajás Domain derived automatically from SRTM images; (d) fractal dimensions obtained from (c).

In order to evaluate the effect of this sort of heterogeneity due to multiple data source, the moving box-counting analysis was also performed in a map of lineaments derived automatically from SRTM images (Fig. 8c–d), because it provides a single data source for the whole area. Following procedures described in Locatelli (2014), lineament extraction was carried out in the PCI-Geomatica software, using four shaded relief images derived from a SRTM digital elevation model, with four different illumination azimuths: 0°, 45°, 90° and 135°, and a constant 10° illumination altitude.

Although the automatic extraction of structures from SRTM images tends to result in short straight lineaments (Fig. 8c), and concentrated mostly in the Cover Assemblage, the resulting map of moving box-count fractal dimensions exhibits close correlation with locations of IOCG deposits/orebodies (Fig. 8d). Also, the automatically extracted lineaments are in agreement with lineaments mapped by Domingos (2009), which indicate that the Cover Assemblage units exhibit abundant, short lineaments forming domains of high density.

Despite apparent differences in the result of using structural maps from multiple and single data sources, there is a general agreement between the maps of moving box-counting fractal dimension derived from the structural maps, such that the IOCG deposits/ orebodies coincide with intermediate to high fractal dimensions (Fig. 8). This suggests that any eventual bias from multiple data sources is not sufficient to significantly distort the results, although caution is critical to interpret results from the structural map obtained from multiple data sources.

4.2. Fry analysis applied to Carajás

Fry analysis was applied to the same 30 IOCG deposits/orebodies (Fig. 6) resulting in 870 Fry points (Fig. 9). The outline of the Fry plot assumes a sigmoidal shape, and the Fry plot shows various internal trends marked by alignments of points. These alignments are oriented to E-W and NW-SE directions, and are spaced between 20 and 40 km. When taken together, the alignments define at least two concentric rhombs. When plotted over a SRTM image, the sigmoidal outline of the Fry plot is similar to those defined by regional geomorphology, which are features described in the literature by several authors (e.g., Holdsworth and Pinheiro, 2000; Veneziani et al., 2004).

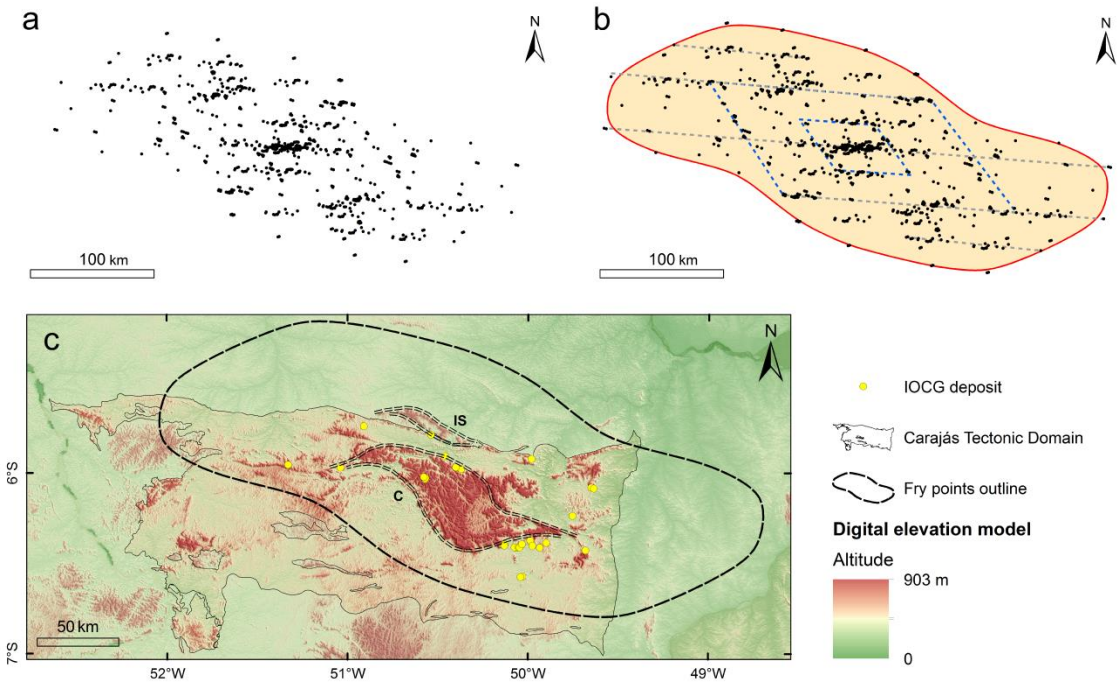

Fig. 9: (a) Fry plot for IOCG deposits/orebodies in Carajás. (b) Interpretations of the Fry plot. See Discussion for details. (c) Relationship between Fry points outline and geomorphological features such as the Carajás (C) and Igarapé Salobo (IS) sigmoids (SRTM digital elevation model).

Rose diagrams for all Fry points indicate preferential E-W, NW-SE and WNW-ESE directions, and subordinate NE-SW and NNE-SSW directions (Fig. 10a). By using all Fry points, one can extract information for a region as a whole, but it can be useful to further limit the analysis to pairs of Fry points at smaller distances in order to evaluate patterns in local scales (Carranza, 2009). In this regard, it is instructive to use the shortest distance within which there is a maximum probability of only one neighbor point next to any one of the points, which for our case is 43 km (similar to one of the break points found in the box-counting method; Fig. 7a). Besides this statistical justification, this distance is relevant because it samples separately IOCG deposits from the southern and northern districts of the Cover Assemblage, thus giving an idea of the geometric relationship among IOCG deposits in each of these two districts (Fig. 6). Additionally, since fractal analyses indicate a change in fractal dimension around 13 to 15 km (Fig. 7a), we also studied trends in pairs of Fry points within 15 km of each other (Fig. 10c).

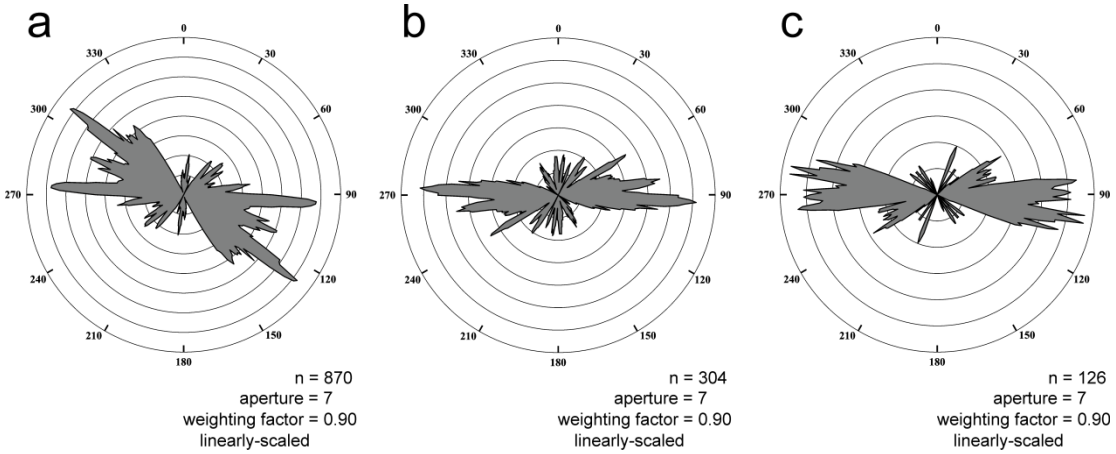

Fig. 10: Rose diagrams for Fry plot of IOCG deposits in Carajás: (a) all pairs of Fry points; (b) only pairs of Fry points within 43 km of each other; (c) only pairs of Fry points within 15 km of each other.

The rose diagram for Fry points within 43 km of each other indicates that the main trends are E-W and ENE-WSW, with secondary trends in N-S, NNE-SSW and NNW-SSE, while the NW-SE trend almost disappears (Fig. 10b). Similarly, for Fry points within 15 km of each other, the main trend remains E-W, with secondary trends in ENE-WSW and NNE-SSW, with the NW-SE trend less significant (Fig. 10c). All secondary trends in the range <15 km (NNE-SSW, ENE-WSW and NW-SE) are also found in the diagram for all points, but here they appear rotated some 10° clockwise.

Rose diagrams were also used to evaluate directions between subsets of IOCG deposits/orebodies according to the estimated ages of mineralization. Results indicate that Neoarchean IOCG deposits present strong trends in NW-SE and E-W directions, and a subordinate one in NNE-SSW, whereas Paleoproterozoic IOCG deposits present the same trends but without a clear predominance (Fig. 11). It is also noticeable that trends for the Paleoproterozoic deposits present a 10° clockwise rotation of directions.

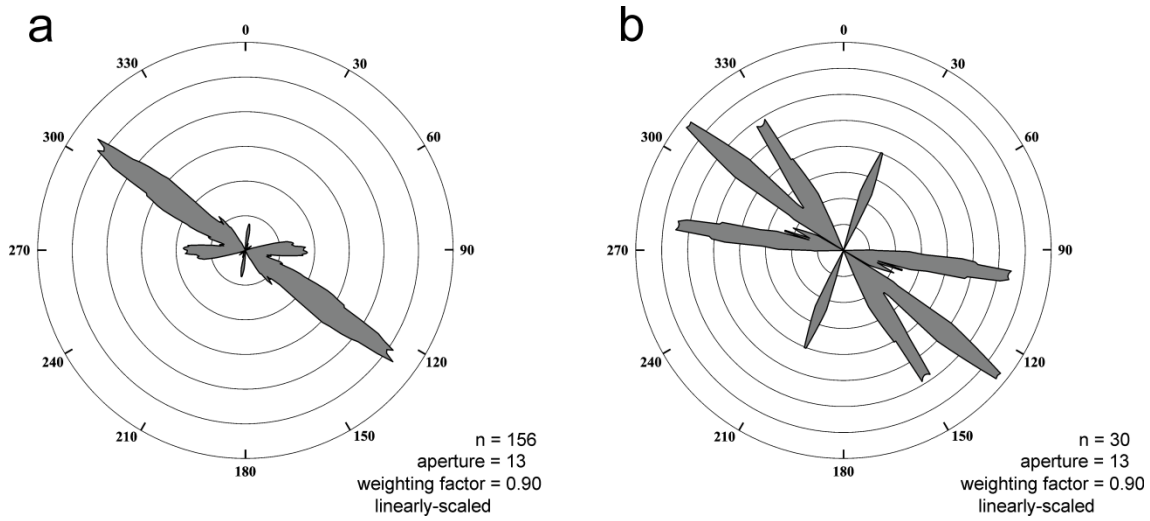

Fig. 11: Rose diagrams for Fry plot of IOCG deposits in Carajás: Fry points representing Neoarchean (a) and Paleoproterozoic (b) deposits.

5. Discussion

5.1. Fry and fractal analyses

The fractal dimensions obtained for the Carajás IOCG deposits using box-counting and radial-density methods do not match exactly, although this is expected because they measure different aspects of the geometric pattern analyzed (Agterberg, 2013; Kruhl, 2013). Nonetheless, the fractal dimensions obtained indicate that the IOCG deposits cluster within 10–15 km (i.e., D_B of 0.5 and 0.19, and D_R of 0.124), and IOCG deposits with scales of at least 40 km form linear trends (i.e., with D_B of 1.48 and D_R of 0.805). These interpretations of the fractal analyses of the IOCG deposits are supported by results of Fry analyses that indicate that IOCG deposits within 43 km of each other form major E-W and WNW-ESE linear trends, but within these alignments, deposits clusters are distributed heterogeneously (Fig. 6 and 9). The two most important trends are recognized in the literature for the southern and northern copper belts (Moreto et al., 2015b), and thought to be situated along or close to two distinct E–W and WNW–ESE trending regional shear zones that form the contacts of the Cover Assemblage with its basement (Moreto et al., 2015a). It is noteworthy that results from Fry plot suggests that there is also a third WNW-ESE trend located in the middle of the Cover Assemblage, roughly at the Bahia-Alemão deposit latitude (Fig. 9b). Although the northern and southern copper belts present several similarities, they are usually treated separately because they present several intrinsic characteristics that differentiate them (Moreto et al.,

2015a, 2015b). Thus, the possibility of a central trend could prove useful for future research, since a more detailed look at the deposits that form this central trend could reveal particularities relevant for mineralization modeling; deposits of the central trend are currently treated as part of the northern trend.

There is discussion whether fractal dimensions obtained for small distances in the box-counting technique are due to under-sampling bias (or roll-off effect), but the fact that the break close to 10 km is found also in radial-density fractal analysis of the Carajás IOCG deposits suggests it could also be related to a geological factor, an interpretation adopted by several authors elsewhere (e.g., Raines, 2008; Carranza, 2009). Furthermore, a similar distance was found in previous lineament analysis for the Carajás region, which indicates that there is a change in the dominant mean direction of topographic lineaments with lengths above and below the 7–10 km range (Domingos, 2009). The synthesis of these results suggests different mineralization controls in prospect (<10km), district (10–43 km) and province (>43 km) scales. This interpretation is supported by results of the Fry analysis.

The Fry plot for all the Carajás IOCG deposits forms a sigmoidal shape (Fig. 9), just like the sigmoidal shape of one of the most striking morphological features in the region, defined by the Cover Assemblage (Pinheiro and Holdsworth, 1997a). This suggests that the topography and the IOCG mineralization in Carajás share the same lithological and structural controls. Originally, the Carajás sigmoid was interpreted to have formed between 2.7 to 2.6 Ga under dextral transtension by the subsidence of supracrustal units into dilatational jogs, although this event was considered in part conjectural by its own proposers (Pinheiro and Holdsworth, 1997a). More recently, authors have reinterpreted the origin of the sigmoid pattern as due to sinistral transpression controlled by large NE-SW structures (Domingos, 2009; Pinheiro et al., 2013). Likewise, internal trends observed in the Fry plot define a rhomb with sides having orientations parallel to several similarly oriented features in Carajás, including anastomosing lineaments that enclose rhomb-shaped units in the Carajás fault zone (Holdsworth and Pinheiro, 2000) and the Cururu strike-slip duplex (Pinheiro, 1997) – both interpreted as sinistral structures. These similarities suggest that the sigmoidal distribution of Fry points of the Carajás IOCG deposits reflects an origin associated with a transcurrent environment with at least one important phase of sinistral dislocation sense.

The rose diagram for all Fry points of the Carajás IOCG deposits indicate that the structures that controlled IOCG mineralization on a regional scale have E-W, NW-SE and WNW-ESE orientations (Fig. 10a). These are the same directions as those of the main structures in the Carajás Tectonic Domain, such as the Carajás fault (Fig. 6), and concur with directions of structures derived from previous remote sensing lineament studies in the region (Carneiro et al., 2006; Domingos, 2009). The NNE-SSW and NE-SW-trending structures seem to have a relevant, though secondary, role in regional-scale control of IOCG mineralization in Carajás. The rose diagrams for Fry points within 43 km and within 15 km of each other indicate the importance of E-W-trending extensional structures, and less so of ENE-WSW, NNE-SSW and NW-SE trending structures, with secondary trends more clearly defined only at prospect scale (i.e., <15 km). The main difference between these local-scale trends and those of regional scale implies a reduction in the importance of the NW-SE trends (Fig. 10), possibly as a reflex of an indirect control exerted by the Carajás fault only at a regional scale. In this context, it is noticeable that the IOCG deposits in the northern copper belt are generally offset to the west in relation to those in the southern copper belt.

5.2. Assessment of results from Fry and fractal analyses

In order to demonstrate the usefulness of Fry and fractal analyses to investigate mineral deposits distribution, an exploratory spatial association analysis was performed to validate the results and discussion presented above. We adopted the distance distribution analysis (Berman, 1977) for comparing cumulative relative frequency graphs of distances from a set of geological features to: (i) mineral deposit locations and (ii) non-deposit locations. Such graphs represent probability-density distributions that are non-random for mineral deposits and random for non-deposit locations. If the difference (*D*) between the graphs is positive (i.e., the graph for IOCG deposits plots above the graph for random points), then there is positive spatial association between the mineral deposit locations and that set of geological features. If *D* is negative (i.e., the graph for IOCG deposits plots below the graph for random points), the spatial association is negative (Carranza, 2008, 2009) (Fig. 12).

Structures with E-W, NW-SE and ENE-WSW trends exhibit positive spatial associations with the Carajás IOCG deposits (blue curves plot above the red curves; Fig. 12a–c), but structures with NNE-SSW trend mostly have negative spatial associations with the Carajás IOCG deposits, becoming positively correlated only beyond distances >17 km (Fig. 12d). In order for the spatial associations to be considered statistically significant, the curve

for deposits pixels should plot above confidence bands. The association with NW-SE structures is the most statistically significant, plotting above both bands for α = 0.01 and α = 0.10, whereas curves for E-W and ENE-WSW are tangent to the confidence band for α = 0.10. The spatial association of the Carajás IOCG deposits with NNE-SSW-trending structures is not statistically significant for the given α.

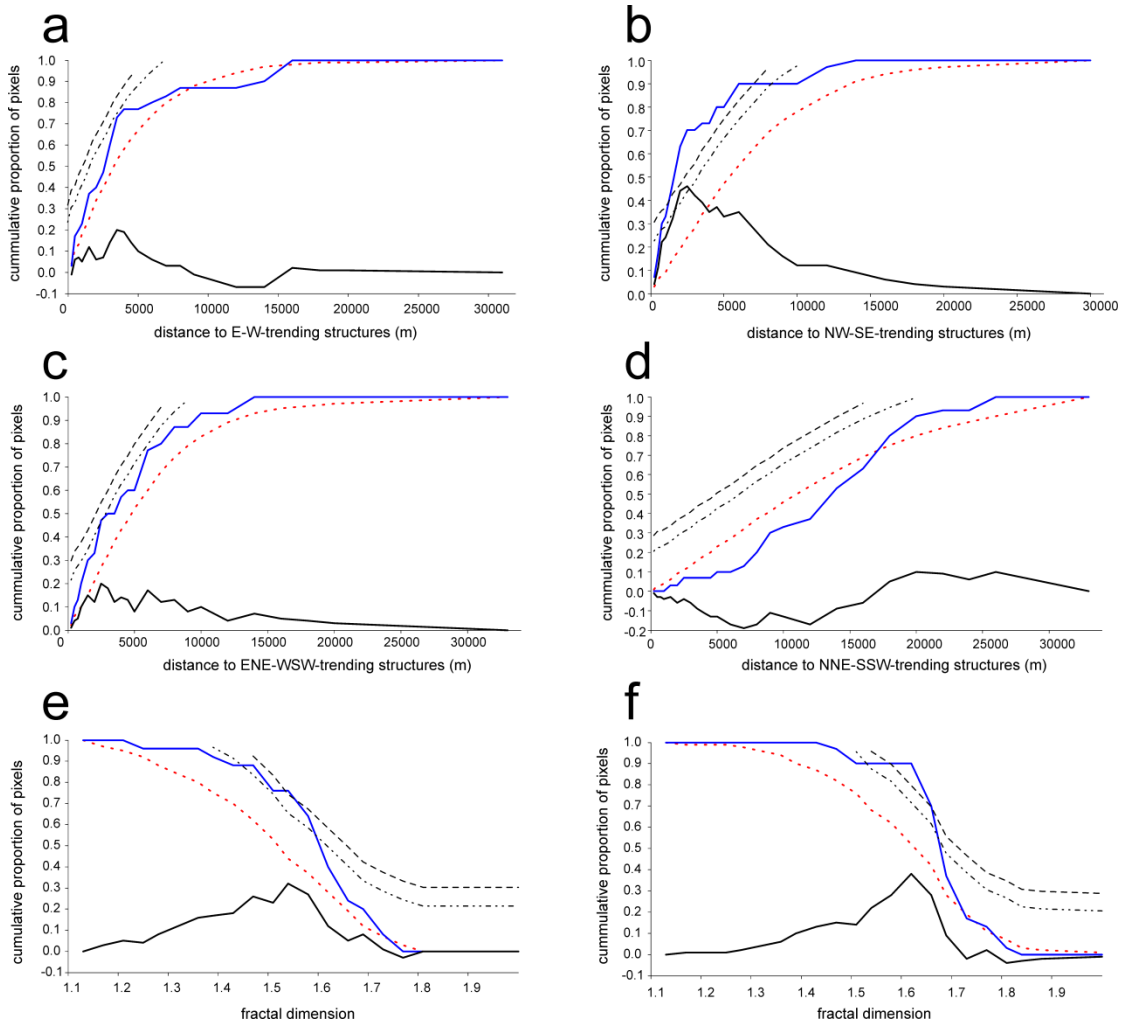

Fig. 12: Graphs of cumulative proportions of distance buffer and deposit pixels around structures (a–d) and cumulative proportions of fractal dimensions and deposit pixels for Neoarchean (e) and Paleoproterozoic (f) IOCG deposits in Carajás. For (e) and (f), IOCG deposits with unknown age were also considered. Blue curves are for IOCG deposits, red curves for random points and black curves for the difference between distributions (*D*). Upper confidence bands are presented as dashed black lines (α = 0.01 and α = 0.10).

Another important information derived from plots in Fig. 12 is the distance within which the difference (*D*) between the distributions is highest. This distance represents the optimal distance from the geological features within which the number of mineral deposits is significantly higher than would be expected due to chance. For structures trending E-W, NW-SE and ENE-WSW, the optimum distance of positive spatial association is around 2.5 km, while for NNE-SSW-trending structures there is no clearly defined peak for *D*.

The results of the spatial association analyses are in agreement with the Fry analyses, indicating important controls on IOCG mineralization by NW-SE and E-W-trending structures, followed by ENE-WSW trending structures. The lack of statistically significant spatial association of the IOCG deposits with NNE-SSW-trending structures is also consistent with Fry analyses, because this trend is invariably subordinate in the rose diagrams.

The spatial association of measured fractal dimensions with Neoarchean (Fig. 12e) and Paleoproterozoic (Fig. 12f) IOCG deposits is also statistically significant. The peaks defined by the *D* curves, which are both significant for $\alpha = 0.01$, represent fractal dimensions of 1.54 for Neoarchean IOCG deposits and 1.62 for Paleoproterozoic IOCG deposits, thus supporting the conclusion obtained from the moving box-counting analysis.

5.3. Structural controls on mineralization

Relating the results from Fry and fractal analyses with the structural and tectonic evolution for Carajás is challenging, because the region is marked by a succession of superimposed deformation events with different kinematics. Furthermore, the overall dynamics is not well defined for the long geological history of the Carajás region, and there is ongoing debate about its evolution. Most authors support the model in which the main structures affecting the Cover Assemblage were formed and reactivated in successive events of sinistral transpression and dextral transtension, with the main displacement zone oriented around E-W and WNW-ESE – a direction inherited from older structures in the basement (Araújo and Maia, 1991; Pinheiro and Holdsworth, 1997a; Veneziani et al., 2004). For this reason, we use the Riedel model to interpret IOCG structural controls. In the Neoarchean, on the inferred ages for IOCG mineralization events (around 2.7 and 2.5 Ga), several authors recognize a sinistral transpressional regime, with the main stress direction oriented to NE-SW, NNE-SSW or ENE-WSW (Pinheiro and Holdsworth, 1997b, 2000; Veneziani et al., 2004; Domingos, 2009). For the IOCG mineralizing event that occurred during the Paleoproterozoic, the consensus is for the occurrence of generalized extension and/or dextral

transtension (Pinheiro and Holdsworth, 1997a, 2000), with the extension direction oriented to NE-SW or E-W. Considering these interpreted kinematics, the trends that define the rhombs in the Fry plot of IOCG deposits mainly reflect a regional control by two sets of structures: (i) WNW-ESE, parallel to the main dislocation direction, and (ii) NW-SE structures, representing oblique antithetic structures X or R' (Fig. 9b and 13). As observed from the rose diagrams, the main trends at the regional scale are associated with Y and P structures, and to a lesser extend with T and R' structures in a sinistral environment, and with Y and T and secondarily to R, R' and X in a dextral environment (Fig. 10 and 13). Based on the rose diagrams for district scales (Fig. 10b), the main structures controlling the Carajás IOCG deposits are oriented approximately parallel to synthetic structures Y and R in a sinistral environment, and Y and P in a dextral environment. At the prospect scale (Fig. 10c), the pattern is the same as at the district scale, but with secondary trends clearer in directions that coincide with R' and P (sinistral) and X and T (dextral).

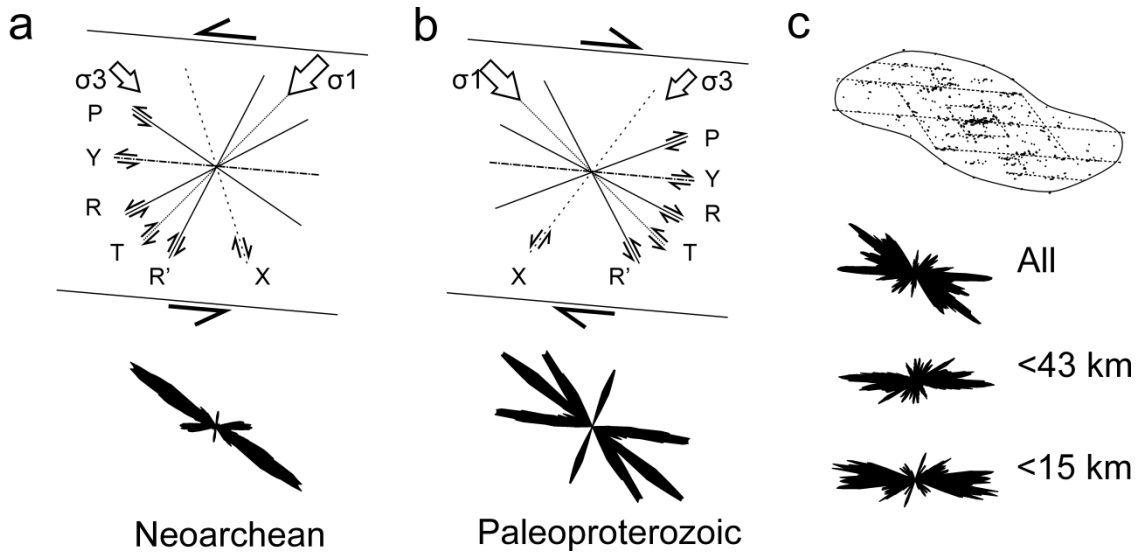

Fig. 13: Angular relations between structures that form in idealized transcurrent simple shear, compiled from clay-cake models and geological examples, with Riedel shear terminology (based on Christie-Blick and Biddle, 1985). (a) model for sinistral transpression inferred to have occurred during the Neoarchean in Carajás, with the simplified rose diagram for Neoarchean IOCG deposits; (b) model for dextral transtension inferred to have occurred during the Paleoproterozoic in Carajás, with the simplified rose diagram for Paleoproterozoic IOCG deposits; (c) Fry plot and rose diagram for all points, for points in the range <43 km and for points in the range <15 km.

Although the number of deposits with available ages is small, an attempt was made to analyze them separately using this parameter in order to evaluate trends according to different kinematics interpreted for the region. The rose diagram for Fry points of Neoarchean IOCG deposits (Fig. 11a) indicates that during the sinistral transpression inferred for the Neoarchean events (~2.7 Ga and 2.5 Ga), the main structures controlling mineralization were oriented approximately in the direction of P structures, and secondarily to Y and R'. For the Paleoproterozoic (*ca.* 1.8 Ga) IOCG deposits, the main control would be related to T and R' structures, and secondarily to Y and X (Fig. 11b and 13). The NE-SW trends present in the rose diagram for 1.8 Ga deposits suggest the importance of NE-SW-trending structures younger than 2.7 Ga but older than 1.8 Ga. Furthermore, the 10° clockwise rotation observed in trends for the Paleoproterozoic in relation to Neoarchean deposits could reflect the rotation of Neoarchean structures during the Proterozoic reactivation. Obviously, the interpretations of the results presented above need to be taken with caution, since the number of IOCG deposits used for each rose diagram in Fig. 11 is small, and a single deposit/orebody can distort results.

The interpretations drawn above are based on theoretical models and depend upon several simplifications. Geological examples tend to be more complicated, and observed arrangements of structures do not necessarily conform to those predicted by models or experiments, especially because (Christie-Blick and Biddle, 1985): (i) rocks are heterogeneous; (ii) structures develop sequentially rather than instantaneously; and (iii) early-formed structures tend to be rotated during extended deformation. Thus, a possible problem with the use of the Riedel model in the Carajás region is that one cannot unequivocally determine which structures are related to a single stress-strain event, as should be the case when applying the Riedel conjugate model. Fry analysis aids to partially overcome this, especially in conjunction with geochronological information (Fig. 13), since it reveals trends among IOCG deposits depending solely on their relative positions.

Bearing in mind the issues pointed out, interpretations derived from Fry analysis are consistent within different spatial ranges and ages, and allows one to infer that the most important structures controlling IOCG mineralization seems to be those parallel to the main dislocation direction (Y) and synthetic faults (P) in a Riedel model, oriented to E-W and WNW-ESE. These trends in all the rose diagrams of the Fry analyses represent important structural controls, both considering deposits as a whole and separating them by age. Classical extension fractures (T) seem to be more relevant in the dextral environment when oriented to NW-SE (thus more important to Paleoproterozoic deposits).

In order to consider other aspects related to how structures control mineralization, fractal dimension can be used to measure their complexity and, by deduction, changes in permeability and porosity of different parts of the study area. The results of the moving box-counting fractal analysis indicate that both Neoarchean and Paleoproterozoic IOCG deposits are associated with intermediate fractal dimensions, as do IOCG deposits with undefined age, meaning that IOCG deposits are not necessarily related to areas with the most complex arrangement of faults. This suggests that IOCG deposits are located in regions of fractal dimension gradients rather than high fractal dimensions, as steep gradients could mark transitions from areas of low complexity to areas with more elements of a permeability network (high complexity), thereby focusing fluid flow and increasing the volume of hydrothermal fluids (Weinberg et al., 2004; Hodkiewicz et al., 2005). These results imply that the degree of interconnectivity of structures, as reflected by fractal dimensions, should be high enough to favor fluid flow, but excessively complex structural patterns could disperse fluid flow rather than focus it, thus not promoting mineralization. Some authors (Ford and Blenkinsop, 2008b; Ford and McCuaig, 2010) suggest that structurally controlled deposits should be present in areas with higher fractal dimensions, and their studies indicate that the relationship between deposits and fractal dimension gradient are due to distortions added by the scale and degree of interpretation of the maps analyzed. In our case study, the structural map was mostly derived from regional scale sheets (1:250,000), and it was assembled from three different sheets that clearly show heterogeneities caused by different approaches to mapping and interpretation. This likely explains why the IOCG deposits do not coincide with the highest fractal dimensions. Nonetheless, fractal analysis of lineaments extracted automatically (Fig. 8d), which are not subject to these biases and are homogeneous throughout the study area, also indicates that Carajás IOCG deposits coincide with intermediate to high fractal dimensions but not with the highest fractal dimensions. Such notion is consistent with the results obtained from the structural map compiled from multiple data sources. The results are to some extent also in agreement with the study of Domingos (2009), who concluded that several of the largest mineral deposits in Carajás are located adjacent to zones of high lineament density, although it is important to note that he used manually extracted lineaments, derived structures density using a different approach and assessed the spatial association visually.

The bulk of the results from fractal and Fry analyses allows to conjecture that regional WNW-ESE trends, which coincide with the main dislocation direction of master faults such as those present in the Carajás and Cinzento strike-slip systems, represent areas where major hydrothermal circulation cells were located, both during the Neoarchean and the Paleoproterozoic. Furthermore, the position of such trends generally coincides with the contacts between the metamorphosed volcano-sedimentary units of the Cover Assemblage and its basement. These are areas where fractal dimension tends to be moderate to high, or where there is relevant fractal dimension gradient, thus suggesting a moderately complex pattern of structures appropriate for fluid percolation, associated with zones with changes in the structural pattern complexity. Within these alignments that controlled regional fluid flow cells, in the district and prospect scales, deposits formed where intersections with secondary structural controls existed, as well as with mineralization controls of other natures such as lithogeochemical controls (not addressed in this work). The secondary structural controls coincide mainly with NW-SE structures, which most likely operated as synthetic, secondary shears (P) during the sinistral transpression regime acting throughout the Neoarchean, and with extension or tension fractures (T) for the dextral transtension regime acting during the Paleoproterozoic. Structures trending ENE-WSW and NNE-SSW also appear to be relevant, which is in agreement with studies carried out in the Sossego deposit indicating that intersections between WNW-ESE and NE-SW structures favored mineralization (Domingos, 2009).

6. Conclusions

Fry analysis is useful to highlight directional trends between mineral deposits, which can be related to structures that controlled mineral deposit formation. Besides trend directions, spacing and repetitions in mineral deposit distribution can also be assessed by the Fry technique, and more detailed information can be derived by subsetting deposits using relevant distances or deposit characteristics (e.g., age). Fractal analyses are suitable to derive information regarding differences in mineralization controls over different spatial scales and their relationship to mineral deposit distribution, as well as to identify relationships between deposits and complex geological patterns, such as regional scale structures. The combination of these techniques results in a powerful methodological approach to obtain information that can be used in understanding mineral deposit genesis and model mineralization controls, which are important for the definition of favorable areas for future exploration work.

The usefulness of the presented methods was demonstrated by applying them to IOCG deposits in the Carajás region, which resulted in the following conclusions regarding their spatial distribution:

(1) Fractal dimensions obtained from box-counting and radial-density techniques suggest that different mineralization controls acted in scales of <10–15 km, 15 to 40 km, and >40 km. Furthermore, the Carajás IOCG deposits cluster at scales of <40 km, and clusters of IOCG deposits in the region form a linear pattern at scales larger than 40 km. These spatial behaviors of the Carajás IOCG deposits are reflected by several well defined linear WNW-ESE trends, separated by distances of 20–40 km, with deposits clusters being heterogeneously distributed within these trends;

(2) Fry analysis indicates that the most important structures that controlled IOCG mineralization in the Carajás region are oriented to WNW-ESE, E-W and NW-SE, with secondary trends to ENE-WSW and NNE-SSW. These trends are clearly marked in the Fry plot, which also indicates a common deformational history for the deposits and the supracrustal sequences, as attested by their common sigmoidal shape;

(3) Trends of the IOCG deposits in Carajás are related mostly to the main direction of dislocation (Y) and synthetic structures (P) in a Riedel model. Classic extension structures (T) seems more relevant during the Paleoproterozoic, when they would be oriented to NW-SE;

(4) The moving box-counting analysis suggests that IOCG deposits in the Carajás region are located in areas with intermediate to high fractal dimensions, reflecting areas with intermediate to high complexity of structural patterns. This probably reflects changes in permeability associated with contact zones between the basement and cover assemblages, which generally display different degrees of complexity in their structural patterns;

(5) Exploratory spatial association analysis indicates that Neoarchean and Paleoproterozoic IOCG deposits in the Carajás region have significant positive spatial associations with NW-SE, E-W and ENE-WSW-trending structures, as well as with intermediate to high fractal dimensions. These

results support those obtained by Fry and fractal analyses, thus reinforcing the relevance of the latter methods to study the spatial distribution of mineral deposits.

Results shown here suggest the following features that could be targeted for exploration work for IOCG deposits in Carajás:

(i) The regional WNW-ENE trends of Salobo, Igarapé Bahia-Alemão and Sossego deposits for scales larger than 40 km. Also, the indication of a possible central trend in addition to the known northern and southern copper belts encourages further studies.

(ii) E-W and ENE-WSW trends of known occurrences and deposits for scales smaller than 40 km.

(iii) Buffer zones up to 2.5 km from structures mapped on a regional scale, especially the NW-SE-trending structures, but also E-W and ENE-WSW. On the other hand, NNE-SSW-trending structures do not appear to be important mineralization controls on a regional scale.

(iv) Regions with intermediate to high complexity of structures patterns, as measured by fractal dimensions values, especially when such values coincide with the contact zone between the cover assemblage and the basement.

Acknowledgments

The authors would like to thank: Vale Company, for the long-term logistic and in-kind support to UNICAMP for research in the Carajás region; FAPESP/CAPES covenant (São Paulo Research Foundation/*Coordenação de Aperfeiçoamento de Pessoal de Nível Superior*), for the scholarship to PMHM (grant FAPESP 2015/11186-3); and CNPq (National Counsel of Technological and Scientific Development), for the financial support (grant 2014-9/401316) and the research grant to CRSF (no. 2008-7/303563). The authors also thank Dr. Martiya Sadeghi, Professor Lydia Maria Lobato (OGR editor) and an anonymous reviewer for their helpful comments, which were instrumental for the improvement of the manuscript.

Appendix A. Supplementary data

Supplementary data to this article can be found online at http://dx.doi.org/10.1016/j.oregeorev.2016.09.038.

References

Agterberg, F.P., 2013. Fractals and spatial statistics of point patterns. J. Earth Sci. 24, 1–11. http://dx.doi.org/10.1007/s12583-013-0305-6.

Andrada de Palomera, R.P., Carranza, E.J.M., 2005. Analysis of Spatial Distribution of Epithermal Gold Deposits in the Deseado Massif, Santa Cruz Province, Argentina. Proceedings of the 16th Argentine Geological Congress. La Plata, Argentina pp. 715–722.

Araújo, O.J.B., Maia, R.G.N., 1991. Programa Levantamentos Geológicos Básicos do Brasil, Programa Grande Carajás, Serra dos Carajás, Folha SB.22-Z-A, Estado do Pará, Escala 1:250.000. Brasília (164 pp).

Austin, J.R., Blenkinsop, T.G., 2009. Local to regional scale structural controls on mineralisation and the importance of a major lineament in the eastern Mount Isa Inlier, Australia: review and analysis with autocorrelation and weights of evidence. Ore Geol. Rev. 35, 298–316. http://dx.doi.org/10.1016/j.oregeorev.2009.03.004.

Beisiegel, V.R., Bernadelli, A.L., Drummond, N.F., Ruff, A.W., Tremaine, J.W., 1973. Geologia recursos minerais da Serra dos Carajás. Rev. Bras. Geosci. 3, 215–242.

Berman, M., 1977. Distance distributions associated with Poisson processes of geometric figures. J. Appl. Probab. 14, 195–199.

Blenkinsop, T.G., Kadzviti, S., 2006. Fluid flow in shear zones: insights from the geometry and evolution of ore bodies at Renco gold mine, Zimbabwe. Geofluids 6, 334–345. http://dx.doi.org/10.1111/j.1468-8123.2006.00154.x.

Blenkinsop, T.G., Sanderson, D.J., 1999. Are gold deposits in the crust fractals? A study of gold mines in the Zimbabwe craton. In: McCaffrey, K.J.W., Lonergan, L., Wilkinson, J.J. (Eds.), Fractures, Fluid Flow and Mineralization Special Publications 155. Geological Society, London, pp. 141–151. http://dx.doi.org/10.1144/GSL.SP.1999.155.01.11.

Boots, B.N., Getis, A., 1988. Point Pattern Analysis, Scientific Geography 8. SAGE Publications Inc., Newbury Park (92 pp).

Carlson, C.A., 1991. Spatial distribution of ore deposits. Geology 19, 111–114. http://dx.oi.org/10.1130/0091-7613(1991)019b0111:SDOODN2.3.CO;2.

Carneiro, C.C., Crósta, A.P., Silva, A.M., Pinheiro, R.V.L., 2006. Fusão de imagens altimétricas aeromagnetométricas como ferramenta de interpretaçao geológica, exemplo da Província mineral de Carajás (PA). Rev. Bras. Geofísica 24, 261–271.

Carranza, E.J.M., 2008. Geochemical Anomaly and Mineral Prospectivity Mapping in GIS, Handbook of Exploration and Environmental Geochemistry. 11. Elsevier B.V, Amsterdam. http://dx.doi.org/10.1016/S1874-2734(09)70001-4 (366 pp).

Carranza, E.J.M., 2009. Controls on mineral deposit occurrence inferred from analysis of their spatial pattern and spatial association with geological features. Ore Geol. Rev. 35, 383–400. http://dx.doi.org/10.1016/j.oregeorev.2009.01.001.

Carranza, E.J.M., 2011a. From predictive mapping of mineral prospectivity to quantitative estimation of number of undiscovered prospects. Resour. Geol. 61, 30–51. http://dx.oi.org/10.1111/j.1751-3928.2010.00146.x.

Carranza, E.J.M., 2011b. Analysis and mapping of geochemical anomalies using logratio-transformed stream sediment data with censored values. J. Geochem. Explor. 110, 167–185. http://dx.doi.org/10.1016/j.gexplo.2011.05.007.

Carranza, E.J.M., Hale, M., 2002a. Spatial association of mineral occurrences and curvilinear geological features. Math. Geol. 34, 203–221. http://dx.doi.org/10.1023/A:1014416319335.

Carranza, E.J.M., Hale, M., 2002b.Where are porphyry copper deposits spatially localized? A case study in Benguet Province. Philippines. Nat. Resour. Res. 11, 45–59.

Carranza, E.J.M., Sadeghi, M., 2010. Predictive mapping of prospectivity and quantitative estimation of undiscovered VMS deposits in Skellefte district (Sweden). Ore Geol. Rev. 38, 219–241. http://dx.doi.org/10.1016/j.oregeorev.2010.02.003.

Carranza, E.J.M., Sadeghi, M., 2014. Post-VMS mineralization deformations (1880–1820 Ma) of the Skellefte district (Sweden): insights from the spatial pattern of VMS occurrences. Front. Earth Sci. 8, 319–324. http://dx.doi.org/10.1007/s11707-014-0466-3.

Carranza, E.J.M., van Ruitenbeek, F.J.A., Hecker, C., van der Meijde, M., van der Meer, F.D., 2008. Knowledge-guided data-driven evidential belief modeling of mineralrospectivity in Cabo de Gata. SE Spain. Int. J. Appl. Earth Obs. Geoinf. 10, 374–387. http://dx.doi.org/10.1016/j.jag.2008.02.008.

Carranza, E.J.M., Owusu, E.A., Hale, M., 2009. Mapping of prospectivity and estimation of number of undiscovered prospects for lode gold, southwestern Ashanti Belt, Ghana. Miner. Deposita 44, 915–938. http://dx.doi.org/10.1007/s00126-009-0250-6.

Christie-Blick, N., Biddle, K.T., 1985. Deformation and basin formation along strike-slip faults. SEPM Spec. Publ. - Strike-slip Deform. basin Form. Sediment. 37, 1–34. http://dx.doi.org/10.2110/pec.85.37.0001.

Diggle, P.J., 1983. Statistical Analysis of Spatial Point Patterns. Academic Press, London (148 pp).

Domingos, F.H.G., 2009. The Structural Setting of the Canaã dos Carajás Region and Sossego-Sequeirinho Deposits, Carajás Brazil. Doctor of Philosophy thesis. University of Durham, Durham (483 pp).

Ford, A., Blenkinsop, T.G., 2008a. Combining fractal analysis of mineral deposit clustering with weights of evidence to evaluate patterns of mineralization: application to copper deposits of the Mount Isa Inlier, NW Queensland, Australia. Ore Geol. Rev. 33, 435–450. http://dx.doi.org/10.1016/j.oregeorev.2007.01.004.

Ford, A., Blenkinsop, T.G., 2008b. Evaluating geological complexity and complexity gradients as controls on copper mineralisation, Mt Isa Inlier. Aust. J. Earth Sci. 55, 13–23.ttp://dx.doi.org/10.1080/08120090701581364.

Ford, A., McCuaig, T.C., 2010. The effect of map scale on geological complexity for computer-aided exploration targeting. Ore Geol. Rev. 38, 156–167. http://dx.doi.org/10.1016/.oregeorev.2010.03.008.

Fry, N., 1979. Random point distributions and strain measurement in rocks. Tectonophysics 60, 89–105. http://dx.doi.org/10.1016/0040-1951(79)90135-5.

Galarza, M.A., Macambira, M.J.B., 2002. Geocronologia e evolução crustal da área do depósito Cu-Au Gameleira, Província Mineral de Carajás (Pará), Brasil. Rev. do Inst. Geociências - USP 2, 143–159.

Goryainov, P.M., Ivanyuk, G.Y., Sharov, N.V., 1997. Fractal analysis of seismic and geological data. Tectonophysics 269, 247–257. http://dx.doi.org/10.1016/S0040-1951(96)00162-X.

Gumiel, P., Sanderson, D.J., Arias, M., Roberts, S., Martín-Izard, A., 2010. Analysis of the fractal clustering of ore deposits in the Spanish Iberian Pyrite Belt. Ore Geol. Rev. 38, 307–318. http://dx.doi.org/10.1016/j.oregeorev.2010.08.001.

Hanna, S.S., Fry, N., 1979. A comparison of methods of strain determination in rocks from southwest Dyfed (Pembrokeshire) and adjacent areas. J. Struct. Geol. 1, 155–162.ttp://dx.doi.org/10.1016/0191-8141(79)90052-X.

He, J., Yao, S., Zhang, Z., You, G., 2013. Complexity and productivity differentiation models of metallogenic indicator elements in rocks and supergene media around Daijiazhuang Pb–Zn deposit in Dangchang County, Gansu Province. Nat. Resour. Res. 22, 19–36. http://dx.doi.org/10.1007/s11053-012-9193-1.

Herbert, S.,Woldai, T., Carranza, E.J.M., van Ruitenbeek, F.J.A., 2014. Predictive mapping of prospectivity for orogenic gold in Uganda. J. Afr. Earth Sci. 99, 666–693. http://dx.doi.rg/10.1016/j.jafrearsci.2014.03.001.

Hitzman, M.W., 2000. Iron oxide-Cu-Au deposits: what, where, when and why. In: Porter, T.M. (Ed.), Hydrothermal Iron Oxide Copper-Gold & Related Deposits: A Global Perspective Volume 1. PGC Publishing, Adelaide, pp. 9–25.

Hodkiewicz, P.F., Weinberg, R.F., Gardoll, S.J., Groves, D.I., 2005. Complexity gradients in the Yilgarn Craton: fundamental controls on crustal-scale fluid flow and the formation of world-class orogenic-gold deposits. Aust. J. Earth Sci. 52, 831–841. http://dx.oi.org/10.1080/08120090500304257.

Holdsworth, R.E., Pinheiro, R.V.L., 2000. The anatomy of shallow-crustal transpressional structures: insights from the Archaean Carajas fault zone, Amazon, Brazil. J. Struct. Geol. 22, 1105–1123. http://dx.doi.org/10.1016/S0191-8141(00)00036-5.

Johnston, J.D., McCaffrey, K.J.W., 1996. Fractal geometries of vein systems and the variation of scaling relationships with mechanism. J. Struct. Geol. 18, 349–358. http://dx.oi.org/10.1016/S0191-8141(96)80055-1.

Justo, A.P., Lopes, E.S., 2014. Programa Geologia do Brasil - PGB, Serra dos Carajás, Folha SB.22-Z-A-II, Estado do Pará, Carta Geológica, Escala 1:100.000. CPRM (Companhia de Pesquisa de Recursos Minerais).

Kreuzer, O.P., Blenkinsop, T.G., Morrison, R.J., Peters, S.G., 2007. Ore controls in the Charters Towers goldfield, NE Australia: constraints from geological, geophysical and numerical analyses. Ore Geol. Rev. 32, 37–80. http://dx.doi.org/10.1016/j.oregeorev. 2006.12.001.

Kruhl, J.H., 2013. Fractal-geometry techniques in the quantification of complex rock structures: special view on scaling regimes, inhomogeneity and anisotropy. J. Struct. Geol. 46, 2–21. http://dx.doi.org/10.1016/j.jsg.2012.10.002.

Lisitsin, V., 2015. Spatial data analysis of mineral deposit point patterns: applications to exploration targeting. Ore Geol. Rev. 71, 861–881. http://dx.doi.org/10.1016/j.regeorev.2015.05.019.

Locatelli, P.E., 2014. Avaliação de Métodos para Correlação entre Morfoestruturas Superficiais e Anomalias Magnéticas em Profundidade com Base em Sensoriamento Remoto e Aerogeofísica. Masters dissertation, Universidade Estadual de Campinas (71 pp).

Luz, F., Mateus, A., Matos, J.X., Gonçalves, M.A., 2014. Cu- and Zn-soil anomalies in the NE border of the South Portuguese Zone (Iberian Variscides, Portugal) identified by multifractal and geostatistical analyses. Nat. Resour. Res. 23, 195–215. http://dx.doi.rg/10.1007/s11053-013-9217-5.

Macambira, E.M.B., Vale, A.G., 1997. Programa Levantamentos Geológicos Básicos do Brasil, São Félix do Xingu, Folha SB.22-Y-B, Estado do Pará, Escala 1:250.000. Brasília (384 pp).

Mandelbrot, B.B., 1983. The Fractal Geometry of Nature (Updated and Augmented Edition). Freeman, New York (495 pp).

McCaffrey, K.J., Petford, N., 1997. Are granitic intrusions scale invariant? J. Geol. Soc. Lond. 154, 1–4. http://dx.doi.org/10.1144/gsjgs.154.1.0001.

Monteiro, L.V.S., Xavier, R.P., Carvalho, E.R., Hitzman, M.W., Johnson, C.A., Souza Filho, C.R., Torresi, I., 2008. Spatial and temporal zoning of hydrothermal alteration and mineralization on the Sossego iron oxide–copper–gold deposit, Carajás Mineral Province, Brazil: paragenesis and stable isotope constraints. Miner. Deposita, 43, 129–159. http://x.doi.org/10.1007/s00126-006-0121-3.

Monteiro, L.V.S., Xavier, R.P., Souza Filho, C.R., Moreto, C.P.N., 2014. Metalogênese da Província Carajás. In: Silva, M.G., Neto, M.B.R., Jost, H., Kuyumjian, R.M. (Eds.), Metalogênese Das Províncias Tectônicas Brasileiras. CPRM (Companhia de Pesquisa de Recursos Minerais), Belo Horizonte, pp. 43–92.

Moreto, C.P.N., Monteiro, L.V.S., Xavier, R.P., Creaser, R.A., DuFrane, S.A.,Melo, G.H.C., Silva, M.A.D., Tassinari, C.C.G., Sato, K., 2015a. Timing of multiple hydrothermal events in the iron oxide–copper–gold deposits of the southern Copper Belt, Carajás Province, Brazil. Miner. Deposita 50, 517–546. http://dx.doi.org/10.1007/s00126-014-0549-9.

Moreto, C.P.N., Monteiro, L.V.S., Xavier, R.P., Creaser, R.A., DuFrane, S.A., Tassinari, C.C.G., Sato, K., Kemp, A.I.S., Amaral, W.S., 2015b. Neoarchean and Paleoproterozoic iron oxide-copper-gold events at the Sossego Deposit, Carajás Province, Brazil: Re-Os and U-Pb geochronological evidence. Econ. Geol. 110, 809–835.

Munro, M.A., Blenkinsop, T.G., 2012. MARD-A moving average rose diagram application for the geosciences. Comput. Geosci. 49, 112–120. http://dx.doi.org/10.1016 /j.cageo.2012.07.012.

Nogueira, A.C.R., Truckenbrodt, W., Pinheiro, R.V.L., 1995. Formação Águas Claras, Pré-Cambriano da Serra dos Carajás: redescrição e redefinição litoestratigráfica. Bol. Mus. Para. Emílio Goeldi - Série Ciências da Terra. 7 pp. 177–277.

Oliveira, J.R., Neto, C.S.S., Costa, E.J.S., 1994. Programa Levantamentos Geológicos Básicoso Brasil, Serra Pelada, Folha SB.22-X-C, Estado do Pará, Escala 1:250.000. Brasília (248 pp).

Pimentel, M.M., Lindenmayer, Z.G., Laux, J.H., Armstrong, R.A., Araújo, J.C., 2003. Geochronology and Nd isotope geochemistry of the Gameleira Cu – Au deposit, Serra dos Carajás, Brazil: 1.8–1.7 Ga hydrothermal alteration and mineralization. J. S. Am. Earth Sci. 15, 803–813.

Pinheiro, R.V.L., 1997. Reactivation History of the Carajas and Cinzento Strike-slip Systems, Amazon, Brazil. PhD thesis. University of Durham, Durham (408 pp).

Pinheiro, R.V.L., Holdsworth, R.E., 1997a. Reactivation of Archaean strike-slip fault systems, Amazon region, Brazil. J. Geol. Soc. Lond. 154, 99–103. http://dx.doi.org/10.1144/gsjgs.154.1.0099.

Pinheiro, R.V.L., Holdsworth, R.E., 1997b. The structure of the Carajás N-4 ironstone deposit and associated rocks: relationship to Archaean strike-slip tectonics and basement reactivation in the Amazon region, Brazil. J. S. Am. Earth Sci. 10, 305–319.ttp://dx.doi.org/10.1016/S0895-9811(97)00018-7.

Pinheiro, R.V.L., Holdsworth, R.E., 2000. Evolução tectono-estratigráfica dos sistemas transcorrentes Carajás e Cinzento, Cinturão Itacaiúnas, na borda leste do Cráton Amazônico. Pará. Rev. Bras. Geociências 30, 597–606.

Pinheiro, R.V.L., Kadekaru, K., Soares, A.V., Freitas, C., Ferreira, S.N., Matos, F.M.V., 2013. Carajás, Brazil - a short tectonic review. Anais Do 13° Simpósio de Geologia Da Amazônia. SBG - Núcleo Norte, Belém, Brazil, pp. 1086–1089.

Pruess, S.A., 1995. Some remarks on the numerical estimation of fractal dimension. In: Barton, C.C., La Pointe, P.R. (Eds.), Fractals in the Earth Sciences. Springer US, Boston, MA, pp. 65–75 http://dx.doi.org/10.1007/978-1-4899-1397-5_3.

Raines, G.L., 2008. Are fractal dimensions of the spatial distribution of mineral deposits meaningful? Nat. Resour. Res. 17, 87–97. http://dx.doi.org/10.1007/s11053-008-9067-8.

Rosière, C.A., Baars, F.J., Seoane, J.C.S., Lobato, L.M., da Silva, L.L., de Souza, S.R.C., Mendes, G.E., 2006. Structure and iron mineralisation of the Carajás Province. Appl. Earth Sci. 115, 126–133. http://dx.doi.org/10.1179/174327506X138986.

Santos, J.O.S., 2003. Geotectônica dos Escudos das Guianas e Brasil-Central. In: Bizzi, L.A., Schobbenhaus, C., Vidotti, R.M., Gonçalves, J.H. (Eds.), Geologia. Tectônica E Recursos Minerais Do Brasil. CPRM, Brasília, pp. 169–226.

Scholz, C.H., 1995. Fractal transitions on geological surfaces. In: Barton, C.C., La Pointe, P.R. (Eds.), Fractals in the Sciences. Springer, New York, pp. 131–140. http://dx.doi.org/10.1007/978-1-4899-1397-5_7.

Silva,M.G., Teixeira, J.B.G., Pimentel, M.M., Vasconcelos, P.M., Arielo, A., Franca-Rocha,W., 2005. Geologia e Mineralizações de Fe-Cu-Au do Alvo GT46 (Igarapé Cinzento), Carajás. Caracterização de Depósitos Minerais Em Distritos Mineiros Da Amazônia. ADIMB, pp. 97–151.

Stubley, M.P., 2004. Spatial distribution of kimberlite in the Slave craton, Canada: a geometrical approach. Lithos 77, 683–693. http://dx.doi.org/10.1016/j.lithos.2004.03.008.

Tavares, F.M., 2014. Programa Geologia do Brasil - PGB, Rio Verde, Folha SB.22-Z-A-III, Estado do Pará, Carta Geológica, Escala 1:100.000. CPRM (Companhia de Pesquisa e Recursos Minerais).

Tavares, F.M., 2015. Evolução Geotectônica do Nordeste da Província Carajás (PhD thesis) Universidade Federal do Rio de Janeiro (143 pp).

Tavares, F.M., Silva, C.M.G., 2013. Programa Geologia do Brasil - PGB, Serra Pelada, Folha SB.22-X-C-VI, Estado do Pará, Carta Geológica, Escala 1:100.000. CPRM (Companhia de Pesquisa de Recursos Minerais).

Turcotte, D.L., 1989. Fractals in geology and geophysics. Pure Appl. Geophys. 131, 171–196. http://dx.doi.org/10.1007/BF00874486.

Turcotte, D.L., 1997. Fractals and Chaos in Geology and Geophysics. second Edition. Cambridge University Press, New York (410 pp).

Turcotte, D.L., Huang, J., 1995. Fractal distributions in geology, scale invariance, and deterministic chaos. In: Barton, C.C., La Pointe, P.R. (Eds.), Fractals in the Earth Sciences. Springer US, Boston, MA, pp. 1–40. http://dx.doi.org/10.1007/978-1-4899-1397-5_1.

Vasquez, M.L., Rosa-Costa, L.T., 2008. Geologia e Recursos Minerais do Estado do Pará: Sistema de Informações Geográficas - SIG: texto explicativo dos mapas Geológico e Tectônico e de Recursos Minerais do Estado do Pará. CPRM (Companhia de Pesquisa de Recursos Minerais), Belém (328 pp).

Vasquez, M.L., Rosa-Costa, L.T., Silva, C.M.G., Klein, E.L., 2008. Compartimentação Geotectônica. In: Vasquez, M.L., Rosa-Costa, L.T. (Eds.), Geologia E Recursos Minerais Do Estado Do Pará: Sistema de Informações Geográficas - SIG: Texto Explicativo Dos Mapas Geológico E Tectônico E de Recursos Minerais Do Estado Do Pará. CPRM (Companhia de Pesquisa de Recursos Minerais), Belém, pp. 39–112.

Vearncombe, J.R., Vearncombe, S., 1999. The spatial distribution of mineralization: applicationsf Fry analysis. Econ. Geol. 94, 475–486. http://dx.doi.org/10.2113 /gsecongeo.94.4.475.

Vearncombe, S., Vearncombe, J.R., 2002. Tectonic controls on kimberlite location, southern Africa. J. Struct. Geol. 24, 1619–1625. http://dx.doi.org/10.1016/S0191-8141(01)00152-3.

Veneziani, P., Santos, A.R., Paradella, W.R., 2004. A evolução tectono-estratigráfica da Província Mineral de Carajás: um modelo com base em dados de sensores remotos orbitais (SAR-C RADARSAT-1, TM LANDSAT-5), aerogeofísica e dados de campo. Rev. Bras. Geosci. 34, 67–78.

Walsh, J.J., Watterson, J., 1993. Fractal analysis of fracture patterns using the standard box-counting technique: valid and invalid methodologies. J. Struct. Geol. 15, 1509–1512. http://dx.doi.org/10.1016/0191-8141(93)90010-8.

Weinberg, R.F., Hodkiewicz, P.F., Groves, D.I., 2004.What controls gold distribution in Archean terranes? Geology 32, 545–548. http://dx.doi.org/10.1130/G20475.1.

Williams, P.J., Barton, M.D., Johnson, D.A., Fontboté, L., Haller, A., Mark, G., Oliver, N.H.S., Marschik, R., 2005. Iron oxide copper-gold deposits: geology, space-time distribution and possible modes of origin. Econ. Geol. 100th Anniv. Vol, 371–405.

Xavier, R.P., Monteiro, L.V.S., Moreto, C.P.N., Pestilho, A.L.S., Melo, G.H.C., Silva, M.A.D., Aires, B., Ribeiro, C., Silva, F.H.F.E., 2012. The iron oxide copper-gold systems of the Carajás Mineral Province, Brazil. In: Hedenquist, J.W., Harris, M., Camus, F. (Eds.), Geology and Genesis of Major Copper Deposits and Districts of the World: A Tribute to Richard H. Sillitoe, SEG Special Publication 16. Society of Economic Geologists Inc., pp. 433–454.

Xu, T., Moore, I.D., Gallant, J.C., 1993. Fractals, fractal dimensions and landscapes — a review. Geomorphology 8, 245–262. http://dx.doi.org/10.1016/0169-555X(93)90022-T.

Zhao, J., Chen, S., Zuo, R., Carranza, E.J.M., 2011. Mapping complexity of spatial distribution of faults using fractal and multifractal models: vectoring towards exploration targets. Comput. Geosci. 37, 1958–1966. http://dx.doi.org/10.1016/j.cageo.2011.04.007.

Zuo, R., Agterberg, F.P., Cheng, Q., Yao, L., 2009. Fractal characterization of the spatial distribution of geological point processes. Int. J. Appl. Earth Obs. Geoinf. 11, 394–402.ttp://dx.doi.org/10.1016/j.jag.2009.07.001.

Zuo, R., Carranza, E.J.M., Cheng, Q., 2012. Fractal/multifractal modelling of geochemical exploration data. J. Geochem. Explor. 122, 1–3. http://dx.doi.org/10.1016/j.gexplo.2012.09.009.

CAPÍTULO 3 CONTROLES ESTRUTURAIS EM MINERALIZAÇÕES EPISÓDICAS IOCG DA PROVÍNCIA MINERAL DE CARAJÁS: EVIDÊNCIAS DA ANÁLISE GEOMÉTRICA E DE PALEOTENSÃO DO DEPÓSITO DE SOSSEGO

Durante o desenvolvimento da pesquisa deste mestrado, o seguinte artigo foi submetido para publicação:

Paulo Miguel Haddad-Martim, Carlos Roberto de Souza Filho, Emmanuel John M. Carranza, *Structural controls on episodic IOCG mineralization in the Carajás Mineral Province: insights from geometric and paleostress analyses at Sossego deposit*, ***Precambrian Research***, submetido.

Tipo: *Research paper*

Conceitos Qualis-CAPES do periódico: A1

Fator de impacto (2016): 3.843

O manuscrito como submetido é apresentado nas próximas páginas.

Structural controls on episodic IOCG mineralization in the Carajás Mineral Province: insights from geometric and paleostress analyses at Sossego deposit

Paulo Miguel Haddad-Martim [a], Carlos Roberto de Souza Filho [a], Emmanuel John M. Carranza [a,b]

[a] Institute of Geosciences, State University of Campinas (UNICAMP), Campinas, São Paulo, Brazil

[b] Economic Geology Research Centre (EGRU), James Cook University, Townsville, QLD, Australia.

The Sossego deposit is one of the largest IOCG deposits and the first copper mine to be operated in the Carajás Mineral Province (CMP). Previous recent studies have shown that its orebodies have formed in two distinct mineralizing events: the Pista-Sequeirinho-Baiano orebodies were formed during the Neoarchean (2.71–2.68 Ga) and the Sossego-Curral orebodies during the Paleoproterozoic (1.90–1.88 Ga). Geometric and paleostress analyses of available data allowed the discrimination of different tectonic events that controlled the deposit. Prior to mineralization, the area was affected by sinistral transpression directed to NNE–SSW. During the Neoarchean mineralization event, the area was affected by a NW–SE extension. The Paleoproterozoic mineralization event occurred during a NW–SE dextral transpression. The arrangement of structures in relation to stress tensors was a key factor that induced the formation of orebodies so close in space but in different time periods and with different morphologies. The change in the tectonic regime from the Neoarchean to the Paleoproterozoic was accompanied by crustal uplift and changes in hydrothermal alteration assemblages, which, taken together, explain the differences observed between the two groups of orebodies. The model for structural control on the Sossego deposit discussed here provides valuable insights for future studies focused on the relationship between tectonic events and mineralization in the CMP.

Keywords: IOCG deposit; Carajás; Sossego deposit; Paleostress analysis; Structural control

1. Introduction

Mineral deposit formation is the result of a complex interplay of geological processes or controls. For the formation of iron oxide-copper-gold (IOCG) deposits, one major control is the genesis and evolution of the structural framework or the plumbing system (Hitzman, 2000; Williams et al., 2005). The presence and effectiveness of structural controls may vary over time, resulting in episodic mineralization events (Hazen et al., 2014). Despite its importance for accumulating metals over time, episodic mineralization can be difficult to detect, as it usually demands detailed surveys to be identified. This is the case for the IOCG deposit at Sossego, located in the Carajás Mineral Province (CMP), Brazil.

Many previous researches have considered all orebodies at Sossego as contemporaneous, and their formation being related to a single tectonic environment albeit at different crustal levels (Carvalho, 2009; Domingos, 2009; Monteiro et al., 2008a; Xavier et al., 2008). However, the more recent research of Moreto et al. (2015b) has indicated the existence of a gap of ~780 Ma between the formation of two sets of orebodies (Pista-Sequeirinho-Baiano and Sossego-Curral) despite their close (< 1 km) spatial proximity. In light of this new geochronological framework, a re-examination of available structural data from previous studies, in conjunction with new data, is fundamental to evaluate the structural control for the Sossego deposit. Such reassessment could prove useful to better understand its genesis and those of other IOCG deposits in the CMP.

Studying the structural control of IOCG deposits in Carajás is challenging, mainly because the region experienced a long evolution, marked by several deformation events (Holdsworth and Pinheiro, 2000; Pinheiro and Holdsworth, 1997). Here we subject fault data available for the Sossego deposit to paleostress analysis coupled with geometric analysis per structural domain. This analytical approach, which has not been used by previous studies (cf. Carvalho, 2009; Domingos, 2009; Monteiro et al., 2008a; Moreto et al., 2015b) allowed a better understanding of processes responsible for the formation of the diachronous Sossego orebodies. Moreover, we address structural aspects for the origin of the pipe breccia at Sossego-Curral orebodies, an issue that has not been addressed in detail by earlier researches.

Our analyses are supported and integrated with information from previous researches that have described in detail the hydrothermal alteration (Carvalho, 2009; Monteiro et al., 2008a,b), structural framework (Domingos, 2009) and geochronology (Moreto et al., 2015b) for the Sossego deposit. Investigating how these aspects are linked to the structural

evolution at the deposit scale could prove critical to addressing regional-scale geological issues, such as the relation between the tectonic evolution of the CMP and the formation of IOCG deposits.

2. Regional context: the Carajás Mineral Province

The CMP is located in the Amazon craton, northern Brazil, specifically in the Carajás Tectonic Domain (Santos, 2003), which is composed of two segments: (1) a Transition Subdomain, to the south, and (2) the Cover Assemblage, to the north (Pinheiro, 1997; Pinheiro and Holdsworth, 1997). The Transition Subdomain is composed of gneisses from the Xingu Complex and granulites from the Pium Complex, both dated to the Archean (Pidgeon et al., 2000; Silva, 2014). The Cover Assemblage is composed of two metamorphosed volcano-sedimentary units (the Rio Novo Group and the Itacaiúnas Supergroup) and a sedimentary unit (the Águas Claras Formation) (Nogueira et al., 1995; Vasquez et al., 2008). At least two important magmatic events have affected the Transition Subdomain and the Cover Assemblage: (1) intrusions of layered mafic-ultramafic rocks (e.g., Luanga Complex) and granites (e.g., Planalto Suite) during the Neoarchean (~2.7 Ga); and (2) intrusion of anorogenic granites (e.g., Central Granite) during the Paleoproterozoic (~1.88 Ga).

Several tectonic models have been proposed for the Carajás region (Araújo and Maia, 1991; Pinheiro, 1997; Rosière et al., 2006; Tavares, 2015; Veneziani et al., 2004). Most of these models support the notion that the structural framework of the Carajás Tectonic Domain resulted from an alternating series of transpressional and transtensional reactivations. Pre-existing Archaean ductile fabrics developed initially in the basement controlled the geometry of subsequent brittle-ductile and brittle tectonic features. These ductile fabrics are characterized mainly by E–W and WNW–ESE-trending moderately to steeply dipping shear zones, represented by the Cinzento and Carajás strike-slip systems, as well as the Canaã shear zone (Fig. 1) (Domingos, 2009; Pinheiro and Holdsworth, 1997).

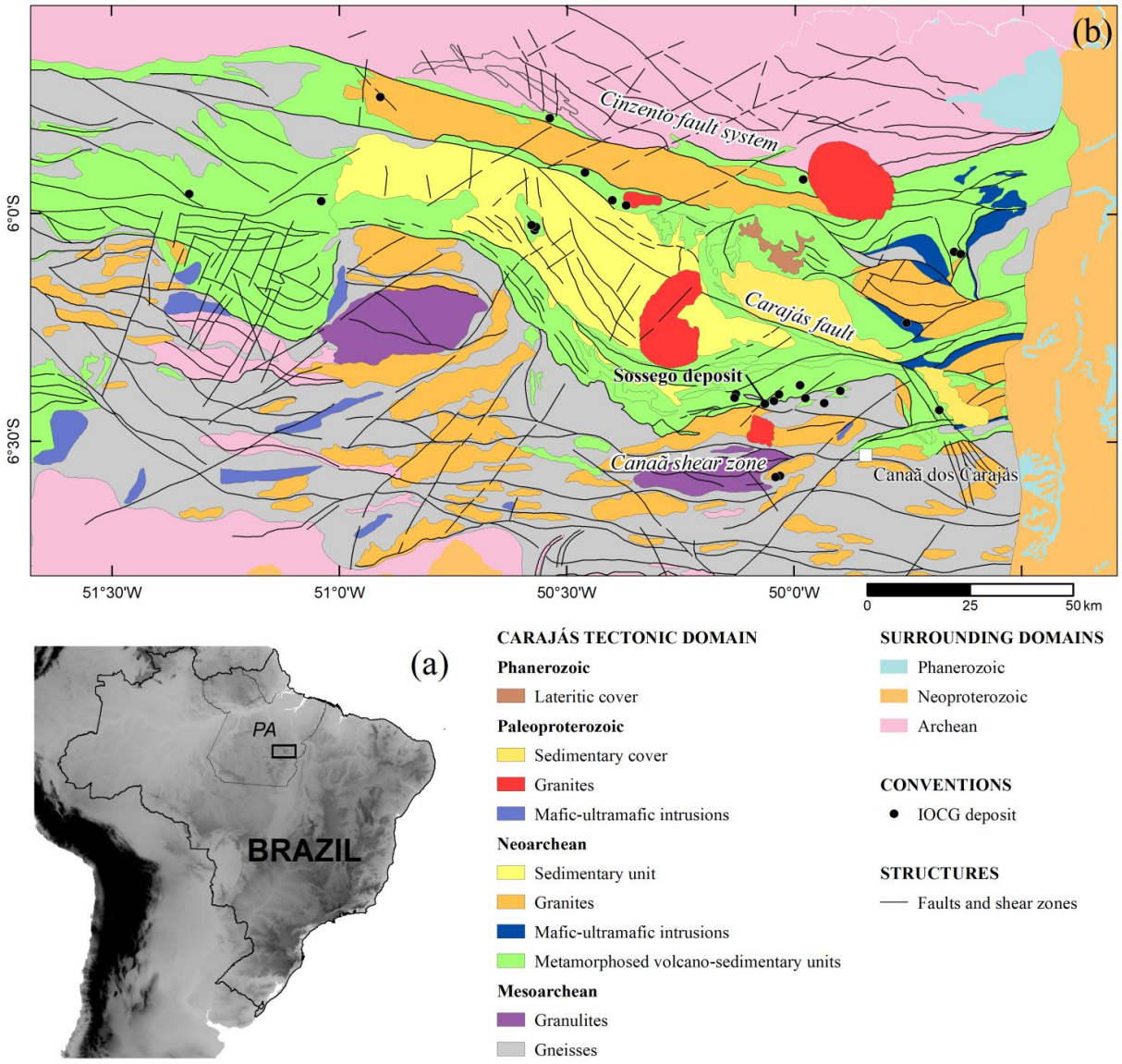

Fig. 1: (a) Location of the study area in southeast Pará State (PA). (b) Simplified regional lithological-structural map of the Carajás Tectonic Domain, where the Sossego deposit is located (modified from Vasquez and Rosa-Costa, 2008).

3. The Sossego deposit

Sossego is a world-class IOCG deposit that came into production in 2004, with mining operations conducted by Vale Company. It is located ~30 km NW of Canaã dos Carajás city (Fig. 1). It is one of the largest IOCG deposits in the region, with estimated resources of 245 Mt at 1.1 wt. % Cu, 0.28 g/t Au (Xavier et al., 2012). The deposit is hosted near the contact between metabasalts of the Itacaiúnas Supergroup (~2.76 Ga) and tonalitic to trondhjemitic gneisses and migmatites of the Xingu Complex (~3.0 Ga). This contact is

located on the northern limits of the Canaã shear zone (Fig. 1) – a set of subvertical ductile shear zones trending WNW–ESE (Domingos, 2009; Pinheiro et al., 2013). Mineralization is distributed amongst five orebodies, which form two groups according to their position and characteristics: Pista-Sequeirinho-Baiano and Sossego-Curral (Fig. 2). In these orebodies, chalcopyrite is the main ore mineral but with local concentrations of pyrite at Sossego and pyrrhotite and pyrite at Sequeirinho.

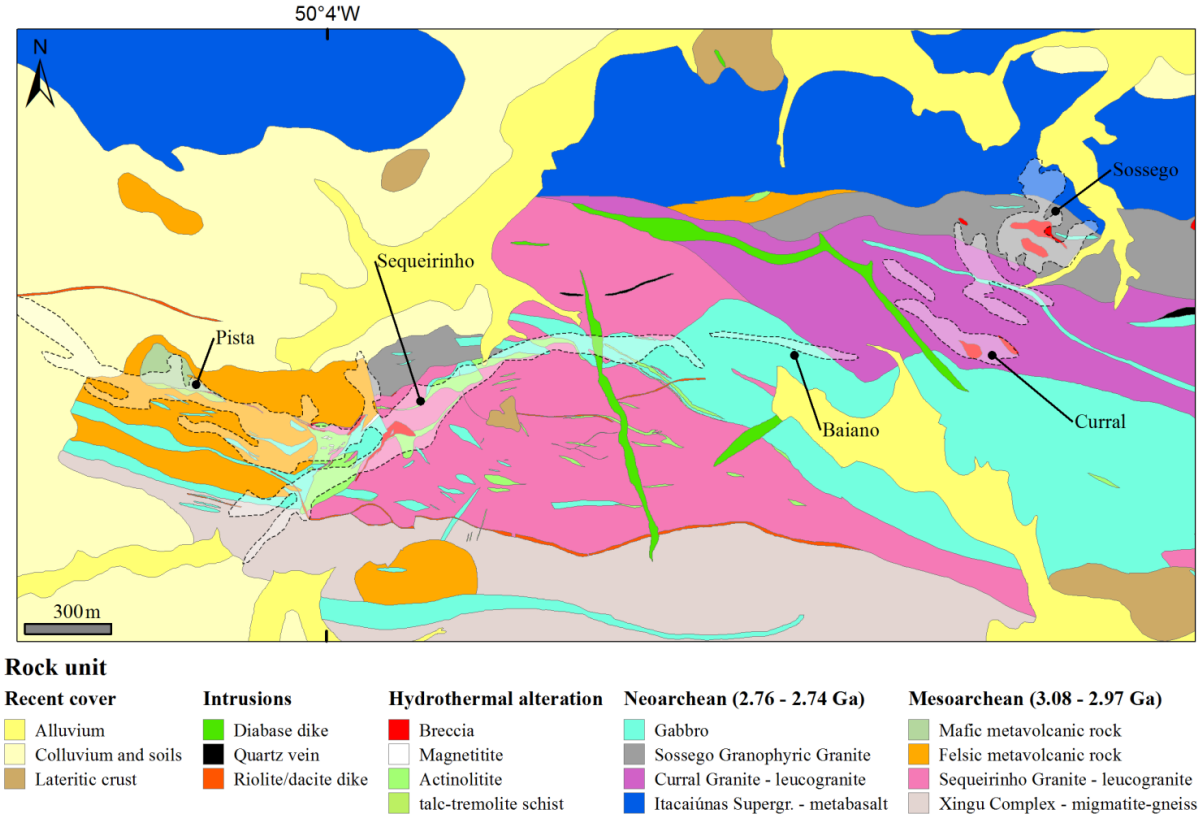

Fig. 2: Sossego deposit geological map (slightly modified from Vale Company map). Dashed outlines are limits of the orebodies projected onto the horizontal plane of the map.

The Pista-Sequeirinho-Baiano mineralization comprises a series of elongated orebodies concordant with the surrounding foliation and shear zones. These orebodies, which define an "S-shaped" form with tips elongated to WNW–ESE and the center to NE–SW (Fig. 2), occur in the hanging wall of major WNW–ESE to NE–SW-trending, steeply-dipping faults (Domingos, 2009; Monteiro et al., 2008a). Hydrothermal alteration is usually more intense in decametric zones along those faults. The Sequeirinho orebody corresponds to the bulk of

mineralization and is characterized by tabular bodies of breccia, dipping steeply to the SE. It is hosted mainly within the Sequeirinho Granite and close to gabbro intrusions, but also within felsic metavolcanic rocks (Fig. 2). The orebody is located in a corridor where structures have dominant trends of NE–SW, while in both flanks structures trend WNW–ESE (Domingos, 2009). The Baiano orebody contains disseminated to venular ore, hosted mainly within gabbros. The Pista orebody consists of disseminations along fractures, foliation planes and small tabular bodies of breccias and sulfide veins, mostly within sheared felsic metavolcanic rocks. An early sodic and then a later sodic–calcic alteration have intensely affected the host rocks of the Pista-Sequeirinho-Baiano orebodies (Monteiro et al., 2008a). The sodic–calcic alteration is associated with replacive actinolite and magnetite bodies that hold later, subvertical, breccia-hosted copper–gold mineralization (Monteiro et al., 2008a). Massive magnetite and actinolite occur as breccia clasts within a matrix of hydrothermal minerals, including sulfides.

The Sossego-Curral orebodies represent an independent feature characterized as vertical pipe breccias with sharp boundaries (Carvalho, 2009; Domingos, 2009), the surface projections of which are elliptical (Fig. 2). The breccias are surrounded by a stockwork of sulfide veins hosted mostly by the Sossego and Curral granites, although some mineralized zones are present within felsic metavolcanic rocks (Monteiro et al., 2008a). Ore breccias comprise angular fragments of the altered host rocks and have open-space filling textures (Monteiro et al., 2008a). Most early sodic alteration at Sossego-Curral has been telescoped by later potassic alteration, which is well developed in the Sossego and Curral orebodies and occurs in replacement zones close to mineralization. The potassic-altered rocks at Sossego-Curral are cut by chlorite veins, and chlorite replacement zones broadly envelope the area of potassic alteration. The latest stage of alteration is represented by a poorly mineralized zone of hydrolytic alteration (Monteiro et al., 2008a).

The bulk characteristics of the mineralization have led previous studies to interpret Sossego deposit as the result of hydrothermal alteration when a predominantly brittle–ductile regime transitioned to a brittle structural regime, with the brittle conditions at both the Sequeirinho and Sossego segments being associated with late sulfide mineralization (Carvalho, 2009; Domingos, 2009; Monteiro et al., 2008a). Evidence for deformation after the mineralization in Pista-Sequeirinho-Baiano orebodies is present in restricted areas with deformed sulfides, while in Sossego-Curral orebody there is no evidence for important deformation events after its formation.

Despite noticeable differences in alteration assemblages, structural characteristics and host rocks, previous studies considered all orebodies to be contemporaneous (Carvalho, 2009; Domingos, 2009; Monteiro et al., 2008a,b). These studies hypothesized that the observed differences would be the result of Sequeirinho orebody being formed at deeper crustal levels in relation to Sossego, and then being juxtaposed laterally due to crustal block uplift. In contrast, Moreto et al. (2015b) indicated that the different groups of orebodies are not contemporaneous because U-Pb dating of hydrothermal monazite and Re-Os dating of molybdenite indicated ages of ~2.71–2.68 Ga for the Sequeirinho and Pista orebodies, whereas monazite from the Sossego-Curral orebodies produced ages of ~1.90–1.88 Ga. This new geochronological framework hints to episodic mineralization at Sossego, although the structural control that acted on each event is not known.

4. Materials and methods

The analyzed data consist of structural measurements and maps, as well as a 3D fault model based on drillhole data. Most of the data were provided by the Vale Company, and these include measurements from mine benches by Domingos (2009). These data are complemented with measurements collected by us during two field trips to the mine pits. Structural maps were compiled by us based on internal maps from Vale Company, as well as from previous studies (Domingos, 2009; Moreto et al., 2015b).

The data were analyzed following a three-step workflow: (i) definition of structural domains based on geological and structural maps, with the support of strike *vs*. distance diagrams (Marshak and Mitra, 1988) and rose diagrams for mapped structures; (ii) basic geometric analysis per structural domain, with support of equal-area nets, rose diagrams and rake histograms (Davis and Reynolds, 1996; Marshak and Mitra, 1988); and (iii) paleostress analysis using the TENSOR software (Delvaux and Sperner, 2003). Equal-area diagrams and data contouring were made using Orient 3.6.0 software (Vollmer, 1995,2016) and rose diagrams using MARD (Munro and Blenkinsop, 2012).

5. Results

5.1. Structural domains definition

The Sossego deposit is located in an area that records multiple deformational events (Moreto et al., 2015a). To identify different deformational phases and their spatio-temporal relationships, we divided the Sossego area into three structural domains, based on

the rock units affected and their dominant structural characteristics. These characteristics include the distribution and shape of rock bodies, the orientation of mapped structures, and structural measurements (Fig. 3).

Structural domain I, located on both sides of the Sequeirinho orebody, is characterized by rock bodies elongated to WNW–ESE conforming to the regional mylonitic foliation. The main constituting units are the Xingu Complex, Sequeirinho Granite, felsic metavolcanic rocks and gabbros. This domain includes Pista and Baiano orebodies, which are elongated according to the foliation and unit contacts (Fig. 3).

Structural domain II is located along the Sequeirinho structural corridor following NE–SW shear zones (Fig. 3b). Its northern and southern limits cross-cut geological units. At its center, the domain is characterized by the re-orientation of geological units of structural domain I to the NE–SW direction, more clearly marked on foliation measurements within the Sequeirinho pit (Fig. 4). Moreover, domain II comprises the majority and the largest hydrothermal rock bodies, which include actinolitites, magnetitites and the Sequeirinho orebody (Fig. 3a). Hydrothermal rock bodies in this domain are hosted mostly within Sequeirinho Granite and gabbros, but also within thinner layers of granophyric granite. According to Domingos (2009), the deflection of geological units in this corridor reflects sinistral kinematics, probably with an offset of hundreds of meters.

Structural domain III includes the Sossego and Curral brecciated orebodies, which present elliptical shapes when projected onto a map (Fig. 3a). The domain is characterized by rock bodies oriented WNW–ESE, similar to structural domain I. This domain is separated from domain I by a WNW–ESE-trending shear zone which marks an important contact between rock units, with this domain comprising almost the whole of the Sossego granophyric granite and Curral granite at the deposit (Fig. 3a). Additionally, the structural morphology of a vertical pipe breccia for Sossego-Curral orebodies is unique in the deposit, and is accompanied by potassic and hydrolytic alteration that is limited to structural domain III (Fig. 3c).

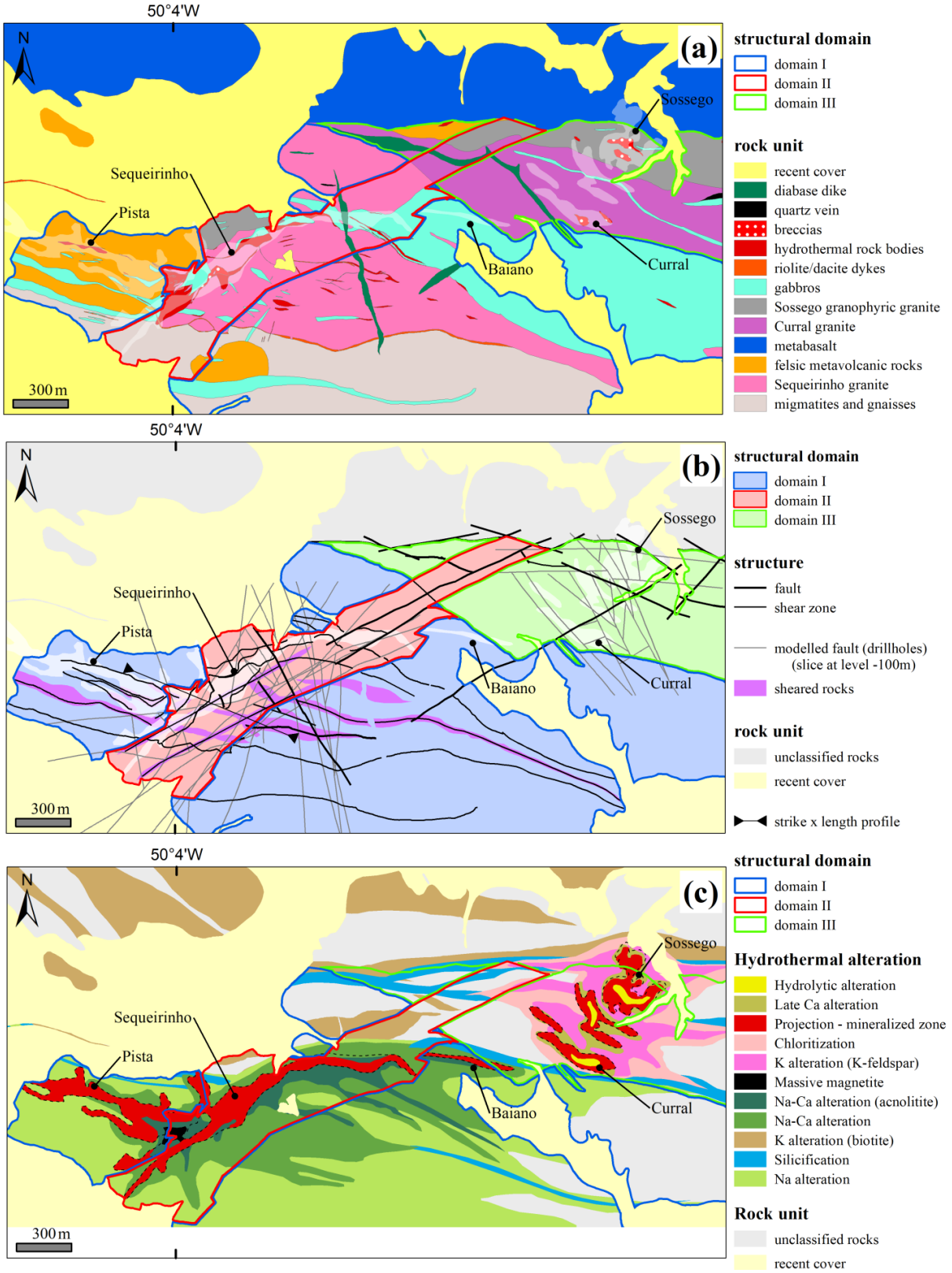

Fig. 3: Structural domains at Sossego deposit and their relationship with: (a) rock units, (b) mapped and modeled structures and (c) hydrothermal alteration. Maps are adapted from Vale Company, Domingos (2009) and Monteiro et al. (2008a).

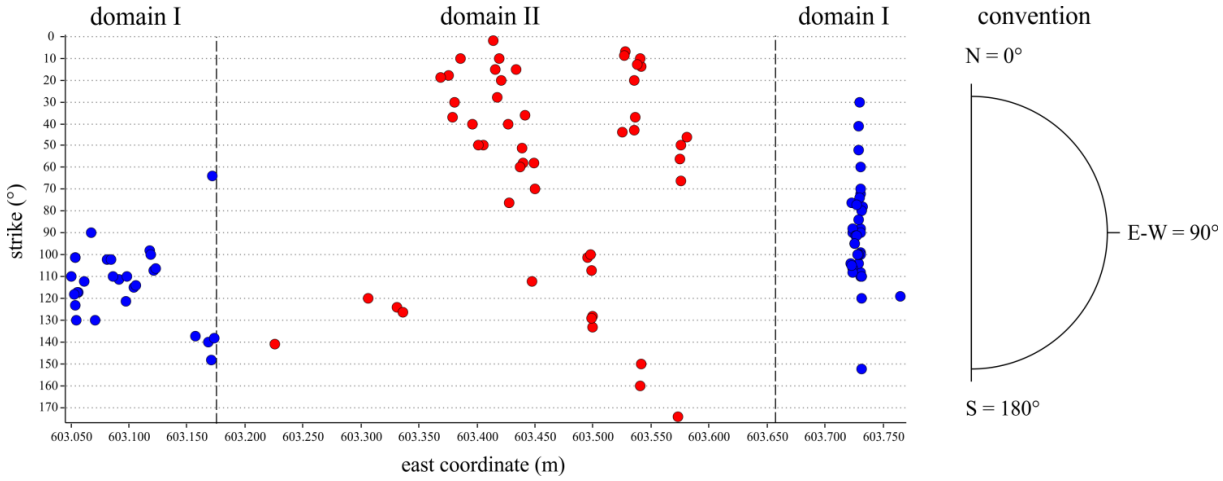

Fig. 4: Foliation strike *vs*. distance diagram along a WNW–ESE profile through domain II. Profile location is marked on Fig. 3b. Measurements taken around the mine pit were projected onto the profile. Diagram indicates that NE–SW-trending foliations predominate in domain II (red dots), whereas WNW–ESE-trending foliations predominate in domain I (blue dots).

5.2. Geometric analysis – map structures

Structural domain I is characterized by narrow and long WNW–ESE-trending shear zones, with local formation of biotite schists in the metavolcanic rocks and granites. Domingos (2009) and Moreto et al. (2015b) interpret these shear zones to have sinistral kinematics. Faults with northerly–southerly orientation, discordant to rock foliation, are infrequent on the geological map, but abundant in the drillhole data model (Fig. 5). The 3D fault model indicates that the NNW-trending faults are subvertical, parallel to the largest diabase dike on the map, and do not appear to significantly displace the geological units in plan view.

Structural domain II is characterized by the occurrence of WNW-trending shear zones similar to those in domain I, truncated by long NE–SW-trending shear zones, occasionally with the development of biotite schists, usually on mineralization footwall (Monteiro et al., 2008a). These shear zones have sinistral kinematic interpretation (Moreto et al., 2015b). Sinistral faults with the same orientation as the NE–SW-trending shear zones also occur (Domingos, 2009). Faults modeled from drillhole data have the same behavior: NE–SW-trending faults dipping moderately to the SE, locally cut by NNW–SSE-trending faults that extend from domain I (Fig. 5).

Structural domain III is characterized by the absence of expressive ductile shear zones – unlike observed in the other two domains – although an important E–W-trending shear zone with biotitization is described to the north (Fig. 3c). Mapped structures are NE–SW- and WNW–ESE-trending faults, forming a rhombic pattern (Fig. 3b). The fault model from drillhole data indicates abundance of NNW–SSE-trending faults (Fig. 5), which are subvertical faults and cut by two parallel E–W-trending faults, with steep dips to the S.

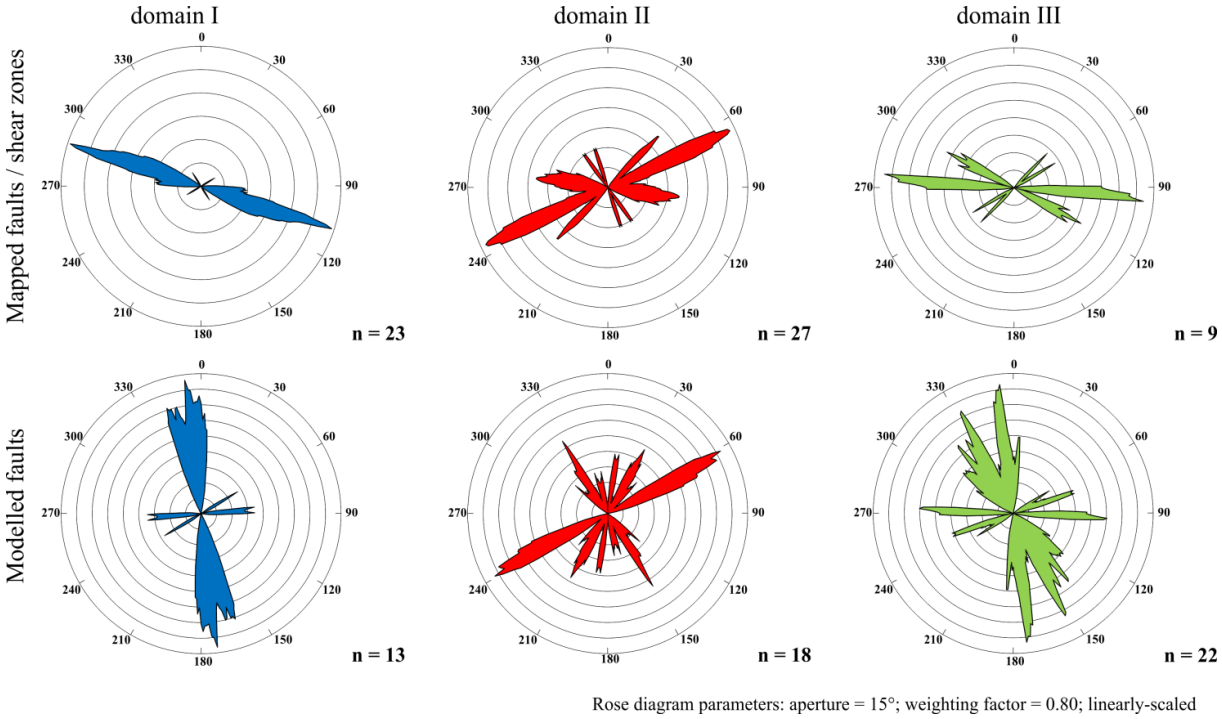

Fig. 5: Rose diagrams for orientations of faults and shear zones in each structural domain (see Fig. 3b). Diagrams at the top comprise data from mapped faults and shear zones, whereas those at the bottom comprise data from modeled faults based on drillhole data provided by Vale Company. Where necessary, faults were assigned to the domain that contained most of the fault's extension.

5.3. Geometric analysis – field measurements

In structural domain I, foliation has clear subvertical WNW–ESE trends, parallel to mapped structures and unit contacts in the domain (Fig. 6a). Mineral lineations measured on foliation planes suggest a dominantly vertical kinematics, probably inverse, as a result of NE–SW compression (Fig. 6b) (Domingos, 2009). Shear zones form two distinct families: (a) subvertical NW–SE trend, slightly oblique to foliation; and (b) nearly orthogonal to (a) with a

NE–SW trend and dipping steeply to SE (Fig. 6c). Shear zones of family (b) are nearly parallel to shear zones in domain II.

Faults exhibit considerable variation in direction, but usually with steep dips (Fig. 6d). Two families of faults stand out: (a) E–W-trending faults steeply dipping to the S; and (b) NW–SE-trending faults steeply dipping to the NE. NE–SW-trending faults tend to have gentler dips to the SE. Fault trending N–S form a subordinate group, barely noticeable in the equal-area plot. Slickenlines measured on fault planes also exhibit great diversity of orientations, from which two groups can be highlighted: (a) a main group, with steep plunges, with maxima roughly parallel to mineral lineation direction; and (b) a subsidiary group, with gentle plunges, suggesting lateral movement in the E–W direction (Fig. 6e). Note that in spite of the significant variation in fault direction, slickenlines are predominantly related to E–W-trending faults. Also, it is noteworthy that despite being a relevant fault population, NW–SE-trending faults dipping to the NE have few slickenlines measured. Mineralized veins are not well-represented in the available data from domain I (Fig. 6f).

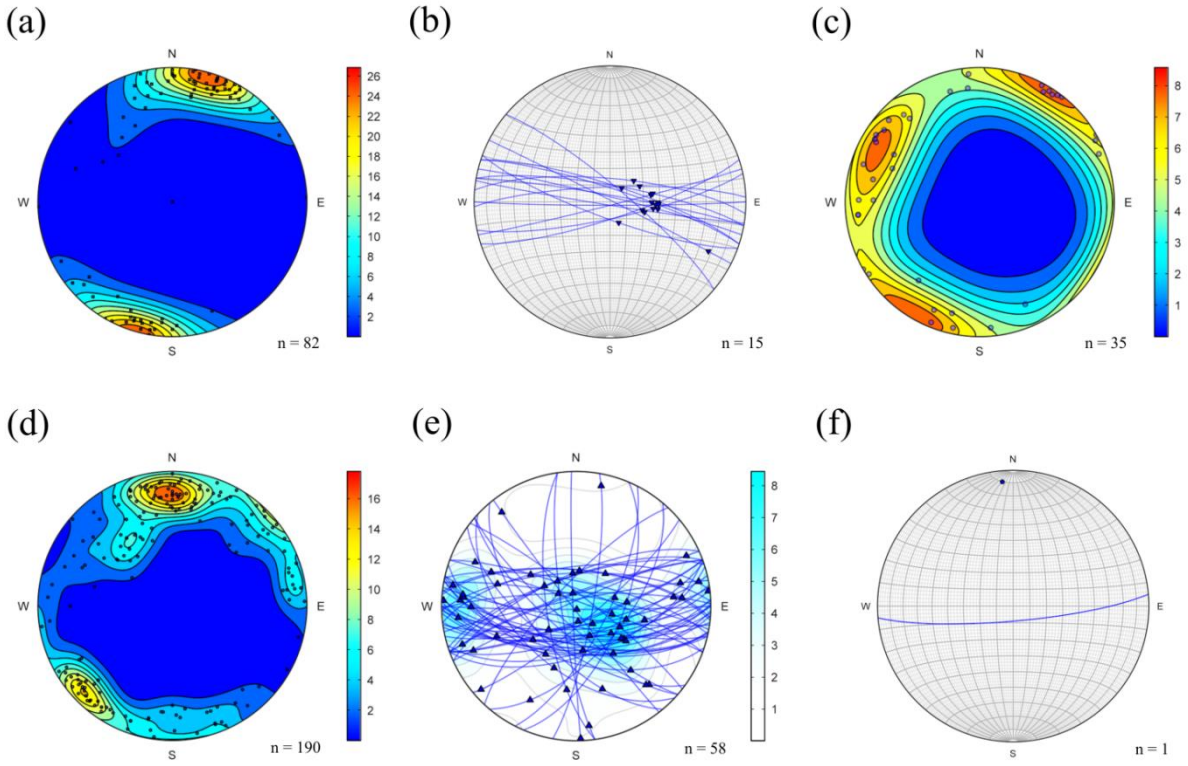

Fig. 6: Equal-area plots (lower hemisphere) for structures in domain I: (a) foliation planes; (b) mineral lineation on foliation; (c) shear zones; (d) faults; (e) slickenlines on fault planes; (f) mineralized veins.

In structural domain II, foliation planes are concentrated in the NE–SW direction, and especially in the NNE–SSW trend, with steep-to-moderate dips to the SE and E (Fig. 7a). Foliation direction is roughly parallel to the direction of the Sequeirinho corridor, showing a clear change when compared to domain I. Mineral lineations measured on foliation planes have steep plunges (Fig. 7b), suggesting a predominantly vertical stretching direction (Domingos, 2009). Also, lineations are predominantly found on NE–SW foliation planes.

Poles to shear zones occupy the entire NW quadrant, indicating a preferred NE–SW direction, parallel to the faults that define the Sequeirinho corridor. In addition, shear zones have moderate-to-steep dips to the SE (Fig. 7c). Subvertical NW–SE-trending shear zones are also observed, roughly parallel to the main trend of shear zones in domain I.

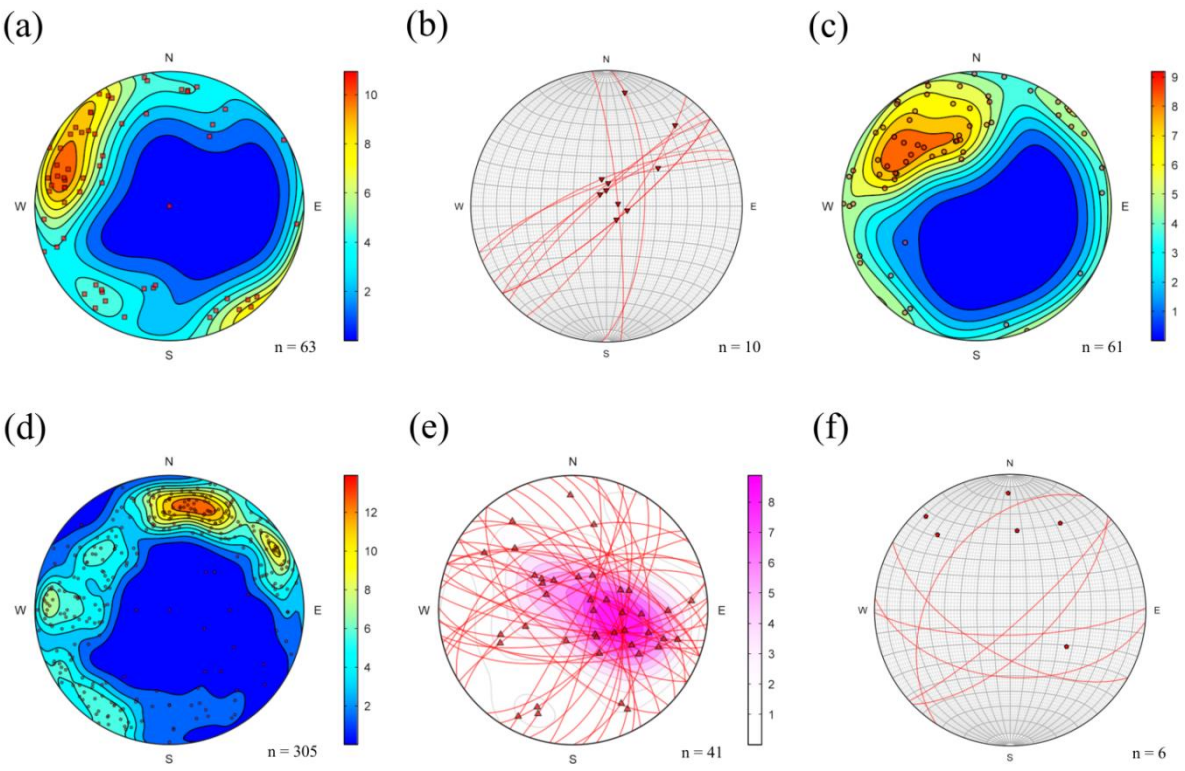

Fig. 7: Equal-area plots (lower hemisphere) for structures in domain II: (a) foliation planes; (b) mineral lineation on foliation; (c) shear zones; (d) faults; (e) slickenlines on fault planes; (f) mineralized veins.

Faults in domain II show large variation of direction and moderate-to-steep dips. Three main families are highlighted: (a) E–W-trending faults with steep-to-moderate dips to the S; (b) NW–SE-trending faults with steep-to-moderate dips to the SW and NE; and (c) N–S- and NE–SW-trending faults dipping to the E and SE, frequently more gently than in (a) and (b) (Fig. 7d). In general, fault distribution in domain II is similar to that in domain I, the main difference being the fact that NW–SE-trending faults in domain II dip predominantly to the SW, but to the NE in domain I.

Slickenlines measured on fault planes show moderate plunges and variable direction (Fig. 7e). The position for the distribution maximum is similar to that in domain I. Slickenlines are found on fault planes with diverse orientation, but with a slight predominance of NW–SE direction. Few measurements that are available for mineralized veins indicate NE–SW to E–W direction, with moderate-to-steep dips (Fig. 7f).

In structural domain III, foliation planes are poorly represented (Fig. 8a). Shear zones define two families: (a) WNW–ESE trend with steep dips to the S; (b) roughly N–S trend, subvertical (Fig. 8b). As in domain I, the WNW–ESE direction predominates.

For domain III, faults can be divided in two populations (Fig. 8c): (a) the main population of subvertical NNW–SSE-trending faults; and (b) a secondary population of ENE–WSW-trending faults with steep-to-moderate dips to the S. Fault trends are roughly opposite to those of the shear zones, but they all dip to the same directions. Slickenlines measured on fault planes have a rather variable orientation, with plunges changing from steep to gentle (Fig. 8d). Subvertical slickenlines exhibit a maximum that roughly coincides with the orientation of the maxima for striae in domains I and II. Slickenlines are found predominantly in NNW–SSE and ENE–WSW trending faults.

In structural domain III, mineralized veins are widespread (Fig. 8e). Two well-defined families are observed, although both exhibit lateral scattering of trends: (a) veins with E–W direction (with slight asymmetry to NW–SE), with steep dips to the S and SW; and (b) veins with N–S direction (with slight asymmetry to NNE–SSW), with steep dips to the E. Vein populations with similar orientations have been described in the regional framework of Canaã dos Carajás (Domingos, 2009). Slickenlines measured on surfaces of mineralized veins suggest a predominantly lateral movement, parallel to the two main directions of the veins, but more commonly in the N–S family (Fig. 8f). The presence of such striations suggests that

at least part of the mineralized veins have a shear component in their formation, probably related with the development of similarly oriented faults (Domingos, 2009).

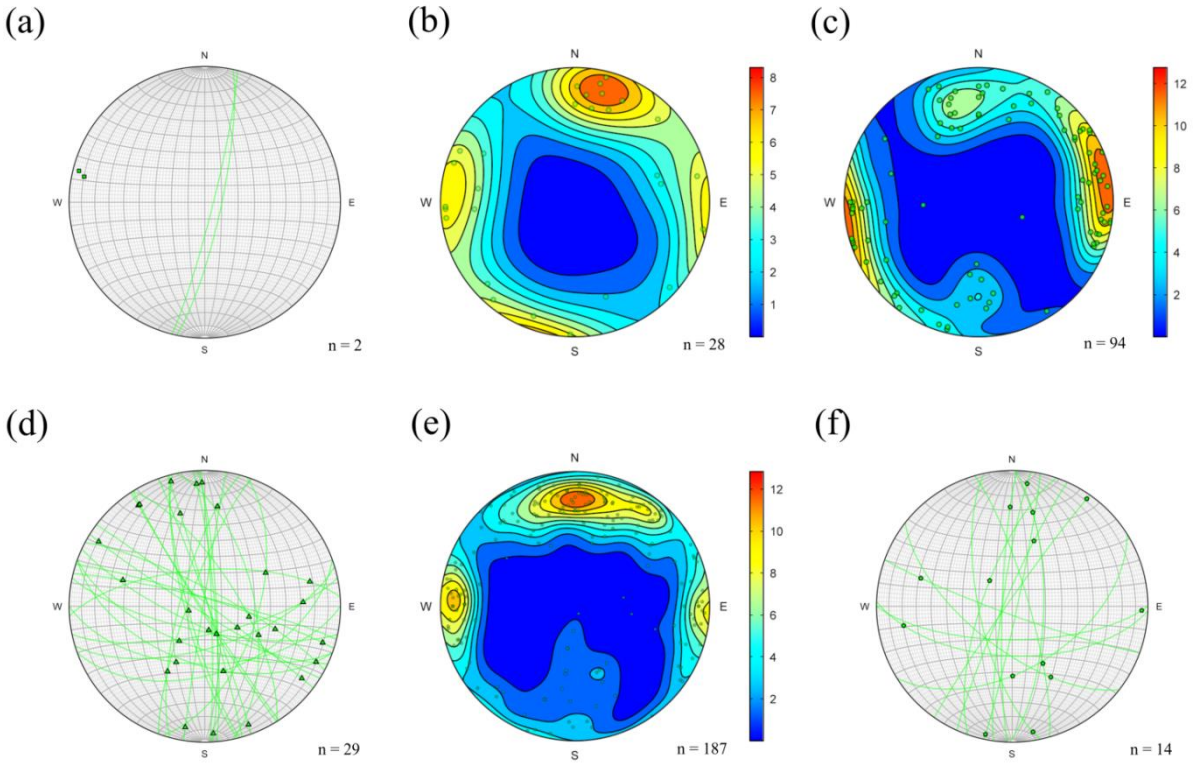

Fig. 8: Equal-area plots (lower hemisphere) for structures in domain III: (a) foliation planes; (b) shear zones; (c) faults; (d) slickenlines on fault planes; (e) mineralized veins; (f) slickenlines on mineralized veins.

5.4. Kinematic analysis of slickensides and slickenlines

Regional interpretation indicates that the Sossego deposit is located in an area that has been subjected to several deformational events (Moreto et al., 2015a; Pinheiro and Holdsworth, 1997). In fact, fault data from Domingos (2009) show variable trends, and dip-slip, strike-slip, and oblique faults are present (Figs. 6, 7, 8). However, assigning faults to different populations is not straightforward because their temporal relation is not well constrained due to the unclear nature of their cross-cutting relations, lack of offset markers and paucity of sense indicators (Domingos, 2009). These characteristics led previous authors to interpret that the bulk of faults at Sossego deposit slipped contemporaneously. However,

newer geochronological data (Moreto et al., 2015b) show that the Sequeirinho and Sossego orebodies are not contemporaneous, but were formed ~2.7 Ga and ~1.8 Ga, respectively. This new geochronological information led us to reinterpret available existing fault data to account for the plausibility that faults at Sossego record at least two deformation events.

In this context, measured slickenlines provide evidence for the existence of at least two groups of structures: the first indicates a predominantly vertical movement, and the second indicates a dominantly horizontal movement. The separation of slickenlines into two groups is suggested mainly by the bimodal character of plunges (and rakes) of slickenlines (Figs. 9, 10), together with the fact that both groups occur with wide directional variation and with no clear separation by fault orientation (Fig. 11). Also, it is important to note that most faults have subvertical dips and thus plunges have large correlation with rakes. This indicates that plunge represents well the kind of dislocation affecting faults (vertical or horizontal), which would not be the case if gently dipping faults were present. The threshold for population separation was defined as a plunge of 40°, since this value is typical for the gap between the populations in the diagrams for all structural domains (Figs. 9, 10).

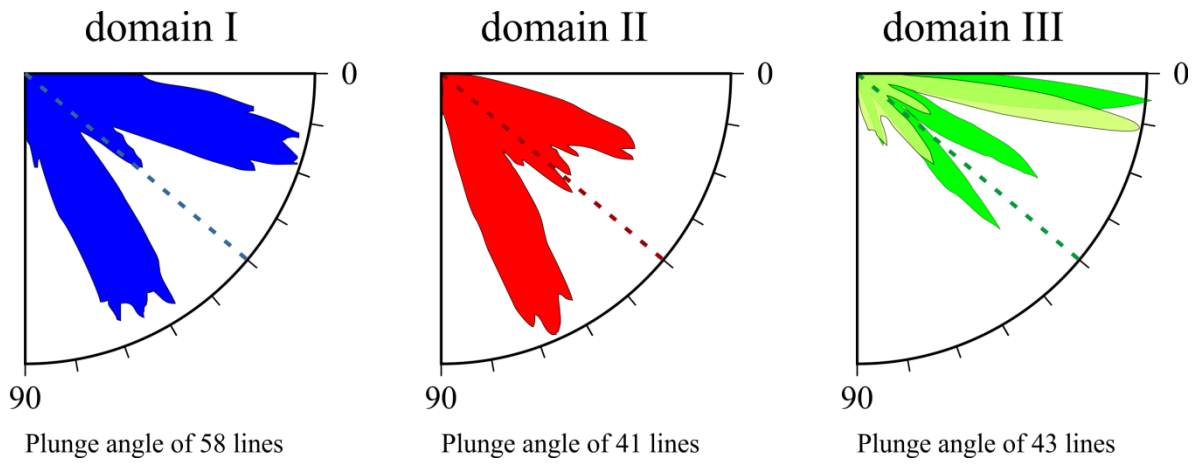

Fig. 9: Plunge diagrams for slickenlines in domains I, II and III. For domain III, data are separated into slickenlines measured on faults (paler green) and mineralized veins (darker green). Dashed lines indicate the 40° plunge threshold. Diagram parameters: aperture = 15°; weighting factor = 0.85; linearly-scaled.

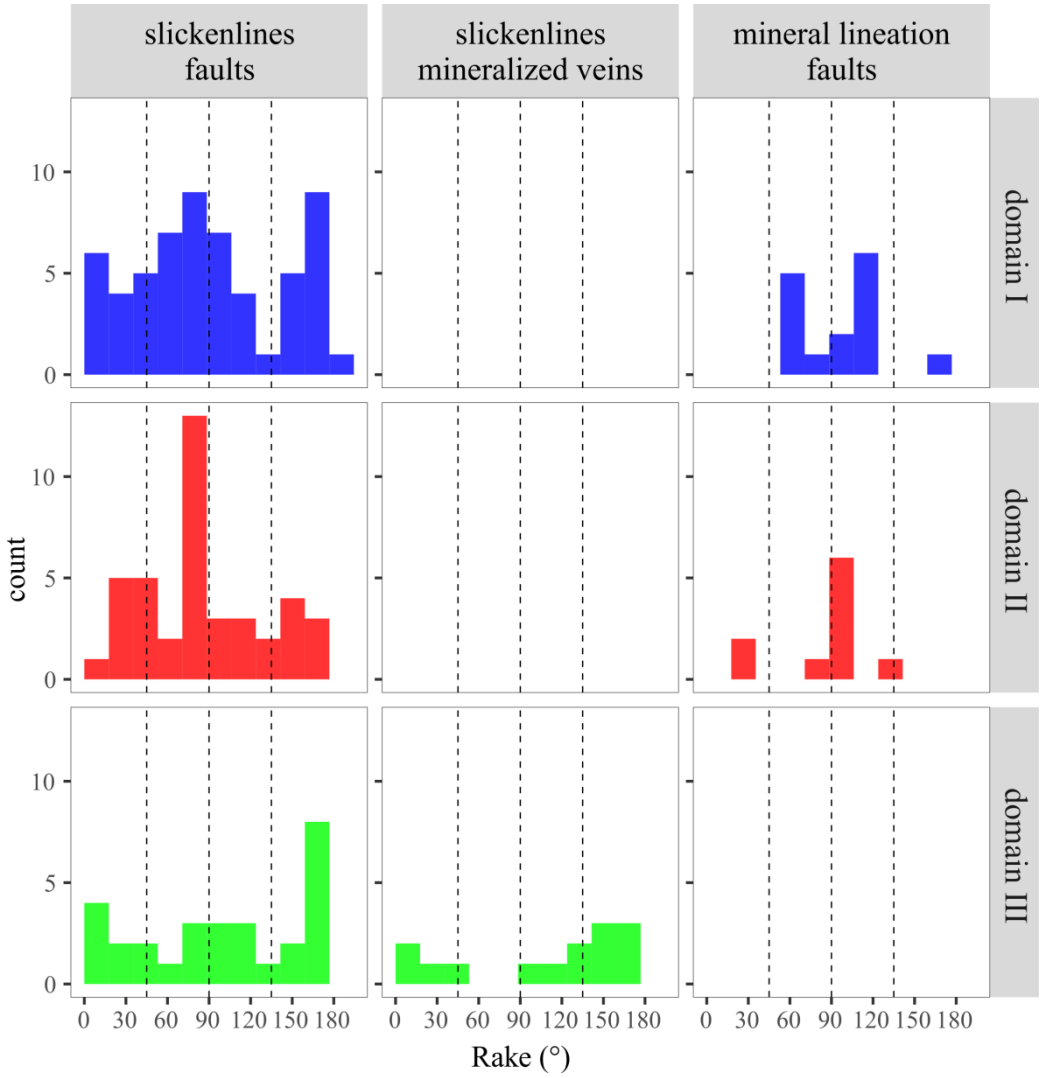

Fig. 10: Rake histograms for lineations at Sossego deposit. Data are separated by structural domains and by structure type. Dashed lines are shown for reference (rakes of 45°, 90° and 135°).

Slickenlines indicate the slip direction of a fault and, as such, planes with similar orientation but with striae almost orthogonal are most likely the result of multiple events of slipping (Fossen, 2010). At Sossego, planes with such characteristics are observed in all domains (Fig. 11). Steeply-to-gently dipping striae are found dispersed all over the mine site, with broad spatial distribution. Since there is no consistent spatial separation between faults with slickenlines with steep and gentle rakes, the presence of which may suggest a spatial grouping of contemporaneous structures, these structures most likely developed during independent events – although previous works do not indicate the presence of cross-cutting relationships between striae. It has been argued by Domingos (2009) that the slickenlines occur close to the intersection of fault planes, which would suggest contemporaneous slipping

of fault planes, but this characteristic is only locally observed and usually does not involve the striae with low rake values, suggestive of lateral displacements.

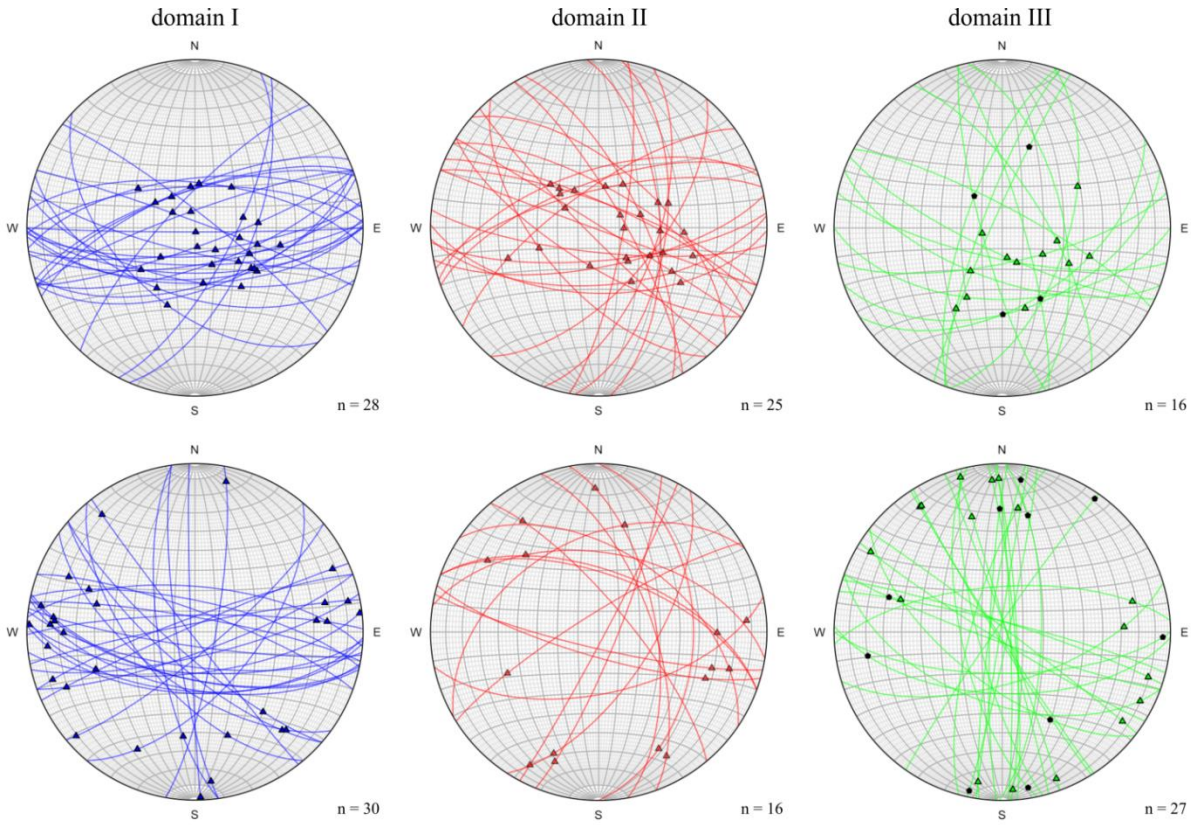

Fig. 11: Equal-area diagrams (lower hemisphere) for fault slickenlines, separated in two groups, accordingly to their plunge: steep plunge (> 40°, top) and gentle plunge (≤ 40°, bottom). For structural domain III, data for mineralized veins are also shown (black dots).

In this context, the recent study by Moreto et al. (2015b), which suggests that Sequeirinho and Sossego orebodies are not contemporaneous, agrees well with the available existing fault data (Domingos, 2009). It is noticeable that gently plunging slickenlines predominate in the Sossego orebody area, especially those observed in mineralized veins (Figs. 9, 10, 11), suggesting that lateral movement is contemporaneous with mineralization at Sossego-Curral orebodies, and thus affected the structural domain III at ~1.8 Ga. The opposite pattern is observed at Sequeirinho, which is located at structural domain II, where faults with steeply plunging slickenlines predominate, suggesting that vertical movements prevailed during mineralization at ~2.7 Ga (Figs. 9, 10, 11). We associate these steeply plunging faults

with mineralization in domains I and II because: (i) these faults are spatially associated with the orebodies, which clearly present characteristics suggesting their formation was associated with deformation – such as brecciated structures and restriction along faults; (ii) these faults have orientations compatible with the directions of mineralization; (iii) the notion that these faults are younger than mineralization is unlikely because these orebodies present evidence only for very limited deformation after its formation (Domingos, 2009; Monteiro et al., 2008a), which can be linked with the formation of the Sossego-Curral orebodies as discussed above. In this context, it is relevant to point out that the latest event recorded in the mine site is the intrusion of diabase dikes. The ages of these dikes are uncertain, but are most likely more recent than any rock in the area, as indicated by their chilled margins and absence of either deformation or hydrothermal alteration. Most likely, these dikes intruded along several previously existing structures, especially those trending NNW–SSE and NW–SE (Figs. 2, 3).

For slickenlines with plunges > 40°, there is a tendency of concentration on faults with ENE–WSW trends, particularly in structural domain I (Fig. 11). For slickenlines with plunge ≤ 40°, there is a predominance of WNW–ESE-trending fault planes, particularly in domains I and II. Also, most N–S and NW–SE-trending striated faults exhibit gently plunging striae, except in domain II. In domain III, lateral movements concentrate on NW–SE-trending faults, which are usually subvertical, while vertical movements are often associated with faults with average dips of < 70° (Fig. 11).

5.5. Paleostress analysis

To derive more information about the structural control on different mineralization events at the Sossego deposit, we performed paleostress analysis on the available existing fault data to evaluate the main characteristics of the stress tensor that affected the area. For this analysis, we used all measurements of striated structures collected by Domingos (2009), which were made available to us by Vale Company. These data include striated fault planes and mineralized veins. Fault planes or mineralized veins without measurements of striae were not used.

Any paleostress analysis involves intrinsic assumptions that must be accepted prior to the application of the method. These assumptions are discussed below.

5.5.1. Assumptions for paleostress analysis

The following assumptions were made prior and during paleostress analysis:

1. In cases where both the plane and line are measured directly, the line-plane pair usually presents an angular deviation. For this reason, slickenlines that were incompatible with their planes were corrected using the projection algorithm available in the software Orient (Vollmer, 2016). Vollmer (2016) also recommended that, when the angular error is too large, the measurement should be discarded as unreliable. In our case, slickenline measurements with errors larger than 20.5° were discarded (8 measurements out of 150).

2. Striated faults have a brittle (or brittle-ductile) origin, as suggested by previous authors due to fault and microstructural characteristics (Domingos, 2009), as well as characteristics of hydrothermal alteration and mineralization events controlled by faults (Carvalho, 2009; Monteiro et al., 2008a).

3. Assumptions inherent to the paleostress method applied include (Delvaux and Sperner, 2003; Viola, 2008): (i) the stress tensor can be considered homogeneous on a macroscopic scale; (ii) blocks bounded by faults are rigid and do not rotate; (iii) faults slip independently; (iv) fault-kinematics is scale-invariant for the faults considered; (v) faults in a sample have movements generated from a single uniform stress tensor.

4. All slickenlines were considered of "well-marked" intensity, which corresponds to the intermediate intensity available in the TENSOR software.

5. As previously discussed, slickenlines with gentle and steep plunges were separated into different populations, and related to the Sossego and Sequeirinho mineralization events, respectively.

6. The defined structural domains (Fig. 3) are meaningful, as well as faults developed within each domain represent its particularities. The significance of the structural domains resides in several differences observed between

Sossego and Sequeirinho orebodies and their host rocks (cf. Domingos, 2009; Monteiro et al., 2008a; Moreto et al., 2015b), including their geometry on maps and equal-area plots.

7. Although the number of striae data is large, none of them has the sense of movement. Yet, we did not make any assumptions on: (i) the sense of motion of faults (and as such, there was no need to assume the quality of sense determination); and (ii) the nature of fault activation (i.e., if it was neoformed or reactivated). For all planes used, these parameters were considered as "unknown". Since the available striae data do not include information on sense of movement, the paleostress analysis performed with the TENSOR software resulted in two possible solutions. As the software developer points out in the program FAQ (http://www.damiendelvaux.be/Tensor/tensor-faq.html), data sets with only the slip direction result in two fully symmetric tensor solutions. As a consequence, the results from paleostress analysis presented below represent a choice between these two symmetrical solutions, supported by previous regional interpretations, as follows.

   For the tensor associated to Sossego (dated ~1.8 Ga), the solution chosen was the one reflecting a strike-slip regime, with dextral kinematics (as opposed to the solution with the strike-slip regime with a sinistral kinematics). This is because dextral strike-slip regime is consistent with the regional understanding for the Carajás region during the Paleoproterozoic, as suggested by several authors who indicated that the region was subjected to a dextral strike-slip regime or an extension regime, with extension direction to NE–SW or E–W (Domingos, 2009; Pinheiro and Holdsworth, 1997,2000; Silva et al., 2005).

   For the tensor related to Sequeirinho (dated ~2.7 Ga), the solution chosen was the one indicating an almost pure extension (as opposed to the solution pointing to an almost pure compression) because the interpretation of regional structural setting at ~2.7 Ga is sinistral transpression, with extension axis directed to NW–SE (Domingos, 2009; Pinheiro and Holdsworth, 1997). This direction coincides well with the extension

direction of the chosen solution, the difference being the inversion of the derived σ1 position (horizontal for the previous regional interpretation, but vertical for ours). Furthermore, this tensor is interpreted as contemporaneous to the Sequeirinho mineralization, and as such would be more plausible since mineralization would be much more susceptible to form under extension instead of under compression (Cox et al., 2001; Sibson, 1994,1986). Moreover, the derived σ2 axis coincides well with the mineralization axis, suggesting an almost perpendicular extension of structures in the Sequeirinho corridor.

5.5.2. Results of paleostress analysis

Considering all the assumptions outlined above, six tensors were obtained for the Sossego deposit: three tensor solutions for steeply dipping striae, indicative of vertical to oblique movement (one for each structural domain), and three tensor solutions for gently dipping striae, indicative of horizontal movement (Fig. 12).

The tensor solutions for striae indicative of oblique to vertical movement suggest an extensional environment, for the three structural domains, with extension directed in roughly NW–SE direction (Fig. 12). In domain I, the maximum horizontal stress (SHmax) is located at azimuth 63°, but with very high standard deviation (41.1°). For domain II, SHmax is at 34 ± 12.2° and for domain III at 25 ± 12.4°. For the three tensor solutions, the indices that measure the quality of the tensor obtained (QRw and QRt) have a "D" value due to the fact that the direction of the striae is unknown. The other parameters that measure errors and uncertainties (including the angular measurement α) are within acceptable levels (Table 1). For all domains, $R' = R$ (i.e., the tensors represent an extensional regime), with values of 0.35, 0.09 and 0.41 for domains I, II and III, respectively. The faults used in these tensors suggest that in domains I and II movement occurred mainly along ENE–WSW trends, slightly oblique to the Sequeirinho corridor, as well as NW–SE trends (see rose diagrams in the background of Fig. 12). In domain III, slipping occurred mainly in faults with WNW–ESE trends, parallel to those of the ductile shear zones and foliation, and to some extent in the N–S direction. It is important to note that four mineralized veins (out of 14) were treated in the tensor for domain III because they present plunges > 40°. Interestingly, the paleostress analysis automatically excluded three of such veins of the tensor solution of domain III, supporting the interpretation

that they are probably related to the subsequent mineralization event at Sossego–Curral orebodies.

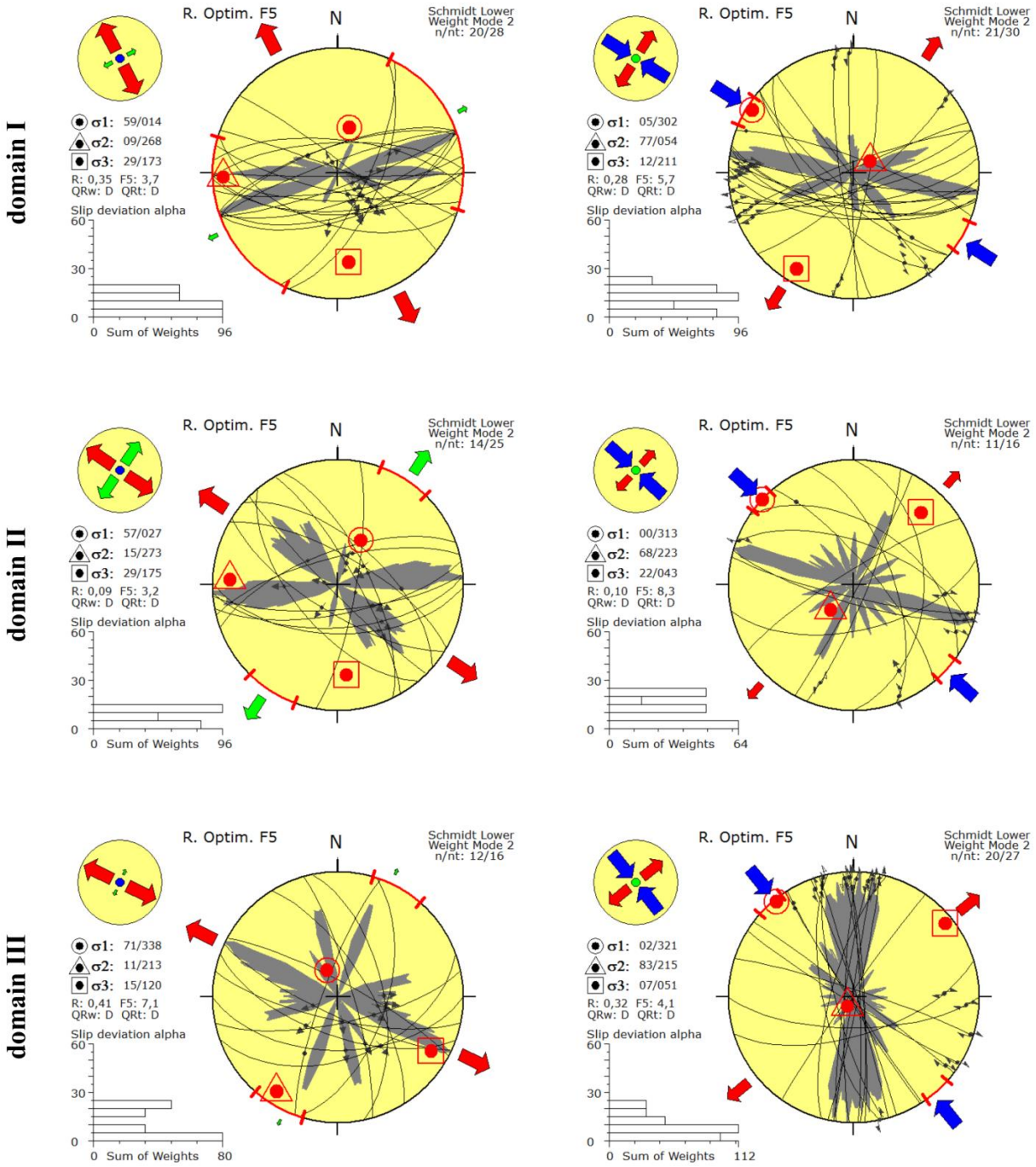

Fig. 12: Tensor solutions for slickenlines indicative of predominant vertical movement (left) and predominant horizontal movement (right).

Table 1: Quality rank results for the six tensor solutions. Colors are attributed accordingly to thresholds presented in Delvaux and Sperner (2003), from A (best) to E (worst).

Solution	n	n/nt	CL_w	α_w	DT_w	Plen	Slen	QRt	Color legend
Steep plunge, domain I	28	0.71	0.25	8.7 ± 4.9	1	0.87	0.93	D	A
Steep plunge, domain II	25	0.56	0.25	7.9 ± 4.9	1	0.77	0.91	D	B
Steep plunge, domain III	16	0.75	0.25	10.7 ± 8.1	1	0.66	0.90	D	C
Gentle plunge, domain I	30	0.70	0.25	11.3 ± 6.7	1	0.79	0.74	D	D
Gentle plunge, domain II	16	0.69	0.25	12.2 ± 8.9	1	0.60	0.66	D	E
Gentle plunge, domain III	27	0.74	0.25	8.8 ± 6.4	1	0.81	0.79	D	

In the case of domain II, it is important to note that the extension would have occurred in the direction perpendicular to the mineralized axis of Sequeirinho (NE–SW), suggesting the opening of previously formed structures and facilitating fluid flow and then mineralization. For domain III, in the Sossego orebody area, the paucity of appropriately directed structures would not have induced fluid flow and mineralization during the time this tensor affected the area (see discussion on section 6).

The tensor solutions indicative of lateral movement suggest a dextral transpressional environment, for the three domains, with the direction of extension grossly in the NE–SW trend (Fig. 12). In domain I, SHmax is oriented towards the azimuth 122 ± 7.4°. For domain II, SHmax is at 133 ± 6.1° and for domain III at 141 ± 6.5°. Similarly to the three previous tensor solutions, the absence of information about the sense of movement of each slickenline renders a "D" value for the quality indices QRw and QRt. The other parameters that measure errors and uncertainties are within acceptable levels (Table 1). For all domains, $R' = 2 - R$ (i.e., the tensors represent a transcurrent regime), with values of 1.72, 1.90 and 1.68, suggesting a compression component (transpression) for domains I, II and III, respectively. The faults used in these tensors indicate that movement occurred mainly in faults directed to WNW–ESE (parallel to the ductile shear zones) and to N–S.

In the case of domain II, it is important to note that the compression would have occurred in the direction roughly perpendicular to the mineralized axis of Sequeirinho, suggesting the closure of previously formed structures, and potentially preventing a new mineralization event.

6. A model for structural control at Sossego deposit

The geometric and paleostress analyses presented above, taken in conjunction with the abundant information available from previous studies (Carvalho, 2009; Domingos, 2009; Monteiro et al., 2008a; Moreto et al., 2015b), allow us to conceive and propose a model for the structural control at Sossego deposit. The main elements of this model portray: (i) some factors responsible for the occurrence of two mutually exclusive mineralization events that were so apart in time (~780 Ma), but close in space (< 1 km); and (ii) the origin for the vertical pipe breccia of Sossego-Curral orebodies, which has not been addressed in detail by previous studies. The model depicts four main stages, each divided into phases, and it is synthesized in Fig. 13.

6.1. Stage (1): Pre-mineralization

Stage (1) involved the development of the latest elements of the ductile framework at Sossego, which was an important control for subsequent deformation events. The age range for this stage can be inferred as 2.74 to 2.71 Ga, since ductile structures such as foliation and shear zones affected gabbronorites and granophyric granites dated 2.74 Ga but hardly affected mineralization at Sequeirinho, which started around 2.71 Ga (Moreto et al., 2015b). The rheological regime is inferred to be ductile, probably associated with lower-to-middle crustal levels, as attested by field characteristics, mineral assemblages, textures and microstructures present in the mylonites at the mine and by regional field observations of gneisses and mylonites in the Canaã dos Carajás area (Domingos, 2009). The stress regime for this stage is inferred as transpression, with $\sigma 1$ oriented around N20°E and $\sigma 3$ horizontal, and a dominant sinistral kinematics (Domingos, 2009).

The first phase of this stage (1.1 in Fig. 13) involved the development of part of a vast network of anastomosing WNW–ESE-trending shear zones, accompanied by the development of foliation and sub-vertical mineral lineation (Fig. 6). Geological units were juxtaposed in rock bodies elongated in WNW–ESE direction, with contacts usually marked by the presence of schistose levels (Carvalho, 2009; Monteiro et al., 2008a). This structural configuration is found both at Sequeirinho and Sossego (Fig. 3). At this phase, fluid flow was pervasive through fractures, foliation and grain boundaries (Monteiro et al., 2008a). Hydrothermal alteration was regional sodic alteration associated with hypersaline deep-seated hot fluids (> 500 °C), probably with a mixed origin (formational/metamorphic or magmatic) (Carvalho, 2009; Monteiro et al., 2008a).

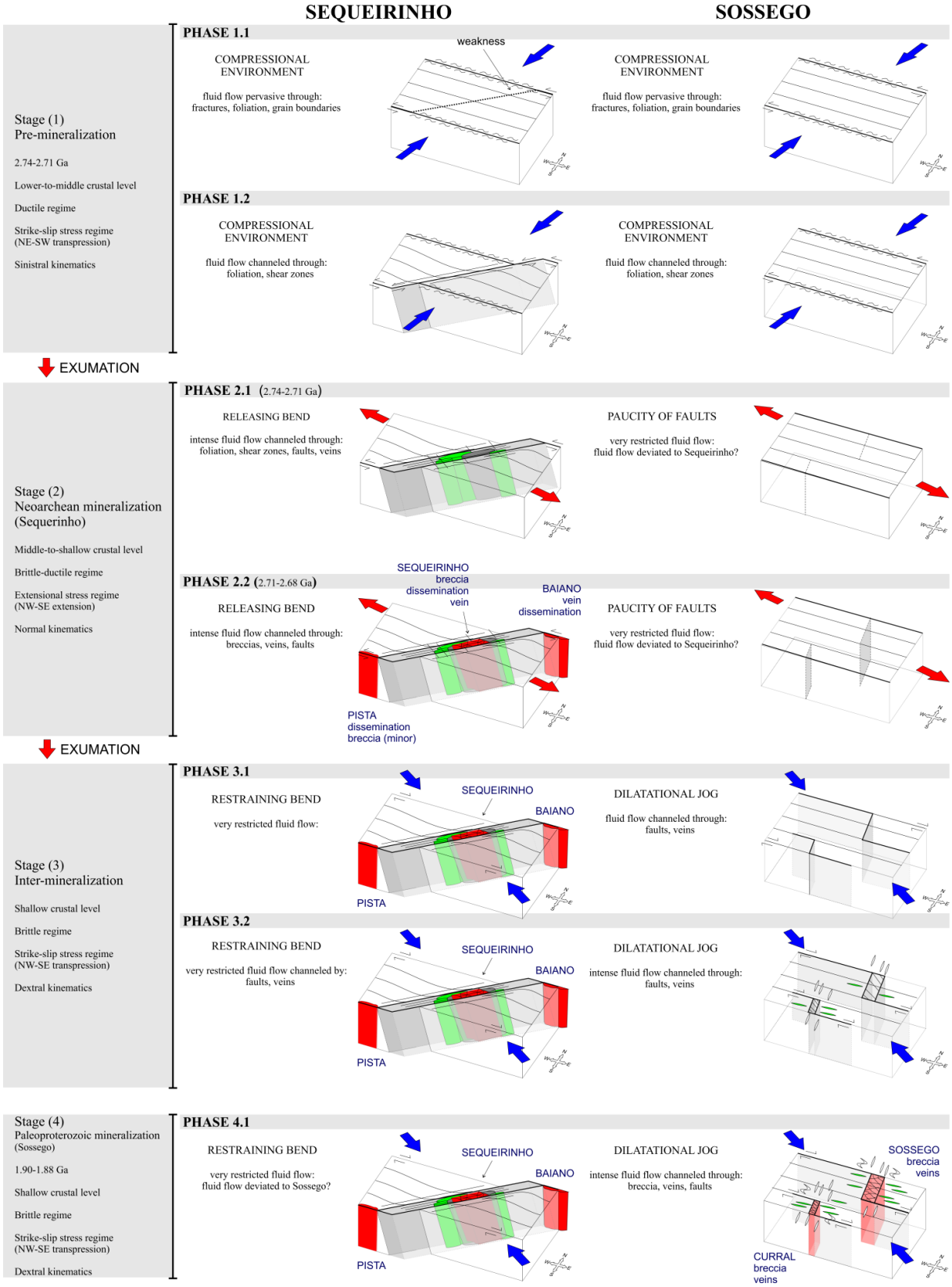

Fig. 13: Schematic model for the structural control of mineralization at Sossego deposit.

The second phase of this stage (1.2 in Fig. 13) marks the beginning of the structural differentiation between Sequeirinho and Sossego. According to Domingos (2009), transpression was responsible for the rupture of rocks along a sinistral brittle-ductile corridor, at the position that now hosts Sequeirinho orebody. This rupture was oriented NE–SW and was marked by partial re-orientation and new development of foliation planes and shear zones (Fig. 7). These shear zones were responsible for the left-lateral offset of geological units, observed especially in gabbros (Fig. 3a) (Domingos, 2009).

At the second phase, predominant hydrothermal alteration was still regional sodic alteration but now controlled by the newly formed NE–SW trending shear zones at Sequeirinho. Silicification and biotitization alteration also occurred, mainly associated with WNW–ESE-trending mylonitic zones north of Sossego (Fig. 3c), but also within the biotitized mylonitic zone on the NE–SW-trending shear zone at Sequeirinho, which now is the footwall of the mineralized zone (Monteiro et al., 2008a).

6.2. Stage (2): Neoarchean mineralization – Sequeirinho, Pista and Baiano orebodies

Stage (2) involved the development of a brittle and brittle-ductile network. At Sequeirinho, this structural network was associated with sodic-calcic alteration that culminated with mineralization (Monteiro et al., 2008a). At Sossego, there is no preserved evidence for this stage. The age range for this stage can be inferred as towards the end of the period between 2.74–2.71 Ga (for the sodic-calcic alteration that preceded mineralization) and 2.71–2.68 Ga (for the mineralization at Sequeirinho) (Moreto et al., 2015b).

The rheological regime was brittle-ductile due to fault characteristics (Domingos, 2009), probably associated with middle-to-shallow crustal level (although shallower than the previous stage), as indicated by the typical deeper IOCG alteration found at Sequeirinho area (Monteiro et al., 2008a). A brittle regime for mineralization is also indicated by textures in the breccias and the fracture control of later alteration minerals (Monteiro et al., 2008a). This stage was associated with the development of faults and scattered veins trending ENE–WSW, NE–SW and NW–SE with oblique to subvertical slickenlines (Fig. 11). Moreover, faults appear to be younger than the ductile fabric developed in the previous stage because the fault patterns in domains I and II are very similar, unlike the pattern for foliation and shear zones (Figs. 6, 7). The stress tensor solutions obtained in paleostress analysis for these structures

suggest an extensional regime, with subvertical σ1 and extension direction around 35° (Fig. 12). The predominant kinematics was normal.

The first phase of this stage (2.1 in Fig. 13) was marked by the extension of structures in the Sequeirinho corridor, since the extension direction was almost perpendicular to the corridor's long axis (NE–SW). The extension of these structures would have allowed intense fluid flow into this area, causing the profound alteration that was necessary for the formation of the abundant hydrothermal bodies elongated along the corridor axis: initially actinolitites followed by magnetitites (Carvalho, 2009; Monteiro et al., 2008a). The lateral block movement was most likely accommodated by WNW–ESE-trending structures, which also exhibit intense hydrothermal alteration and were later mineralized (Pista and Baiano orebodies). Fluid flow was intense, and channeled through foliation, shear zones, faults and veins. The fluid possessed characteristics similar to those in the pre-mineralization stage, i.e., deep-seated hot (> 500°C) hypersaline fluids probably of mixed origin (Monteiro et al., 2008a).

The second phase of this stage (2.2 in Fig. 13) was marked by the mineralization event itself. The main characteristic was the development of NE–SW-trending tabular breccias, associated with the dislocation planes in the Sequeirinho corridor, and affected mainly the hydrothermal rocks of the previous phase (actinolitites and magnetitites). The probable deformation mechanism associated with the breccia generation was a mixture of attrition and implosion breccias (cf. Sibson, 1986). The “S” shaped distribution of mineralization suggests that, despite concentration of fluid flow along the Sequeirinho corridor, important fluxes also occurred at the structures that most likely accommodated the lateral displacement of the blocks, generating WNW–ESE-trending tabular attrition breccias at Pista and veins in Baiano orebodies. This interpretation is in agreement with the results of textural analysis of deposit breccias performed by Domingos (2009), which indicate that attrition was the dominant process of fragmentation for breccias at Sequeirinho, while at the Sossego orebody the main mechanism would be due to explosive brecciation. At this phase, there was a mixture of fluids. According to Carvalho (2009) and Monteiro et al. (2008a), fluid characteristics suggest that mineralization was conditioned by the mixing of endogenous and meteoric fluids, resulting in a fluid with lower temperatures (< 300°C) and mixed salinity.

At the Sossego area, structural phases 2.1 and 2.2 are not recognized, mainly because of the paucity/absence of hydrothermal alteration zones with sodic and sodic-calcic composition, but also due to the paucity of similarly oriented structures as at Sequeirinho. Nucleation of N–S-trending structures may have occurred at this time, but with the available existing data this assertion is speculative. For the absence of hydrothermal alteration and mineralization at this time at Sossego, we hypothesize three reasons: (i) lack of structures favorable to opening as in the Sequeirinho corridor; (ii) preferred fluid migration to Sequeirinho due to the effect of a "suction pump" area (cf. Sibson, 1994), which would have attracted most of the fluid flow into that location; (iii) presence of another form of mineralization control at the time, such as lithogeochemical control (e.g., proximity to gabbronorites, which are abundant at Sequeirinho, but scarce at Sossego).

6.3. Stage (3): Inter-mineralization

This stage mostly involved the development of faults with predominantly lateral movements. The age range for this stage is poorly constrained, since it is only possible to affirm that it was developed sometime between ~2.68 and ~1.90 Ga, that is, after the end of the mineralization event at Sequeirinho and before the beginning of mineralization at Sossego. The rheological regime was brittle, as indicated by field characteristics of faults, veins and breccias, as well as microstructures (Domingos, 2009). The evident brittle regime, as observed in the Sossego orebody, is interpreted to be associated with regional exhumation that affected the area (Moreto et al., 2015b). Moreover, as Domingos (2009) pointed out for the data he collected in the Canaã dos Carajás region, around the mine, microstructures and mineral assemblages suggest a progressive regional uplift accompanied by temperature reduction. Also, a shallower crustal level is indicated by alteration assemblages of potassic and chloritic nature that affected the Sossego orebody area at this stage, similar to those found in high structural levels of IOCG systems (Monteiro et al., 2008a; Moreto et al., 2015b), and also by their morphology as breccia pipes and veins. The stress regime was transpression, with calculated tensors suggesting a horizontal $\sigma 1$ around 132° and a horizontal $\sigma 3$ around 42° (Fig. 12). The predominant kinematics was dextral.

The first phase of this stage (3.1 at Fig. 13) marks the beginning of hydrothermal alteration at Sossego. It involved generation of several dilational jogs defined by the occurrence of dextral strike-slip faults with right-hand offsets, which can be deduced from the orientation of faults associated with this phase (NNW–SSE- and E–W-trending faults) and the

shape of the breccia body at Sossego (vertical pipe breccia) (Figs. 3b, 8). Considering the calculated tensors, these jogs were dilational. It is important to note that the notion of these jogs is conceptual, since they have not been observed directly in the field. However, faults modeled with drillhole data indicate that this is a reasonable assumption, especially for the Sossego orebody (Fig. 3b). Additionally, Sibson (1986) pointed out that it is not uncommon for master faults that generate breccias in dilational jogs to be barren and concealed.

The second phase of this stage (3.2 at Fig. 13) involved continuous widening of the dilational jogs, with consequent fluid flow channeled through faults and veins and the widening of the potassic and chloritic hydrothermal alterations halos. This phase was accompanied by the development of two populations of subvertical extensional- and shear-veins, which also controlled the hydrothermal alteration: a family oriented to N–S, and another to E–W (Fig. 8). During this stage, there is no evidence at Sequeirinho for pervasive potassic or chloritic alterations, which are observed only as narrow fractures assemblages (Monteiro et al., 2008a).

6.4. Stage (4): Paleoproterozoic mineralization – Sossego and Curral orebodies

Sossego mineralization was dated by Moreto et al. (2015b) to be 1.90–1.88 Ga (phase 4.1 at Fig. 13). The overall characteristics of this stage are the same as in the preceding stage: a brittle regime associated with shallow crustal level, with a strike-slip stress regime (NW–SE transpression) with a dominant dextral kinematics. The main difference is that with the continuous evolution of the dilational jogs, brecciation started to develop in a subcircular and vertical pipe-like structure, most likely by a process of implosive brecciation (Sibson, 1986,1985) and analogous to what is illustrated by Melosh et al. (2014). As breccias, veins and faults were generated, both porosity and permeability increased, and fluid flow was intensified and concentrated there, allowing mineralization to develop. Similarly to what is observed at Sequeirinho orebody, geochemical data suggest that mineralization was formed by colder fluids (< 300°C) with mixed salinity, probably reflecting the mixture of deep-seated and meteoric fluids (Carvalho, 2009; Monteiro et al., 2008a).

During this stage, there is no evidence at Sequeirinho for relevant ore remobilization or re-mineralization, which suggests that during Sossego mineralization the Sequeirinho area was not subjected to relevant fluid percolation. We hypothesize two reasons for this: (i) considering the tensor solution, Sequeirinho would have been at a restraining

bend, with its long axis roughly perpendicular to the compression axis, thus preventing fluid flow; and (ii) with the generation and evolution of pipe breccias at Sossego, a low stress area would form and the resulting hydraulic gradient would drive most of the fluid flow towards this dilational structure (Sibson, 1994).

7. Discussion and conclusions

The stress tensors described in this study can be related to regional tectonic events as follows.

(i) NNE–SSW-directed sinistral transpression during 2.74–2.71 Ga (tensor obtained from Domingos, 2009): regionally, this event is interpreted as part of the convergence between the Rio Maria and Carajás tectonic domains, from south to north. This convergence caused reactivation of WNW–ESE-trending ductile regional shear zones, originally formed at ~2.85 Ga, such as the Canaã Shear Zone. At Sossego, this event would be responsible for the formation of part of the ductile fabric of the area and the nucleation of the Sequeirinho corridor.

(ii) NW–SE-directed extension during 2.71–2.68 Ga: for this period the interpretation is a tectonic reactivation by sinistral transpression directed to NE–SW (Domingos, 2009; Pinheiro and Holdsworth, 1997). This period is also related to the emplacement of syn-tectonic granites such as the Planalto Granite Suite (Feio et al., 2012), which could have caused circulation of hydrothermal fluids at regional scale through major crustal discontinuities, leading to metal leaching and ore deposition at this time. Despite the difference in the tectonic regime in relation to the tensors obtained for Sossego, in both cases this period would be related to extension in the NW–SE direction, which for Sossego is linked to the formation of Pista-Sequeirinho-Baiano orebodies.

(iii) NW–SE-directed dextral transpression during 1.90–1.88 Ga: this event is associated with an important A-type granite magmatism, recorded all over the Carajás Tectonic Domain (e.g. Central Granite, Machado et al., 1991). This magmatism could be responsible for fluid circulation at a regional scale and related to the formation of several Cu-Au deposits in the region

(Moreto et al., 2015a). Most authors agree that during this period the region was subjected to an extension directed to NE–SW or E–W, either as a result of transtension or pure extension (Pinheiro and Holdsworth, 1997,2000; Tavares, 2015). Such tectonic movements are most likely related to the collapse of Paleoproterozoic orogens (Tavares, 2015) or as a response to a super-plume installed in the region (Dall'Agnol et al., 2005). This extension axis coincides well with the tensors obtained for the formation of Sossego-Curral orebodies.

The Transamazonian cycle (~2.2–2.0 Ga; Teixeira et al., 1989) – an event that records the convergence between the Carajás Province and the northern Bacajá Domain – does not appear to be recorded at Sossego. This interpretation is in agreement with previous studies that indicate evidence for this event in Sossego area is very restricted (Moreto et al., 2015a; Tavares, 2015).

The integration of information from previous studies and the new results from paleostress analysis shown here indicates that mineralization at Sossego represents a remarkable example of episodic mineralization at neighboring locations, but separated by hundreds of millions of years. For the Sossego deposit, the favorable orientation of structures in regard to stresses affecting the area appears to be a fundamental component to explain the development of orebodies with such characteristics. Additionally, the relationship between orientation of structures and main stresses seems a reasonable explanation to account for mutually exclusive fluid flow at Sossego: during the older mineralization at Pista-Sequeirinho-Baiano there is no evidence for mineralization in Sossego-Curral, and the opposite is true – there is no evidence of remobilization of ore from Sequeirinho to Sossego during the younger mineralization event. These are important features to observe, due to their implications to ore genesis and its relation to tectonic environment. The interpretations presented here can be used to constrain mineralization controls in similar IOCG deposits in the region, and could provide useful insights for future studies and exploration work.

Acknowledgments

The authors thank Vale Company, for the long-term support to UNICAMP for research in the Carajás region, and especially Roberto Albuquerque, Péterson Barbosa, Fabrício Franco, Rafael Sposito, Fernando Matos, Sérgio B. Huhn and the short-term planning staff who accompanied us during field trips to the mine site. We also thank

FAPESP/CAPES covenant (São Paulo Research Foundation/ *Coordenação de Aperfeiçoamento de Pessoal de Nível Superior*) for the scholarship to PMHM (grant FAPESP 2015/11186-3); and CNPq (National Counsel of Technological and Scientific Development), for the financial support (grant 2014-9/401316) and the research grant to CRSF (no. 2008-7/303563).

References

Araújo, O.J.B. de, Maia, R.G.N., 1991. Programa Levantamentos Geológicos Básicos do Brasil, Programa Grande Carajás, Serra dos Carajás, Folha SB.22-Z-A, Estado do Pará, Escala 1:250.000. Brasília.

Carvalho, E. de R., 2009. Caracterização Geológica e Gênese das Mineralizações de Óxido de Fe-Cu-Au e metais associados na Província Mineral de Carajás: Estudo de Caso do Depósito de Sossego. Universidade Estadual de Campinas.

Cox, S.F., Knackstedt, M.A., Braun, J., 2001. Principles of structural control on permeability and fluid flow in hydrothermal systems. Rev. Econ. Geol. 14, 1–24.

Dall'Agnol, R., Teixeira, N.P., Rämö, O.T., Moura, C.A. V., Macambira, M.J.B., de Oliveira, D.C., 2005. Petrogenesis of the Paleoproterozoic rapakivi A-type granites of the Archean Carajás metallogenic province, Brazil. Lithos 80, 101–129.

Davis, G.H., Reynolds, S.J., 1996. Structural Geology of Rocks and Regions, 2nd ed. Wiley.

Delvaux, D., Sperner, B., 2003. New aspects of tectonic stress inversion with reference to the TENSOR program. In: Nieuwland, D.A. (Ed.), New Insights into Structural Interpretation and Modelling. Geological Society, London, pp. 75–100.

Domingos, F.H.G., 2009. The structural setting of the Canaã dos Carajás region and Sossego-Sequeirinho deposits, Carajás Brazil. Doctor of Philosophy thesis, University of Durham, Durham.

Feio, G.R.L., Dall'Agnol, R., Dantas, E.L., Macambira, M.J.B., Gomes, A.C.B., Sardinha, A.S., Oliveira, D.C., Santos, R.D., Santos, P.A., 2012. Geochemistry, geochronology, and origin of the Neoarchean Planalto Granite suite, Carajás, Amazonian craton: A-type or hydrated charnockitic granites? Lithos 151, 57–73.

Fossen, H., 2010. Structural Geology, 1st ed. Cambridge University Press, Cambridge.

Hazen, R.M., Liu, X.-M., Downs, R.T., Golden, J., Pires, A.J., Grew, E.S., Hystad, G., Estrada, C., Sverjensky, D.A., 2014. Mineral Evolution: Episodic Metallogenesis, the Supercontinent Cycle, and the Coevolving Geosphere and Biosphere. Spec. Publ. 18, 1–15.

Hitzman, M.W., 2000. Iron Oxide-Cu-Au Deposits: What, Where, When and Why. In: Porter, T.M. (Ed.), Hydrothermal Iron Oxide Copper-Gold & Related Deposits: A Global Perspective, Volume 1. PGC Publishing, Adelaide, pp. 9–25.

Holdsworth, R.E., Pinheiro, R.V.L., 2000. The anatomy of shallow-crustal transpressional structures: Insights from the Archaean Carajas fault zone, Amazon, Brazil. J. Struct. Geol. 22, 1105–1123.

Machado, N., Lindenmayer, Z., Krogh, T.E., Lindenmayer, D., 1991. U-Pb geochronology of Archean magmatism and basement reactivation in the Carajás area, Amazon shield, Brazil. Precambrian Res. 49, 329–354.

Marshak, S., Mitra, G., 1988. Basic Methods of Structural Geology. Prentice-Hall, Englewood Cliffs, NJ.

Melosh, B.L., Rowe, C.D., Smit, L., Groenewald, C., Lambert, C.W., Macey, P., 2014. Snap, Crackle, Pop: Dilational fault breccias record seismic slip below the brittle–plastic transition. Earth Planet. Sci. Lett. 403, 432–445.

Monteiro, L.V.S., Xavier, R.P., Carvalho, E.R. de, Hitzman, M.W., Johnson, C.A., Souza Filho, C.R. de, Torresi, I., 2008a. Spatial and temporal zoning of hydrothermal alteration and mineralization in the Sossego iron oxide–copper–gold deposit, Carajás Mineral Province, Brazil: paragenesis and stable isotope constraints. Miner. Depos. 43, 129–159.

Monteiro, L.V.S., Xavier, R.P., Hitzman, M.W., Juliani, C., Souza Filho, C.R. de, Carvalho, E.R. de, 2008b. Mineral chemistry of ore and hydrothermal alteration at the Sossego iron oxide-copper-gold deposit, Carajás Mineral Province, Brazil. Ore Geol. Rev. 34, 317–336.

Moreto, C.P.N., Monteiro, L.V.S., Xavier, R.P., Creaser, R.A., DuFrane, S.A., Melo, G.H.C., Silva, M.A.D. da, Tassinari, C.C.G., Sato, K., 2015a. Timing of multiple hydrothermal events in the iron oxide–copper–gold deposits of the Southern Copper Belt, Carajás Province, Brazil. Miner. Depos. 50, 517–546.

Moreto, C.P.N., Monteiro, L.V.S., Xavier, R.P., Creaser, R.A., DuFrane, S.A., Tassinari, C.C.G., Sato, K., Kemp, A.I.S., Amaral, W.S., 2015b. Neoarchean and Paleoproterozoic Iron Oxide-Copper-Gold events at the Sossego Deposit, Carajás Province, Brazil: Re-Os and U-Pb geochronological evidence. Econ. Geol. 110, 809–835.

Munro, M.A., Blenkinsop, T.G., 2012. MARD-A moving average rose diagram application for the geosciences. Comput. Geosci. 49, 112–120.

Nogueira, A.C.R., Truckenbrodt, W., Pinheiro, R.V.L., 1995. Formação Águas Claras, Pré-Cambriano da Serra dos Carajás: redescrição e redefinição litoestratigráfica. Bol. Mus. Para. Emílio Goeldi - Série Ciências da Terra 7, 177–277.

Pidgeon, R.T., MacAmbira, M.J.B., Lafon, J.M., 2000. Th-U-Pb isotopic systems and internal structures of complex zircons from an enderbite from the Pium Complex, Carajas Province, Brazil: Evidence for the ages of granulite facies metamorphism and the protolith of the enderbite. Chem. Geol. 166, 159–171.

Pinheiro, R.V.L., 1997. Reactivation History of the Carajas and Cinzento Strike-slip Systems, Amazon, Brazil. PhD thesis, University of Durham, Durham.

Pinheiro, R.V.L., Holdsworth, R.E., 1997. Reactivation of Archaean strike-slip fault systems, Amazon region, Brazil. J. Geol. Soc. London. 154, 99–103.

Pinheiro, R.V.L., Holdsworth, R.E., 2000. Evolução tectonoestratigráfica dos sistemas transcorrentes Carajás e Cinzento, Cinturão Itacaiúnas, na borda leste do Cráton Amazônico, Pará. Rev. Bras. Geociências 30, 597–606.

Pinheiro, R.V.L., Kadekaru, K., Soares, A.V., Freitas, C., Ferreira, S.N., Matos, F.M.V., 2013. Carajás, Brazil - a short tectonic review. Anais Do 13o Simpósio de Geologia Da Amazônia. SBG - Núcleo Norte, Belém, Brazil, pp. 1086–1089.

Rosière, C.A., Baars, F.J., Seoane, J.C.S., Lobato, L.M., da Silva, L.L., de Souza, S.R.C., Mendes, G.E., 2006. Structure and iron mineralisation of the Carajás Province. Appl. Earth Sci. 115, 126–133.

Santos, J.O.S., 2003. Geotectônica dos Escudos das Guianas e Brasil-Central. In: Bizzi, L.A., Schobbenhaus, C., Vidotti, R.M., Gonçalves, J.H. (Eds.), Geologia, Tectônica E Recursos Minerais Do Brasil. CPRM, Brasília, pp. 169–226.

Sibson, R.H., 1985. Stopping of earthquake ruptures at dilational fault jogs. Nature 316, 248–251.

Sibson, R.H., 1986. Brecciation processes in fault zones: Inferences from earthquake rupturing. Pure Appl. Geophys. 124, 159–175.

Sibson, R.H., 1994. Crustal stress, faulting and fluid flow. Geol. Soc. London, Spec. Publ. 78, 69–84.

Silva, M.A.D. Da, 2014. Metatexitos e diatexitos do Complexo Xingu na região de Canaã dos Carajás: implicações para a evolução mesoarqueana do Domínio Carajás. Universidade Estadual de Campinas.

Silva, M. da G. da, Teixeira, J.B.G., Pimentel, M.M., Vasconcelos, P.M., Arielo, A., Franca-Rocha, W. da, 2005. Geologia e Mineralizações de Fe-Cu-Au do Alvo GT46 (Igarapé Cinzento), Carajás. In: Caracterização de Depósitos Minerais Em Distritos Mineiros Da Amazônia. ADIMB, pp. 97–151.

Tavares, F.M., 2015. Evolução Geotectônica do Nordeste da Província Carajás. Ph.D. thesis, Universidade Federal do Rio de Janeiro, Rio de Janeiro.

Teixeira, W., Tassinari, C.C.G., Cordani, U.G., Kawashita, K., 1989. A review of the geochronology of the Amazonian Craton: Tectonic implications. Precambrian Res. 42, 213–227.

Vasquez, M.L., Rosa-Costa, L.T. da, 2008. Geologia e Recursos Minerais do Estado do Pará: Sistema de Informações Geográficas - SIG: texto explicativo dos mapas Geológico e Tectônico e de Recursos Minerais do Estado do Pará. Belém.

Vasquez, M.L., Rosa-Costa, L.T. da, Silva, C.M.G. da, Klein, E.L., 2008. Compartimentação Geotectônica. In: Vasquez, M.L., Rosa-Costa, L.T. da (Eds.), Geologia E Recursos Minerais Do Estado Do Pará: Sistema de Informações Geográficas - SIG: Texto Explicativo Dos Mapas Geológico E Tectônico E de Recursos Minerais Do Estado Do Pará. CPRM, Belém, pp. 39–112.

Veneziani, P., Santos, A.R. dos, Paradella, W.R., 2004. A evolução tectono-estratigráfica da Província Mineral de Carajás: um modelo com base em dados de sensores remotos orbitais (SAR-C RADARSAT-1, TM LANDSAT-5), aerogeofísica e dados de campo. Rev. Bras. Geociências 34, 67–78.

Viola, G., 2008. Ductile and brittle structural evolution of the Laxemar- Simpevarp area: an independent analysis based on local and regional constraints, SKB Report R-08-124. Stockholm.

Vollmer, F.W., 1995. C program for automatic contouring of spherical orientation data using a modified Kamb method. Comput. Geosci. 21, 31–49.

Vollmer, F.W., 2016. Orient 3: Spherical projection and orientation data analysis software user manual.

Williams, P.J., Barton, M.D., Johnson, D.A., Fontboté, L., Haller, A. de, Mark, G., Oliver, N.H.S., Marschik, R., 2005. Iron oxide copper-gold deposits: Geology, space-time distribution, and possible modes of origin. Econ. Geol. 100th Anniv. Vol. 371–405.

Xavier, R.P., Monteiro, L.V.S., Moreto, C.P.N., Pestilho, A.L.S., Melo, G.H.C. de, Silva, M.A.D. da, Aires, B., Ribeiro, C., Silva, F.H.F. e, 2012. The Iron Oxide Copper-Gold Systems of the Carajás Mineral Province, Brazil. In: Hedenquist, J.W., Harris, M., Camus, F. (Eds.), SEG Special Publication 16. Society of Economic Geologists Inc., pp. 433–454.

Xavier, R.P., Wiedenbeck, M., Trumbull, R.B., Dreher, A.M., Monteiro, L.V.S., Rhede, D., Araújo, C.E.G. de, Torresi, I., 2008. Tourmaline B-isotopes fingerprint marine evaporites as the source of high-salinity ore fluids in iron oxide copper-gold deposits, Carajás Mineral Province (Brazil). Geology 36, 743–746.

CAPÍTULO 4 A NATUREZA FRACTAL DE CONTROLES ESTRUTURAIS NA FORMAÇÃO DE MINÉRIO: O CASO DOS DEPÓSITOS *IRON OXIDE-COPPER-GOLD* DA PROVÍNCIA MINERAL DE CARAJÁS, BRASIL

Durante o desenvolvimento da pesquisa deste mestrado, o seguinte artigo foi preparado para submissão:

Paulo Miguel Haddad-Martim, Emmanuel John M. Carranza, Carlos Roberto de Souza Filho, *The fractal nature of structural controls on ore formation: the case of the iron oxide-copper-gold deposits in the Carajás Mineral Province, Brazilian Amazon*, preparado para submissão.

A íntegra do manuscrito preparado é apresentada nas próximas páginas.

O material suplementar para este trabalho está disponível no APÊNDICE B.

The fractal nature of structural controls on ore formation: the case of the iron oxide-copper-gold deposits in the Carajás Mineral Province, Brazilian Amazon

Paulo Miguel Haddad-Martim [a], Emmanuel John M. Carranza [a,b], Carlos Roberto de Souza Filho [a]

[a] Institute of Geosciences, State University of Campinas (UNICAMP), Campinas, São Paulo, Brazil

[b] Economic Geology Research Centre (EGRU), James Cook University, Townsville, QLD, Australia.

The formation of ore minerals in hydrothermal deposits is the result of a complex interplay between physical and chemical processes that are conditioned by the geological environment where they occur. In the last decades, research has increasingly indicated that many of these processes display different forms of scale invariance, i.e., they show fractal geometry. This characteristic suggests that behind the apparent disorder and irregularity of the geometry of mineral deposits at different scales, an underlying regular pattern is present. If properly understood, this regular geometrical pattern could be useful in a variety of theoretical and applied fields. A great portion of this scale invariance is given by the structural framework during mineralization, since structures are a dominant factor controlling fluid flow. Here, we assess the geometry of iron oxide-copper-gold (IOCG) mineralization in the worldly known Carajás Mineral Province, focusing in one of the largest and most economically important mineralization, the Sossego deposit. The geometry of mineralization is evaluated at the microscale (ore minerals in thin sections), local scale (orebodies in mine maps) and regional scale (deposits distribution in regional maps). We show that the spatial distribution and shape of ore minerals in the microscale is largely non-random, presents fractal geometry and displays defined trends in spatial distribution and anisotropy. Additionally, the geometric trends observed at the microscale mimics those of the local-scale geometry of orebodies, as well as the regional-scale distribution of mineralization. The main property controlling the observed scale invariance is permeability, which is intrinsically associated with multiple scale structures. These results contribute to the advancement of the understanding of the fractal nature of processes controlling mineral deposits formation, as well as suggest new multi-scale approaches to investigate the structural controls on ore deposition.

1. Introduction

Obtaining information about the regional and local-scale distribution and geometry of mineral deposits is an important task because these properties have direct impact on exploration programs and mining operations (Monteiro et al., 2004). The concept of fractal geometry provides a useful framework to address this task, since a broad range of geological features and events have been described as fractals, including rock fragmentation, ore grade and tonnage, seismicity and fluid convection (Turcotte, 1989). Of particular interest in this context is the fact that the spatial distribution of mineral deposits has been modeled as *fractal dusts*, which means that deposits exhibit clustering at many different scales (Mandelbrot, 1983; Carlson, 1991; Blenkinsop and Sanderson, 1999). Theoretical fractal dusts present systematic clusters across all scales, but natural fractals are usually bound within a range (Kruhl, 2013). For mineral deposits, the lower bound of fractality is usually established as a single deposit, while the upper bound is its geological province (Carlson, 1991).

The scale invariance in the spatial distribution of mineral deposits is interpreted mainly as the result of the fractal nature of the structures that controlled the mineralizing systems (Blenkinsop and Sanderson, 1999; Hodkiewicz et al., 2005). This interpretation is supported by studies on several types of structures. For example, veins, including mineralized ones, show fractal geometry in a range of spatial scales (Brooks and Manning, 1994; Johnston and McCaffrey, 1996; Hippertt and Massucatto, 1998; Roberts et al., 1999). Scale invariance has also been described for different aspects of faults, strike-slip duplexes (Jensen et al., 2011), S-C structures (Hippertt, 1999), and breccias (Jébrak, 1997). In the context of ore deposits, fractal geometry was also described for ore banding (Goryainov et al., 1997) and in mineralized stockworks (Gumiel et al., 2010).

The fractal property of mineral deposits implies the existence of systematic patterns in their geometry that are considered independent of the spatial scale. Despite the intense research on this subject in the last decades, the relation between the geometry of mineral deposits in the microscopic, local and regional scales has not been properly demonstrated. As indicated above, previous work has shown relationships of this kind on the regional and local scales, but not simultaneously on the microscale. The present study has investigated whether the fractal properties of mineral deposits are consistent from the microscopic to the regional scale, with a particular interest to describe the possible small- and

large-scale structural features that plausibly defined the permeability that controlled fluid flow.

To apply the proposed approach, we have chosen the iron oxide-copper-gold (IOCG) deposit type, which typically exhibits strong structural control, and an area with abundant data: the Sossego deposit in the Carajás Mineral Province, Brazil. Mineralization at Sossego and other IOCG deposits in the province present characteristics which suggest that they are structurally-controlled (Xavier et al., 2012; Haddad-Martim et al., 2017). However, the means by which the regional-scale mechanisms of structural control are related to the local-scale and microscale mechanisms on mineralization are not known. This study integrates information at microscale (ore minerals in thin section), local scale (orebodies in the mineral deposit) and regional scale (distribution of mineral deposits in the province) to investigate if the spatial pattern of ore minerals at microscale provides insights into the structural control on mineralization at the macroscales (local- and regional-scales). Insights to this relationship can be useful in the current understanding of IOCG formation in the province as well in defining other potential exploration targets.

2. The study area

2.1. Regional geology and characteristics of Carajás IOCG deposits

The Sossego deposit is located in the Carajás Tectonic Domain (Santos, 2003), an Archean block located in the northern region of Brazil (Fig. 1). The Carajás Tectonic Domain is composed of a Mesoarchean basement (~3,0 Ga) that assembles granulites of the Pium Complex and gneisses and migmatites of the Xingu Complex (Pidgeon et al., 2000; Silva, 2014). This basement is partially covered by Neoarchean (~2.76–2.74 Ga) metamorphosed volcano-sedimentary units, including the Rio Novo Group (Hirata et al., 1982) and the Itacaiúnas Supergroup (Machado et al., 1991). These units include variable metamorphosed associations of mafic and felsic volcanic rocks, banded iron formations, pelites and psammites. These supracrustal rocks are intruded by penecontemporaneous (~2.75–2.70 Ga) alkaline granites, such as the Estrela, Planalto and Plaquê intrusions (Barros et al., 2009; Feio et al., 2012), and by mafic-ultramafic layered complexes, such as Luanga (Machado et al., 1991). The metamorphosed volcano-sedimentary units are covered by sediments affected by low-grade metamorphism, the Águas Claras Formation, which was deposited in shallow-marine to fluvial environments (Nogueira et al., 1995). Late Neoarchean alkaline and

metaluminous granites (e.g. Velho Salobo Granite, 2.57 Ga, Machado et al., 1991) are of limited occurrence, but are also found.

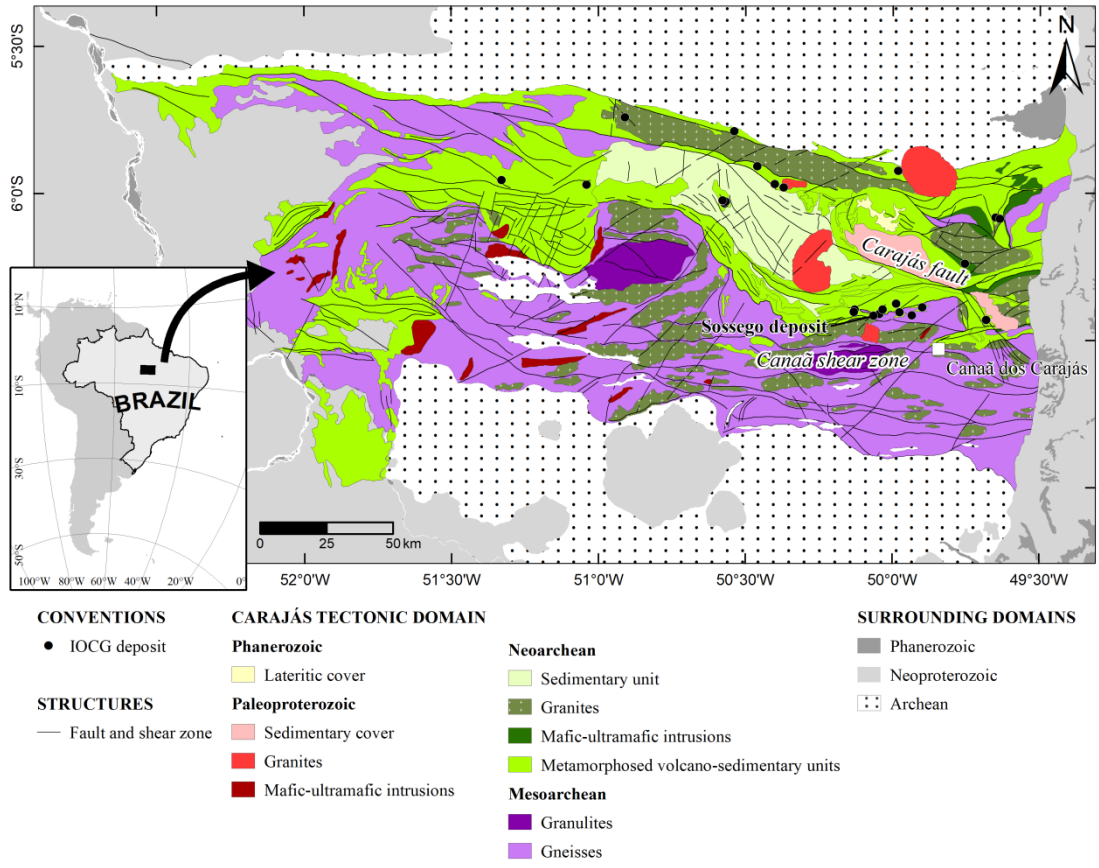

Fig. 1: Regional-scale geology of the Carajás Tectonic Domain (modified from Vasquez and Rosa-Costa, 2008).

The Archean units are affected by Paleoproterozoic magmatism, represented by mafic-ultramafic intrusions (e.g., Cateté Intrusive Suite, Macambira and Vale, 1997) and intracontinental felsic magmatism (A-type alkaline to subalkaline granites), such as the Serra dos Carajás Intrusive Suite (~1.88–1.87 Ga, Machado et al., 1991; Tallarico et al., 2004). This period is also marked by the limited deposition of immature sediments of the Caninana Formation, characterized as poorly selected psammites and psephites (Pereira et al., 2009).

The widely accepted models for the structural evolution of the Carajás Tectonic Domain sustain that the main structural features of the region are the result of an alternating series of transpressional and transtensional reactivations that occurred intermittently during

the Archean and the Proterozoic (Araújo and Maia, 1991; Pinheiro and Holdsworth, 1997; Holdsworth and Pinheiro, 2000). The older structural fabric is represented by E–W and WNW–ESE-trending, moderately to steeply dipping ductile shear zones, with significant strain partitioning, and it is supposed to have developed in the basement during the Mesoarchean. This fabric defines the basic outline of the domain (Fig. 1), and in the Sossego deposit region it is represented by the Canaã shear zone (Domingos, 2009). This ductile fabric was then reactivated in a series of transcurrent events partially controlled by this previous geometry, but also associated with the new development of brittle-ductile and brittle faults, as exemplified by the Carajás fault and later structures, mostly oriented to NE–SW and N–S (Fig. 1; Pinheiro and Holdsworth, 1997).

The Carajás Tectonic Domain comprises one of the most important mineral provinces in the world, encompassing several world-class mineral deposits (Monteiro et al., 2014). This rich endowment includes an uncommon abundance of large IOCG deposits (Xavier et al., 2012), including their first representatives of Archean age (Williams et al., 2005). These IOCG deposits form two spatial clusters, the northern and southern copper belts (Moreto et al., 2015b). Deposits are structurally controlled and present a great variety of host rocks and geochemical signatures (Xavier et al., 2012). Geochronological data indicate three regional episodes of IOCG mineralization (Moreto et al., 2015b): two in the Archean (~2.7 and 2.5 Ga) and one in the Paleoproterozoic (~1.8 Ga). In this context, Sossego deposit presents great economic importance, being one of the largest IOCG deposit in the southern copper belt and currently being mined by Vale Company. Additionally, it is surrounded by several smaller occurrences currently under exploration.

2.2. Local geology and characteristics of IOCG mineralization at Sossego deposit

The Sossego deposit is located on the northern limit of the Canaã shear zone, near the contact between Mesoarchean tonalitic to trondhjemitic gneisses and migmatites of the Xingu Complex and Neoarchean metabasalts of the Itacaiúnas Supergroup (Fig. 1). Mineralization is distributed in five orebodies, which form two sets with particular characteristics: Pista-Sequeirinho-Baiano and Sossego-Curral (Fig. 2). Host rocks and alteration assemblages are thoroughly described in previous works (Monteiro et al., 2008a,b; Carvalho, 2009). Here we present some of the main characteristics of these orebodies.

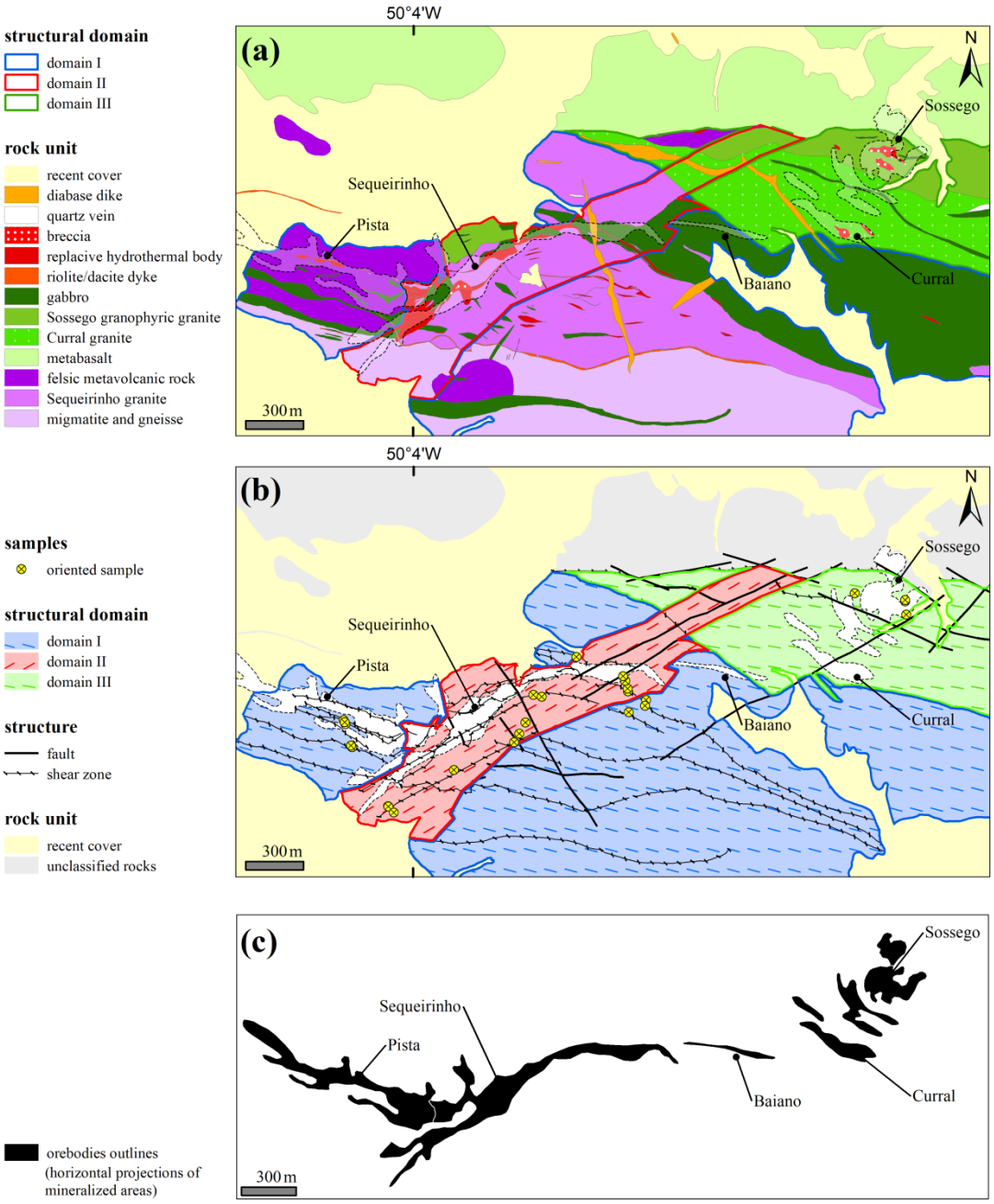

Fig. 2: Local-scale geology of Sossego deposit. (a) Geological map. (b) Structural map, with location for oriented samples used in this study. (c) Orebodies outlines. Maps are adapted from Vale Company and Domingos (2009).

For Pista-Sequeirinho-Baiano orebodies, the main characteristics are:

- *Host rocks*: Sequeirinho Granite in areas close to gabbro intrusions, but also within sheared felsic metavolcanic rocks and gabbros. Different host rocks are juxtaposed by ductile shear zones, forming subvertical WNW–ESE elongated

rock bodies (Neves, 2006). These shear zones have an anastomosing pattern, defining zones with intense deformation (ultramylonites), grading to less-deformed areas where host rocks are isotropic (Carvalho, 2009).

- *Hydrothermal alteration*: host rocks are intensely affected by a regional early Na-alteration (mainly albitization), and then a later Na-Ca alteration (rich in actinolite-epidote) (Monteiro et al., 2008a). Hydrothermal alteration is usually more intense in decametric zones along faults. Na-alteration is pervasive, but fracture-controlled veinlets also occur, with textural evidence that it occurred before and during ductile deformation. Na-Ca alteration is fracture-controlled, but pervasive towards mineralized areas, especially in rocks with mylonitic fabric. Where pervasive, it is associated with replacive bodies of actinolite and magnetite that hold later, subvertical, breccia-hosted Cu–Au mineralization (Monteiro et al., 2008a). Biotitization and silicification are found in mylonitic rocks at footwalls immediately adjacent to faults controlling mineralization, attesting to deformation coupled with metasomatism (Carvalho, 2009).

- *Orebody morphology*: encompasses an "S-shaped" mineralization concordant with the surrounding foliation and shear zones. Pista and Baiano comprise the tips of this trend and are elongated to WNW–ESE, while Sequeirinho is located at the center and is oriented to NE–SW (Fig. 2). Limiting faults are steeply-dipping and orebodies are located in their hanging wall (Monteiro et al., 2008a). Sequeirinho orebody holds the bulk of mineralization, which is characterized by tabular bodies of breccia steeply-dipping to SE, surrounded by an envelope of disseminated ore (Domingos, 2009).

- *Orebody structural domain*: Sequeirinho is hosted in a NE–SW trending zone with apparent sinistral offset, while Pista and Baiano are hosted in its flanks, where structures trend WNW–ESE (Domingos, 2009). These different trends define structural domains II and I, respectively (Fig. 2).

- *Ore structure and texture*: Sequeirinho presents chaotic breccias with subrounded fragments of Na-Ca altered wall-rock in a matrix of ore minerals. The broad range of shapes and fragments sizes (millimeter-decimeter) suggest a milled texture with some comminution (Carvalho, 2009; Domingos, 2009). The disseminated envelope around breccias is characterized by sulfides occurring

parallel to foliation, accompanied by millimeter-centimeter wide veins (Domingos, 2009). Ore at Pista orebody consists of disseminated sulfides and thin films along the mylonitic foliation and fractures, filling fissures, fractures and steeply-dipping veins and in the matrix of small tabular breccia bodies (Carvalho, 2009). Ore at Baiano orebody consists of sulfides in veinlets, fractures and disseminations.

- *Ore main minerals*: both veins and breccia matrix contain an ore assemblage with chalcopyrite, with local concentrations of pyrrhotite and pyrite, accompanied by magnetite (Monteiro et al., 2008a).

- *Mineralization age*: dating of hydrothermal monazite (U-Pb) and molybdenite (Re-Os) indicated Neoarchean ages of ~2.71–2.68 Ga for the Sequeirinho and Pista orebodies (Moreto et al., 2015b).

The main characteristics for Sossego-Curral orebodies are:

- *Host rocks*: Sossego and Curral granites, with minor areas of felsic metavolcanic rocks (Monteiro et al., 2008a). These rocks are subvertical, elongated to WNW–ESE and heterogeneously deformed.

- *Hydrothermal alteration*: early Na- and Na-Ca alterations are poorly developed (Monteiro et al., 2008a). Na-alteration is limited to fractures and concentrated in highly-deformed levels, accompanying mylonitic foliation. K-alteration is well-developed and varies from pervasive near the mineralized zones to vein-controlled further away. Chloritization occurs as veins and replacement zones that cut and envelope the area of K-alteration. The latest stage of alteration is represented by a poorly mineralized zone of hydrolytic alteration (Monteiro et al., 2008a).

- *Orebody morphology*: the Sossego-Curral orebodies represent an independent feature characterized as vertical pipe breccias with sharp boundaries (Carvalho, 2009; Domingos, 2009). The surface projections of these pipes are irregular or elliptical (Fig. 2). Ore breccias are surrounded by a stockwork of steeply-dipping sulfide veins.

- *Orebody structural domain*: Sossego-Curral orebodies are located in structural domain III, which is characterized as a set of WNW–ESE ductile shear zones separated from domain I by a major steeply-dipping fault (Monteiro et al., 2008a).

- *Ore structure and texture*: orebodies here comprise breccias with millimeter-decimeter angular to subrounded fragments of K-altered wall-rock in a matrix of ore minerals and other hydrothermal phases. Breccias are predominantly clast-supported, but matrix-supported breccias are also recognized. Textural evidence indicates that crackle breccia predominates, but chaotic breccias are also present (Carvalho, 2009; Domingos, 2009). Open-space filling textures are present (Monteiro et al., 2008a). The surrounding stockwork domain presents millimeter-centimeter wide veins containing the same assemblage than the breccia matrix (Carvalho, 2009). Veins can be brecciated or massive, and episodic opening is indicated by the occurrence of different mineral phases within them. Vein contacts exhibit evidence of shearing, whereas slickenlines are evidence of potential link with nearby faults (Domingos, 2009). Sulfides also occur disseminated along the wall rock foliation or forming pods.

- *Ore main minerals*: chalcopyrite, with local concentrations of pyrite and magnetite (Monteiro et al., 2008a).

- *Mineralization age*: dating of hydrothermal monazite (U-Pb) from the Sossego-Curral orebodies produced Paleoproterozoic ages of ~1.90–1.88 Ga (Moreto et al., 2015b).

Hydrothermal alteration associated with the mineralization took place during the transition from a predominantly brittle–ductile to a brittle structural regime, with brittle conditions both at Sequeirinho and Sossego segments being associated with late sulfide mineralization (Monteiro et al., 2008a; Carvalho, 2009; Domingos, 2009). Evidence for deformation after mineralization is scarce in the deposit and only observed in the Pista-Sequeirinho-Baiano orebodies, where deformed sulfides can be occasionally found (Monteiro et al., 2008a). Additionally, isotopic and fluid inclusion studies indicate that mineralization was the result of a mixture between deep-seated fluids, with mantle-metamorphic-magmatic origin, and surface meteoric waters or basinal brines (Monteiro et al., 2008a; Carvalho, 2009; Xavier et al., 2012; Moreto et al., 2015b).

3. Data acquisition

3.1. Sample collection and preparation

Field work was done at the Sossego mine pits to collect local-scale data, including measurements of prominent structures and oriented samples of ore and its host rocks. Although the bulk of the deposit is comprised of breccia ore, most samples were collected away from it because breccia ore consists of massive sulfide that is not suitable for the microscale analyses proposed. From all samples collected, 25 oriented rock samples showed evidence of mineralization at variable degrees, and thus were used in subsequent analyses (Fig. 2b). These mineralized samples were prepared for the extraction of oriented thin sections (Hansen, 1990). Considering that this work aims to relate the micro-, local- and regional-scale datasets, we chose to extract the thin sections from the horizontal plane of the samples. The reason for this is that local and regional data maps represent this plane, and thus data acquired in microscale will be directly comparable. Therefore, 25 oriented polished thin sections were prepared, one for each sample. Most samples present the main ore mineral (chalcopyrite), with a few samples containing only magnetite. Considering that magnetite was also formed by hydrothermal alteration related to mineralization (Monteiro et al., 2008a), samples with both minerals were subjected to further analyses.

3.2. Thin section photomicrography and image analysis

Microscale data collection was done through a well-defined workflow that consisted of: (i) inspection of the thin section under the microscope; (ii) selection of areas in thin section for the acquisition of photomicrographs; (iii) georeferencing of the photomicrographs obtained in a GIS; (iv) conversion of the photomicrograph to a binary map of ore mineral distribution; (v) georeferencing of the binary map in a GIS; (vi) analysis of the binary map (Fig. 3).

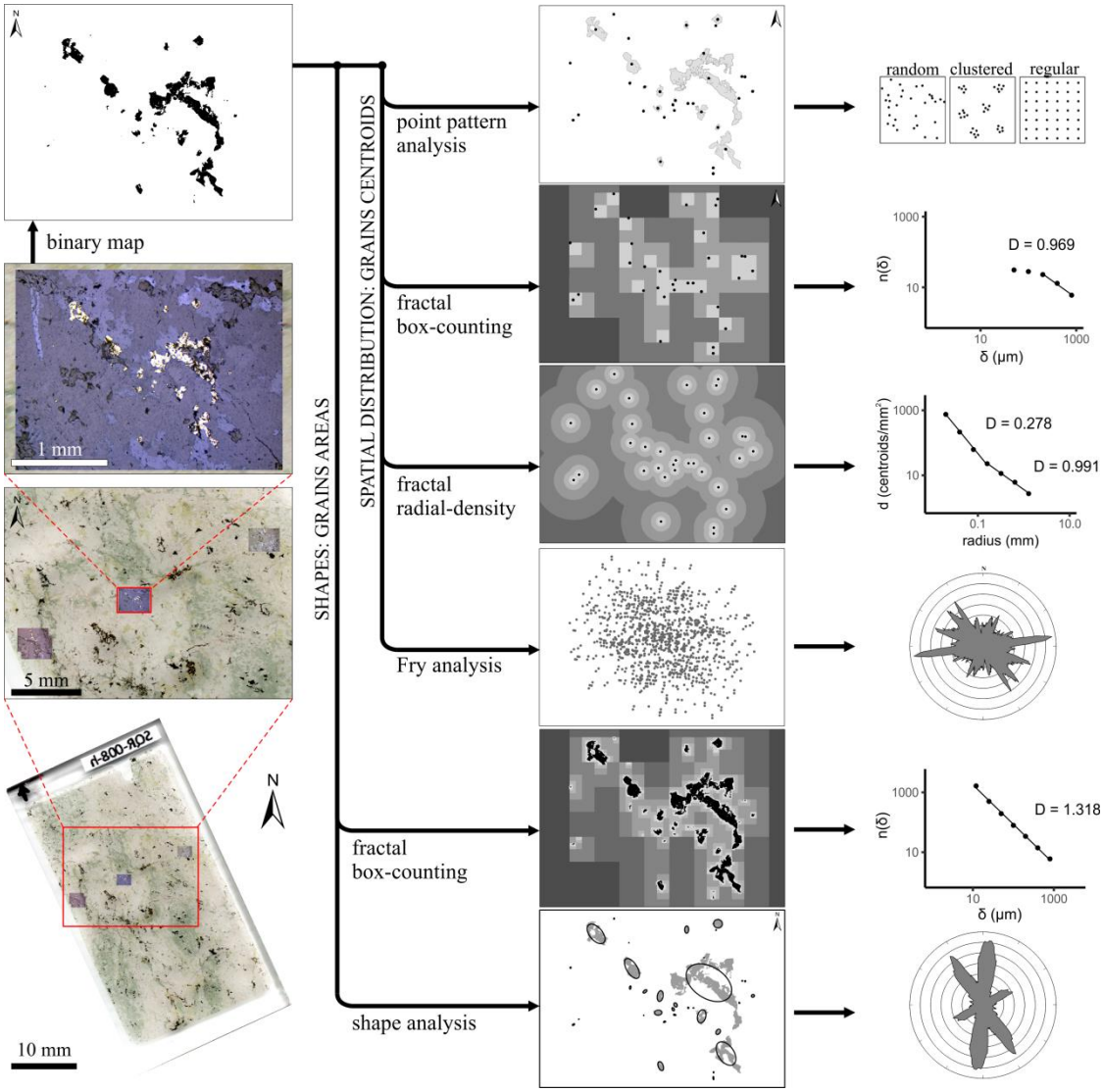

Fig. 3: Workflow for microscale data collection and analysis. The thin section image was georeferenced in a GIS environment (bottom left), including its three photomicrographs obtained under reflected light. During this process, scaling and orientation of images are preserved. From each photomicrography, the binary image of the ore minerals was obtained (top left). From this image, six microscale geometric analyses were carried out. The same workflow was followed for each of the 72 photomicrographs.

Photomicrographs were obtained in a way so that its borders coincided with the N–S and E–W directions. All photos were taken using a camera attached to the microscope, under reflected light, with the same magnification and with the same picture format. In exceptional occasions, where the magnification was not enough to sample an appropriate number of sulfide grains, adjoining pictures were taken and stitched together using the

MosaicJ Plugin (Thévenaz and Unser, 2007) available in the Fiji software (Schindelin et al., 2012).

To improve sampling of different ore minerals patterns, every sample was photographed more than once. For every thin section with homogeneous structure, three locations were chosen to obtain the photomicrographs (Fig. 3), preferably along a profile orthogonal to the dominant structure of the sample (e.g. foliation direction). For every thin section without a clear dominant structure, we chose areas with representative forms of ore minerals. Thus, at the end of the process, 72 photomicrographs were collected, distributed among the 25 thin sections available. Photomicrographs were then georeferenced in a GIS over the thin section scanned images, to check for consistency of scale and orientation (Fig. 3). Each photo was then converted to a binary map by image processing to represent ore mineral distribution.

Image processing was performed in the Fiji software (Schindelin et al., 2012). The binary images were obtained by applying a color threshold to the reflected-light images, focusing on the yellow and high brightness areas, with high saturation being used to separate sulfides from magnetite. We chose reflected light images for the high accuracy in classification and because they closely represent a 2D surface, which is desirable for image analysis (Heilbronner and Barrett, 2014). With this setting, the ore minerals were separated from gangue minerals in each binary image. The raw binary images were then processed to remove inconsistencies [e.g. incorrectly classified isolated pixels or polishing pits inside coarse (> 70 μm) grains]. Image processing was performed in two steps: (i) using a median filter with 1 pixel radius; (ii) manual retouching, using a transparent digital overlay of the binary map over the original photomicrography.

The resulting binary images were then submitted to the ‘Analyze Particles’ algorithm implemented in Fiji, which calculates the geometric parameters of each particle including its centroid position, area, perimeter, best-fit ellipses, etc. Particles touching the image boundaries were excluded from particle analysis and subsequent spatial analytical methods because their shapes were not completely contained in the image. Binary images and particle parameters were then georeferenced in a GIS for further spatial analyses. The methods of spatial analysis applied are grounded on two basic geometric aspects of ore minerals: (i) their spatial distribution (point pattern analysis, fractal analysis and Fry analysis), and (ii) their shape (fractal analysis and shape analysis) (Fig. 3).

Ore formation at Sossego is the outcome of hydrothermal fluids activity, so it will be important to examine results considering their permeability controls, or channelways (cf. Taylor, 2009). In a simplified scheme, ore components can be classified either as formed by precipitation in fluid-filled void space (infill), or by reaction with the wall rocks (alteration). In geological settings such as Sossego, permeability is controlled by variable styles of fracturing, which resulted in a combination of infill and alteration ore components that could have masked the nature of the original channelways. Therefore, it is essential to separate these two ore components to understand the permeability that controlled ore-forming processes. As such, each photomicrograph obtained was classified as either infill or alteration. Pictures were classified as infill only when directly within veins and fractures. All remaining pictures were classified as alteration, and they are usually associated with foliation planes, intergranular contacts or adjacent to fractures. To account for different textures reflecting the intensity of alteration in the picture, images classified as alteration were further subdivided into disseminated alteration (abundant grains distributed more homogeneously in the whole photo) and sparse alteration (usually scant grains, distributed heterogeneously throughout the photo). Examples of each texture can be found in Supplementary Material (Appendix A).

4. Analysis of the spatial distribution pattern of ore minerals in the microscale

For each of the photomicrographs analyzed, the spatial pattern of ore minerals – represented by their centroids – were subjected to the spatial analytical methods explained below.

4.1. Point pattern analysis

The spatial distribution of minerals in thin sections can provide insights into their forming processes (Kretz, 1969; Jerram et al., 1996). As such, we applied Point Pattern Analysis (PPA) to examine the spatial distribution of ore minerals at the microscale. For that we used the Average Nearest Neighbor (ANN) algorithm available in ArcMap™. The ANN analysis measures the distance between each point and its nearest neighbor. The average of all distances observed ($\overline{D}_O$) is then compared to the averaged distance expected ($\overline{D}_E$) between points of a hypothetical random distribution, with the same number of points and within the same total area. If the observed mean distance is less than the average for the random distribution, the analyzed pattern is considered clustered; if it is larger, it is considered dispersed. The z-score for the ANN statistic is then calculated for a given p-value, in order to evaluate if the departure from the random distribution is statistically significant. The general

concepts supporting ANN can be found on classic PPA textbooks (e.g., Boots and Getis, 1988).

The ANN analysis is very sensitive to study area size, and so it is effective for comparing patterns in a fixed study area. This limitation is not relevant here since most photomicrographs analyzed are rectangles with exactly the same area. Additionally, the representation of mineral grains as points is suitable only if the number of analyzed grains in contact with each other is low (Kretz, 1969); otherwise, the possibility for a given mineral to have a random distribution would be limited (Jerram et al., 1996). Since ore minerals in our samples are mostly not in contact with each other, this issue has likely not expressively affected the results.

The results of PPA indicate that for the majority of images analyzed the distribution of ore minerals is clustered, with eight images returning random patterns and a single image displaying a dispersed pattern (Fig. 4). It is noticeable that some random patterns plot away from the strictly random line, and that the larger the observed distance, the further away from the line a random pattern can be found. ANN z-scores are dependent on $\overline{D}_O$, thus as $\overline{D}_O$ increases the ratio $\overline{D}_O/\overline{D}_E$ can increasingly depart from the 1:1 relationship and still be statistically random.

PPA results suggests that clustered features have controlled the circulation and concentration (i.e., focusing) of mineralizing fluids and thus the crystallization of ore minerals in clusters at the microscale. This inference can be examined in more detail with the application of fractal analysis.

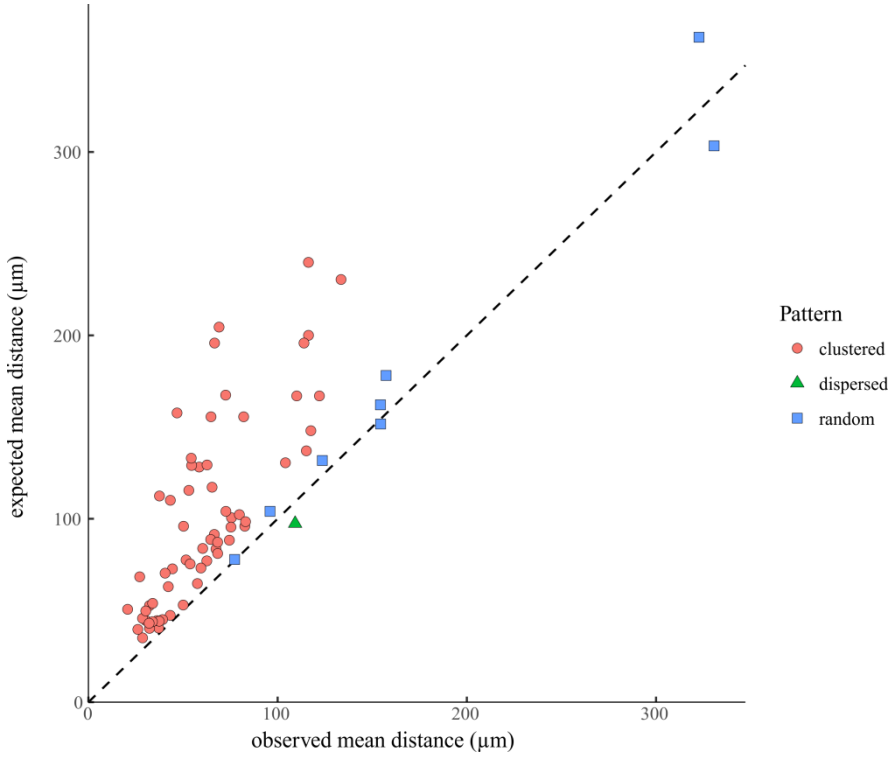

Fig. 4: Scatter plot illustrating results of ANN analysis for 72 photomicrographs of ore minerals. Classification of patterns is given for p-value < 0.1. The dashed line marks the trend for patterns where the observed mean distance ($\overline{D}_O$) equals the expected mean distance ($\overline{D}_E$), i.e., a strictly random pattern.

4.2. Fractal analysis

Fractal geometry describes the shapes of fractals, which are irregular objects that cannot be adequately described by Euclidean geometry (Kreuzer et al., 2007). The fundamental characteristic of a fractal is *self-similarity* (or *self-affinity*), which means that a segment of the fractal contains a copy of the entire design (Mandelbrot, 1983). A fractal is commonly manifested via its fractal dimension, which represents a measurement of object irregularity (Xu et al., 1993). In this study, we applied fractal analysis to examine if the factor that controls the spatial distribution of ore minerals at the microscale is fractal. To do so, we subjected the same centroid sets examined by PPA to two fractal methods: the box-counting and the radial-density (Carlson, 1991; Carranza, 2008,2009; Agterberg, 2013). The box-counting and radial-density methods were implemented in ArcMap™ (Wang et al., 2007; Raines, 2008; Carranza et al., 2009).

The box-counting method derives the fractal dimension of a geometric pattern by covering it with a grid of boxes with a given size δ and then counting the number of boxes $n(\delta)$ that covers a part of the pattern. The geometric pattern can be a set of points, lines or areas. The box side is then halved, and a new counting of the number of boxes covering the pattern is performed. The procedure is repeated several times, and then plotted in a log-log graph of $n(\delta) \times \delta$. If the points obtained can be fitted with a straight line through least-squares regression, then the geometric pattern can be considered fractal and its fractal dimension (D_{bc}) is obtained from the equation of the regression line.

The radial-density method is used to derive the fractal dimension of a geometric pattern of points. Each point is covered by a circle with radius r, and then the point density d is calculated by the relationship between number of points and the area covered by all the circles, excluding overlapping areas of individual circles. The radius is doubled and the point density is re-calculated. The procedure is repeated a number of times until the defined study area is completely covered by circles. The results are plotted in a log-log graph of $d \times r$. If the plots obtained can be fitted with a straight line through least-squares regression, then the point pattern can be considered fractal and its fractal dimension (D_{rc}) is obtained by the inclination of the regression line.

Here, the box-counting analysis of centroids was carried out using an initial box side with 800 μm. This box side was halved four times, with a final box side of 50 μm. These upper and lower limits were chosen because they are compatible with the mean centroids distribution and the photomicrograph area, and thus avoid sampling effects of the method (Walsh and Watterson, 1993). The whole area covered by the box-counting method (2400 x 1600 μm) is slightly different than the photomicrograph area (2215.33 x 1661.50 μm), in order for the fractal study area to be completely covered by the initial boxes used. Most pictures do not present ore minerals that are so close to the border of the picture, so the area used for fractal analysis does not affect the results. The radial-density analysis of centroids was performed with an initial radius of 20 μm, and doubling the radius in each iteration until the same area covered by the box-counting analysis was completely covered by circles.

The results of the fractal analysis indicate that the spatial pattern of ore minerals is fractal, as suggested by the linear relationships obtained for the box-counting and the radial-density methods for the majority of images analyzed (Supplementary Material, Appendix B). Previous authors have attested the goodness of fit of spatial patterns to the fractal model by

using R^2 values (Peternell and Kruhl, 2009; Peternell et al., 2011). In our analysis, most results present $R^2 > 0.99$ (Fig. 5).

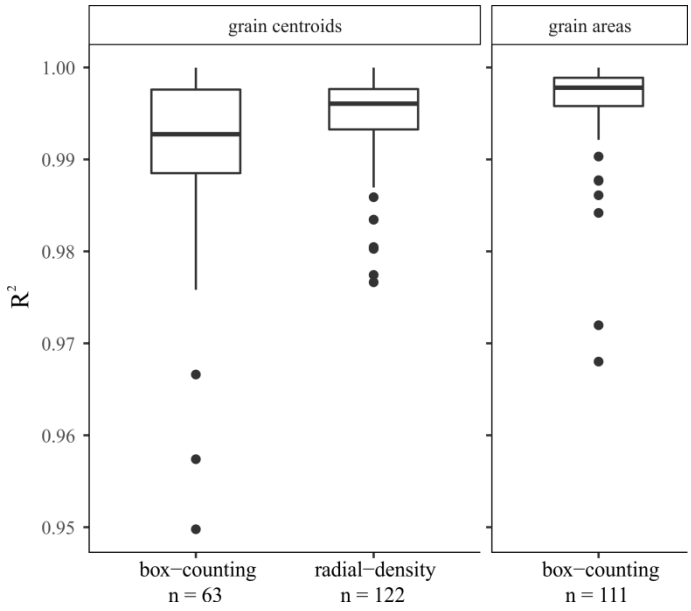

Fig. 5: Box-plots for R^2 values obtained for linear regressions of fractal analyses.

In the box-counting method, the results for nine of the analyzed patterns could not be properly fit with straight line segments in the log-log graphs, suggesting that fractal geometry is not present at the scale of the microphotographs. For the remaining 63 microphotographs the results could be fitted with regression lines, indicating that most of the analyzed patterns present a fractal distribution. Within the sampled range, it is noted that results for box sides (or distances) smaller than 100–200 μm fall below the fitted regression line. This departure from the linear relationship at small distances is common in the box-counting method and is due to sampling effects (Walsh and Watterson, 1993). In our analysis, each small-sided box samples a single centroid and therefore represents only one feature, which generates a horizontal line in the log-log graph ($D_{bc} = 0$). This effect is reinforced in our analysis due to the fact that there is a minimum distance between adjacent centroids given by the grain areas. As a result of this departure, these data points in the log-log graphs of $n(\delta)$ x δ were not considered in the linear regression and determination of D_{bc} of the spatial patterns.

Fractal dimension values present a scatter of results. The box-counting of centroids for all images indicate values of D_{bc} ranging from 0.58 to 1.90, but with most of the D_{bc} values above 1.0 (Fig. 6a). These results are expected since the spatial patterns represent different ore components, with different textures. When results for alteration and infill ore components are separated, some trends emerge (Fig. 6b). Disseminated alteration presents a narrower range of higher D_{bc}, with values tending to be space-filling ($D \rightarrow 2$). The ranges of D_{bc} for sparse alteration and infill ore components overlap, although sparse alteration presents a tendency to higher D_{bc} values. Infill presents the broadest range for D_{bc}, which tend to be lower in comparison with alteration ore components.

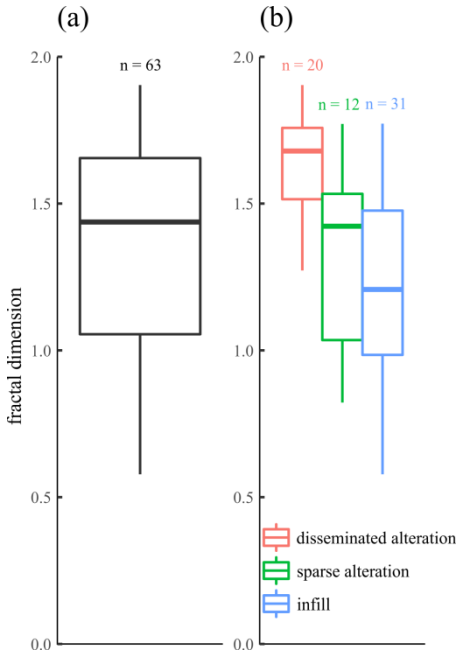

Fig. 6: Box-plots of box-counting fractal dimensions for grain centroids. (a) All images. (b) Per ore component type.

As we are measuring the dimension of point distributions representing centroids of ore mineral grains, D_{bc} values are directly proportional both to grain abundance and distribution (Zuo et al., 2009a). Additionally, centroid abundance is inversely related to grain size in the image, as too many coarse grains result in fewer centroids and in lower fractal dimensions. As such, box-counting results can be interpreted as a consequence of the geometric patterns of the different ore components (Fig. 7).

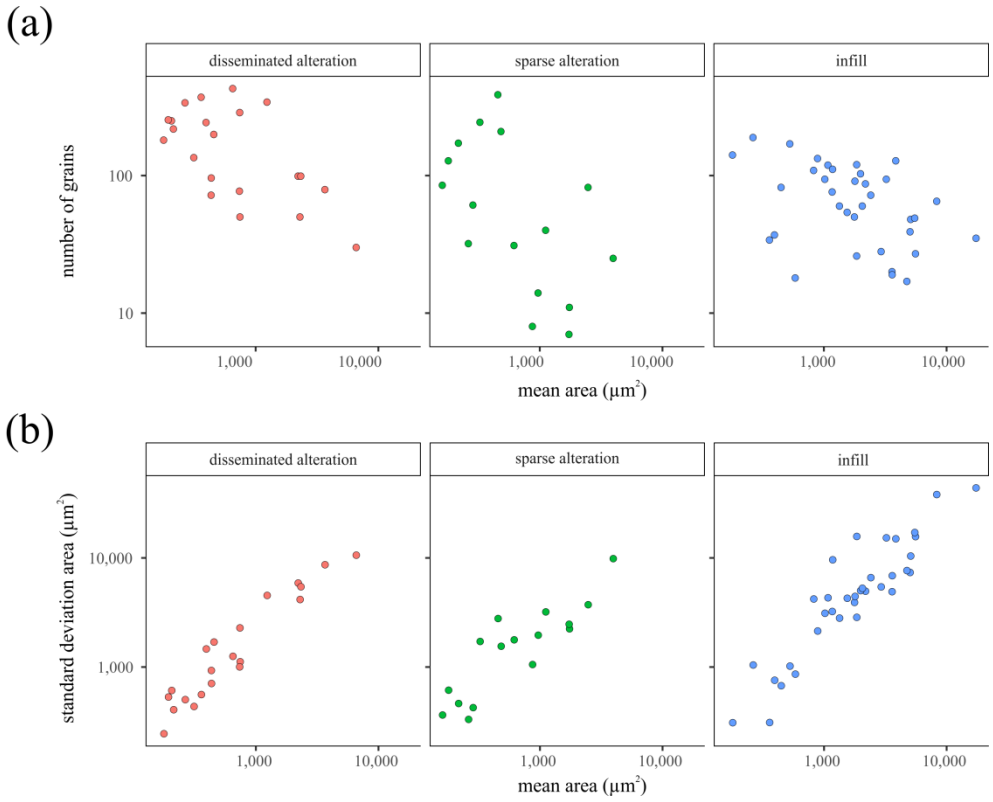

Fig. 7: Basic trends in the geometric patterns of ore components of the Sossego deposit. (a) Relationship between the number of ore mineral grains and mean area per analyzed image. Disseminated alteration is commonly characterized by images with abundant fine grains, while infill images present few, but coarse grains. Sparse alteration presents patterns with both characteristics, and the images with the fewest grains. (b) Relationship between standard deviation from the mean area and mean area per analyzed image. Finer grain sizes in disseminated and sparse alteration are usually associated with lower standard deviations, suggesting a more homogeneous grain size. On the other hand, the larger mean areas in images of infill are usually accompanied by higher standard deviations, suggesting a more heterogeneous texture. Note logarithmic scales. Grains with areas < 30 μm^2 are excluded (see details in section 5.2).

Disseminated alteration, which presents a high number of fine grains scattered over the whole image and a rather homogeneous texture, displays a narrow range of higher D_{bc} values. In contrast, sparse alteration and infill, which present fewer grains and with more heterogeneity in grain abundance and size, show a wider range of lower D_{bc}.

In the radial-density analysis, the results for six images could not be properly fitted with straight line segments in the log-log graphs. For the remaining 66 images, results could be fitted with regression lines, thus indicating that most of the analyzed patterns present

a fractal distribution in the range of 20 to 2,560 μm. Unlike results of the box-counting analysis, the results of radial-density show that D_{rc} is not unique throughout the analyzed scale interval. Some results are best fitted by two line segments with different inclinations, thus reflecting two D_{rc} for different spatial ranges (Supplementary Material, Appendix B). Such patterns are called *bifractals*, in contrast to patterns with a single dimension, which are called *monofractals* (Ord et al., 2016). In the log-log graphs, the distance where D_{rc} changes is marked by a break point that indicates the transition between the two ranges with different fractal dimensions.

Results of radial-density analysis indicate that patterns in 56 images are bifractal with breaks situated in 80–160 μm, while the patterns in the remaining 10 images are monofractal (Fig. 8a). The range for D_{rc} in monofractal patterns is mostly between 0.50 and 1.00, with median around 0.75. For the bifractal patterns, D_{rc} values for smaller radii are mostly between 0.25 and 0.50, while for larger radii values increase to the range $1.00 < D_{rc} < 1.25$. Monofractals patterns usually present intermediate D_{rc} values in relation to the smaller and larger radii in the bifractal patterns (Fig. 8a).

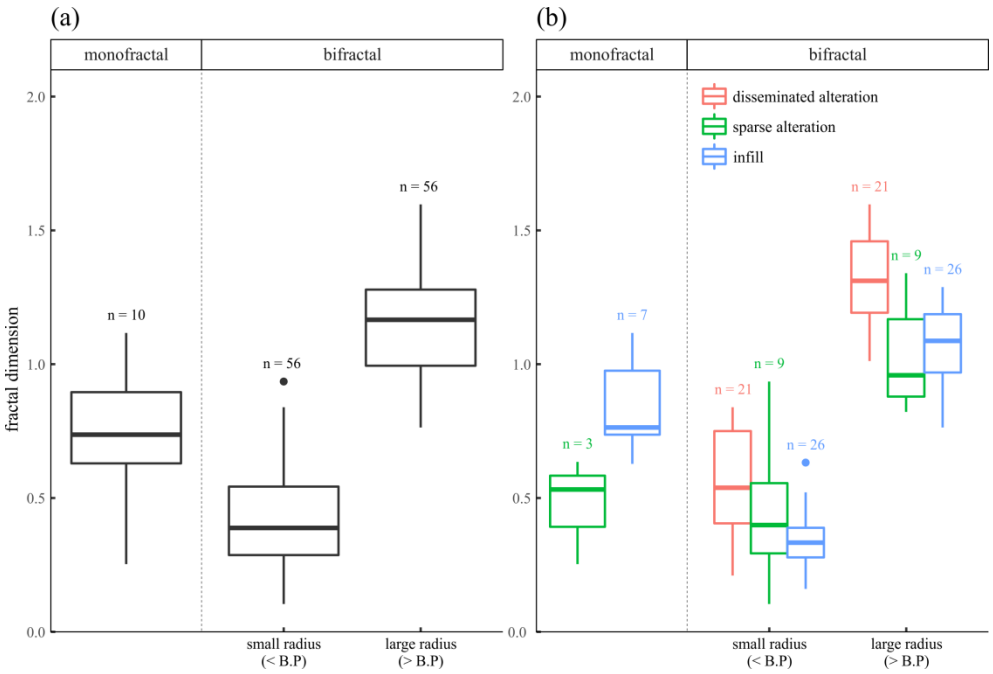

Fig. 8: Box-plots of radial-density fractal dimensions for grain centroids. (a) All images. (b) Per ore component type. B.P. = break point.

The textures of different ore components influence the observed radial-density results (Fig. 8b). All ore components exhibit either monofractal or bifractal patterns, except disseminated alteration, which exhibits only bifractal patterns. Additionally, infill presents higher D_{rc} compared to sparse alteration for monofractal patterns. Fractal dimensions overlap greatly for ore components in the range of smaller radii, although there is a tendency of increasing dimension from infill to disseminated alteration. Additionally, infill presents a narrower range for D_{rc}. In the range of larger radii, disseminated alteration shows higher dimension values compared to sparse alteration and infill, which, in turn tends to present higher D_{rc} than sparse alteration.

The radial-density method investigates the density of points, which in this case is sensitive to the degree of clustering in each image, as well as the shape of clusters. From this, it can be inferred that infill or sparse alteration with monofractal patterns present a rather homogeneous clustering within the distances analyzed. This inference is supported by images representing either monofractal infill or sparse alteration, since they are characterized by strong linear patterns or by the presence of sparse grains. The absence of monofractals in the disseminated alteration images suggests that this component is rather prone to present heterogeneities in grain clustering. Additionally, the lower D_{rc} for sparse alteration in relation to infill in monofractal patterns is in agreement with the fact that this alteration usually is more clustered and presents fewer grains, and thus is less space-filling (Figs. 7, 8b). Disseminated alteration presents a tendency for higher D_{rc} compared to sparse alteration and infill, both in the smaller and larger radii of bifractal patterns. This should be expected because in disseminated alteration points are spread far apart (finer and more abundant grains – Fig. 7a), resulting in a more space-filling pattern.

The bulk of results from PPA and fractal analyses indicate that the pattern for the spatial distribution of ore minerals at Sossego deposit is essentially non-random, and that its deterministic portion seems to be fractal. These interpretations can be examined further through the use of Fry analysis.

4.3. Fry analysis

We have subjected the same set of images examined by PPA and fractal analyses to Fry analysis (Fry, 1979; Vearncombe and Vearncombe, 1999), using centroids of ore mineral grains to examine the preferential directions between grains. Fry analysis is a form of autocorrelation analysis that can be used to enhance preferential directions between points in a

point distribution (Vearncombe and Vearncombe, 2002). It has been used successfully in regional and local scales to examine structural control on ore deposits (Vearncombe and Vearncombe, 1999; Stubley, 2004; Blenkinsop and Kadzviti, 2006; Carranza, 2009; Zuo et al., 2009a; Lisitsin, 2015). The method's principle is to compute all possible direction-distance vectors between point pairs in the distribution ('Fry points'), and include them in a single diagram called the 'Fry plot'. The results highlight the preferential direction within a point population, and can be better visualized with the aid of rose diagrams. A review of the basic concepts of Fry analysis can be found in several works (Fry, 1979; Vearncombe and Vearncombe, 1999; Carranza, 2009). Here, Fry analysis was performed using DotProc shareware. Rose diagrams were made using the Windows® version of MARD (Munro and Blenkinsop, 2012), the TENSOR software (Delvaux and Sperner, 2003) and the spatstat package in R (Baddeley et al., 2015).

A possible limitation with Fry analysis is that it can be sensitive to the study area shape, especially if it is too narrow (Austin and Blenkinsop, 2009). These authors suggest that the autocorrelation directions over lengths greater than the smallest side of the study area may be influenced by shape. Considering our images are slightly rectangular (2215.33 x 1661.50 μm), we have performed Fry analysis both in the whole photomicrograph (thus considering all pairs of Fry points), but also limited to the smallest image side, thus only considering an 800 μm radius around each point. Fry analysis was performed per image, and the obtained results were grouped according to structural domain (Fig. 2b) and ore component (Figs. 9, 10).

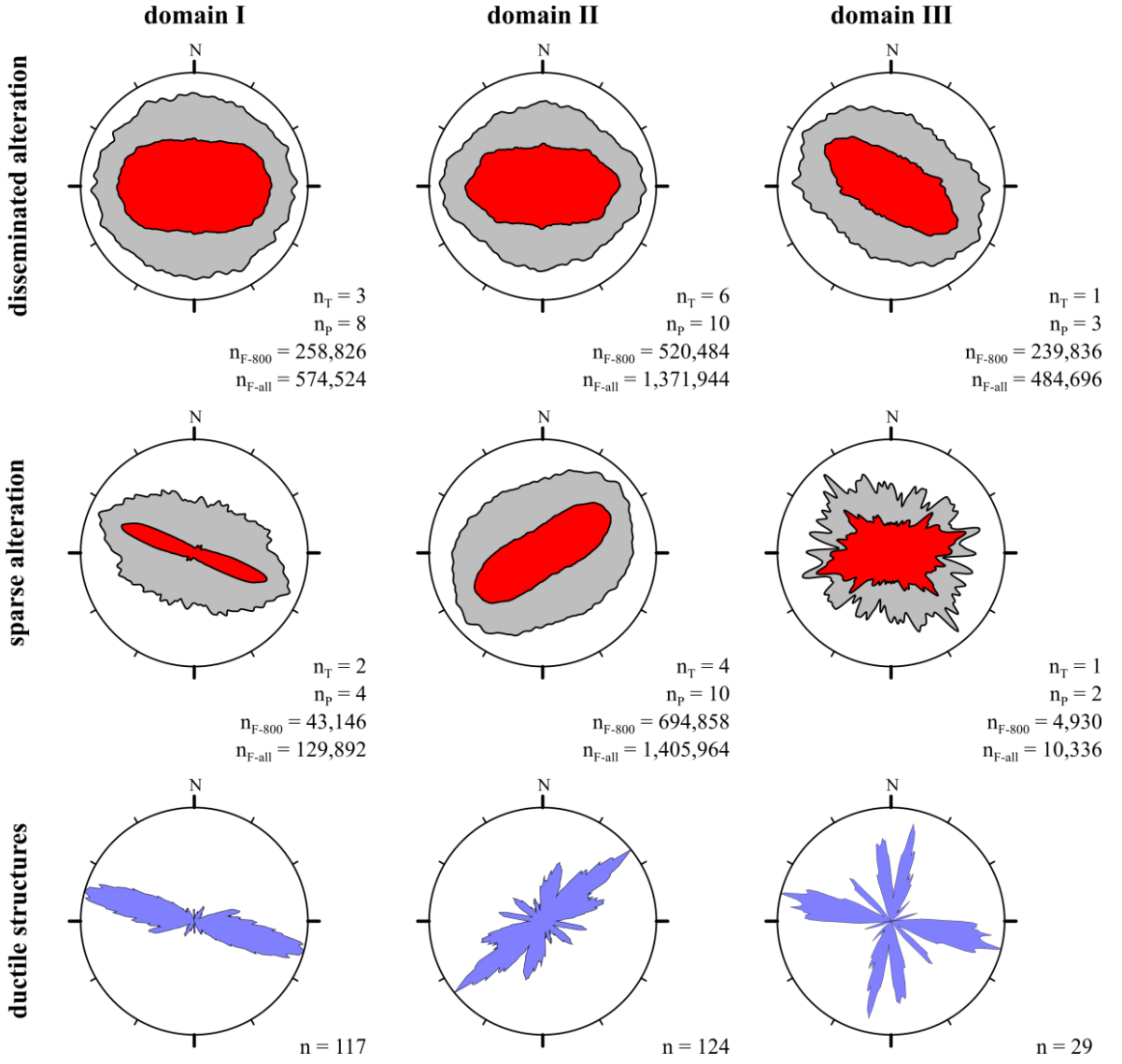

Fig. 9: Rose diagrams for ore minerals trends in the microscale (alteration ore component) and structures from mine benches. Red: Fry points for the whole image; Gray: Fry points for distances ≤ 800 μm. Results for the whole image were arbitrarily reduced by a factor of 0.25 to facilitate comparison. Ductile structures: strike direction for foliation and shear zones. Sample sizes for each rose diagram: n_T = thin sections; n_P = photomicrographs; n_{F-800} = Fry points (< 800 μm); n_{F-all} = Fry points (all).

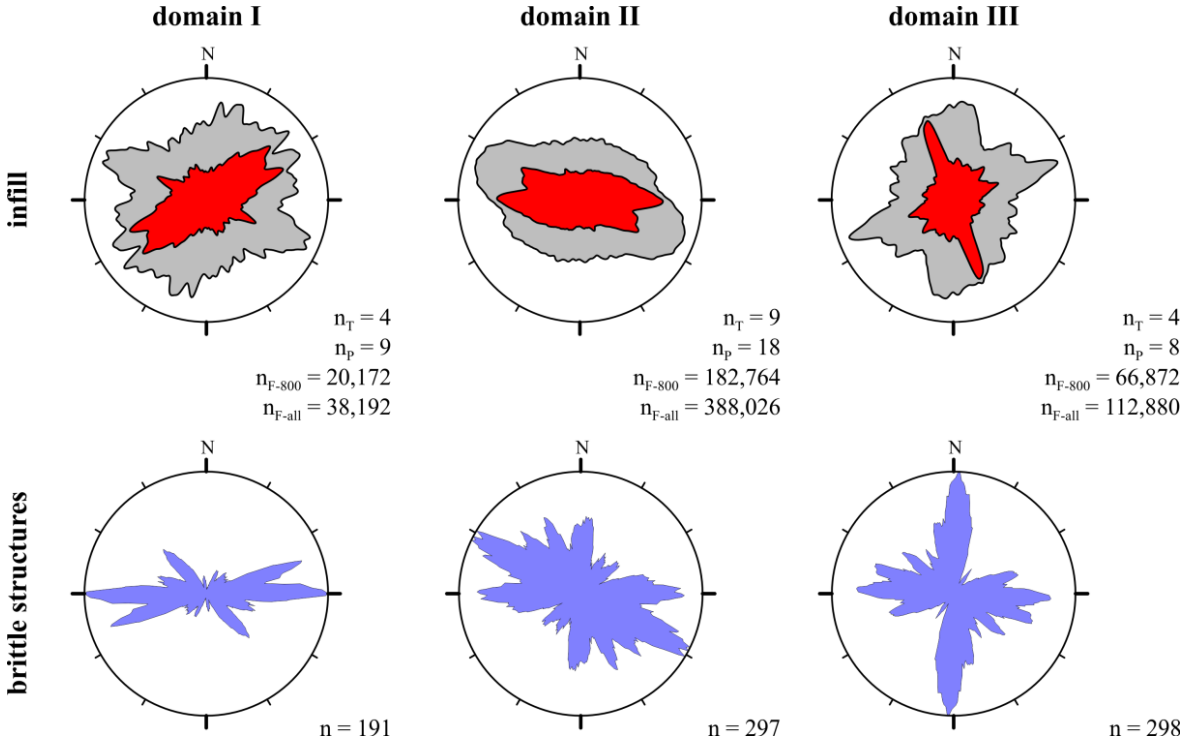

Fig. 10: Rose diagrams for ore minerals trends in the microscale (infill ore component) and structures from mine benches. Red: Fry points for the whole image; Gray: Fry points for distances ≤ 800 μm. Results for the whole image were arbitrarily reduced by a factor of 0.25 to facilitate comparison. Brittle structures: strike direction for faults, mineralized veins and fractures. Symbols for sample sizes as in Fig. 9.

Results for Fry points for lengths ≤ 800 μm are generally consistent with those for all Fry points, although trends are less defined in the shorter range. This effect is particularly noted in images of disseminated alteration, especially in structural domain I, where results for lengths ≤ 800 μm indicate near absence of preferential direction (Fig. 9). For all other groups, observed trends are usually preserved, suggesting that they are independent of the shape of the study area (cf. Austin and Blenkinsop, 2009).

Ore minerals in disseminated alteration in domain II have a poorly defined E–W trend, while those in domain III have a better defined NW–SE trend (Fig. 9). Unlike in disseminated alteration, ore minerals in sparse alteration exhibit distinct trends. In domain I they are oriented WNW–ESE, while in domain II they are directed NE–SW. In domain III a main NW–SE trend is highlighted, together with a subordinate ENE–WSW trend.

Fry analysis of infill ore components indicates main trends that are oriented opposite to those of alteration components, although secondary trends of the former coincide with those of the latter (Fig. 10). For infill in domain I, trends are oriented NE–SW and WNW–ESE, while in domain II trends are oriented mainly WNW–ESE, with a gentle dispersion over the NE–SW quadrants. For infill in domain III preferential orientations are N–S and ENE–WSW.

Disseminated and sparse alteration in the thin section are mainly associated with foliation and related intergranular boundaries, which in Sossego are connected mostly to the development of the ductile framework of shear zones and foliation planes (Carvalho, 2009; Domingos, 2009). For disseminated alteration, the abundance of ore grains in the thin sections as a whole generates a pattern with diffused E–W trends, which are slightly oblique to the trends of ductile structures. In contrast, sparse alteration exhibit trends that are very similar to those structures, especially in domains I and II (Fig. 9). The similarity is less evident in domain III, with the NW–SE direction observed in Fry analysis being slightly oblique to the WNW–ESE trend of structures, and with the N–S trend being unrepresented. However, it is important to note that domain III has the smallest number of samples, and thus, some of these differences could be the result of under-sampling.

Infill ore components are associated with fractures and veins in the thin sections. These structures are related to the brittle framework of Sossego deposit, which was developed after the ductile structures (Domingos, 2009). As such, when results for Fry analysis of the infill components are compared to available structural data for brittle structures in the mine pit, there is a good coincidence of trends, especially for domains II and III. For domain II, main trends are WNW–ESE, and for domain III, N–S, ENE–WSW and WNW–ESE. For domain I, the shape of the distribution is very similar, but ore mineral trends are rotated ~20° counterclockwise (Fig. 10).

The rose diagrams for Fry points of ore minerals in the Sossego deposit strengthen the results of the PPA and fractal analyses, suggesting that ore minerals show defined trends that can be related to the structural controls at the deposit scale. The relationship between the geometry of ore minerals at the microscale and their structural control can be investigated further by examining the individual shapes of grains and the shapes of mineralized areas. This is the topic of the next section.

5. Shape analysis of ore minerals in the microscale

Shape analysis derives information about the origin of a feature based in their resulting shape, which can be informative about a variety of geological processes (Heilbronner and Barrett, 2014). It is routinely used in different geological settings to assess metamorphic conditions, deformation mechanisms, strain, and porosity, just to name a few applications (Peternell and Kruhl, 2009). Here, we have examined the shape of ore minerals using two complementary methods: (i) fractal analysis; and (ii) best-fit ellipses. We employed the geometric parameters obtained during image analysis of the same set of binary images utilized in the analysis of spatial distribution of grains (Section 4).

5.1. Fractal analysis

Earlier studies show that shapes of minerals can present fractal geometry in the microscale as a response to deformation mechanism (Mamtani, 2012), deformation intensity (Wang et al., 2007), physicochemical conditions (Peternell and Kruhl, 2009), petrogenesis (Xie et al., 2010) and growth history (Zuo et al., 2009b). All these processes can play a role in mineralization control. To complement the results discussed in Section 4, we applied fractal analysis to examine if the shapes of ore mineral grains at the Sossego deposit present fractal geometry.

We subjected the binary images of ore mineral grains to the box-counting method to examine their shape (D_{bg}, Wang et al., 2007; Zuo et al., 2009b). We used the same algorithm applied in the box-counting of centroids shown above, including the same initial box side (800 μm), but in this case with seven iterations, down to a final box side of 12.5 μm.

The results indicate that the shape of ore minerals is fractal, as attested by linear relationships obtained for the majority of patterns analyzed and the high R^2 values (Fig. 5; Supplementary Material, Appendix B). The results for three images cannot be fitted with straight line segments in the log-log graphs. For the remaining 69 images, the results of linear regression indicate that the analyzed patterns present fractal geometry in the range of 12.5 μm to 800 μm. The box-counting of grain areas show that D_{bg} is not homogeneous throughout the analyzed interval for all images, resulting in monofractal (27 images) and bifractal (42 images) patterns, the latter with break points situated in the range 100–200 μm.

The D_{bg} interquartile range for monofractal patterns range between 1.20 and 1.40 (Fig. 11a). For bifractal patterns, the interquartile range for small-sided boxes span between 0.90 and 1.25, while for large-sided boxes values are within $1.40 < D_{bg} < 1.90$. These results indicate that monofractals patterns present intermediate D_{bg} values compared to bifractals. Additionally, a great scatter of values is observed, especially for bifractal patterns. This can be investigated further once data for alteration and infill are examined independently (Fig. 11b).

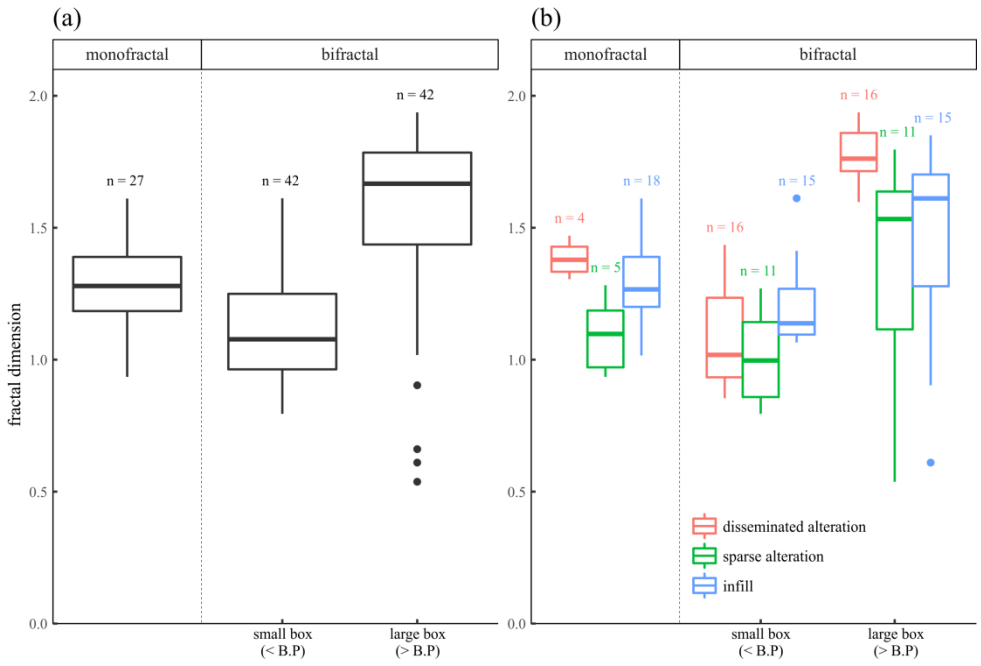

Fig. 11: Box-plots of box-counting fractal dimensions for grain areas. (a) All images. (b) Per ore component type. B.P. = break point.

Infill ore components are predominantly monofractals. Alterations are mainly bifractals. The ranges of D_{bg} values for the different ore components overlap, although interquartile ranges and medians suggest that disseminated alteration presents higher values, especially relative to sparse alteration (Fig. 11b). In the distance range for small-sided boxes of bifractal patterns, there is an important overlap. For the range of large-sided boxes, disseminated alteration is well-separated from the other components, with a narrower range of higher D_{bg}. Sparse alteration and infill present a broad range of D_{bg} values, although for infill the range is narrower and higher.

For the box-counting of grain areas, small-sided boxes sample the grain shape individually, while large-sided boxes are sensitive to the spatial arrangement of the grains. Therefore, box-counting of grains is reflecting not only the shape and size of grains, but also the shape and size of their clusters. As such, the bifractal patterns can be inferred to be the result of marked difference in grain shapes and their clusters throughout the distances investigated. In contrast, monofractals are the result of patterns with a more homogeneous size and clustering of grains. This is supported by the tendency of the monofractal patterns to be related with images with the coarsest grains, or where coarse grains are more common. In this case, the single dimension represents less the change between grains clusters and grains individually, and more the general shape of the grains, thus resulting in more homogeneous sampling. Thus, the predominance of monofractal patterns among infill relative to alteration could be partially explained by the abundance of coarse grains, as explained above (Fig. 7). The large overlap of D_{bg} values between different ore components suggests relative homogeneity in grain shape in monofractals, although the greater abundance of grains in disseminated alteration compared to sparse alteration results in higher D_{bg}.

The overlap in the range of small-sided boxes of bifractal patterns suggests that the grain shape is rather indifferent between ore component types. The tendency for lower D_{bg} values in disseminated alteration can be explained considering the resolution imposed by the smallest box size used (12.5 μm). As such, small-sided boxes sample coarse grains effectively as areas, while fine grains are too small and tend to be sampled as points. If the grains are sampled as points, then the measured fractal dimension will tend to zero. For the range of large-sided boxes, the homogeneity of disseminated alteration has to do with the fact that box-counting with large boxes will be almost the same for different images, since all boxes will present sulfides. Conversely, infill and sparse alteration present more variation in grain abundance and size and yield heterogeneous D_{bg} values.

The results discussed above suggest that ore mineral shapes present fractal geometry, which could prove useful to gain insight into the structural control on mineralization. To investigate this possibility further, we examined the simplified version of each grain shape: their best-fit ellipses.

5.2. Shape analysis: best-fit ellipses

For various applications it is convenient to simplify the shapes under study to fundamental parameters, such as size, axial ratio (or anisotropy) and orientation (Heilbronner and Barrett, 2014). In this context, best-fit ellipses are especially useful because their shape is defined by these three parameters. Although not all natural shapes are elliptical, the use of best-fit ellipses is usually justified as a representation of these parameters for a given shape, especially in terms of axial ratio and orientation (Heilbronner and Barrett, 2014). Here, we focus on the anisotropy and orientation of the best-fit ellipses for the ore minerals available in the analyzed images. Anisotropy was assessed by the axial ratio between the minor and major axes. The preferential orientation was extracted from the orientations of the ellipses' major axes. To avoid spurious results, grains with areas < 30 μm^2 were excluded from analysis, because their sizes were too small considering the pixel size and their shape parameters could render imprecise results.

Results indicate that the average grain departs from a circular shape, as indicated by axial ratios < 1.00 and usually > 0.25, suggesting that the average shape is anisotropic (Fig. 12). The angular coefficient of the linear model fitted through the data and placed at the origin, represents the average axial ratio of the grain population (Heilbronner and Barrett, 2014). In the present case, results indicate that the axial ratio is close to 0.5 both for alteration and infill.

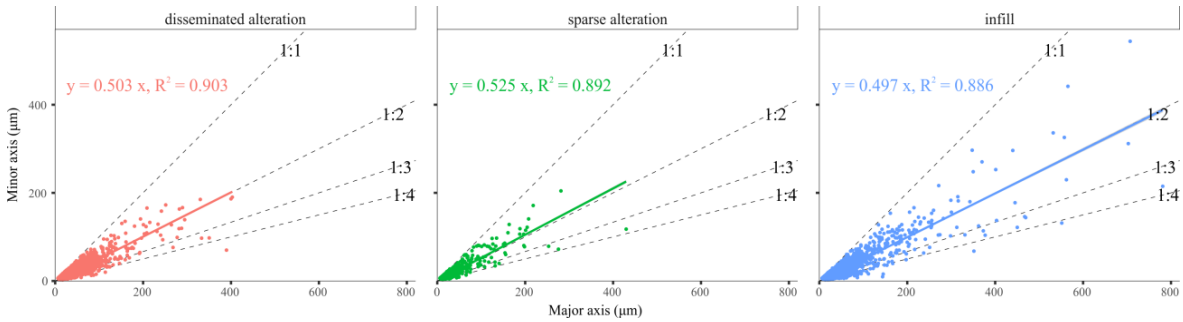

Fig. 12: Anisotropy of ore minerals grains (axial ratio for best-fit ellipses). Equations for linear models are given in each diagram. Dashed lines represent ratios used as references for discussion in the text.

Since ore mineral shapes suggest the existence of anisotropy, it is useful to investigate if this anisotropy has a particular orientation. To examine this, we produced rose

diagrams representing the orientation of the major axis of ellipses. As different structural domains present different orientation trends, the analysis was also separated by structural domain (Fig. 13a).

Rose diagrams in Fig. 13a reveal that although major axis orientations can be highly scattered, preferential trends can be found in almost every structural domain, for each ore component. For domain I, major axes are oriented WNW–ESE and E–W for all ore components. Important NE–SW trends are also present for sparse alteration and N–S for infill. For domain II, there is a NE–SW trend, well-defined for sparse alteration but subtle for disseminated alteration and infill. For infill, a NW–SE trend is also present. For domain III, trends are well-defined, directed ENE–WSW for infill, ENE–WSW and WNW–ESE for disseminated alteration, and NW–SE and NE–SW for sparse alteration. Disseminated alteration also displays a secondary N–S trend.

Ore minerals at Sossego deposit are not deformed, so their best-fit ellipses are not a proxy for the strain ellipse during the mineralization. So, what could these preferential orientations mean? To answer this question it is interesting to bring forward the concept of mineralization ellipsoid, which has been used before to model mineralization control on the deposit scale (Monteiro et al., 2004; Blenkinsop and Kadzviti, 2006). The geometry of an orebody can be represented simply and accurately by a set of three mutually perpendicular axes (major, intermediate and minor), which define an ellipsoid that is an approximation of the shape of the orebody (Blenkinsop, 2004). This ellipsoid can be defined by ore grade or by the structural setting, and it can encompass the whole orebody or have the same volume. These ellipsoids represent general trends of mineralization and their major axis can be interpreted as the vector of mineralization, which can be linked to the orientation of controlling structures (Monteiro et al., 2004).

When dealing with 2D analyses one can refer to mineralization ellipses, which in our case represent the horizontal projection of the mineralization ellipsoid. Additionally, the ellipses' major axes represent the mineralization vector in the horizontal plane. It is important to note that true orientation and size of mineralization vectors should only be defined in 3D, considering that the horizontal plane is an arbitrary cut through the mineralization ellipsoid. Nonetheless, since we will only compare information from the horizontal plane, and considering that mineralization in Sossego is almost vertical, this issue is less relevant (Blenkinsop, 2004).

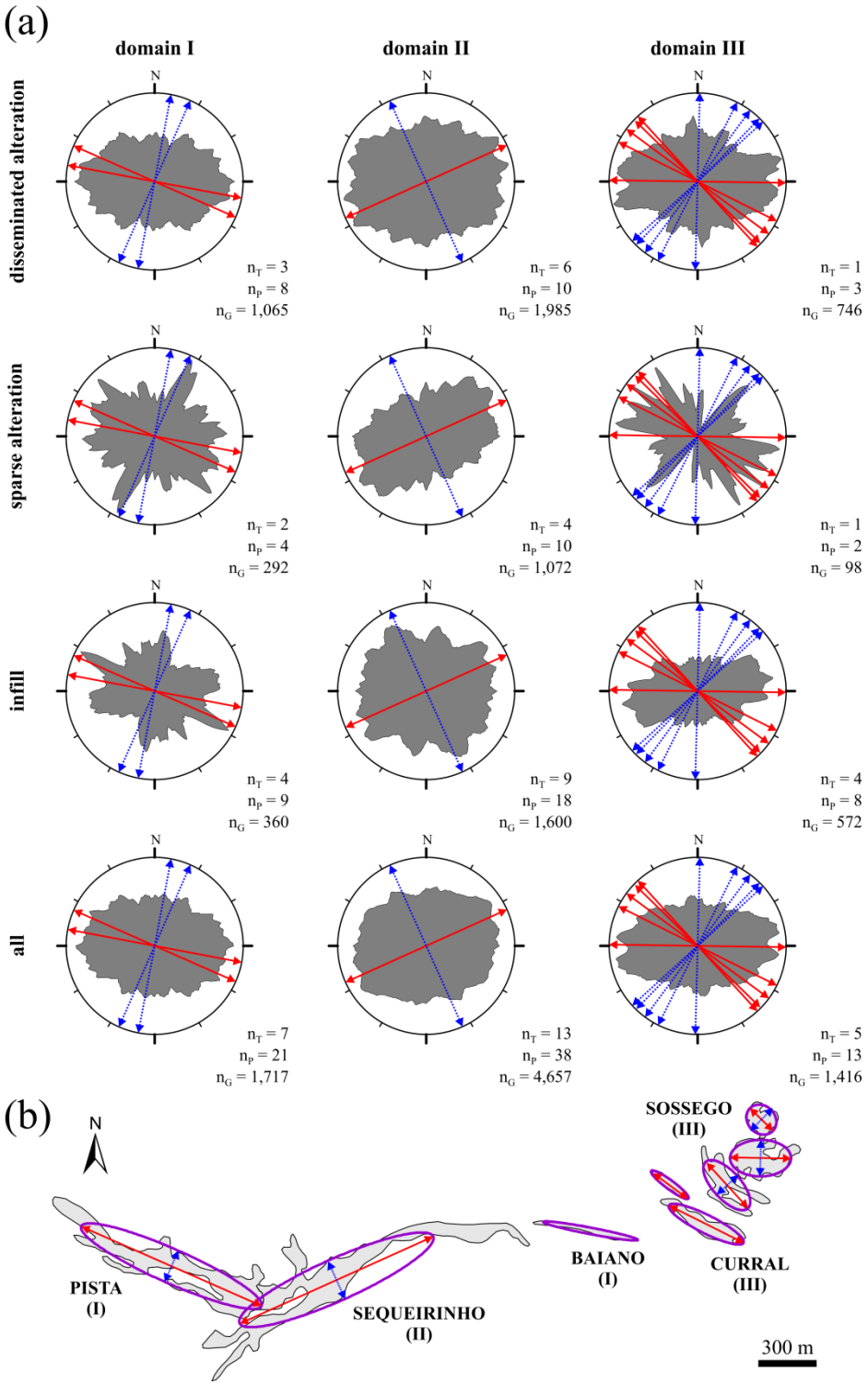

Fig. 13: (a) Rose diagrams for orientation of ore minerals grains (major axis for best-fit ellipses). Grains with high roundness (≥ 0.9) are excluded. Rose diagrams are classified by ore component and structural domain. Sample sizes for each rose diagram: n_T = thin sections; n_P = photomicrographs; n_G = grains. Directions for horizontal mineralization vectors [as shown in (b)] are given for each domain: red (major vector), blue (minor vector). (b) Mineralization ellipses and mineralization vectors for orebodies at Sossego deposit. Structural domains are indicated for each orebody (as in Fig. 2b). See text for details.

To define the mineralization ellipses for Sossego, we generated ellipses for the orebodies using the same processing used for ore minerals, but in this case using a binary map of orebodies (Fig. 13b). Comparison between results of microscale and local scale shows that the orientations of major mineralization vectors coincide well with the trends of grains' major axes, especially in domains I, II and the largest orebody in domain III (Fig. 13a). These shape analysis patterns are explored further in the following sections, where they are integrated and discussed with all other results.

6. Interpretation of microscale structural controls on Sossego mineralization

The microscale distribution of ore minerals at the Sossego deposit is dominantly non-random, and both their spatial distribution and their shape present fractal geometry. Furthermore, the distribution and shape of ore minerals mimic the geometry of local-scale structural controls and orebodies.

Three aspects of the fractal geometry provide clues about ore formation: (i) the ranges on which the patterns are fractal, (ii) the variability of fractal dimension values and (iii) the different characters of fractality (mono- *vs* bifractal). The range for the observed fractality is constrained by the maximum microscale interval analyzed (12.5 to 2,560.0 μm), which covers around three orders of magnitude. This is compatible with ranges observed in previous studies dealing with fractal dimension of mineral grains (Wang et al., 2007; Peternell and Kruhl, 2009). However, if we consider that many of the patterns analyzed are bifractals, the scale covered by each fractal dimension is smaller. These short ranges are the rule for natural fractals and, as such, fractal dimensions of many different geological features usually cover less than two orders of magnitude (Kruhl, 2013). This behavior does not necessarily indicate a problem in modelling the feature as a fractal, but rather that the process responsible for the formation of a given feature has a limited scale of influence, or that the feature is influenced by more than one fractal process.

The fractal dimensions measured for the spatial distribution and shape of ore minerals vary considerably. Part of this variability can be explained by different trends in the geometry of the different ore components (Section 4.2 and 5.1). *D* values reflect changes in grain abundance, grain size and degree of clustering that are found between disseminated, sparse alteration and infill. Nonetheless, a significant variation in *D* is observed in each type of ore component. This is partially explained by the natural variably in texture of each ore component, but some scatter of *D* is likely related to other reasons (Xu et al., 1993): (i)

natural fractals show a statistical form of self-similarity and the parts are only statistically similar to the whole; (ii) natural fractals are usually not self-similar, but rather self-affine, i.e., their scaling properties vary differently in different directions.

Similarly, results indicate that the nature of the fractality of ore minerals at the microscale is not homogeneous, with both mono- and bifractal patters being found. Monofractal patterns suggest a single pattern-forming process, while bifractal patterns suggest several pattern-forming processes (Peternell and Kruhl, 2009). Moreover, the existence of bifractal patterns is especially true for the range analyzed, where the scaling of the fractal dimension is a fundamental property (Kruhl, 2013). This change in fractal dimension in the grain scale is related to differences between the small entities themselves and the clusters of such small entities, or with irregularities in the grain borders and their shape. These different behaviors in the grain scale have been defined previously as textural and structural fractality (Kaye, 1978; Orford and Whalley, 1983; Horovistiz et al., 2010). In such cases, one process is responsible for generating the entities, and another process originates their clusters. In general, this indicates that the different processes lead to patterns of changed fractality at distinct scales (Kruhl, 2013). Our results support such interpretation. Here, bifractals were yielded through a variety of methods, each resulting in different dimensions for ranges in the grain scale and above. Furthermore, this effect is observed in the ore minerals distribution and shape.

Mono- and bifractal patterns are observed both in alteration and infill, and sometimes in different images of the same thin section. Therefore, the difference between the forming processes appears to be related dominantly with local characteristics at/within the crystallization site, and less to the ore component under analysis. The predominance of bifractal patterns and the heterogeneity of fractal dimensions observed indicate that the spatial distribution of ore minerals at Sossego is related to a complex interplay of processes, and that the geometry of ore minerals in the microscale represents a composite of two or more fractals interwoven.

In fact, recent work indicates that mineralization processes are actually multifractal across a range of scales, which means that ore formation is the result of many intertwining fractals (Ord et al., 2016). This characteristic is most likely the result of the fact that precipitation processes are fractal, but so is permeability. The distribution and shape of ore minerals would express the interaction between these fractals in the following way:

(i) Precipitation: precipitation is regulated by several mechanisms, including competitive reaction sites, different forms of catalysis and chaotic mixing (Ord et al., 2012). These are conveyed as chemical potential gradients of Eh and pH, present in scales from nanometers to kilometers (Lester et al., 2012; Ord et al., 2016).

(ii) Permeability: amongst the several variables that control fluid flow, permeability is a fundamental one and it is intrinsically related to the existing structures (Sibson, 1994,1996; Oliver, 1996; Roberts et al., 1999; Cox et al., 2001; Oliver and Bons, 2001). Moreover, fluid flow can be greatly concentrated in the network, with few structures being responsible for the bulk of fluid flow (Ledésert et al., 1993; Sanderson and Zhang, 1999). Consequently, permeability is highly dependent on fracture geometry, which includes its aperture, tortuosity, termination mode, density, length, orientation and filling minerals (Nolte et al., 1989; Ledésert et al., 1993; Berkowitz and Hadad, 1997). The orientation of discontinuities is of particular interest, as it has a major effect on the permeability magnitude and direction (Zhang et al., 1996). Flow path geometry is also greatly influenced by stress, which affects several of the geometry variables indicated above, particularly the aperture of structures (Zhang et al., 1996; Sanderson and Zhang, 1999). Considering several authors have shown the ubiquity of fractal geometry in structures at different scales, including at the microscale (Kruhl, 2013), it is reasonable to infer that the distribution of ore minerals should then be fractal, regardless of the scale considered. In fact, several studies have shown that fluid flow is fractal or multifractal as a response to the structural framework (Nolte et al., 1989; Berkowitz and Hadad, 1997; Roberts et al., 1999), and that spatial scale invariance is strongly influenced by the local permeability of hydrothermal systems (Ord et al., 2012).

The fact that both the spatial distribution and the shape of ore minerals are fractal strengthen the notion that the processes controlling the formation of ore minerals at the microscale are scale-invariant, which can be important to understand the mineralization control at other scales. This is because, in theory, the geometry observed at a certain scale of a fractal can be extrapolated to another scale (Arias et al., 2011). Obviously, considering the

stated limitations of natural fractals, this extrapolation cannot be performed in every instance. In the present study, we examined if the orientation and shape of ore minerals in the microscale preserve some of its geometric attributes across scales, and our results suggest they do. The preferential orientations of ore minerals distribution obtained in the Fry analysis and the main directions for anisotropy obtained in the shape analysis are compatible with local-scale trends in their structural domain and orebodies, and thus are compatible with structures considered to be controlling mineralization. This suggests that the fractality of mineralization at Sossego is not restricted to the range directly analyzed (image scale), but extends, at least in some aspects, to the local scale.

Considering the above inferences, what can be derived in terms of structural control? In our interpretation, the key to understand the scale invariance of the structural control resides in the permeability and how it controls fluid. Fluid flow can be pervasive through microfractures, or channelized through large, interconnect fractures (Oliver, 1996). The first form is associated with greater potential for fluid-rock interaction and is closely related to alteration. The second can present limited interaction (Oliver and Bons, 2001), and is associated with infill. The way infill and alteration are related can vary considerably, with fluid flowing in either direction: from infill to alteration and vice versa (Oliver and Bons, 2001; Taylor, 2009). In the first case, veins and fractures represent the initial conduit for fluids by their advection, and then promote the alteration of wall rocks. In the second case, veins would mark the remobilization of pre-existing minerals from the wall rock to the veins. This interplay between pervasive and channelized fluid flow is fundamental in the mass and temperature exchanges necessaries to induce mineralization. Although several paths for hydrothermal activity exists, it is common that its evolution progresses from flows initially pervasively distributed in microscopic channels in the rock matrix to flows progressively channeled to larger and larger macroscopic fractures, which in turn can present a fractal clustering (Brooks and Manning, 1994). The pervasive flows permit extensive mineral-fluid reactions to take place and is characteristic of the initial parts of hydrothermal events, because rocks are subjected to higher temperatures and pressure (Manning, 1994). The channeled flows take place as the rock cools and is exhumed.

The above inferences agree well with Sossego deposit characteristics. First of all, hydrothermal activity at Sossego is a combination of alteration and infill (Monteiro et al., 2008a; Carvalho, 2009; Domingos, 2009). Furthermore, fluid flow related to the earlier regional events of Na- and Na-Ca alterations is pervasively distributed in microscopic flow

channels in the rock matrix (Monteiro et al., 2008a). These are associated with the earlier WNW-ESE ductile fabric characterized by shear zones and foliation planes that affect all rocks at the mine site (Figs. 2, 9). Conversely, although part of mineralization is distributed along permeability pathways within rock fabrics that were inherited from this ductile events, the bulk of ore is associated with later brittle and brittle-ductile structures that were active during mineralization and partially cut the previous fabrics (Domingos, 2009). These brittle fabrics are defined mostly by WNW–ESE, NE–SW, E–W and N–S faults, veins and breccia bodies (Monteiro et al., 2008a; Domingos, 2009) (Figs. 2, 10). Each of these fabrics is associated predominantly with a type of channelway for fluids and to a different type of ore component. The ductile fabric is more related to alteration, while the brittle fabric to infill.

The occurrence of sulfide as infill and alteration indicates that fluid flow at Sossego deposit was pervasive, as well as channelized during mineralization. Therefore, both fabrics played a role in mineralization. Considering the host rocks are typically depleted in sulfide, the mineral paragenesis, fluid isotopic and geochemical characteristics (Monteiro et al., 2008a), the relative abundance of infill to alteration, and the presence of selvages in veins borders (Domingos, 2009), all suggest that fluid advection was an important process at Sossego during mineralization, with addition of externally derived fluids and the subsequent alteration of wall rocks. Thus, using the classification scheme for fluid flow presented in Oliver (1996), the Na- and Na-Ca alteration preceding mineralization would be an example of an open system of pervasive fluid flow. In contrast, the mineralization at Pista-Sequeirinho-Baiano and Sossego-Curral orebodies would be characterized as channelized, fractured, open systems fluid flows. For Sequeirinho orebodies, wall rocks were partly open (fluid interacts with local wall rock), while at Sossego they are more closed (cf. Oliver, 1996). This last inference is made because Pista-Sequeirinho-Baiano orebodies are closely related to ductile shear zones with a broad mineralization envelope (Fig. 2), while Sossego-Curral are characterized as vertical pipe breccias surrounded by a network of veins that cut previous structures, with a limited interaction with the wall rock. These different flow patterns are most likely associated with different structural regimes and stress conditions during ore formation of the different sets of orebodies, as attested by the large age gap between them (Moreto et al., 2015b).

These different permeability styles help explaining the relationship between patterns at different scales. Fry results show there is a relationship between the spatial distributions of ore minerals in the microscale and the structural trends in the local scale.

Sparse alteration is associated mostly with foliation, which explains why its trends reflect the local-scale structural trends, especially in domains I and II, where wall rock alteration is more developed (Fig. 9). On the other hand, trends for disseminated alteration are less-defined. This is because in disseminated alteration the number of ore grains started to increase, and as this process advanced, orientation started to get lost in the microscale. Considering the natural progression of the alteration process, with disseminated masses merging into a massive texture, no direction could be obtained by the methods employed. As such, results indicate that the sparse alteration is the best to examine the permeability in the microscale. Similarly, infill preserves the main directions between micro- and local scales, especially for domain III, where infill is relatively more important than alteration (Fig. 10). This is because veins and fractures form elongated spaces for fluids percolation. As fluids crystallize in voids, the orientation of grains would usually follow the rupture direction, especially for fine veins and fractures, like the ones analyzed in this study. This holds true for veins with crystals that grow perpendicular to the vein wall. Despite their orthogonal orientation, the distribution of crystals (as measured by the directions between their centroids) would be parallel to the vein border and would highlight the void direction.

The consistency between the anisotropy of micro- and local scales as evidenced by shape analysis also supports the above inferences. A general relationship between the geometry of mineralization and the underlying permeability has been observed before for different scales. In hand-specimen scale, shape can be an important indicator that a mineral is the result of alteration or infill, also providing clues on the type of permeability it is associated with (Taylor, 2009). In the deposit scale, the geometry of mineral deposits can give insights into fluid flow in shear zones, although the relationship between orebodies geometry and shear direction can be complicated by other factors, as growth history (Blenkinsop and Kadzviti, 2006). Nonetheless, shear direction is a critical factor controlling fluid flow, because it forms a preferable pathway for fluids. For some deposits, this increasing of permeability in the shear direction is directly related to microcracking, which creates permeability anisotropy (Kisters et al., 2000; Blenkinsop and Kadzviti, 2006).

For the Sossego deposit, the usual notion that the best-fit ellipses of grains can be used to define the deformation is not feasible, considering that sulfides rarely record deformation (Monteiro et al., 2008a). The anisotropic patterns that emerge are most likely a result of the way the sulfide masses have grown, which must be a reflection, among other things, of the permeability control that occurred during mineralization. As such, the

anisotropy directions for the micro- and local scales coincide well for domains I and II, where the shear directions appear to have a higher control on fluid flow and ore formation (Monteiro et al., 2008a; Domingos, 2009) (Fig. 13). A potential explanation for these results is that in domains I and II foliation and parallel microfracturing are important permeability controls. Accordingly, crystallization occurred mostly along foliation direction, not as much in the orthogonal direction and, thus, the anisotropy direction was conserved. Ore minerals in domain III show a strong anisotropy, revealing a preferential E–W direction. This is roughly coincident with one of the major directions of brittle structures in domain III, and to the mineralization vector representing the bulk of mineralization. Nonetheless, three mineralization vectors do not concur with microscale trends. This could be due to: (i) our samples are in the periphery of the main mineralized area, where the ellipse is E–W; (ii) mineralization in Sossego orebodies is controlled mainly by veins and breccias, where ore minerals can be oriented more freely.

The above inferences are in agreement with previous studies that state that flow rates in anisotropic fracture system are expected to be anisotropic, with fracture orientation being the stronger factor controlling permeability anisotropy (Zhang and Sanderson, 1995). Interestingly, the relationship between geometric and permeability anisotropy follows a power-law relation (Zhang and Sanderson, 1995).

The overall results indicate that the Sossego deposit is characterized by permeable areas that are conformable with the foliation, fractures and veins, which are the fabric elements that controlled the geometry of the mineralization at the micro- and local-scales. This reinforces the notion that mineral deposits geometry is fractal, and as such, can preserve geometric characteristic in a broad range of scales.

7. The fractal nature of structural controls on IOCG mineralization in the Carajás Mineral Province

Regional patters described in previous work seem to suggest that the scale invariance of mineralization extend beyond the Sossego deposit. Fractal and Fry analyses performed for the regional-scale spatial distribution of IOCG deposits in the Carajás Mineral Province indicates it displays fractal geometry (Haddad-Martim et al., 2017). Regional IOCG distribution shows that deposits are aligned in at least two WNW-ESE structural corridors (the northern and southern copper belts, cf. Moreto et al., 2015a). These corridors are parallel to the regional ductile E–W structural framework, which is interpreted as the oldest fabric in the region and related to the amalgamation of the Carajás Tectonic Domain (Holdsworth and Pinheiro, 2000; Domingos, 2009). They also coincide with the contact areas between the basement and the supracrustal rocks (Fig. 1), which suggests these IOCG corridors probably mark areas of crustal discontinuities where large-scale fluid circulation took place. This ductile structural framework shows highly anisotropic geometries of fractured rock masses that can be observed in all scales in the Carajás domain (Figs. 1, 2). Therefore, this structural configuration present anisotropic permeability and deformability, proprieties that are controlled by fractures density, length and orientation at all scales (Zhang and Sanderson, 1995), and that are also affected by the stress state of the region (Sanderson and Zhang, 1999).

Particular combinations of permeability anisotropy and superimposed structural permeability may lead to the localized high-volume flows needed to develop hydrothermal mineral deposits (Sibson, 1996), and apparently this is the case in Carajás. Within the regional WNW-ESE alignments, IOCG deposits are irregularly distributed and controlled by secondary trends: ENE–WSW, NE–SW, NNE–SSW (Haddad-Martim et al., 2017). This is probably the result of later reactivation and deformation by successive brittle, transcurrent events, also associated with large scale tectonic movements (Pinheiro and Holdsworth, 1997). Some of these events are related to igneous activity and are most likely responsible for controlling IOCG deposit formation within the regional corridors. Local-scale controls are associated to favorable traps, such as dilational jogs, lateral ramps, transfer faults, and other forms of link structures (Sibson, 1996).

Favorable sites for the convergence of factors leading to mineralization are observed in all scales. Trends obtained in this study for local- and micro- scales are analogous to the spatial distribution of IOCG mineralization in the regional scale, both in spatial distribution and anisotropy (Figs. 14, 15).

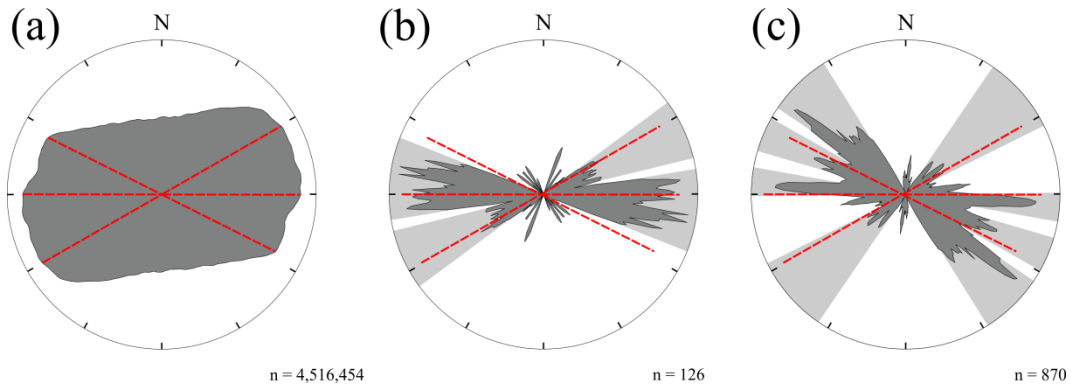

Fig. 14: Rose diagrams for the spatial distribution of Carajás IOCG mineralization at different scales. (a) Microscale: trends for ore minerals at Sossego deposit (combination of results for all Fry points in Figs. 9, 10). (b) Local scale: trends between IOCG deposits < 15 km apart. (c) Regional scale: trends between all IOCG deposits in Carajás [results in (b) and (c) as presented in Haddad-Martim et al. (2017)]. Dashed-lines represent microscale trends. Gray sectors represent trends in the local and regional scales.

A consistency of directions between shear zones of different scales of magnitude have been documented before, particularly in transcurrent settings, such as that affecting the Carajás Mineral Province (Tchalenko, 1970). This helps to explain why the general trends for the IOCG mineralization are conserved at different scales (Fig. 14). Likewise, similar anisotropy trends are observed in all scales observed. Interestingly, the anisotropy of mineralization in the regional scale is similar when considering all IOCG deposits, or when considering only IOCG deposits dated to the Archean or the Paleoproterozoic (Fig. 15). These anisotropic patterns indicate that the permeability defined by the ductile fabric was consistent through time and spatial scales, controlling the general trends of deposit distribution. Also, if we consider only the Archean deposits (~2.7 Ga) in the southern copper belt, where the Sossego deposit is located, the trend observed is also consistent with those observed in Sequeirinho, the largest Archean orebody in the area.

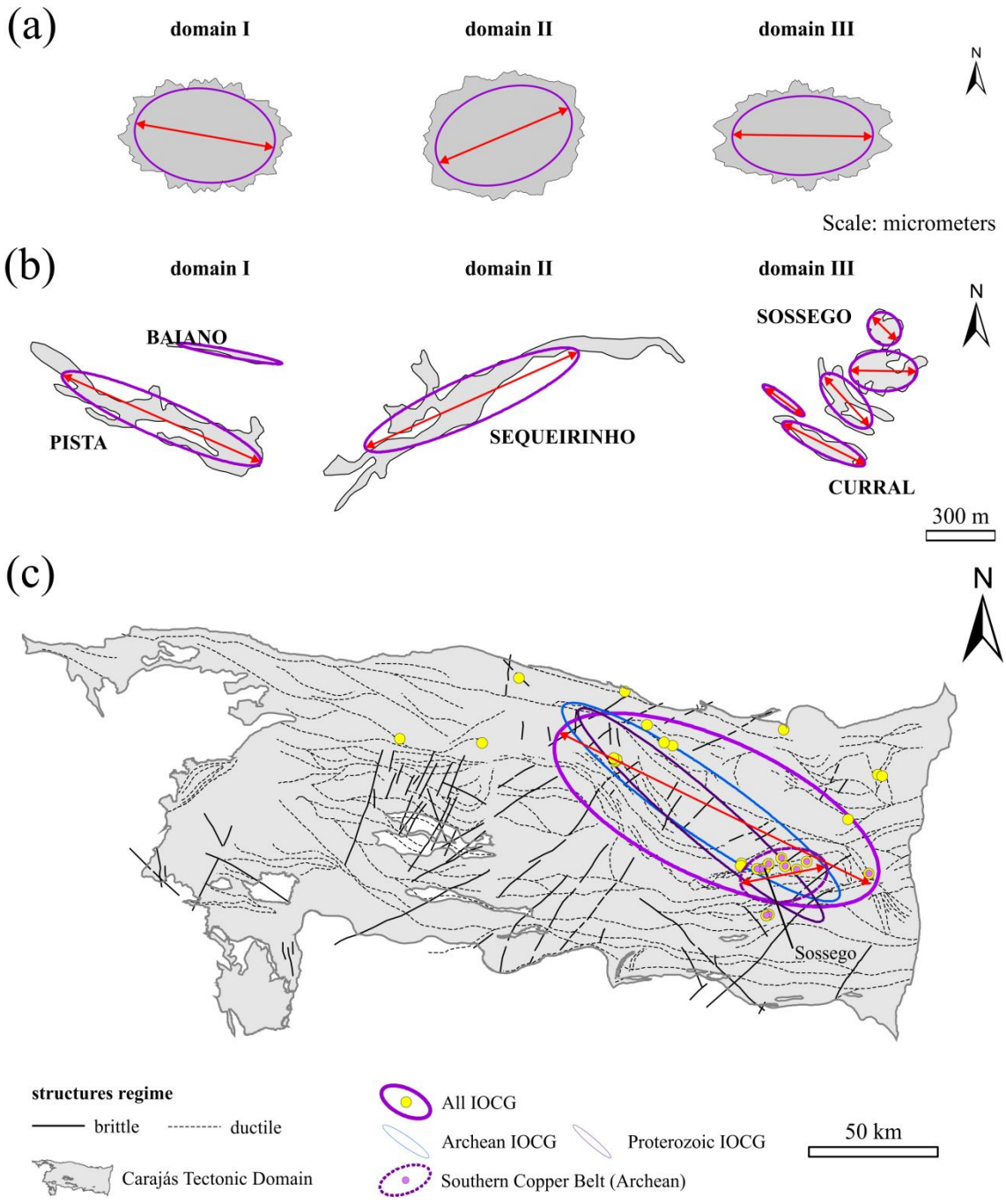

Fig. 15: Anisotropy for Carajás IOCG mineralization at different scales. (a) Microscale: trends for major axes of best-fit ellipses of ore minerals, per structural domain at Sossego deposit. (b) Local scale: horizontal mineralization ellipses and mineralization axes for orebodies. Orebodies are grouped per structural domain. (c) Regional scale: standard deviational ellipse [as discussed in Lisitsin (2015)] for the spatial pattern of IOCG deposits in the Carajás Mineral Province.

Our interpretations imply that a multifractal system is the underlying control for the spatial distribution of mineral deposits, which is consistent with the current knowledge of fracturing processes and related fluid flow (Zuo et al., 2009a; Gumiel et al., 2010; Ord et al., 2016). In fact, recent work suggests that hydrothermal mineral deposits are open flow, stochastic (i.e., probabilistic) and chaotic (i.e., sensitive to initial conditions) systems (Lester et al., 2012; Ord et al., 2012,2016). This notion is relevant since it stresses out that a hydrothermal deposit is the result of a complex interplay of systems, which include mass balance, heat transfer, fluid transport, chemical reaction kinetics and mechanical deformation. The outcome of such a complex interplay is a mineralizing system that is intrinsically multifractal (Ord et al., 2016). Thus, mineralizing systems represent the combination of the fractal distribution of hydrothermal alteration, fluid and mineral chemistry and structure, and our results suggest this is the case for IOCG deposits in Carajás. The fundamental reason for this is that scale invariance is a pervasive characteristic in aggregation and fragmentation processes (Nolte et al., 1989). This characteristic results from the fact that in many natural systems the driving forces that put the system in motion are imposed by forces in large-length scales, but the dissipative processes operate at small-length scales (Ord et al., 2016). This is particularly true for deformation, which is affected by regional-scale stresses that are dissipated in structures that develop in a cascading process, from regional faults and shear zones, all the way through microfractures and foliation in the microscale. This cascading processes – although irregular due to properties such as intermittency (Ord et al., 2016) – generates the regular patterns observed by the use of fractal geometry.

Despite the useful inferences presented above, some limitations with the fractal approach should be pointed out. For instance, the geometry of some fracture patterns have been reported as not being fractal (Walsh and Watterson, 1993; Brooks et al., 1996), which can be a result of the aforementioned intermittency of natural fractals, where the pattern displays fractal geometry at one point, but not in another (Ord et al., 2016). Additionally, the range where scale invariance is present most likely will vary from region to region, although it is expected to be present between millimeter to kilometer scales (Kruhl, 2013; Ord et al., 2016). Moreover, relationships are most likely nonlinear (Ord et al., 2016), which could make the link of geometric parameters between different scales more complex in other instances. Some of these limitations could be overcome by the use of an approach that takes into account heterogeneities in fractal dimension, both in space as in nature. For this, the patterns studied here could be examined by multifractal analyses to investigate in more detail the spatial

proprieties of the mineralization system in Carajás, and similar approaches could be used in other mineral provinces around the world.

8. Concluding remarks

Our study has shown that IOCG mineralization at the Sossego deposit, and more generally in the Carajás Mineral Province, present fractal geometry, mainly through the consistency of trends of spatial distribution and anisotropy directions over a wide range of scales (scale invariance). This suggests that some of the broad characteristics of regional structural mineralization controls can be inferred from microscale patterns of ore minerals and from local-scale structures close to mineral deposits. In this context, the fractal character of mineral deposits could be used to improve the prediction of the location of deposits, especially in greenfields. Regional mineralization controls are only well known in brownfields, where the discovery of many deposits allows their detailed study. In greenfields, precisely the areas with the greatest potential for the location of unknown deposits, the scarcity of occurrences makes it difficult to interpret the controls. If mineral deposits are fractals, and some properties of their controls can be assessed on thin sections and at local scales, then the mineralization controls can be understood at these scales, and then extrapolated to the regional scale. This suggestion could prove important to predict mineral favorability in the regional scale, a topic of major interest for future research.

References

Agterberg, F.P., 2013. Fractals and spatial statistics of point patterns. J. Earth Sci. 24, 1–11. doi:10.1007/s12583-013-0305-6

Araújo, O.J.B. de, Maia, R.G.N., 1991. Programa Levantamentos Geológicos Básicos do Brasil, Programa Grande Carajás, Serra dos Carajás, Folha SB.22-Z-A, Estado do Pará, Escala 1:250.000. Brasília, 164 pp.

Arias, M., Gumiel, P., Sanderson, D.J., Martin-Izard, A., 2011. A multifractal simulation model for the distribution of VMS deposits in the Spanish segment of the Iberian Pyrite Belt. Comput. Geosci. 37, 1917–1927. doi:10.1016/j.cageo.2011.07.012

Austin, J.R., Blenkinsop, T.G., 2009. Local to regional scale structural controls on mineralisation and the importance of a major lineament in the eastern Mount Isa Inlier, Australia: Review and analysis with autocorrelation and weights of evidence. Ore Geol. Rev. 35, 298–316. doi:10.1016/j.oregeorev.2009.03.004

Baddeley, A., Rubak, E., Turner, R., 2015. Spatial Point Patterns: Methodology and Applications with R. Chapman and Hall/CRC Press, London, 810 pp.

Barros, C.E. de M., Sardinha, A. de S., Barbosa, J. dos P. de O., Macambira, M.J.B., Barbey, P., Boullier, A.-M., 2009. Structure, petrology, geochemistry and zircon U/Pb and Pb/Pb geochronology of the synkinematic Archean (2.7 Ga) A-type granites from the Carajás metallogenic province, northern Brazil. Can. Mineral. 47, 1423–1440. doi:10.3749/canmin.47.6.1423

Berkowitz, B., Hadad, A., 1997. Fractal and multifractal measures of natural and synthetic fracture networks. J. Geophys. Res. 102, 12,205–12,218. doi:10.1029/97JB00304

Blenkinsop, T.G., 2004. Orebody geometry in lode gold deposits from Zimbabwe: Implications for fluid flow, deformation and mineralization. J. Struct. Geol. 26, 1293–1301. doi:10.1016/j.jsg.2003.11.010

Blenkinsop, T.G., Kadzviti, S., 2006. Fluid flow in shear zones: Insights from the geometry and evolution of ore bodies at Renco gold mine, Zimbabwe. Geofluids 6, 334–345. doi:10.1111/j.1468-8123.2006.00154.x

Blenkinsop, T.G., Sanderson, D.J., 1999. Are gold deposits in the crust fractals? A study of gold mines in the Zimbabwe craton. In: McCaffrey, K.J.W., Lonergan, L., Wilkinson, J.J. (Eds.), Fractures, Fluid Flow and Mineralization. Special Publications 155. Geological Society, London, pp. 141–151. doi:10.1144/GSL.SP.1999.155.01.11

Boots, B.N., Getis, A., 1988. Point Pattern Analysis, Scientific Geography 8. SAGE Publications Inc., Newbury Park, 92 pp.

Brooks, B.A., Allmendinger, R.W., de la Barra, I.G., 1996. Fault spacing in the El Teniente Mine, central Chile: Evidence for nonfractal fault geometry. J. Geophys. Res. 101, 13633–13653. doi:10.1029/96jb00800

Brooks, B.A., Manning, C.E., 1994. Fractal clustering of metamorphic veins: Comment and Reply. Geology 22, 1147–1149.

Carlson, C.A., 1991. Spatial distribution of ore deposits. Geology 19, 111–114. doi:10.1130/0091-7613(1991)019<0111:SDOOD>2.3.CO;2

Carranza, E.J.M., 2008. Geochemical Anomaly and Mineral Prospectivity Mapping in GIS, Handbook of Exploration and Environmental Geochemistry, volume 11. Elsevier B.V., Amsterdam, 366 pp. doi:10.1016/S1874-2734(09)70001-4

Carranza, E.J.M., 2009. Controls on mineral deposit occurrence inferred from analysis of their spatial pattern and spatial association with geological features. Ore Geol. Rev. 35, 383–400. doi:10.1016/j.oregeorev.2009.01.001

Carranza, E.J.M., Owusu, E.A., Hale, M., 2009. Mapping of prospectivity and estimation of number of undiscovered prospects for lode gold, southwestern Ashanti Belt, Ghana. Miner. Depos. 44, 915–938. doi:10.1007/s00126-009-0250-6

Carvalho, E. de R., 2009. Caracterização Geológica e Gênese das Mineralizações de Óxido de Fe-Cu-Au e metais associados na Província Mineral de Carajás: Estudo de Caso do Depósito de Sossego. Universidade Estadual de Campinas, 141 pp.

Cox, S.F., Knackstedt, M.A., Braun, J., 2001. Principles of structural control on permeability and fluid flow in hydrothermal systems. Rev. Econ. Geol. 14, 1–24.

Delvaux, D., Sperner, B., 2003. New aspects of tectonic stress inversion with reference to the TENSOR program. In: Nieuwland, D.A. (Ed.), New Insights into Structural Interpretation and Modelling. Geological Society, London, pp. 75–100. doi:10.1144/GSL.SP.2003.212.01.06

Domingos, F.H.G., 2009. The structural setting of the Canaã dos Carajás region and Sossego-Sequeirinho deposits, Carajás Brazil. Doctor of Philosophy thesis, University of Durham, Durham, 483 pp.

Feio, G.R.L., Dall'Agnol, R., Dantas, E.L., Macambira, M.J.B., Gomes, A.C.B., Sardinha, A.S., Oliveira, D.C., Santos, R.D., Santos, P.A., 2012. Geochemistry, geochronology, and origin of the Neoarchean Planalto Granite suite, Carajás, Amazonian craton: A-type or hydrated charnockitic granites? Lithos 151, 57–73. doi:10.1016/j.lithos.2012.02.020

Fry, N., 1979. Random point distributions and strain measurement in rocks. Tectonophysics 60, 89–105. doi:10.1016/0040-1951(79)90135-5

Goryainov, P.M., Ivanyuk, G.Y., Sharov, N. V., 1997. Fractal analysis of seismic and geological data. Tectonophysics 269, 247–257. doi:10.1016/S0040-1951(96)00162-X

Gumiel, P., Sanderson, D.J., Arias, M., Roberts, S., Martín-Izard, A., 2010. Analysis of the fractal clustering of ore deposits in the Spanish Iberian Pyrite Belt. Ore Geol. Rev. 38, 307–318. doi:10.1016/j.oregeorev.2010.08.001

Haddad-Martim, P.M., Souza Filho, C.R. de, Carranza, E.J.M., 2017. Spatial analysis of mineral deposit distribution: A review of methods and implications for structural controls on iron oxide-copper-gold mineralization in Carajás, Brazil. Ore Geol. Rev. 81, 230–244. doi:10.1016/j.oregeorev.2016.09.038

Hansen, V.L., 1990. Collection and preparation of thin sections of oriented samples. J. Geol. Educ. 38, 294–297.

Heilbronner, R., Barrett, S.D., 2014. Image Analysis in Earth Sciences, 1st ed. Springer Verlag, Berlin Heidelberg, 520 pp. doi:10.1007/978-3-642-10343-8

Hippertt, J., 1999. Are S-C structures, duplexes and conjugate shear zones different manifestations of the same scale-invariant phenomenon? J. Struct. Geol. 21, 975–984. doi:10.1016/S0191-8141(99)00047-4

Hippertt, J.F., Massucatto, A.J., 1998. Phyllonitization and development of kilometer-size extension gashes in a continental-scale strike-slip shear zone, north Goiás, central Brazil. J. Struct. Geol. 20, 433–445. doi:10.1016/S0191-8141(97)00106-5

Hirata, W.K., Rigon, J.C., Kadekaru, K., Cordeiro, A.A.C., Meireles, E.A., 1982. Geologia Regional da Província Mineral de Carajás. Anais Do I Simpósio de Geologia Da Amazônia. pp. 100–110.

Hodkiewicz, P.F., Weinberg, R.F., Gardoll, S.J., Groves, D.I., 2005. Complexity gradients in the Yilgarn Craton: Fundamental controls on crustal-scale fluid flow and the formation of world-class orogenic-gold deposits. Aust. J. Earth Sci. 52, 831–841. doi:10.1080/08120090500304257

Holdsworth, R.E., Pinheiro, R.V.L., 2000. The anatomy of shallow-crustal transpressional structures: Insights from the Archaean Carajas fault zone, Amazon, Brazil. J. Struct. Geol. 22, 1105–1123. doi:10.1016/S0191-8141(00)00036-5

Horovistiz, A.L., de Campos, K.A., Shibata, S., Prado, C.C.S., Hein, L.R. de O., 2010. Fractal characterization of brittle fracture in ceramics under mode I stress loading. Mater. Sci. Eng. A 527, 4847–4850. doi:10.1016/j.msea.2010.04.014

Jébrak, M., 1997. Hydrothermal breccias in vein-type ore deposits: A review of mechanisms, morphology and size distribution. Ore Geol. Rev. 12, 111–134. doi:10.1016/S0169-1368(97)00009-7

Jensen, E., Cembrano, J., Faulkner, D., Veloso, E., Arancibia, G., 2011. Development of a self-similar strike-slip duplex system in the Atacama Fault system, Chile. J. Struct. Geol. 33, 1611–1626. doi:10.1016/j.jsg.2011.09.002

Jerram, D.A., Cheadle, M.J., Hunter, R.H., Elliott, M.T., 1996. The spatial distribution of grains and crystals in rocks. Contrib. to Mineral. Petrol. 125, 60–74. doi:10.1007/s004100050206

Johnston, J.D., McCaffrey, K.J.W., 1996. Fractal geometries of vein systems and the variation of scaling relationships with mechanism. J. Struct. Geol. 18, 349–358. doi:10.1016/S0191-8141(96)80055-1

Kaye, B.H., 1978. Specification of the ruggedness and/or texture of a fine particle profile by its fractal dimension. Powder Technol. 21, 1–16. doi:10.1016/0032-5910(78)80103-X

Kisters, A.F.M., Kolb, J., Meyer, F.M., Hoernes, S., 2000. Hydrologic segmentation of high-temperature shear zones: Structural, geochemical and isotopic evidence from auriferous mylonites of the Renco mine, Zimbabwe. J. Struct. Geol. 22, 811–829. doi:10.1016/S0191-8141(00)00006-7

Kretz, R., 1969. On the spatial distribution of crystals in rocks. Lithos 2, 39–65. doi:10.1016/S0024-4937(69)80005-8

Kreuzer, O.P., Blenkinsop, T.G., Morrison, R.J., Peters, S.G., 2007. Ore controls in the Charters Towers goldfield, NE Australia: Constraints from geological, geophysical and numerical analyses. Ore Geol. Rev. 32, 37–80. doi:10.1016/j.oregeorev.2006.12.001

Kruhl, J.H., 2013. Fractal-geometry techniques in the quantification of complex rock structures: A special view on scaling regimes, inhomogeneity and anisotropy. J. Struct. Geol. 46, 2–21. doi:10.1016/j.jsg.2012.10.002

Ledésert, B., Dubois, J., Velde, B., Meunier, A., Genter, A., Badri, A., 1993. Geometrical and fractal analysis of a three-dimensional hydrothermal vein network in a fractured granite. J. Volcanol. Geotherm. Res. 56, 267–280.

Lester, D.R., Ord, A., Hobbs, B.E., 2012. The mechanics of hydrothermal systems: II. Fluid mixing and chemical reactions. Ore Geol. Rev. 49, 45–71. doi:10.1016/j.oregeorev.2012.08.002

Lisitsin, V., 2015. Spatial data analysis of mineral deposit point patterns: Applications to exploration targeting. Ore Geol. Rev. 71, 861–881. doi:10.1016/j.oregeorev.2015.05.019

Macambira, E.M.B., Vale, A.G., 1997. Programa Levantamentos Geológicos Básicos do Brasil, São Félix do Xingu, Folha SB.22-Y-B, Estado do Pará, Escala 1:250.000. Brasília, 384 pp.

Machado, N., Lindenmayer, Z., Krogh, T.E., Lindenmayer, D., 1991. U-Pb geochronology of Archean magmatism and basement reactivation in the Carajás area, Amazon shield, Brazil. Precambrian Res. 49, 329–354. doi:10.1016/0301-9268(91)90040-H

Mamtani, M.A., 2012. Fractal analysis of magnetite grains - implications for interpreting deformation mechanism. J. Geol. Soc. India 80, 308–313. doi:10.1007/s12594-012-0149-1

Mandelbrot, B.B., 1983. The Fractal Geometry of Nature (Updated and Augmented Edition). Freeman, New York, 495 pp.

Manning, C.E., 1994. Fractal clustering of metamorphic veins. Geology 22, 335–338. doi:10.1130/0091-7613(1994)022<0335:FCOMV>2.3.CO

Monteiro, L.V.S., Xavier, R.P., Carvalho, E.R. de, Hitzman, M.W., Johnson, C.A., Souza Filho, C.R. de, Torresi, I., 2008a. Spatial and temporal zoning of hydrothermal alteration and mineralization in the Sossego iron oxide–copper–gold deposit, Carajás Mineral Province, Brazil: paragenesis and stable isotope constraints. Miner. Depos. 43, 129–159. doi:10.1007/s00126-006-0121-3

Monteiro, L.V.S., Xavier, R.P., Hitzman, M.W., Juliani, C., Souza Filho, C.R. de, Carvalho, E.R. de, 2008b. Mineral chemistry of ore and hydrothermal alteration at the Sossego iron oxide-copper-gold deposit, Carajás Mineral Province, Brazil. Ore Geol. Rev. 34, 317–336. doi:10.1016/j.oregeorev.2008.01.003

Monteiro, L.V.S., Xavier, R.P., Souza Filho, C.R. de, Moreto, C.P.N., 2014. Metalogênese da Província Carajás. In: Silva, M. da G. da, Neto, M.B. da R., Jost, H., Kuyumjian, R.M. (Eds.), Metalogênese Das Províncias Tectônicas Brasileiras. CPRM, Belo Horizonte, pp. 43–92.

Monteiro, R.N., Fyfe, W.S., Chemale Jr., F., 2004. The impact of the linkage between grade distribution and petrofabric on the understanding of structurally controlled mineral deposits: Ouro Fino Gold Mine, Brazil. J. Struct. Geol. 26, 1195–1214. doi:10.1016/j.jsg.2003.11.023

Moreto, C.P.N., Monteiro, L.V.S., Xavier, R.P., Creaser, R.A., DuFrane, S.A., Melo, G.H.C., Silva, M.A.D. da, Tassinari, C.C.G., Sato, K., 2015a. Timing of multiple hydrothermal events in the iron oxide–copper–gold deposits of the Southern Copper Belt, Carajás Province, Brazil. Miner. Depos. 50, 517–546. doi:10.1007/s00126-014-0549-9

Moreto, C.P.N., Monteiro, L.V.S., Xavier, R.P., Creaser, R.A., DuFrane, S.A., Tassinari, C.C.G., Sato, K., Kemp, A.I.S., Amaral, W.S., 2015b. Neoarchean and Paleoproterozoic Iron Oxide-Copper-Gold events at the Sossego Deposit, Carajás Province, Brazil: Re-Os and U-Pb geochronological evidence. Econ. Geol. 110, 809–835.

Neves, M.P., 2006. Estudos Isotópicos (Pb-Pb, Sm-Nd, C e O) do Depósito Cu-Au do Sossego, Província Mineral de Carajás. M.Sc dissertation, Universidade Federal do Pará, Belém, 104 pp.

Nogueira, A.C.R., Truckenbrodt, W., Pinheiro, R.V.L., 1995. Formação Águas Claras, Pré-Cambriano da Serra dos Carajás: redescrição e redefinição litoestratigráfica. Bol. Mus. Para. Emílio Goeldi - Série Ciências da Terra 7, 177–277.

Nolte, D.D., Pyrak-Nolte, L.J., Cook, N.G.W., 1989. The Fractal Geometry of Flow Paths in Natural Fractures in Rock and the Approach to Percolation. Pure Appl. Geophys. 131, 111–138.

Oliver, N.H.S., 1996. Review and classification of structural controls on fluid flow during regional metamorphism. J. Metamorph. Geol. 14, 477–492. doi:10.1046/j.1525-1314.1996.00347.x

Oliver, N.H.S., Bons, P.D., 2001. Mechanisms of fluid flow and fluid-rock interaction in fossil metamorphic hydrothermal systems inferred from vein-wallrock patterns, geometry and microstructure. Geofluids 1, 137–162. doi:10.1046/j.1468-8123.2001.00013.x

Ord, A., Hobbs, B.E., Lester, D.R., 2012. The mechanics of hydrothermal systems: I. Ore systems as chemical reactors. Ore Geol. Rev. 49, 1–44. doi:10.1016/j.oregeorev.2012.08.003

Ord, A., Munro, M., Hobbs, B., 2016. Hydrothermal mineralising systems as chemical reactors: Wavelet analysis, multifractals and correlations. Ore Geol. Rev. 79, 155–179. doi:10.1016/j.oregeorev.2016.03.026

Orford, J.D., Whalley, W.B., 1983. The use of the fractal dimension to quantify the morphology of irregular-shaped particles. Sedimentology 30, 655–668. doi:10.1111/j.1365-3091.1983.tb00700.x

Pereira, R.M.P., Rosière, C.A., Santos, J.O.S., Lobato, L.M., Figueiredo e Silva, R.C., McNaughton, N.J., 2009. Unidade Caninana: sequência clástica paleoproterozoica revelada por datação U-Pb em zircões detríticos da Província Mineral Carajás. 11o Simpósio de Geologia Da Amazônia. Manaus, pp. 376–379.

Peternell, M., Bitencourt, M. de F., Kruhl, J., 2011. Combined quantification of anisotropy and inhomogeneity of magmatic rock fabrics - An outcrop scale analysis recorded in high resolution. J. Struct. Geol. 33, 609–623. doi:10.1016/j.jsg.2011.01.011

Peternell, M., Kruhl, J.H., 2009. Automation of pattern recognition and fractal-geometry-based pattern quantification, exemplified by mineral-phase distribution patterns in igneous rocks. Comput. Geosci. 35, 1415–1426. doi:10.1016/j.cageo.2008.11.001

Pidgeon, R.T., MacAmbira, M.J.B., Lafon, J.M., 2000. Th-U-Pb isotopic systems and internal structures of complex zircons from an enderbite from the Pium Complex, Carajas Province, Brazil: Evidence for the ages of granulite facies metamorphism and the protolith of the enderbite. Chem. Geol. 166, 159–171. doi:10.1016/S0009-2541(99)00190-4

Pinheiro, R.V.L., Holdsworth, R.E., 1997. Reactivation of Archaean strike-slip fault systems, Amazon region, Brazil. J. Geol. Soc. London. 154, 99–103. doi:10.1144/gsjgs.154.1.0099

Raines, G.L., 2008. Are fractal dimensions of the spatial distribution of mineral deposits meaningful? Nat. Resour. Res. 17, 87–97. doi:10.1007/s11053-008-9067-8

Roberts, S., Sanderson, D.J., Gumiel, P., 1999. Fractal analysis and percolation properties of veins. Geol. Soc. London, Spec. Publ. 155, 7–16. doi:10.1144/GSL.SP.1999.155.01.03

Sanderson, D.J., Zhang, X., 1999. Critical stress localization of flow associated with deformation of well-fractured rock masses, with implications for mineral deposits. Geol. Soc. London, Spec. Publ. 155, 69–81. doi:10.1144/GSL.SP.1999.155.01.07

Santos, J.O.S., 2003. Geotectônica dos Escudos das Guianas e Brasil-Central. In: Bizzi, L.A., Schobbenhaus, C., Vidotti, R.M., Gonçalves, J.H. (Eds.), Geologia, Tectônica E Recursos Minerais Do Brasil. CPRM, Brasília, pp. 169–226.

Schindelin, J., Arganda-Carreras, I., Frise, E., Kaynig, V., Longair, M., Pietzsch, T., Preibisch, S., Rueden, C., Saalfeld, S., Schmid, B., Tinevez, J.-Y., White, D.J., Hartenstein, V., Eliceiri, K., Tomancak, P., Cardona, A., 2012. Fiji: an open-source platform for biological-image analysis. Nat. Methods 9, 676–682. doi:10.1038/nmeth.2019

Sibson, R.H., 1994. Crustal stress, faulting and fluid flow. Geol. Soc. London, Spec. Publ. 78, 69–84. doi:10.1144/GSL.SP.1994.078.01.07

Sibson, R.H., 1996. Structural permeability of fluid-driven fault-fracture meshes. J. Struct. Geol. 18, 1031–1042. doi:10.1016/0191-8141(96)00032-6

Silva, M.A.D. Da, 2014. Metatexitos e diatexitos do Complexo Xingu na região de Canaã dos Carajás: implicações para a evolução mesoarqueana do Domínio Carajás. Universidade Estadual de Campinas, 102 pp.

Stubley, M.P., 2004. Spatial distribution of kimberlite in the Slave craton, Canada: a geometrical approach. Lithos 77, 683–693. doi:10.1016/j.lithos.2004.03.008

Tallarico, F.H.B., McNaughton, N.J., Groves, D.I., Fletcher, I.R., Figueiredo, B.R., Carvalho, J.B., Rego, J.L., Nunes, A.R., 2004. Geological and SHRIMP II U-Pb constraints on the age and origin of the Breves Cu-Au-(W-Bi-Sn) deposit, Carajás, Brazil. Miner. Depos. 39, 68–86. doi:10.1007/s00126-003-0383-y

Taylor, R., 2009. Ore Textures - Recognition and Interpretation. Springer-Verlag, Berlin, Heidelberg, 288 pp. doi:10.1007/978-3-642-01783-4

Tchalenko, J.S., 1970. Similarities between shear zones of different magnitudes. Geol. Soc. Am. Bull. 81, 1625–1640. doi:10.1130/0016-7606(1970)81[1625:SBSZOD]2.0.CO;2

Thévenaz, P., Unser, M., 2007. User-friendly semiautomated assembly of accurate image mosaics in microscopy. Microsc. Res. Tech. 70, 135–146. doi:10.1002/jemt.20393

Turcotte, D.L., 1989. Fractals in geology and geophysics. Pure Appl. Geophys. 131, 171–196. doi:10.1007/BF00874486

Vasquez, M.L., Rosa-Costa, L.T. da, 2008. Geologia e Recursos Minerais do Estado do Pará: Sistema de Informações Geográficas - SIG: texto explicativo dos mapas Geológico e Tectônico e de Recursos Minerais do Estado do Pará. Belém, 328 pp.

Vearncombe, J.R., Vearncombe, S., 1999. The spatial distribution of mineralization: Applications of Fry analysis. Econ. Geol. 94, 475–486. doi:10.2113/gsecongeo.94.4.475

Vearncombe, S., Vearncombe, J.R., 2002. Tectonic controls on kimberlite location, southern Africa. J. Struct. Geol. 24, 1619–1625. doi:10.1016/S0191-8141(01)00152-3

Walsh, J.J., Watterson, J., 1993. Fractal analysis of fracture patterns using the standard box-counting technique: valid and invalid methodologies. J. Struct. Geol. 15, 1509–1512. doi:10.1016/0191-8141(93)90010-8

Wang, Z., Cheng, Q., Cao, L., Xia, Q., Chen, Z., 2007. Fractal modelling of the microstructure property of quartz mylonite during deformation process. Math. Geol. 39, 53–68. doi:10.1007/s11004-006-9065-5

Williams, P.J., Barton, M.D., Johnson, D.A., Fontboté, L., Haller, A. de, Mark, G., Oliver, N.H.S., Marschik, R., 2005. Iron oxide copper-gold deposits: Geology, space-time distribution, and possible modes of origin. Econ. Geol. 100th Anniv. Vol. 371–405.

Xavier, R.P., Monteiro, L.V.S., Moreto, C.P.N., Pestilho, A.L.S., Melo, G.H.C. de, Silva, M.A.D. da, Aires, B., Ribeiro, C., Silva, F.H.F. e, 2012. The Iron Oxide Copper-Gold Systems of the Carajás Mineral Province, Brazil. In: Hedenquist, J.W., Harris, M., Camus, F. (Eds.), SEG Special Publication 16. Society of Economic Geologists Inc., pp. 433–454.

Xie, S., Cheng, Q., Zhang, S., Huang, K., 2010. Assessing microstructures of pyrrhotites in basalts by multifractal analysis. Nonlinear Process. Geophys. 17, 319–327. doi:10.5194/npg-17-319-2010

Xu, T., Moore, I.D., Gallant, J.C., 1993. Fractals, fractal dimensions and landscapes — a review. Geomorphology 8, 245–262. doi:10.1016/0169-555X(93)90022-T

Zhang, X., Sanderson, D.J., 1995. Anisotropic features of geometry and permeability in fractured rock masses. Eng. Geol. 40, 65–75. doi:10.1016/0013-7952(95)00040-2

Zhang, X., Sanderson, D.J., Harkness, R.M., Last, N.C., 1996. Evaluation of the 2-D permeability tensor for fractured rock masses. Int. J. Rock Mech. Min. Sci. Geomech. Abstr. 33, 17–37. doi:10.1016/0148-9062(95)00042-9

Zuo, R., Agterberg, F.P., Cheng, Q., Yao, L., 2009a. Fractal characterization of the spatial distribution of geological point processes. Int. J. Appl. Earth Obs. Geoinf. 11, 394–402. doi:10.1016/j.jag.2009.07.001

Zuo, R., Cheng, Q., Xia, Q., Agterberg, F.P., 2009b. Application of fractal models to distinguish between different mineral phases. Math. Geosci. 41, 71–80. doi:10.1007/s11004-008-9191-3

CAPÍTULO 5 IMPLICAÇÕES PARA PESQUISA MINERAL E CONSIDERAÇÕES FINAIS

1. Implicações para pesquisa mineral

A exploração por novos depósitos minerais é uma atividade que consome expressivos recursos financeiros, se estende por longos períodos e está sujeita a uma alta taxa de insucesso. Estas características fazem com que a exploração mineral necessite de intenso planejamento na tentativa de ampliar a chance de acerto na localização de uma jazida (Nykänen & Ojala 2007). Uma ferramenta muito utilizada para planejar a exploração mineral adequadamente são os mapas de favorabilidade mineral (Carranza 2008).

Mapas de favorabilidade mineral reúnem diversos tipos de informação pertinentes à localização de um depósito mineral, tais como mapas geológicos, dados geoquímicos, dados geofísicos e imagens de sensoriamento remoto (Carranza 2008). Cada um destes temas é usado para criar uma camada que é dividida, de acordo com critérios específicos, em áreas com maior ou menor potencial para conter um depósito mineral. Estas camadas, também chamadas de *mapas evidenciais* (Leite & Souza Filho 2009), são então integradas em uma mesma base cartográfica, que reúne todo o conjunto de critérios aplicáveis à localização do depósito de interesse. A região com a sobreposição das áreas com os maiores potenciais e segundo os critérios mais relevantes é considerada a região com maior potencial metalogenético e, portanto, aquela que deverá ser priorizada durante a pesquisa mineral. Portanto, para a elaboração de um mapa de favorabilidade mineral são usados todos os conhecimentos disponíveis sobre os processos geológicos atuantes na metalogênese da região de interesse.

Neste contexto a trama estrutural de uma região é de fundamental importância, em especial para a investigação de depósitos hidrotermais, uma vez que estruturas de diversas escalas formam os condutos permeáveis pelos quais se movem os fluidos mineralizantes (Sibson 1994; Oliver 1996; Cox *et al.* 2001). Quando não estão disponíveis informações detalhadas sobre a forma de atuação do controle estrutural, é comum o uso de mapas onde são definidos *buffers* genéricos ao redor de todas as estruturas, onde se considera que quanto mais próximos do eixo central do *buffer*, maior a chance de ocorrência do depósito mineral (Leite & Souza Filho 2009). No entanto, quando estudos são feitos para detalhar o caráter do

controle estrutural, é possível individualizar aquelas estruturas que apresentam maior potencial para mineralização – seja por sua natureza ou geometria – atribuindo pesos maiores para as estruturas mais favoráveis (Carranza 2009). Em geral, esta classificação mais refinada gera modelos mais realistas e precisos, sendo, portanto desejável para a pesquisa mineral.

As informações levantadas nesta pesquisa sobre o controle estrutural dos depósitos IOCG em escala regional, bem como do depósito de Sossego nas escalas local e microscópica, fornecem interpretações relevantes para a pesquisa mineral na região de Carajás. Estas interpretações para as características dos controles estruturais podem ser incorporadas em um modelo de favorabilidade regional, servindo para balizá-lo e torná-lo mais realista. Neste contexto, as conclusões mais relevantes deste estudo são:

- Em escala microscópica, o controle estrutural para o depósito de Sossego é dado por diferentes tipos de microestruturas, tais como planos de foliação, microfraturas, microbrechas e vênulas – em especial para as áreas ao redor das brechas mineralizadas. Minerais de minério ocorrem como preenchimento hidrotermal destas estruturas, ou então como alteração hidrotermal de suas rochas encaixantes imediatas. Estas formas de ocorrência documentam diferentes estilos de permeabilidade na escala microscópica, e indicam que a mineralização resulta de combinações de alteração e preenchimento hidrotermais tardios de sulfeto. As microestruturas observadas estão diretamente relacionadas ao desenvolvimento de zonas de cisalhamento, falhas e veios de escala local. Devido à autossimilaridade das estruturas, a forma e distribuição espacial dos minerais de minério documentam padrões geométricos semelhantes àqueles observados nas estruturas de escala local, incluindo a orientação preferencial para a distribuição da mineralização e sua anisotropia. Estes parâmetros geométricos marcam as direções mais susceptíveis à mineralização e variam de acordo com cada um dos domínios estruturais do depósito (CAPÍTULO 4).

- Em escala local, nota-se que os diferentes domínios estruturais do depósito de Sossego apresentam algumas das características dos principais elementos estruturais descritos em escala regional, incluindo uma trama dúctil mais antiga, de orientação WNW–ESE, que é afetada por estruturas rúpteis posteriores, orientadas para E–W, NW–SE, NE–SW e N–S. O controle estrutural da mineralização é dado por áreas onde a configuração geométrica em relação aos

esforços regionais facilitou o desenvolvimento ou reativação de estruturas. Dessa forma, os sítios favoráveis à mineralização são interpretados como *releasing bends* ou *jogs* dilatacionais com orientações opostas para os corpos Pista-Sequeirinho-Baiano e os corpos Sossego-Curral. No modelo proposto, a mudança nos campos de tensão regionais e locais – associadas à orientação oposta entre os *bends*/*jogs* – teria favorecido a mineralização em épocas distintas, no Neoarqueano e no Paleoproterozóico. Esta interpretação é suportada pelo fato de que as estrias de falhas encontradas nas cavas da mina parecem documentar dois eventos principais de movimentação, um com movimentação predominantemente vertical e outro com movimentação predominantemente horizontal (CAPÍTULO 3). Em ambos os casos, os eventos deformacionais são interpretados como responsáveis pela geração de permeabilidade estrutural documentada na escala microscópica, e registrada na escala local pela ocorrência de corpos de minério com geometrias características e distintas entre si.

- Em escala regional, o controle estrutural para a mineralização IOCG – conforme documentado pela distribuição espacial de depósitos – está associado principalmente às estruturas orientadas para WNW–ESE, E–W e NW–SE, com tendências secundárias para ENE–WSW e NNE–SSW. Portanto, a distribuição espacial dos depósitos IOCG de Carajás apresenta tendências de direção e anisotropia consistentes com a configuração estrutural regional. Estas tendências são confirmadas pela análise de associação espacial entre os depósitos IOCG e estruturas regionais, especialmente para NW–SE, E–W e ENE–WSW, e menos para NNE-SSW (CAPÍTULO 2). As orientações entre as mineralizações em escala regional são consistentes com aquelas observadas para o depósito de Sossego em escala local, e sugere que a autossimilaridade das estruturas que controlaram a permeabilidade em escala regional se estende até as escalas local e microscópica.

Cada um dos elementos de controle estrutural destacados acima, nas diferentes escalas especiais, está inter-relacionado e pode ser incorporado em análises de favorabilidade mineral. Para isso, é necessário identificar em mapas estruturais regionais as áreas que reúnem estes elementos estruturais (e.g. estruturas com orientações apropriadas, *bends* e *jogs* com formato apropriado) e integrá-los com informações geológicas, geofísicas e geoquímicas.

2. Considerações finais

A propriedade fractal dos depósitos IOCG de Carajás indica haver padrões sistemáticos na geometria dos depósitos que se conservam independente da escala espacial, mesmo considerando a complexidade inerente aos processos metalogenéticos. O conjunto de resultados obtidos nesta pesquisa permite inferir que padrões de escala microscópica de minerais de minério, bem como estruturas de escala local próximas de depósitos minerais, apresentam relações geométricas consistentes com as estruturas regionais às quais estão relacionadas, principalmente devido à invariância escalar que apresentam. Dessa forma, parece ser possível extrair informações úteis das escalas microscópica e local para inferir algumas das propriedades dos controles estruturais regionais. Além disso, controles estruturais inferidos a partir de feições das escala microscópica e local apresentam potencial para a previsão da favorabilidade mineral regional, uma vez que permitem individualizar estruturas mais favoráveis à mineralização e, portanto, mais prospectivas.

O conjunto de inferências deste trabalho sugere que a geometria fractal é uma ferramenta útil à prospecção mineral, e indicam que futuros trabalhos podem identificar aplicações para as técnicas aqui apresentadas. A abordagem aqui utilizada tem potencial particularmente interessante para *greenfields*, onde é comum a falta de dados e conhecimento sobre depósitos minerais e seus possíveis controles de mineralização.

REFERÊNCIAS

Berman M. 1977. Distance distributions associated with Poisson processes of geometric figures. *Journal of Applied Probability*, **14**(1):195–199.

Blenkinsop T.G. and Sanderson D.J. 1999. Are gold deposits in the crust fractals? A study of gold mines in the Zimbabwe craton. *In*: McCaffrey K.J.W., Lonergan L., & Wilkinson J.J. (eds.) *Fractures, Fluid Flow and Mineralization. Special Publications*, 155, London, Geological Society, p. 141–151.

Carlson C.A. 1991. Spatial distribution of ore deposits. *Geology*, **19**(2):111–114.

Carranza E.J.M. 2008. *Geochemical Anomaly and Mineral Prospectivity Mapping in GIS*. Amsterdam, Elsevier B.V., 366 p.

Carranza E.J.M. 2009. Controls on mineral deposit occurrence inferred from analysis of their spatial pattern and spatial association with geological features. *Ore Geology Reviews*, **35**(3–4):383–400.

Carvalho E. de R. 2009. Caracterização Geológica e Gênese das Mineralizações de Óxido de Fe-Cu-Au e metais associados na Província Mineral de Carajás: Estudo de Caso do Depósito de Sossego: Universidade Estadual de Campinas, 141 p.

Cox S.F., Knackstedt M.A. and Braun J. 2001. Principles of structural control on permeability and fluid flow in hydrothermal systems. *Reviews in Economic Geology*, **14**:1–24.

Davis G.H. and Reynolds S.J. 1996. *Structural Geology of Rocks and Regions*. Wiley, 800 p.

Delvaux D. and Sperner B. 2003. New aspects of tectonic stress inversion with reference to the TENSOR program. *In*: Nieuwland D.A. (ed.) *New Insights into Structural Interpretation and Modelling*, London, Geological Society, p. 75–100.

Domingos F.H.G. 2009. The structural setting of the Canaã dos Carajás region and Sossego-Sequeirinho deposits, Carajás Brazil [Doctor of Philosophy thesis]: University of Durham, 483 p.

Ford A. and Blenkinsop T.G. 2008. Evaluating geological complexity and complexity gradients as controls on copper mineralisation, Mt Isa Inlier. *Australian Journal of Earth Sciences*, **55**:13–23.

Fry N. 1979. Random point distributions and strain measurement in rocks. *Tectonophysics*, **60**(1–2):89–105.

Hansen V.L. 1990. Collection and preparation of thin sections of oriented samples. *Journal of Geological Education*, **38**:294–297.

Heilbronner R. and Barrett S.D. 2014. *Image Analysis in Earth Sciences*. Berlin Heidelberg, Springer Verlag, 520 p.

Hippertt J. 1999. Are S-C structures, duplexes and conjugate shear zones different manifestations of the same scale-invariant phenomenon? *Journal of Structural Geology*, **21**(8–9):975–984.

Hippertt J.F. and Massucatto A.J. 1998. Phyllonitization and development of kilometer-size extension gashes in a continental-scale strike-slip shear zone, north Goiás, central Brazil. *Journal of Structural Geology*, **20**(4):433–445.

Hitzman M.W. 2000. Iron Oxide-Cu-Au Deposits: What, Where, When and Why. *In*: Porter T.M. (ed.) *Hydrothermal Iron Oxide Copper-Gold & Related Deposits: A Global Perspective, Volume 1*, Adelaide, PGC Publishing, p. 9–25.

Hodkiewicz P.F., Weinberg R.F., Gardoll S.J. and Groves D.I. 2005. Complexity gradients in the Yilgarn Craton: Fundamental controls on crustal-scale fluid flow and the formation of world-class orogenic-gold deposits. *Australian Journal of Earth Sciences*, **52**(6):831–841.

Holdsworth R.E. and Pinheiro R.V.L. 2000. The anatomy of shallow-crustal transpressional structures: Insights from the Archaean Carajas fault zone, Amazon, Brazil. *Journal of Structural Geology*, **22**(8):1105–1123.

Jébrak M. 1997. Hydrothermal breccias in vein-type ore deposits: A review of mechanisms, morphology and size distribution. *Ore Geology Reviews*, **12**(3):111–134.

Jensen E., Cembrano J., Faulkner D., Veloso E. and Arancibia G. 2011. Development of a self-similar strike-slip duplex system in the Atacama Fault system, Chile. *Journal of Structural Geology*, **33**(11):1611–1626.

Jerram D.A., Cheadle M.J., Hunter R.H. and Elliott M.T. 1996. The spatial distribution of grains and crystals in rocks. *Contributions to Mineralogy and Petrology*, **125**(1):60–74.

Johnston J.D. and McCaffrey K.J.W. 1996. Fractal geometries of vein systems and the variation of scaling relationships with mechanism. *Journal of Structural Geology*, **18**(2–3):349–358.

Kretz R. 1969. On the spatial distribution of crystals in rocks. *Lithos*, **2**(1):39–65.

Kruhl J.H. 2013. Fractal-geometry techniques in the quantification of complex rock structures: A special view on scaling regimes, inhomogeneity and anisotropy. *Journal of Structural Geology*, **46**:2–21.

Leite E.P. and Souza Filho C.R. de. 2009. Artificial neural networks applied to mineral potential mapping for copper-gold mineralizations in the Carajás Mineral Province,

Brazil. *Geophysical Prospecting*, **57**(6):1049–1065.

Mandelbrot B.B. 1983. *The Fractal Geometry of Nature (Updated and Augmented Edition)*. New York, Freeman, 495 p.

Marshak S. and Mitra G. 1988. *Basic Methods of Structural Geology*. Englewood Cliffs, NJ, Prentice-Hall, 446 p.

Monteiro L.V.S., Xavier R.P., Carvalho E.R. de, Hitzman M.W., Johnson C.A., Souza Filho C.R. de and Torresi I. 2008a. Spatial and temporal zoning of hydrothermal alteration and mineralization in the Sossego iron oxide–copper–gold deposit, Carajás Mineral Province, Brazil: paragenesis and stable isotope constraints. *Mineralium Deposita*, **43**(2):129–159.

Monteiro L.V.S., Xavier R.P., Hitzman M.W., Juliani C., Souza Filho C.R. de and Carvalho E.R. de. 2008b. Mineral chemistry of ore and hydrothermal alteration at the Sossego iron oxide-copper-gold deposit, Carajás Mineral Province, Brazil. *Ore Geology Reviews*, **34**(3):317–336.

Morais R.P.S. de and Alkmim F.F. de. 2005. O controle litoestrutural da mineralização de cobre do depósito Sequeirinho, Canaã dos Carajás, PA. *In*: *1º Simpósio Brasileiro de Metalogenia*, Gramado, Sociedade Brasileira de Geologia, p. CD-ROM.

Moreto C.P.N., Monteiro L.V.S., Xavier R.P., Creaser R.A., DuFrane S.A., Melo G.H.C., Silva M.A.D. da, Tassinari C.C.G. and Sato K. 2015a. Timing of multiple hydrothermal events in the iron oxide–copper–gold deposits of the Southern Copper Belt, Carajás Province, Brazil. *Mineralium Deposita*, **50**(5):517–546.

Moreto C.P.N., Monteiro L.V.S., Xavier R.P., Creaser R.A., DuFrane S.A., Tassinari C.C.G., Sato K., Kemp A.I.S. and Amaral W.S. 2015b. Neoarchean and Paleoproterozoic Iron Oxide-Copper-Gold events at the Sossego Deposit, Carajás Province, Brazil: Re-Os and U-Pb geochronological evidence. *Economic Geology*, **110**:809–835.

Nykänen V. and Ojala V.J. 2007. Spatial analysis techniques as successful mineral-potential mapping tools for orogenic gold deposits in the northern Fennoscandian shield, Finland. *Natural Resources Research*, **16**(2):85–92.

Oliver N.H.S. 1996. Review and classification of structural controls on fluid flow during regional metamorphism. *Journal of Metamorphic Geology*, **14**:477–492.

Ord A., Munro M. and Hobbs B. 2016. Hydrothermal mineralising systems as chemical reactors: Wavelet analysis, multifractals and correlations. *Ore Geology Reviews*, **79**:155–179.

Pinheiro R.V.L. and Holdsworth R.E. 2000. Evolução tectonoestratigráfica dos sistemas

transcorrentes Carajás e Cinzento, Cinturão Itacaiúnas, na borda leste do Cráton Amazônico, Pará. *Revista Brasileira de Geociências*, **30**(4):597–606.

Raines G.L. 2008. Are fractal dimensions of the spatial distribution of mineral deposits meaningful? *Natural Resources Research*, **17**(2):87–97.

Sibson R.H. 1994. Crustal stress, faulting and fluid flow. *Geological Society, London, Special Publications*, **78**(1):69–84.

Sibson R.H. 1996. Structural permeability of fluid-driven fault-fracture meshes. *Journal of Structural Geology*, **18**(8):1031–1042.

Turcotte D.L. 1989. Fractals in geology and geophysics. *Pure and Applied Geophysics*, **131**(1/2):171–196.

Turcotte D.L. and Huang J. 1995. Fractal Distributions in Geology, Scale Invariance, and Deterministic Chaos. *In*: Barton C.C. & La Pointe P.R. (eds.) *Fractals in the Earth Sciences*, Boston, MA, Springer US, p. 1–40.

Vasquez M.L., Rosa-Costa L.T. da, Silva C.M.G. da and Klein E.L. 2008. Compartimentação Geotectônica. *In*: Vasquez M.L. & Rosa-Costa L.T. da (eds.) *Geologia e Recursos Minerais do Estado do Pará: Sistema de Informações Geográficas - SIG: texto explicativo dos mapas Geológico e Tectônico e de Recursos Minerais do Estado do Pará*, Belém, CPRM, p. 39–112.

Vearncombe J.R. and Vearncombe S. 1999. The spatial distribution of mineralization: Applications of Fry analysis. *Economic Geology*, **94**(4):475–486.

Wang Z., Cheng Q., Cao L., Xia Q. and Chen Z. 2007. Fractal modelling of the microstructure property of quartz mylonite during deformation process. *Mathematical Geology*, **39**(1):53–68.

Weinberg R.F., Hodkiewicz P.F. and Groves D.I. 2004. What controls gold distribution in Archean terranes? *Geology*, **32**(7):545–548.

Williams P.J., Barton M.D., Johnson D.A., Fontboté L., Haller A. de, Mark G., Oliver N.H.S. and Marschik R. 2005. Iron oxide copper-gold deposits: Geology, space-time distribution, and possible modes of origin. *Economic Geology 100th Anniversary Volume*,:371–405.

Xavier R.P., Monteiro L.V.S., Moreto C.P.N., Pestilho A.L.S., Melo G.H.C. de, Silva M.A.D. da, Aires B., Ribeiro C. and Silva F.H.F. e. 2012. The Iron Oxide Copper-Gold Systems of the Carajás Mineral Province, Brazil. *In*: Hedenquist J.W., Harris M., & Camus F. (eds.) *SEG Special Publication*, 16, Society of Economic Geologists Inc., p. 433–454.

APÊNDICE A – Material suplementar do CAPÍTULO 2

Supplementary Material

Here we expand and complement key concepts on Fry and fractal analysis used in the manuscript.

1. Randomness of point patterns and suitability of Fry analysis

For point objects, a completely random distribution is the result of a Poisson process (Fry, 1979; Boots and Getis, 1988), in which the point pattern follows two basic conditions: (i) ***uniformity*** – any location in the studied spatial pattern has equal chance of a point occurrence; and (ii) ***independence*** – the occurrence of a point at a certain location in the spatial pattern does not influence the chance of occurrence of another point at another location. The resulting distribution is known as ***complete spatial randomness*** (CSR) (Diggle, 1983). The importance of a distribution with CSR is that it serves as an ideal reference for the definition of two basic patterns of point distributions (Fig. 1, Boots and Getis, 1988): (i) a ***clustered*** pattern, in which points display a significantly higher grouping than is expected in CSR (Fig. 1b); and (ii) a ***regular*** pattern, in which points show a spread that is significantly higher than is expected in CSR (Fig, 1c). A clustered pattern suggests objects resulting from an interplay of processes that involve 'concentration' of groups of such objects into certain locations; whereas a regular pattern suggests objects resulting from an interplay of processes that involve 'circulation' of such objects toward certain locations (Carranza, 2009).

Clustered and regular patterns can be generated by the lack of at least one of the basic conditions for CSR, i.e., non-uniformity or dependence. As a consequence, such patterns can contain some randomness, meaning they are not completely random. Fry analysis is suitable for these types of patterns.

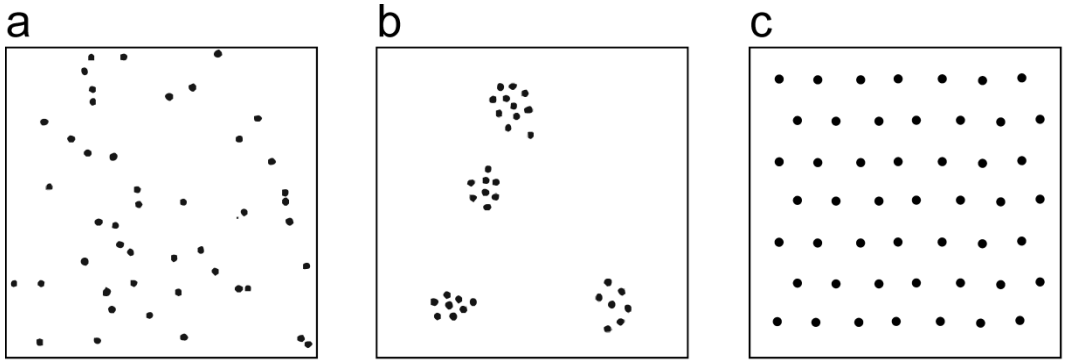

Fig. 1: Fundamental types of point pattern distributions (from Boots and Getis, 1988): (a) complete spatial randomness (CSR); (b) clustered; (c) regular.

2. Dimension concepts and the origin of the fractal dimension

Dimension is a concept usually defined as "the number of parameters needed to uniquely identify all points of space". This dimension concept can be extended to higher dimensional spaces, and is known as **Euclidean dimension**. Although useful, the definition of the Euclidean dimension of certain objects is unsatisfactory in certain situations, so that mathematicians of the transition between the 19^{th} and 20^{th} centuries proposed an alternative definition, known as the **topological** or **Lebesgue dimension** ($\boldsymbol{D_T}$). In this concept, the dimension of a space is the largest of its local dimensions, where the local dimension is defined as the sum of a unit and the Euclidean dimension of the smallest object capable of dividing the original space into two parts. For example: a point is the object with the smallest Euclidean dimension (0), which is able to separate a line into two parts. So the D_T for a line is 1 (i.e., 1 + 0). A line is the object with the smallest Euclidean dimension (1) which is capable of separating a plan (or area) in two parts. So, the D_T for a plane is 2 (i.e., 1 + 1). Although wider than the Euclidean concept, the concept of topological dimension also shows limitations, illustrated by features such as the Koch and Peano curves (Fig. 2).

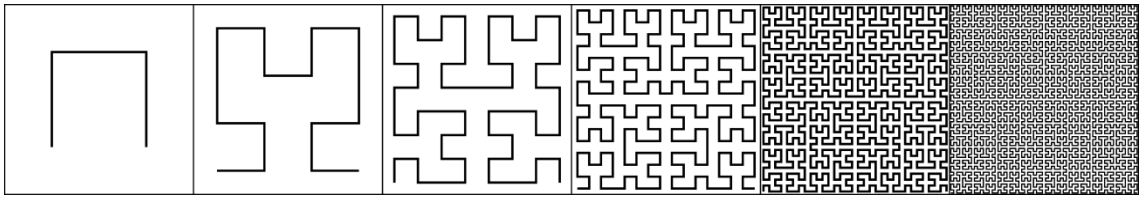

Fig. 2: First six iterations for the construction of a Hilbert curve, a variation of the Peano curve (modified from "Hilbert curve". Licensed under CC BY-SA 3.0 via Wikipedia). In the figure scale, the sixth iteration already reveals a curve with indistinguishable contours. These curves are known as space-filling curves, precisely because as the iterations advance, their length tends to fill up the whole plan.

The curve shown in Fig. 2 contradicts the definition of topological dimension. Although it is a line (D_T = 1), it has an intricate pattern that fills the entire space of the plane, becoming indistinguishable of it (D_T = 2). Considering the existence of such geometric features, a new concept of dimension was necessary in order to describe them. Following work considered that the dimension of a feature *S* is given by the smallest possible union of *n* subsets that cover *S*, and each subset has a diameter equal to or smaller than δ and δ approaches 0 (Pruess, 1995). In practice, this abstract definition means that the size of a feature *S* is measured by covering it with regular geometric features with diagonal δ (usually squares) and the dimension of *S* is given by Eq. (1) (Pruess, 1995):

$$\mu_D = \lim_{\delta \to 0} n(\delta)\delta^D \quad (1)$$

Where $n(\delta)$ is the number of squares with diagonal δ necessary to cover the feature *S* whose dimension is to be determined, and μ_D is a constant of proportionality (Pruess, 1995). Such dimension, firstly known as the **Hausdorff-Besicovitch dimension** (***D***), was later renamed as **fractal dimension** (Mandelbrot, 1983). Rearranging Eq. (1) and representing it in logarithmic form, we have the dimension *D* as in Eq. (2) (Pruess, 1995):

$$D = \lim_{\delta \to 0} \frac{\log n(\delta) - \log \mu_D}{\log(\frac{1}{\delta})} \quad (2)$$

In practice, it is not possible to reduce the size of the squares that cover the feature of interest to the limit 0. So, the above equation is reorganized and *D* is approximated by the slope of a line on a log-log graph as in Eq. (3):

$$\log n(\delta) = \log \mu_D - D \log \delta \quad (3)$$

To build a log *n(δ)* x log *δ* graph, appropriate values of *δ* are chosen, data points obtained are fitted with a straight line and its slope is used as an estimate of the Hausdorff-Besicovitch dimension (Fig. 3).

According to the concept of Hausdorff- Besicovitch dimension, a point has $D = 0$, a line $D = 1$ and a plane $D = 2$, coinciding with D_T of these features. However, for complex objects, D does not coincide with D_T. For the Peano curve of Fig. 2, $D_T = 1$ and $D = 2$; for the Koch curve of Fig. 3, $D_T = 1$ and $D \approx 1.26$ (Mandelbrot, 1983). In both cases, the Hausdorff-Besicovitch dimension is greater than the topological dimension of the curves ($D > D_T$), which is the definition of a fractal (a feature in which the Hausdorff-Besicovitch dimension is larger than the topological dimension). Note that D for the Koch curve is a fractional number (a ubiquitous characteristic in this type of feature); this is the reason why the term "fractal" was chosen by Mandelbrot.

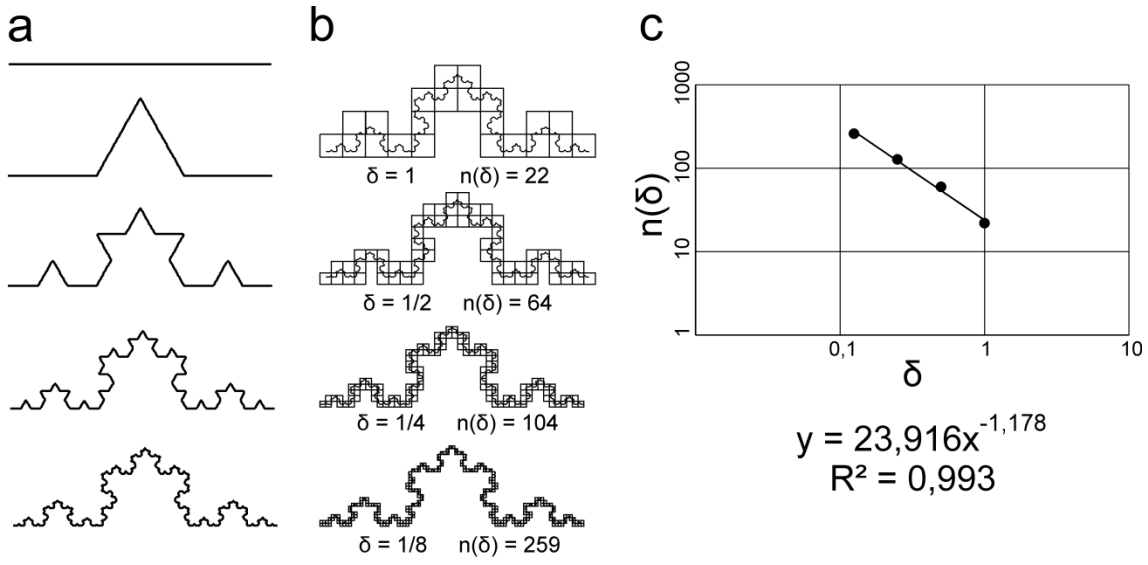

Fig. 3: Procedure for estimating the Hausdorff-Besicovitch dimension of a Koch curve. (a) First five iterations for making the curve. (b) The curve is covered by grids of squares with increasingly small diagonal *δ*. As *δ* decreases, the number of squares *n(δ)* needed to cover the curve increases. (c) The slope of line in the log *n(δ)* x log *δ* graph provides an estimate of $D = 1.178$. For a theoretical curve such as the one illustrated here, D can be determined exactly from the Hausdorff-Besicovitch equation ($D \approx 1.261$; Mandelbrot 1983). Deviation from the theoretical value is inherent to the method applied, but can be reduced by using more grids.

References

Boots, B.N., Getis, A., 1988. Point Pattern Analysis, Scientific Geography 8. SAGE Publications Inc., Newbury Park, 92 pp.

Carranza, E.J.M., 2009. Controls on mineral deposit occurrence inferred from analysis of their spatial pattern and spatial association with geological features. Ore Geol. Rev. 35, 383–400. doi:10.1016/j.oregeorev.2009.01.001

Diggle, P.J., 1983. Statistical Analysis of Spatial Point Patterns. Academic Press, London, 148 pp.

Fry, N., 1979. Random point distributions and strain measurement in rocks. Tectonophysics 60, 89–105. doi:10.1016/0040-1951(79)90135-5

Mandelbrot, B.B., 1983. The Fractal Geometry of Nature (Updated and Augmented Edition). Freeman, New York, 495 pp.

Pruess, S.A., 1995. Some Remarks on the Numerical Estimation of Fractal Dimension. In: Barton, C.C., La Pointe, P.R. (Eds.), Fractals in the Earth Sciences. Springer US, Boston, MA, pp. 65–75. doi:10.1007/978-1-4899-1397-5_3

APÊNDICE B – Material suplementar do CAPÍTULO 4

Appendix A. Supplementary figure

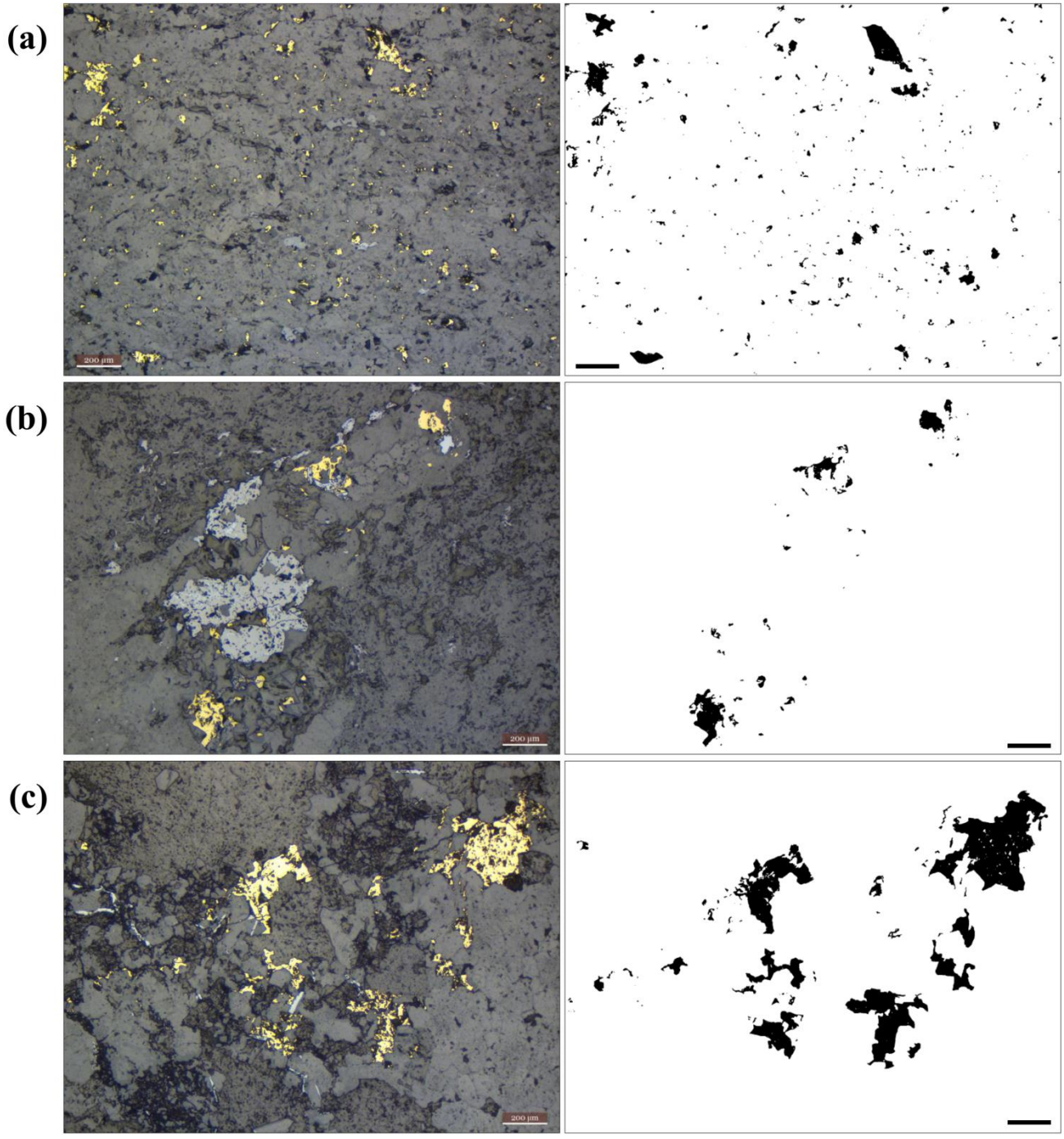

Fig. A1. Examples of texture classification as used in this study. (a) Disseminated alteration (photo SQR-005-h_b1). (b) Sparse alteration (photo SQR-016-h_a1). (c) Infill (photo SSG-002-h_a1). Left: Reflected light. Right: bitmap of ore minerals (chalcopyrite for these samples). Scale bar: 200 µm.

Appendix B. Supplementary data (fractal analysis results per photomicrograph)

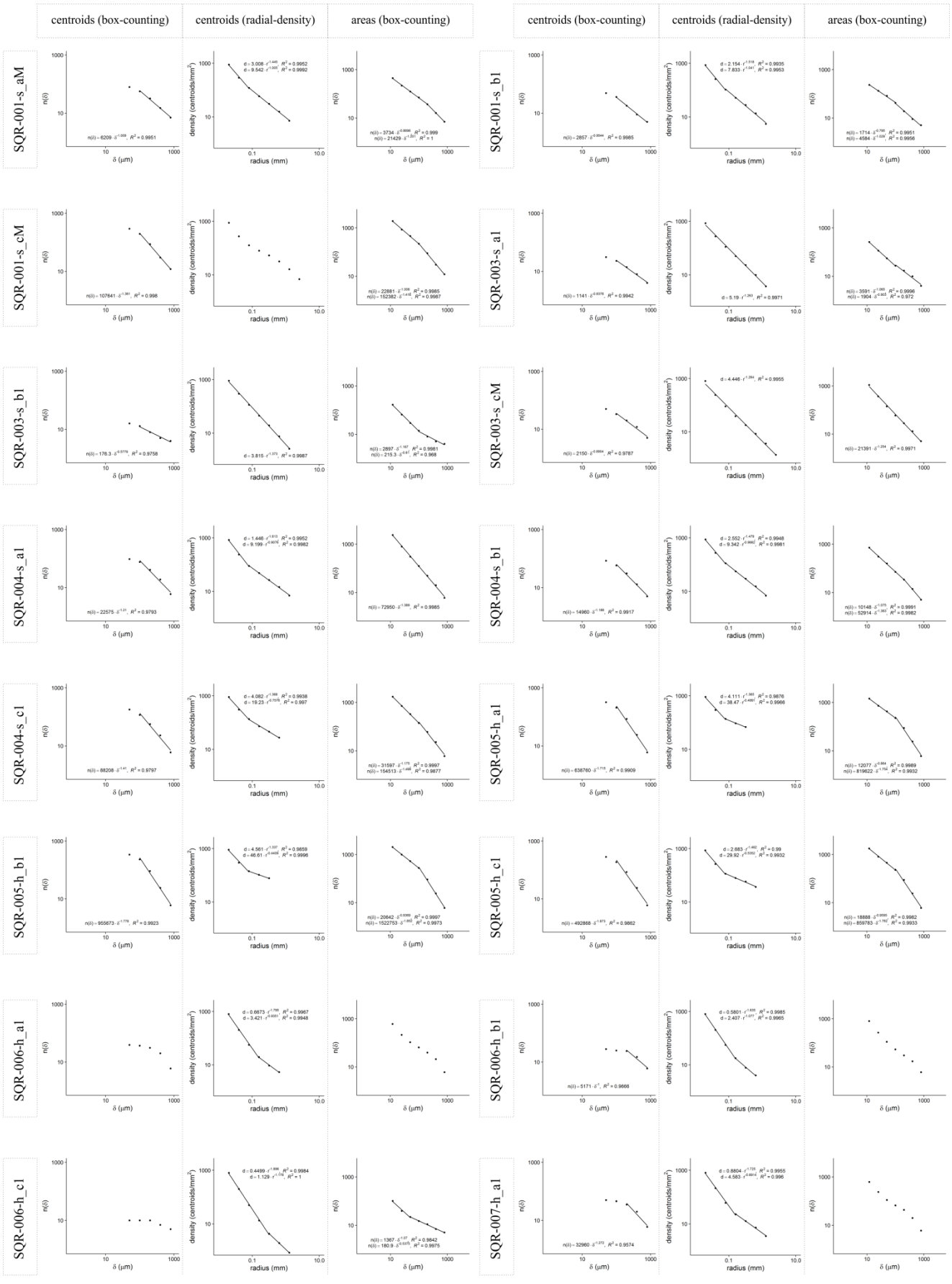

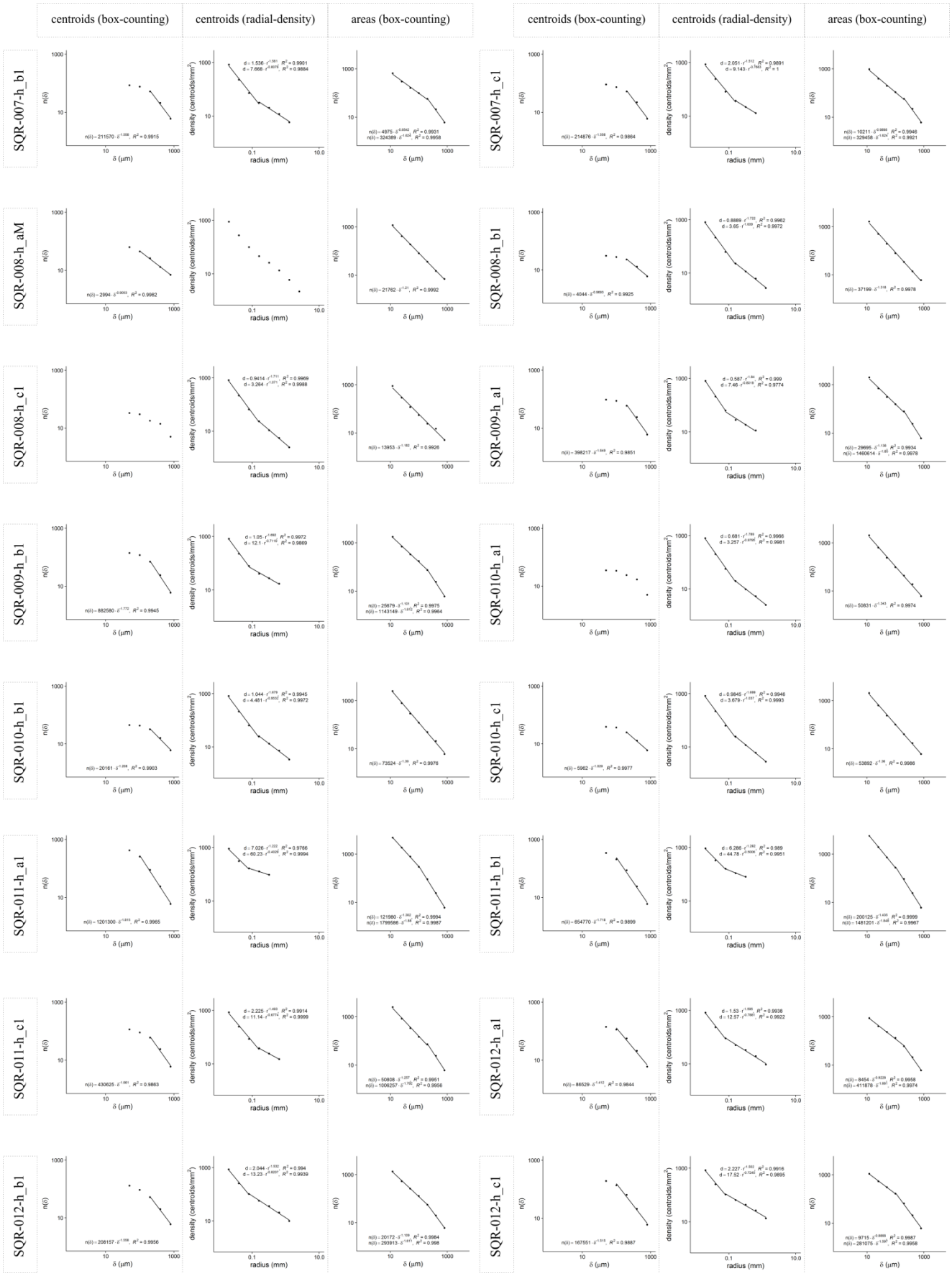
centroids (box-counting)
centroids (radial-density)
areas (box-counting)
centroids (box-counting)
centroids (radial-density)
areas (box-counting)
SQR-007-h_b1
SQR-007-h_c1
SQR-008-h_aM
SQR-008-h_b1
SQR-008-h_c1
SQR-009-h_a1
SQR-009-h_b1
SQR-010-h_a1
SQR-010-h_b1
SQR-010-h_c1
SQR-011-h_a1
SQR-011-h_b1
SQR-011-h_c1
SQR-012-h_a1
SQR-012-h_b1
SQR-012-h_c1
n(δ)
δ (µm)
density (centroids/mm²)
radius (mm)

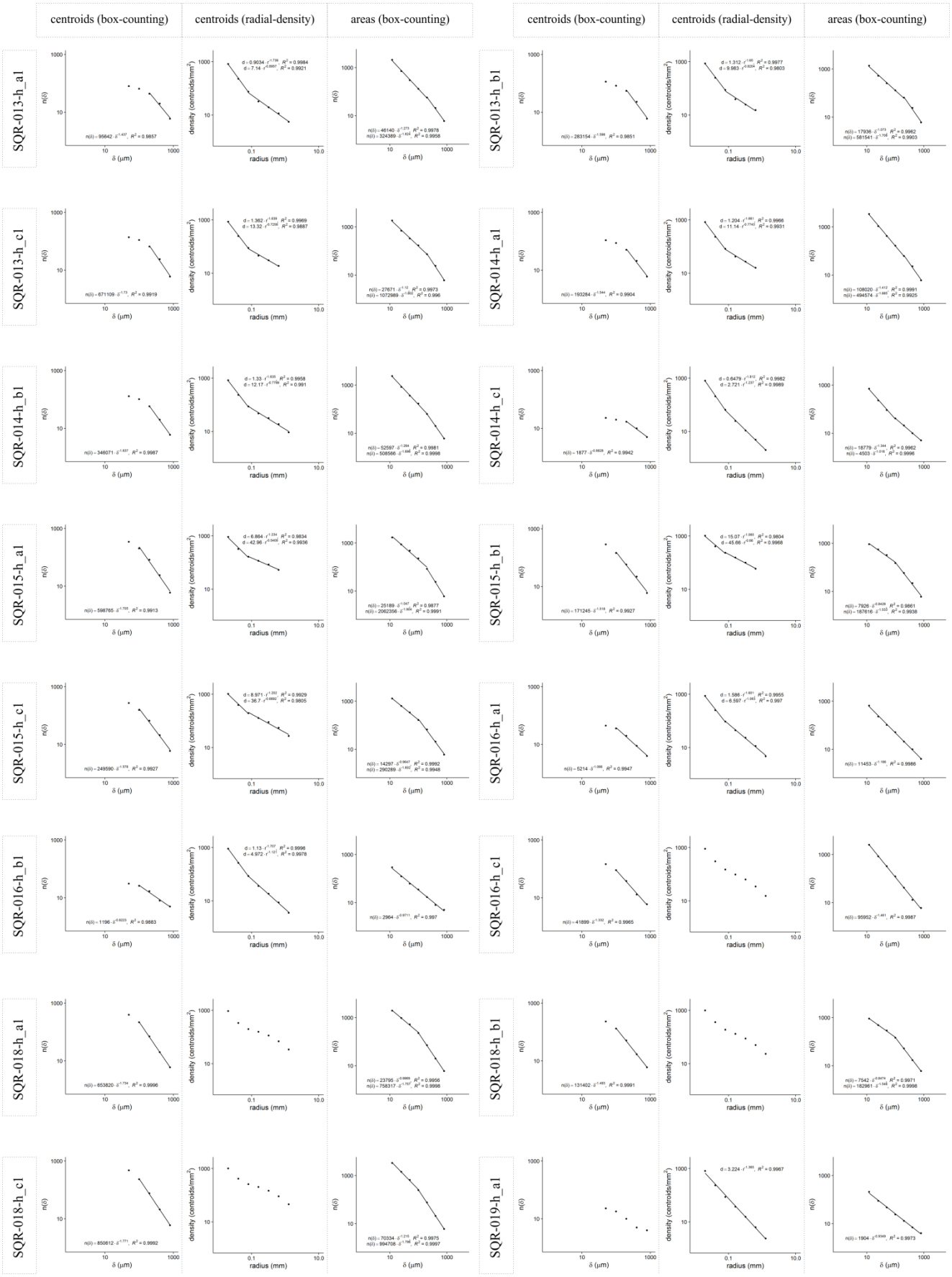
centroids (box-counting)
centroids (radial-density)
areas (box-counting)
centroids (box-counting)
centroids (radial-density)
areas (box-counting)
SQR-013-h_a1
SQR-013-h_b1
SQR-013-h_c1
SQR-014-h_a1
SQR-014-h_b1
SQR-014-h_c1
SQR-015-h_a1
SQR-015-h_b1
SQR-015-h_c1
SQR-016-h_a1
SQR-016-h_b1
SQR-016-h_c1
SQR-018-h_a1
SQR-018-h_b1
SQR-018-h_c1
SQR-019-h_a1
n(δ)
δ (μm)
density (centroids/mm²)
radius (mm)

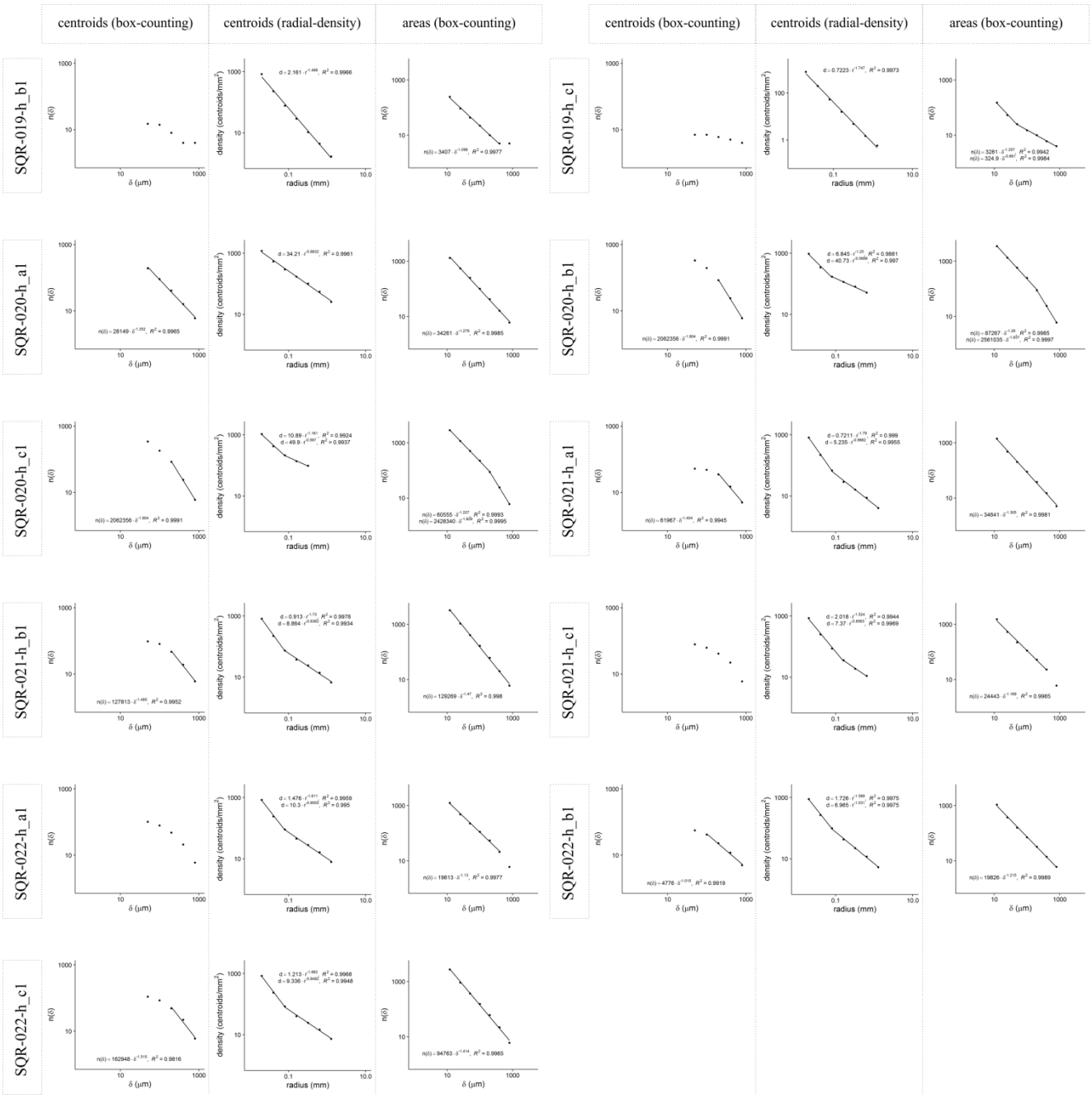
centroids (box-counting)
centroids (radial-density)
areas (box-counting)
centroids (box-counting)
centroids (radial-density)
areas (box-counting)
SQR-019-h_b1
SQR-019-h_c1
SQR-020-h_a1
SQR-020-h_b1
SQR-020-h_c1
SQR-021-h_a1
SQR-021-h_b1
SQR-021-h_c1
SQR-022-h_a1
SQR-022-h_b1
SQR-022-h_c1
n(δ)
density (centroids/mm²)
δ (μm)
radius (mm)

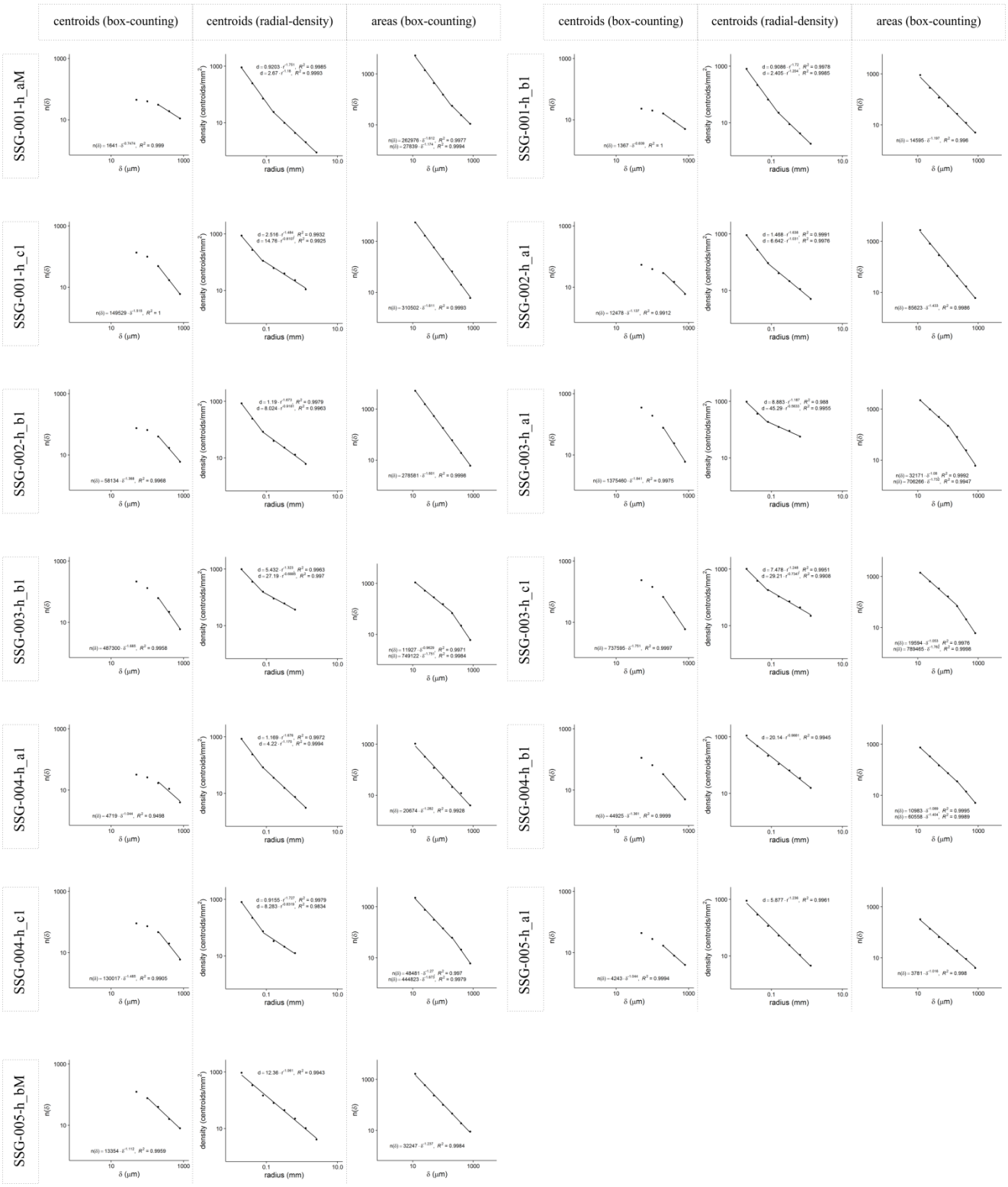
centroids (box-counting)
centroids (radial-density)
areas (box-counting)
centroids (box-counting)
centroids (radial-density)
areas (box-counting)
SSG-001-h_aM
SSG-001-h_b1
SSG-001-h_c1
SSG-002-h_a1
SSG-002-h_b1
SSG-003-h_a1
SSG-003-h_b1
SSG-003-h_c1
SSG-004-h_a1
SSG-004-h_b1
SSG-004-h_c1
SSG-005-h_a1
SSG-005-h_bM
n(δ)
density (centroids/mm²)
δ (μm)
radius (mm)